FROM CHRONIC INFLAMMATION TO CANCER: HOW FAR CAN IMMUNOTHERAPY GO?

EDITED BY: Zhaogang Yang, Xuefeng Li and Lesheng Teng
PUBLISHED IN: Frontiers in Pharmacology

frontiers Research Topics

frontiers

ISSN 1664-8714
ISBN 978-2-88974-429-9
DOI 10.3389/978-2-88974-429-9

About Frontiers

Frontiers is more than just an open-access publisher of scholarly articles: it is a pioneering approach to the world of academia, radically improving the way scholarly research is managed. The grand vision of Frontiers is a world where all people have an equal opportunity to seek, share and generate knowledge. Frontiers provides immediate and permanent online open access to all its publications, but this alone is not enough to realize our grand goals.

Frontiers Journal Series

The Frontiers Journal Series is a multi-tier and interdisciplinary set of open-access, online journals, promising a paradigm shift from the current review, selection and dissemination processes in academic publishing. All Frontiers journals are driven by researchers for researchers; therefore, they constitute a service to the scholarly community. At the same time, the Frontiers Journal Series operates on a revolutionary invention, the tiered publishing system, initially addressing specific communities of scholars, and gradually climbing up to broader public understanding, thus serving the interests of the lay society, too.

Dedication to Quality

Each Frontiers article is a landmark of the highest quality, thanks to genuinely collaborative interactions between authors and review editors, who include some of the world's best academicians. Research must be certified by peers before entering a stream of knowledge that may eventually reach the public - and shape society; therefore, Frontiers only applies the most rigorous and unbiased reviews.
Frontiers revolutionizes research publishing by freely delivering the most outstanding research, evaluated with no bias from both the academic and social point of view. By applying the most advanced information technologies, Frontiers is catapulting scholarly publishing into a new generation.

What are Frontiers Research Topics?

Frontiers Research Topics are very popular trademarks of the Frontiers Journals Series: they are collections of at least ten articles, all centered on a particular subject. With their unique mix of varied contributions from Original Research to Review Articles, Frontiers Research Topics unify the most influential researchers, the latest key findings and historical advances in a hot research area! Find out more on how to host your own Frontiers Research Topic or contribute to one as an author by contacting the Frontiers Editorial Office: frontiersin.org/about/contact

FROM CHRONIC INFLAMMATION TO CANCER: HOW FAR CAN IMMUNOTHERAPY GO?

Topic Editors:
Zhaogang Yang, University of Texas MD Anderson Cancer Center, United States
Xuefeng Li, Guangzhou Medical University, China
Lesheng Teng, Jilin University, China

Citation: Yang, Z., Li, X., Teng, L., eds. (2022). From Chronic Inflammation to Cancer: How Far Can Immunotherapy Go? Lausanne: Frontiers Media SA.
doi: 10.3389/978-2-88974-429-9

Table of Contents

04 ***Editorial: From Chronic Inflammation to Cancer: How Far Can Immunotherapy Go?***
Xuefeng Li, Lesheng Teng and Zhaogang Yang

06 ***An m6A-Related Prognostic Biomarker Associated With the Hepatocellular Carcinoma Immune Microenvironment***
Yingxi Du, Yarui Ma, Qing Zhu, Tongzheng Liu, Yuchen Jiao, Peng Yuan and Xiaobing Wang

22 ***Emerging Biological Functions of IL-17A: A New Target in Chronic Obstructive Pulmonary Disease?***
Meiling Liu, Kang Wu, Jinduan Lin, Qingqiang Xie, Yuan Liu, Yin Huang, Jun Zeng, Zhaogang Yang, Yifan Wang,Shiyan Dong, Weiye Deng, Mingming Yang, Song Wu, Wen Jiang and Xuefeng Li

36 ***EGFR-IL-6 Signaling Axis Mediated the Inhibitory Effect of Methylseleninic Acid on Esophageal Squamous Cell Carcinoma***
Yu Wang, Xianghe Liu, Guanghui Hu, Chenfei Hu, Yang Gao, Miaomiao Huo, Hongxia Zhu, Mei Liu and Ningzhi Xu

47 ***Inhibition of BCL9 Modulates the Cellular Landscape of Tumor-Associated Macrophages in the Tumor Immune Microenvironment of Colorectal Cancer***
Zhuang Wei, Mengxuan Yang, Mei Feng, Zhongen Wu, Rina Rosin-Arbesfeld, Jibin Dong and Di Zhu

64 ***FDX1 can Impact the Prognosis and Mediate the Metabolism of Lung Adenocarcinoma***
Zeyu Zhang, Yarui Ma, Xiaolei Guo, Yingxi Du, Qing Zhu, Xiaobing Wang and Changzhu Duan

76 ***Aberrant ROS Mediate Cell Cycle and Motility in Colorectal Cancer Cells Through an Oncogenic CXCL14 Signaling Pathway***
Jun Zeng, Mei Li, Jun-Yu Xu, Heng Xiao, Xian Yang, Jiao-Xiu Fan, Kang Wu and Shuang Chen

87 ***Carnitine Palmitoyltransferase System: A New Target for Anti-Inflammatory and Anticancer Therapy?***
Muyun Wang, Kun Wang, Ximing Liao, Haiyang Hu, Liangzhi Chen, Linlin Meng, Wei Gao and Qiang Li

103 ***lncRNA OR3A4 Promotes the Proliferation and Metastasis of Ovarian Cancer Through KLF6 Pathway***
Fangfang Guo, Jianan Du, Lingling Liu, Yawei Gou, Mingming Zhang, Wei Sun, Hongmei Yu and Xueqi Fu

113 ***Therapeutic Development by Targeting the cGAS-STING Pathway in Autoimmune Disease and Cancer***
Qiumei Li, Shuoran Tian, Jiadi Liang, Jiqiang Fan, Junzhong Lai and Qi Chen

127 ***Targeting TIGIT Inhibits Bladder Cancer Metastasis Through Suppressing IL-32***
Kang Wu, Jun Zeng, Xulian Shi, Jiajia Xie, Yuqing Li, Haoxiang Zheng, Guoyu Peng, Guanghui Zhu, Dongdong Tang and Song Wu

frontiers in Pharmacology

EDITORIAL
published: 12 January 2022
doi: 10.3389/fphar.2021.838917

Editorial: From Chronic Inflammation to Cancer: How Far Can Immunotherapy Go?

Xuefeng Li[1], *Lesheng Teng*[2] *and Zhaogang Yang*[3]*

[1]The Sixth Affiliated Hospital of Guangzhou Medical University, Qingyuan People's Hospital, State Key Laboratory of Respiratory Disease, Sino-French Hoffmann Institute, School of Basic Medical Sciences, Guangzhou Medical University, Guangzhou, China, [2]School of Life Sciences, Jilin University, Changchun, China, [3]Department of Radiation Oncology, The University of Texas MD Anderson Cancer Center, Houston, TX, United States

Keywords: chronic inflammation, cancer, target therapy, immunotherapy, drug

Editorial on the Research Topic

From Chronic Inflammation to Cancer: How Far Can Immunotherapy Go?

Inflammation is divided into acute inflammation and chronic inflammation. Chronic inflammation has been proved to be one of the major culprits of tumor occurrence and development (Ameri et al., 2019). Once acute inflammation does not subside in time, it will turn into chronic inflammation, and then induce a variety of malignant tumors. Chronic inflammatory diseases, systemic chronic inflammation (obesity, depression, etc.,) and chronic inflammation caused by treatment can affect the immune system, thereby promoting the occurrence and development of tumors. In recent years, people have achieved many gratifying results, including in-depth research on the relationship between inflammation and tumors, the occurrence and regression mechanism of inflammation, and the role of chronic inflammation in tumorigenesis and development.

Here, we are committed to developing new strategies and treatments to activate the immune system of patients with chronic inflammation and cancer, in order to discover new drugs that can be used to combat chronic inflammation and induce cancer immune activation. In our research topic, Liu et al. described the role of IL-17A in Chronic Obstructive Pulmonary Disease (COPD), and discussed that IL-17A and its downstream regulators are potential therapeutic targets for COPD and subsequently COPD-derived lung cancer. Zhang et al. explored the role of FDX1 in the prognosis and metabolism of lung adenocarcinoma. They showed that FDX1 was closely related to glucose metabolism, fatty acid oxidation and amino acid metabolism. Another interesting study performed by Zeng et al. found chemokine ligand 14 (CXCL14) is involved in the proliferation and migration of ROS-induced colorectal cancer (CRC) cells, suggesting that aberrant ROS may promote colorectal cancer cell proliferation and migration through an oncogenic CXCL14 signaling pathway. Also, Wang et al., from another aspect, discussed the carnitine palmitoyltransferase system as a new target for anti-inflammatory and anti-cancer therapy, which may work as a promising anti-inflammatory/anti-tumor therapeutic strategy for numerous disorders. In tumor microenvironment field, Du et al. studied the tumor microenvironmental m6A as a prognostic biomarker associated with the hepatocellular carcinoma (HCC). And Wei et al. found that inhibition of BCL9 modulates the cellular landscape of tumor-associated macrophages in colorectal cancer.

Today, in cancer prevention and treatment, many clinical trials aiming at evaluating the efficacy of inflammatory regulators are underway. Though the single use of anti-inflammatory drugs has shown limited efficacy in cancer treatment, inflammation modulators can synergistically increase the anti-cancer drug's efficacy in cancer therapies (chemotherapy, immunotherapy, etc.). For example, in some patients with advanced cancer, after conventional treatment, immunotherapy can still alleviate

OPEN ACCESS

Edited and reviewed by:
Paola Patrignani,
University of Studies G. d'Annunzio Chieti and Pescara, Italy

***Correspondence:**
Zhaogang Yang
zyang12@mdanderson.org

Specialty section:
This article was submitted to Inflammation Pharmacology, a section of the journal Frontiers in Pharmacology

Received: *18 December 2021*
Accepted: *22 December 2021*
Published: *12 January 2022*

Citation:
Li X, Teng L and Yang Z (2022) Editorial: From Chronic Inflammation to Cancer: How Far Can Immunotherapy Go? Front. Pharmacol. 12:838917. doi: 10.3389/fphar.2021.838917

or even prevent the further development of disease (Ramagopalan et al., 2021). It is worth noting that the side effects suffered by patients during the remission period of several years are also lighter. Thus, there are still many key issues to be addressed on how to apply immunotherapy to regulate inflammation, or to improve the efficacy of cancer treatment or anti-cancer efficacy. For example: how to identify the most critical driving factors affecting the inflammatory response of cancer patients (Golder et al., 2021)? How to reduce or avoid side effects such as severe inflammation in the process of anti-cancer treatment (inflammatory storm induced by CAR-T treatment) (Hescot et al., 2018)? In addition, in the process of anti-tumor immunotherapy, we should also consider that different cancer patients will have different inflammatory responses. Personalized treatment strategies (precision medicine) for specific tumor-related inflammation will help improve anti-cancer efficacy. To answer these questions, our topic authors, through different ways and methods, in different tumors, have studied in depth some application cases of immunotherapy. Wu et al. explored T cell immunoreceptor with immunoglobulin and immunoreceptor tyrosine-based inhibitory motif domain (TIGIT), which is highly expressed in a subset of Treg cells, as a novel target for bladder cancer immunotherapy. Li et al. discussed the cGAS-STING pathway to explore the DNA immune recognition regulation in autoimmune disease and cancer. They summarized the current progress on cGAS-STING pathway modulators and laid the foundation for further investigating therapeutic development in autoimmune diseases and tumors. Wang et al. discussed the inhibitory effect of methylseleninic acid on esophageal squamous cell carcinoma through EGFR-IL-6 signaling axis. For metastatic cancer, Guo et al. used a xenograft model in zebra fish, and found lncRNA OR3A4 acts as the inflammatory cytokine to promote the proliferation and metastasis of ovarian cancer through KLF6 pathway.

In summary, the collection of aforementioned articles in this research topic provide either overview of novel targets in immunotherapy, or new fundamental findings and summaries related to chronic inflammation and cancer. Additional researches, for example, drug delivery systems and synthetic antibody engineering, are needed to gain further insights as we move toward to improve the safety and efficacy of novel immunotherapy applications in chronic inflammation and cancer.

AUTHOR CONTRIBUTIONS

XL: drafting manuscript. XL, LT, and ZY: revision, editing, and final approval. All authors listed contributed to the work and approved it for publication.

ACKNOWLEDGMENTS

We thank the authors, editors, and reviewers who contributed to this Research Topic.

REFERENCES

Ameri, A. H., Moradi Tuchayi, S., Zaalberg, A., Park, J. H., Ngo, K. H., Li, T., et al. (2019). IL-33/regulatory T Cell axis Triggers the Development of a Tumor-Promoting Immune Environment in Chronic Inflammation. *Proc. Natl. Acad. Sci. U S A.* 116, 2646–2651. doi:10.1073/pnas.1815016116

Golder, A. M., McMillan, D. C., Park, J. H., Mansouri, D., Horgan, P. G., and Roxburgh, C. S. (2021). The Prognostic Value of Combined Measures of the Systemic Inflammatory Response in Patients with colon Cancer: an Analysis of 1700 Patients. *Br. J. Cancer* 124, 1828–1835. doi:10.1038/s41416-021-01308-x

Hescot, S., Haissaguerre, M., Pautier, P., Kuhn, E., Schlumberger, M., and Berdelou, A. (2018). Immunotherapy-induced Addison's Disease: A Rare, Persistent and Potentially Lethal Side-Effect. *Eur. J. Cancer* 97, 57–58. doi:10.1016/j.ejca.2018.04.001

Ramagopalan, S. V., Leahy, T. P., Ray, J., Wilkinson, S., Sammon, C., and Subbiah, V. (2021). The Value of Innovation: Association between Improvements in Survival of Advanced and Metastatic Non-small Cell Lung Cancer and Targeted and Immunotherapy. *BMC Med.* 19, 209. doi:10.1186/s12916-021-02070-w

Conflict of Interest: The authors declare that the research was conducted in the absence of any commercial or financial relationships that could be construed as a potential conflict of interest.

frontiers in Pharmacology

ORIGINAL RESEARCH
published: 24 June 2021
doi: 10.3389/fphar.2021.707930

An m6A-Related Prognostic Biomarker Associated With the Hepatocellular Carcinoma Immune Microenvironment

Yingxi Du[1†], Yarui Ma[1], Qing Zhu[1], Tongzheng Liu[2], Yuchen Jiao[1], Peng Yuan[3] and Xiaobing Wang[1]**

[1]State Key Laboratory of Molecular Oncology, National Cancer Center/National Clinical Research Center for Cancer/Cancer Hospital, Chinese Academy of Medical Sciences and Peking Union Medical College, Beijing, China, [2]College of Pharmacy, Jinan University, Guangzhou, China, [3]National Cancer Center/National Clinical Research Center for Cancer/Cancer Hospital, Chinese Academy of Medical Sciences and Peking Union Medical College, Beijing, China*

OPEN ACCESS

Edited by:
Xuefeng Li,
Guangzhou Medical University, China

Reviewed by:
Shiyan Dong,
Jilin University, China
Yifan Wang,
University of Texas MD Anderson Cancer Center, United States

***Correspondence:**
Peng Yuan
yuanpeng01@hotmail.com
Xiaobing Wang
wangxb@cicams.ac.cn

[†]*These author share first authorship*

Specialty section:
This article was submitted to Inflammation Pharmacology, a section of the journal Frontiers in Pharmacology

Received: *11 May 2021*
Accepted: *14 June 2021*
Published: *24 June 2021*

Citation:
Du Y, Ma Y, Zhu Q, Liu T, Jiao Y, Yuan P and Wang X (2021) An m6A-Related Prognostic Biomarker Associated With the Hepatocellular Carcinoma Immune Microenvironment. Front. Pharmacol. 12:707930. doi: 10.3389/fphar.2021.707930

Background: N6-methyladenosine (m6A) is related to the progression of multiple cancers. However, the underlying influences of m6A-associated genes on the tumor immune microenvironment in hepatocellular carcinoma (HCC) remain poorly understood. Therefore, we sought to construct a survival prediction model using m6A-associated genes to clarify the molecular and immune characteristics of HCC.

Methods: HCC case data were downloaded from The Cancer Genome Atlas (TCGA). Then, by applying consensus clustering, we identified two distinct HCC clusters. Next, four m6A-related genes were identified to construct a prognostic model, which we validated with Gene Expression Omnibus (GEO) and International Cancer Genome Consortium (ICGC) datasets. Additionally, the molecular and immune characteristics in different subgroups were analyzed.

Results: m6A RNA methylation regulators were differentially expressed between HCC and normal samples and linked with immune checkpoint expression. Using consensus clustering, we divided HCC samples into two subtypes with distinct clinical features. Cluster 2 was associated with unfavorable prognosis, higher immune checkpoint expression and immune cell infiltration levels. In addition, the immune and carcinogenic signaling pathways were enriched in cluster 2. Furthermore, we constructed a risk model using four m6A-associated genes. Patients with different risk scores had distinct survival times, expression levels of immunotherapy biomarkers, TP53 mutation rates, and sensitivities to chemotherapy and targeted therapy. Similarly, the model exhibited an identical impact on overall survival in the validation cohorts.

Conclusion: The constructed m6A-based signature may be promising as a biomarker for prognostics and to distinguish immune characteristics in HCC.

Keywords: M6A, hepatocellular carcinoma, prognosis, immune microenvironment, therapy

INTRODUCTION

Epidemiological surveys have found that hepatocellular carcinoma (HCC) is among the most lethal cancers in terms of its incidence and mortality (Bray et al., 2018). Despite great improvements in diagnosis and treatment, the overall prognosis of HCC patients remains unsatisfactory. Therefore, predictive prognostic biomarkers of HCC are immediately needed to improve the clinical outcome of HCC patients.

Recently, inhibiting immune checkpoints, such as cytotoxic T lymphocyte-associated protein 4 (CTLA4), programmed death 1 (PD1), and programmed death-ligand 1 (PD-L1), has shown clear benefits in the survival of cancer patients (Larkin et al., 2015; Bellmunt et al., 2017; Garassino et al., 2020). Compared with traditional therapies, immune checkpoint inhibitor (ICI) treatment has become an emerging strategy for HCC therapy with a significantly favorable outcome (El-Khoueiry et al., 2017; Zhu et al., 2018). Nonetheless, a major limitation is the low response rate of patients to immunotherapy (Ferris et al., 2016; Ma et al., 2019). Multiple factors, including the tumor immune microenvironment (TIME), can affect ICI effectiveness, and few biomarkers can effectively predict patient outcomes (Nishino et al., 2017). The identification of potential prognostic markers associated with treatment benefit will allow individualized immunotherapy for HCC patients. Unfortunately, we know little about the TIME of HCC. Therefore, sensitive prognostic and therapeutic biomarkers are urgently needed to predict the HCC response to ICIs. Many studies on the TIME have demonstrated the critical function of infiltrating immune cells in cancer development and the therapeutic response to immunotherapy (Jiang et al., 2018; Zeng et al., 2018). For example, tumor-infiltrating lymphocytes (TILs), such as CD4+ T cells and CD8+ T cells, have emerged as potential prognostic factors for therapeutic responsiveness to immunotherapy (Vassilakopoulou et al., 2016). Due to the high enrichment of infiltrating regulatory T cells (Tregs) and exhausted CD8+ T cells in HCC, the regulatory imbalance in the tumor immune microenvironment has an important impact on the initiation, progression and resistance of HCC, which possesses features of immunosuppressive disease (Zheng et al., 2017; Ringelhan et al., 2018; Ruf et al., 2020). Therefore, the potential mechanisms that regulate the tumor immune microenvironment should be further clarified to enable the determination of precise and accurate biomarkers that effectively render a prognosis and predict the immune response to personalized immunotherapy.

N6-methyladenosine (m6A) is the most important and prevalent internal modification of mRNA (Wang et al., 2017). m6A regulators comprise three types of factors: writers, readers, and erasers (Yang et al., 2018). A variety of studies have shown that m6A regulators make a huge difference in the modification of noncoding RNAs, including microRNAs, long non-coding RNAs, and circular RNAs, gene expression, alternative splicing, and protein translation (Dominissini et al., 2012; Alarcón et al., 2015; Lin et al., 2019; He et al., 2020; Rao et al., 2020). The aberrant expression levels of m6A regulators are tightly linked to stem cell differentiation, germ cell maturity and fertility, T cell differentiation, heart disease, and nervous system activity (Geula et al., 2015; Li et al., 2017a; Fang et al., 2020). m6A RNA methylation regulators have also been investigated extensively in a variety of tumors (Huo et al., 2020). m6A methylation has a great effect on the tumor development and progression by modulating the expression of a wide variety of oncogenes and cancer suppressor genes. For instance, depletion of METTL3 makes pancreatic cancer cells sensitive to anticancer therapy (Taketo et al., 2018). Additionally, downregulation of METTL14 may serve as a prognostic factor for HCC patients (Weng et al., 2018).

Although many efforts have been made to study the intrinsic mechanisms of m6A-related regulators in cancer progression and metastasis, the underlying roles of m6A regulators in the immune microenvironment continue to be largely unclear. A study found that neoantigen-dependent tumor-specific immunity is considerably controlled by YTHDF1 (Han et al., 2019). In addition, FTO might decrease the response to anti-PD-1 blockade immunotherapy in melanoma (Yang et al., 2019). These results suggested that m6A-associated genes might become underlying predictive factors and therapeutic targets to improve the clinical response to ICI treatment. However, whether m6A RNA methylation regulators are correlated with the TIME or immune checkpoints such as PD-L1 is unknown in HCC. There is no doubt that a comprehensive understanding of m6A-associated genes in HCC still needs to be further demonstrated.

A significant amount of research has focused on constructing a useful tool to provide better survival prediction for patients with HCC. However, little of this research has been useful. To systematically analyze the correlations of m6A-associated regulators with prognosis, the expression of immune checkpoints, therapeutic response, and TIME in HCC, we carried out this study. Specifically, we studied the expression levels of m6A-associated genes in HCC and normal tissues and the correlation between m6A regulators and immune checkpoints. Then, we identified two different HCC subtypes that had different prognostic outcomes and clinicopathological features. Next, we established a risk model for m6A-related regulators to improve the accuracy of their prognosis for HCC, which led to the categorization of HCC samples in the TCGA, GEO, and ICGC cohorts into two risk subgroups. Next, the relationships between the risk models and immune checkpoints, immune cell infiltration levels, total mutation burden (TMB), neoantigen counts, gene mutation status, and therapeutic sensitivity were fully elucidated on the basis of the m6A-related signature to systematically examine the effects of m6A regulators on the survival and tumor immune microenvironment of HCC. These results demonstrated that m6A-associated regulators play key roles in HCC prognosis, TIME, and therapeutic responses.

METHODS

Data Collection

The mRNA expression profiles and the corresponding clinicopathological data of HCC patients were simultaneously

downloaded from the TCGA on August 3, 2020, and consisted of data on 374 HCC and 50 normal case samples. The RNA-seq data and survival data of 221 HCC samples (GSE14520 dataset) were obtained from the GEO database. The RNA-seq data and clinical information of another 232 HCC cases were downloaded from the ICGC database. We removed the batch effect *via* the "sva" R package.

Identification of m6A RNA Methylation Regulators

After searching the recently published literature on m6A, we found 18 m6A-related genes (Huo et al., 2020). A total of 15 of these genes were selected based on the mRNA expression data of HCC obtained from the TCGA. Ten genes (YTHDC2, FTO, ZC3H13, YTHDC1, YTHDF3, YTHDF1, METTL3, RBM15, YTHDF2, and WTAP) were identified for subsequent prognostic analysis because they are listed in the GSE14520 dataset.

Construction and Validation of the Prognostic Gene Signature

The risk model of four m6A regulators was constructed using least absolute shrinkage and selection operator (LASSO) regression analysis of the TCGA cohort data. The coefficients were derived from the LASSO regression analysis. The risk score was obtained from the equation: risk score = $\sum_{i=1}^{n}$ (coefficient of mRNAi*expression of mRNAi). Then, according to the median value of the risk score, HCC patients were classified into the high-risk subgroup or the low-risk subgroup.

Gene Ontology and Gene Set Enrichment Analysis

To elucidate the biological features of two distinct clusters, the "clusterProfiler" package was employed for the Gene Ontology (GO) enrichment analysis, and *p*. adjust <0.05 showed significance (Yu et al., 2012). GSEA was carried out using the Hallmark gene set "h.all.v7.0.symbols.gmt" to illustrate the different enriched terms between different HCC subtypes.

Immune Cell Infiltration Estimation, Tumor Mutation Burden and Neoantigen Analyses

The immune score and stromal score for each patient were obtained by using the "estimate" package (Yoshihara et al., 2013). The immune cell infiltration levels were assessed comprehensively through The Tumor Immune Estimation Resource (TIMER), which estimates the abundance of six immune cell infiltrates (Li et al., 2017b). The somatic mutational profile of HCC was downloaded from the TCGA. The quantity and quality of the gene mutations were analyzed in the two groups with the "Maftools" package of R (Mayakonda et al., 2018). Neoantigens in the TCGA-LIHC dataset were obtained from a previously published study (Thorsson et al., 2018).

Chemotherapy and Targeted Therapy Response Prediction

To estimate the predictive role of the model for HCC treatment, we used the R package "pRRophetic" to evaluate the half maximal inhibitory concentration (IC50) of common chemotherapy and targeted therapy drugs, such as sorafenib, mitomycin, and doxorubicin.

Statistical Analysis

Statistical tests were conducted using R version 4.0.2 and GraphPad Prism 8.0. The group comparisons of two groups were compared by *t*-test. The expression correlation analysis between m6A-associated genes and immune checkpoints was performed by Pearson correlation test. Using "km" method in the R package "ConsensusClusterPlus," we classified 374 HCC patients into different subtypes. We performed a chi-square test to explore the relationship between the clusters and clinicopathological characteristics. Survival curves and survival differences were generated by the Kaplan-Meier method with log rank test. Univariate and multivariate analyses were performed by adopting the Cox regression method to determine whether the risk score combined with other clinical characteristics was an independent prognostic factor. In addition, a receiver operating characteristic (ROC) curve analysis was performed to evaluate the predictive power of the prognostic model. A p value (two-sided) less than 0.05 was accepted as statistically significant: not significant (ns), $p < 0.05$ (*), $p < 0.01$ (**), $p < 0.001$ (***) and $p < 0.0001$ (****).

RESULTS

m6A RNA Methylation Regulators Were Largely Overexpressed and Associated With Immune Checkpoints in Hepatocellular Carcinoma

To systematically investigate the potential impact of m6A-related genes on HCC development and progression, we assessed the distinct expression levels of 15 m6A-associated genes between HCC and normal tissues in the TCGA dataset. It was evident that the expression levels of m6A-associated genes in the HCC and normal patients were different (**Figure 1A**). All m6A regulators, except METTL14 and ZC3H13, were significantly overexpressed in the HCC samples. Then, we assessed the correlation of immune checkpoints, including HAVCR2 (also known as TIM3), LAG3, PD-L1, CTLA4, IDO1, and PD1, with m6A-related genes. The expression levels of immune checkpoints showed a positive correlation with m6A-associated genes (**Figure 1B**). These findings demonstrated that m6A-related regulators might have essential effects on HCC development and progression. Considering the known roles of checkpoints in the immunosuppressive microenvironment, m6A-associated

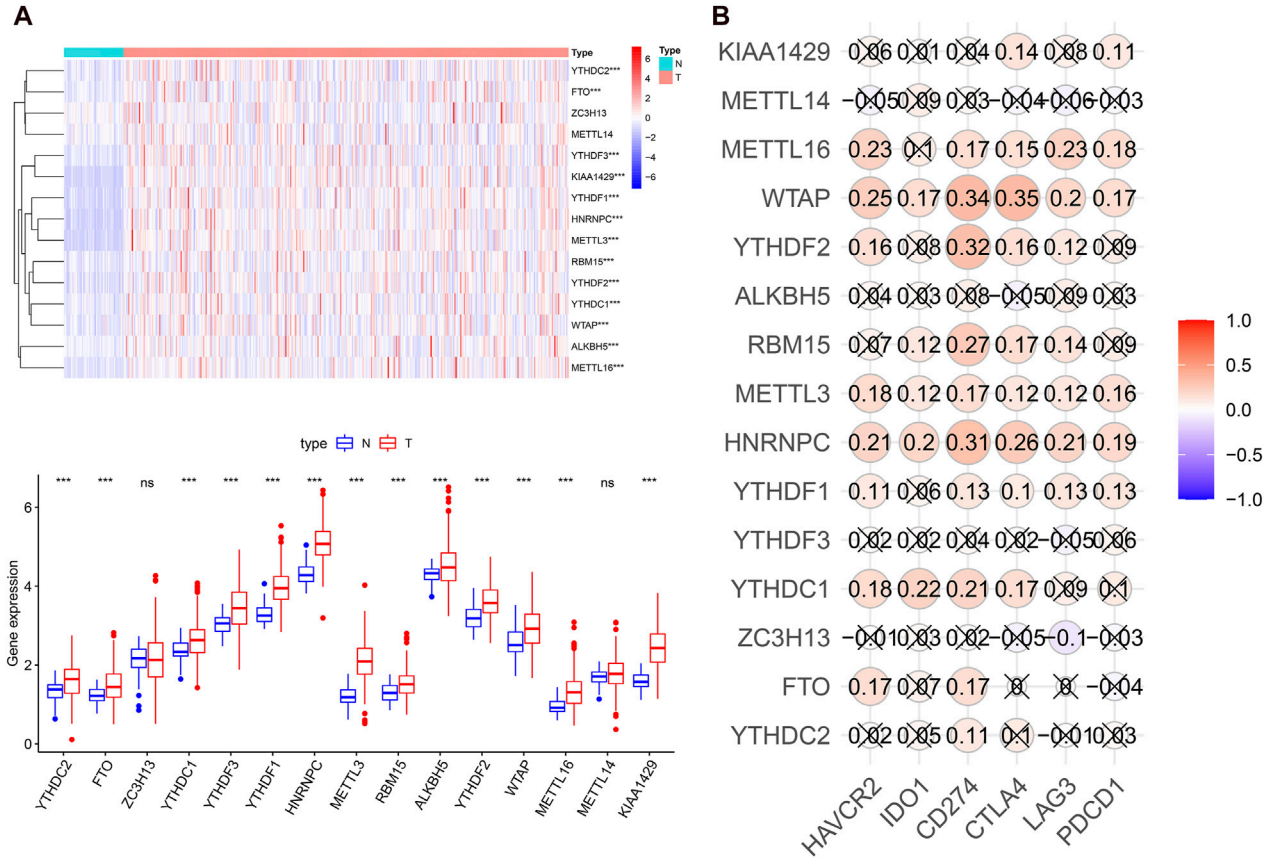

FIGURE 1 | m6A regulators expression levels and correlation with immune checkpoint expression in HCC. **(A)**, heatmap and boxplot of 15 m6A-related genes expression in HCC. N: normal tissue; T: tumor tissue. **(B)**, the expression correlation between the immune checkpoints and m6A regulators. "X" means $p > 0.05$.

regulators may have crucial biological functions in HCC immunotherapy.

The Association of Consensus Clustering With the Clinicopathological Features, Survival Status, Tumor Signaling Pathways, and Immune Cell Infiltration in Hepatocellular Carcinoma

Considering the optimal clustering stability, k = 2 was ultimately identified (**Supplementary Figure S1**), and the samples from 374 patient with HCC were categorized into two different subtypes (**Figure 2A**). Then, the overall survival (OS) and other clinical information of cluster 1 (n = 260) and cluster 2 (n = 114) were compared comprehensively. The OS (p = 0.0008) of cluster 1 with downregulated m6A regulator expression was better than that of cluster 2 with upregulated m6A regulator expression (**Figure 2B**). We found that the expression level of individual m6A-associated genes in cluster 2 was higher than that in cluster 1, expect that of ZC3H13. Then, we fully compared the clinical characteristics between the two clusters (**Figure 2C**). Cluster 1 mostly consisted of samples from male and elderly patient with HCC ($p < 0.05$). Cluster 2 was closely linked with a higher histological grade and a lower stromal score than cluster 1 ($p < 0.05$). We also performed PCA to find the gene expression profiles that differed between the two subtypes (**Supplementary Figure S1D**). The results indicated that the clusters defined by m6A-related genes were tightly linked to HCC tumor heterogeneity. Next, to further explore potential functional pathways, Gene Ontology (GO) enrichment analysis was conducted for the differentially expressed genes (DEGs) between the two subtypes. The DEGs were closely related to biological processes (BPs) of the immune response, such as the immunoglobulin-mediated immune response and complement activation (**Figure 3A**). Because of the possible difference in the immune microenvironment between the two clusters, GSEA was conducted to further analyze the underlying regulatory mechanisms. The findings revealed that cluster 2 samples expectedly possessed several canonical hallmarks of malignancy, such as DNA repair, G2M checkpoint, mTORC1 pathway, Wnt/β-Catenin pathway, P53 pathway, and PI3K/AKT/mTOR pathway (**Figure 3B**). Hence, these pathways linked with the development and progression of cancers, particularly the PI3K/AKT/mTOR pathway, P53 pathway, and Wnt/β-Catenin pathway, might be connected with the distinct immune microenvironment of the two clusters. To explore the influence of m6A-associated regulators on the tumor immune microenvironment of HCC, we assessed the immune cell infiltrate level, immune score, and stromal score between the two clusters. The stromal score was significantly different between the two clusters (**Figure 2C**). Next, the infiltration levels of immune cells in the two

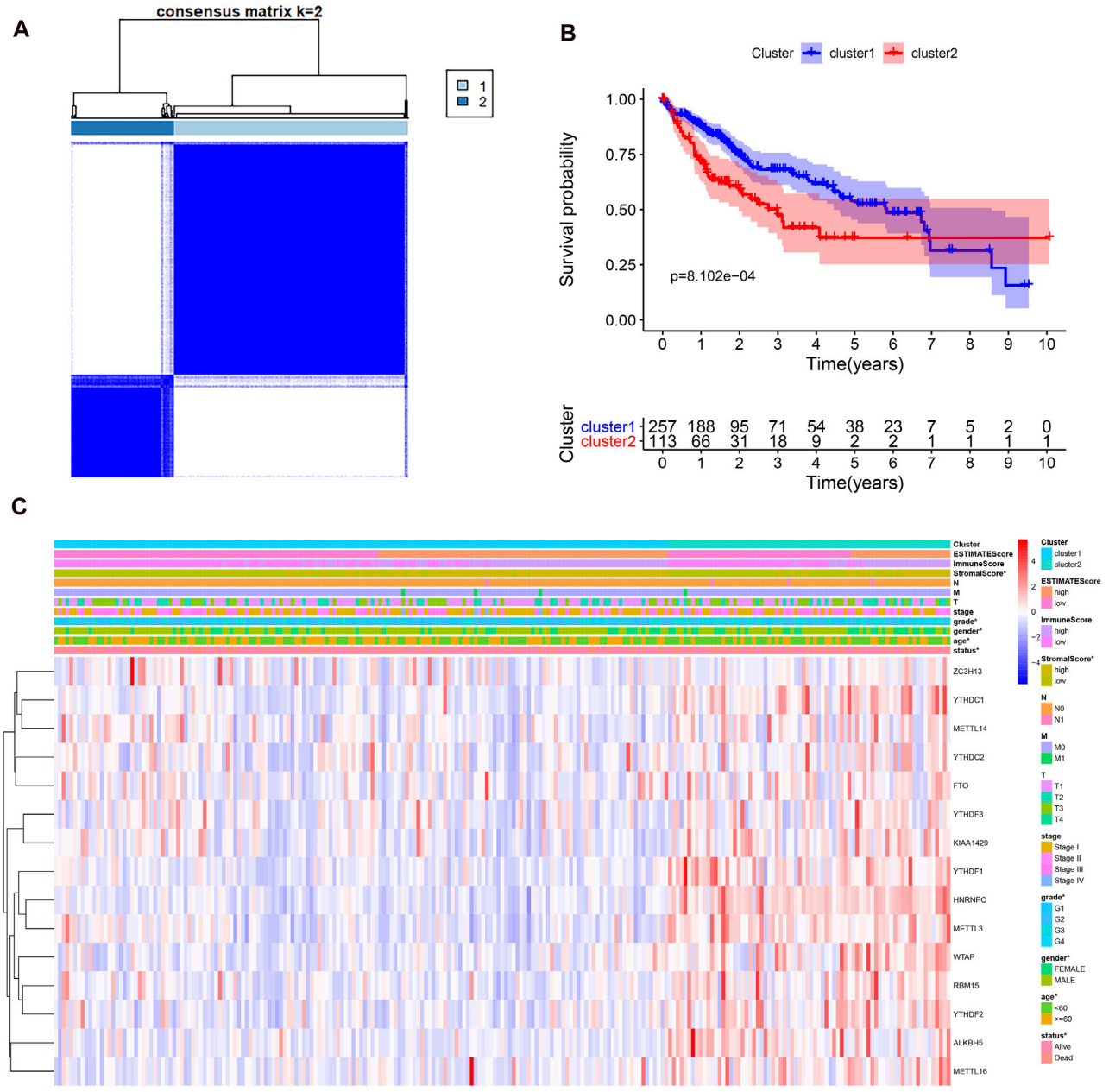

FIGURE 2 | Different clinicopathological characteristics and survival of HCC in two clusters in the TCGA-LIHC. **(A)**, consensus clustering heatmap for k = 2 in HCC. **(B)**, survival curve of overall survival in two clusters. **(C)**, heatmap and clinicopathological characteristics of the two clusters.

clusters were explored. Cluster 2 samples showed a higher abundance of immune cells (**Figure 3C**). To further investigate the involvement of immune checkpoints with m6A-associated genes, we evaluated the expression levels of immune checkpoints between the two clusters. The immune checkpoints were highly expressed in cluster 2 samples ($p < 0.01$; **Figure 3D**). The expression levels of immune checkpoints were also compared between HCC and normal patient samples (**Supplementary Figure S2A**). Given these results, the patients represented by cluster 2 may potentially have a higher response rate to ICI treatment.

Construction of an m6A RNA Methylation Regulator-Based Prognostic Model

Next, we elucidated the prognostic function of m6A-related genes in HCC patients. Univariate Cox regression analysis was used to identify seven survival-related genes (**Supplementary Figure S2B**). Then, LASSO regression analysis was performed based on the expression levels of seven identified m6A-associated genes in the TCGA cohort. As a consequence, four m6A-related genes, namely, METTL3, YTHDF2, YTHDF1, and ZC3H13, were identified (**Figure 4A**). The risk score of

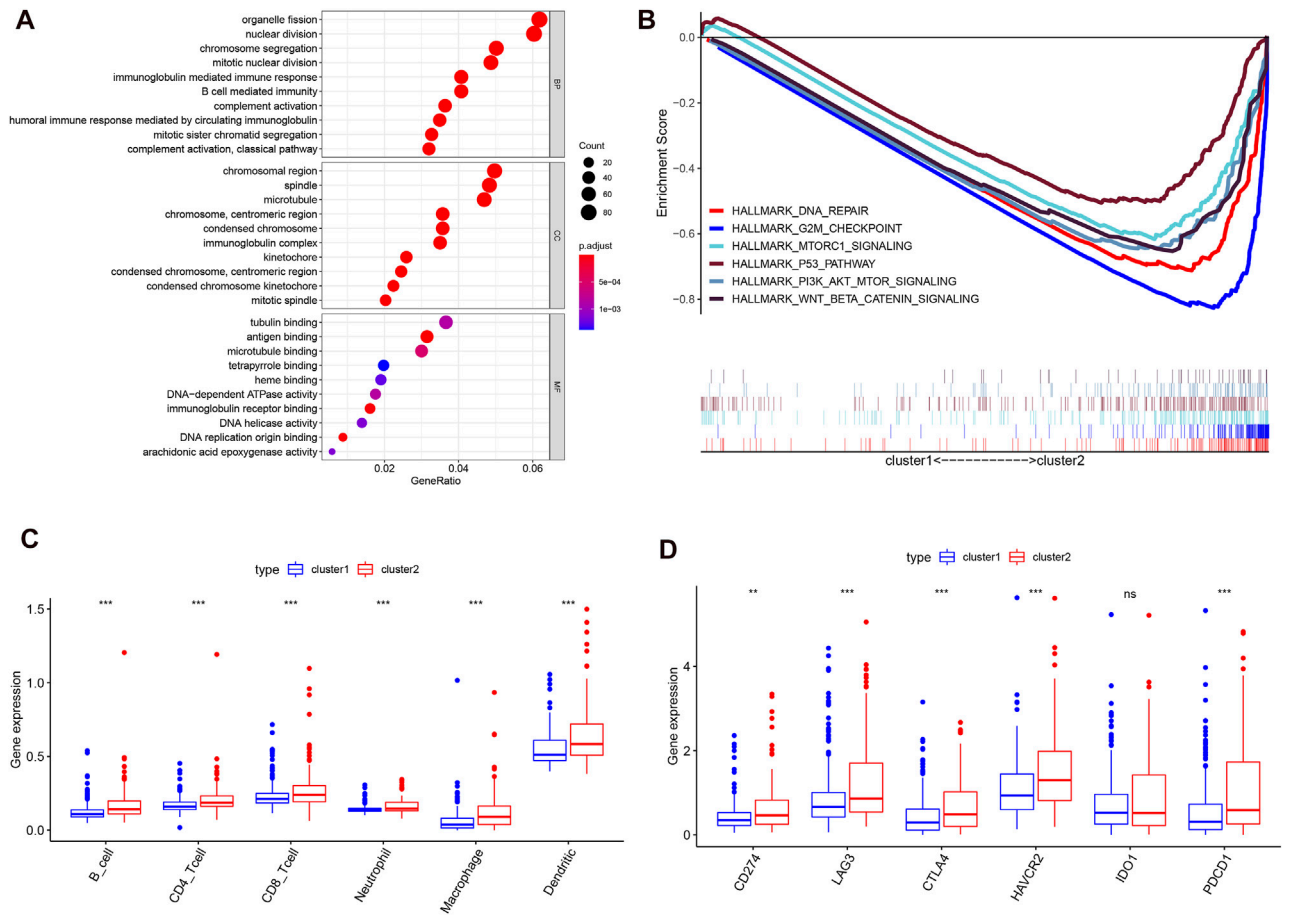

FIGURE 3 | Different cancer pathways and immune cell infiltration level in two subtypes in the TCGA-LIHC. **(A)**, top enriched pathways in distinct two clusters. **(B)**, several differential enriched pathways in GSEA. **(C)**, the infiltrating level of six immune cell types in two clusters. **(D)**, the expression level of immune checkpoints in two clusters.

each patient in the TCGA, GEO, and ICGC datasets was calculated by employing the following equation: risk score = (0.1503* expression level of METTL3) + (0.0877* expression level of YTHDF2) + (0.0274* expression level of YTHDF1) − (0.1197* expression level of ZC3H13). Subsequently, 185 cases were classified into the high-risk group and 185 cases were classified into the low-risk group according to the median risk score in the TCGA dataset. We studied the associations between the risk score and clinicopathological characteristics. The heatmap results showed that the four m6A regulators had distinct expression levels in the two risk subgroups in the TCGA cohort (**Figure 4B**). METTL3, YTHDF2, and YTHDF1 were mainly overexpressed in the high-risk subgroup, whereas ZC3H13 was upregulated in the low-risk subgroup. The differences in status ($p < 0.05$), grade ($p < 0.01$), stage ($p < 0.01$), and T stage ($p < 0.05$) between the two risk subgroups were significant. In addition, we studied the associations between risk score and clustering subtypes and stromal score. Not surprisingly, we found that patients in cluster 2 showed an evidently higher risk score than patients in cluster 1 ($p < 0.0001$, **Figure 4C**). Compared to the group of patients with a high-risk score, the group of patients with a high-risk score had a higher stromal score ($p < 0.05$, **Figure 4D**). The immune score between two groups was no statistical significance (**Supplementary Figure S2C**). To further test the robustness of the risk model, we plotted a Kaplan-Meier curve. Patients in the high-risk group had a reduced survival time compared with those in the low-risk group ($p < 0.001$). In addition, the time-dependent ROC analysis were performed to assess the predictive accuracy of the risk model, and the area under the curve (AUC) was as high as 0.766 at 1 year, 0.728 at 3 years, and 0.616 at 5 years (**Figure 4E**). These findings indicate that the risk score was dramatically related to clustering subtypes, degree of liver cancer malignancy, stromal score, and survival time for patients with HCC.

The Independent Prognostic Role of the Risk Model Based on the Gene Expression Omnibus and International Cancer Genome Consortium Cohorts

To validate that the m6A-associated genes had a similar impact on other HCC cases, we selected the GSE14520 dataset and ICGC dataset to serve as the external validation cohorts. Patient data

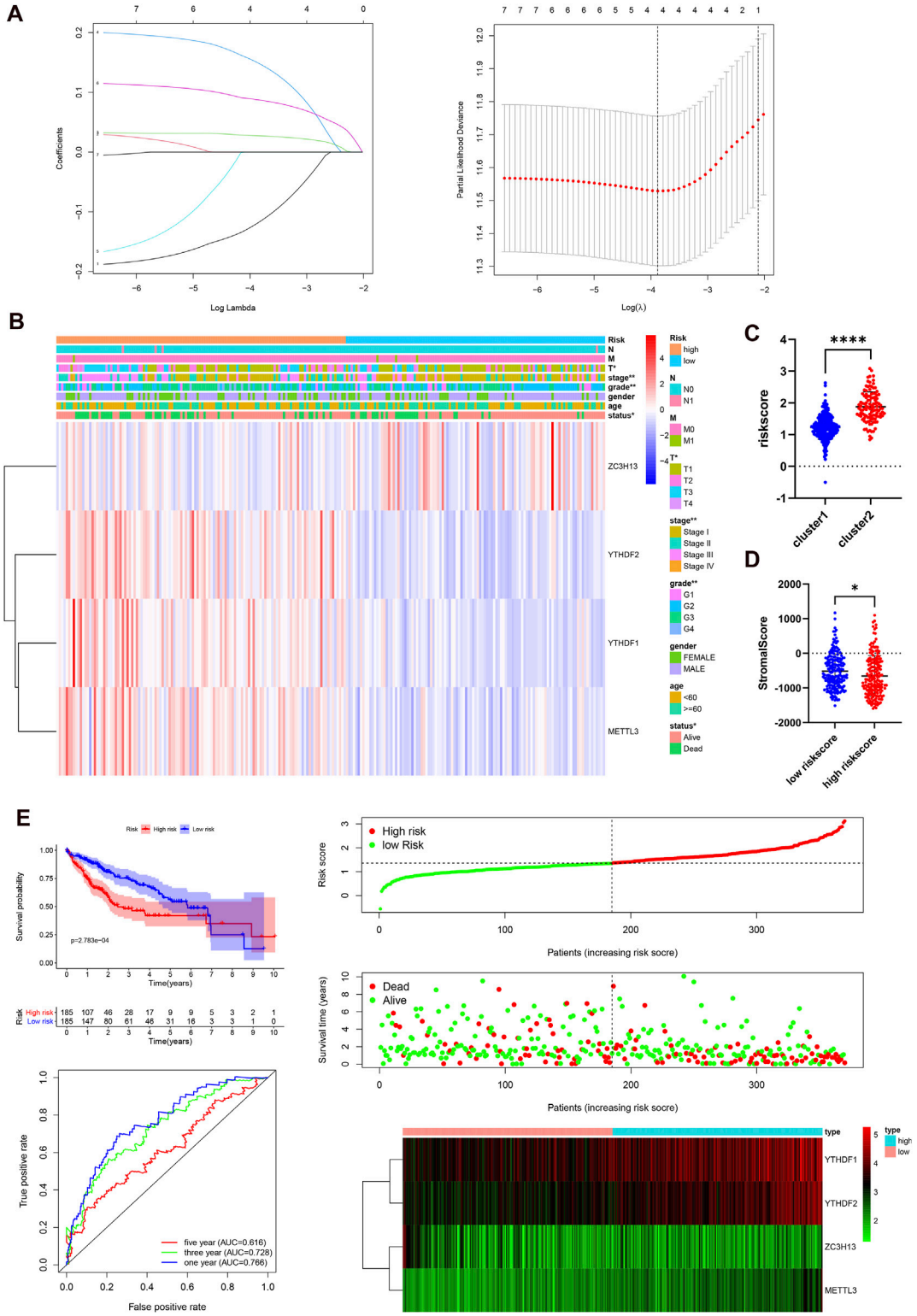

FIGURE 4 | Prognostic risk signatures correlated with clinicopathological characteristics in the TCGA-LIHC. **(A)**, construction of the risk signature model. **(B)**, heatmap and clinicopathological characteristics of two risk subgroups. **(C)**, distribution of risk scores stratified by cluster. **(D)**, the relationship between risk score and stromal score. **(E)**, survival curve, ROC curve, and risk score analysis in the TCGA-LIHC cohort.

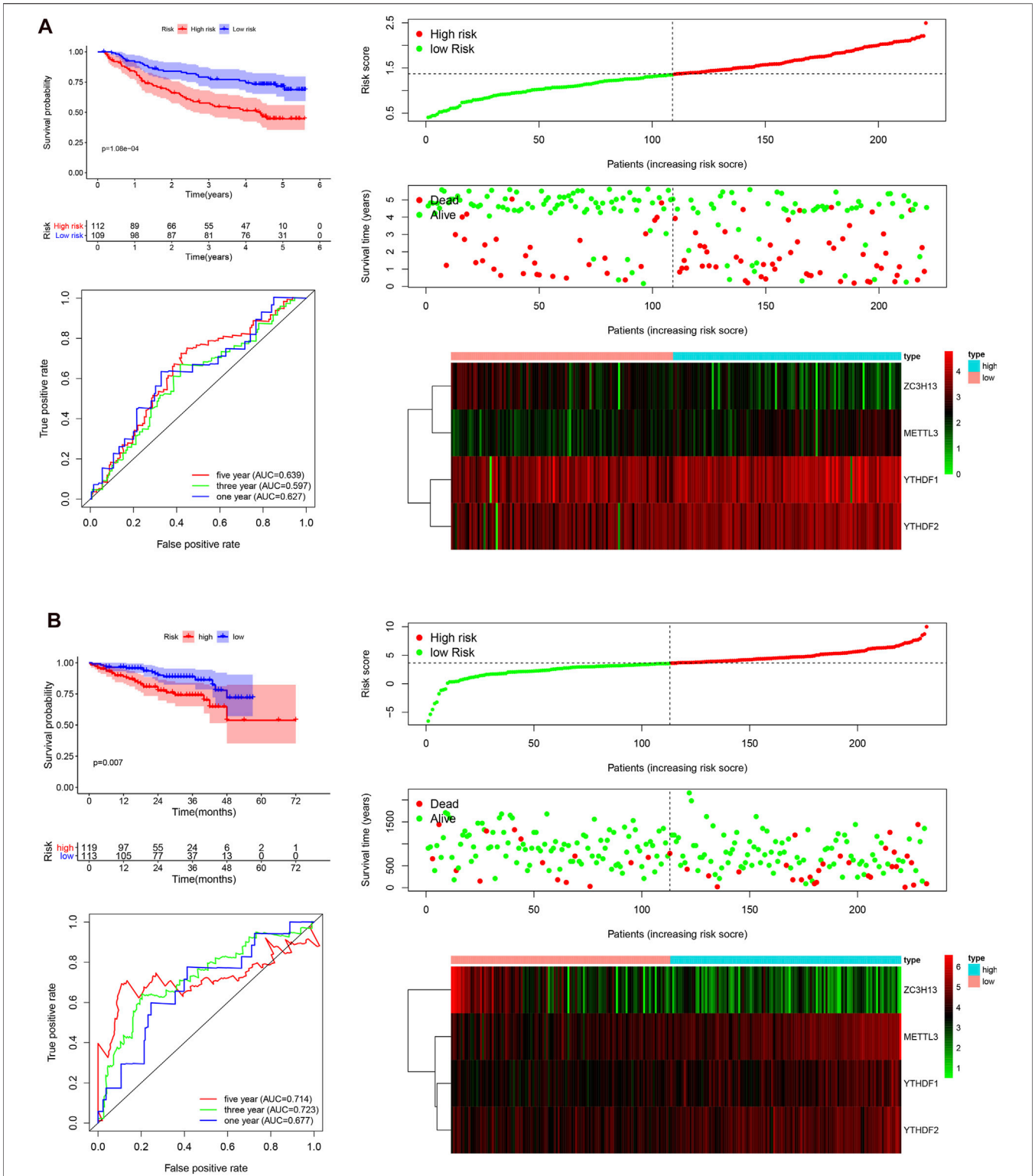

FIGURE 5 | Survival curve analysis, time-dependent ROC curve analysis, and risk score analysis in the GEO and ICGC datasets. **(A)**, survival curve, ROC curve, and risk score analysis in the GSE14520 cohort. **(B)**, survival curve, ROC curve, and risk score analysis in the ICGC cohort.

were then categorized into two groups according to the median risk score of the TCGA cohort. The overall survival status, ROC curves, and expression details related four selected m6A-related genes and the corresponding risk scores in the GEO and ICGC cohorts are exhibited in **Figure 5**. The heatmaps show that METTL3, YTHDF2, and YTHDF1 are mainly overexpressed

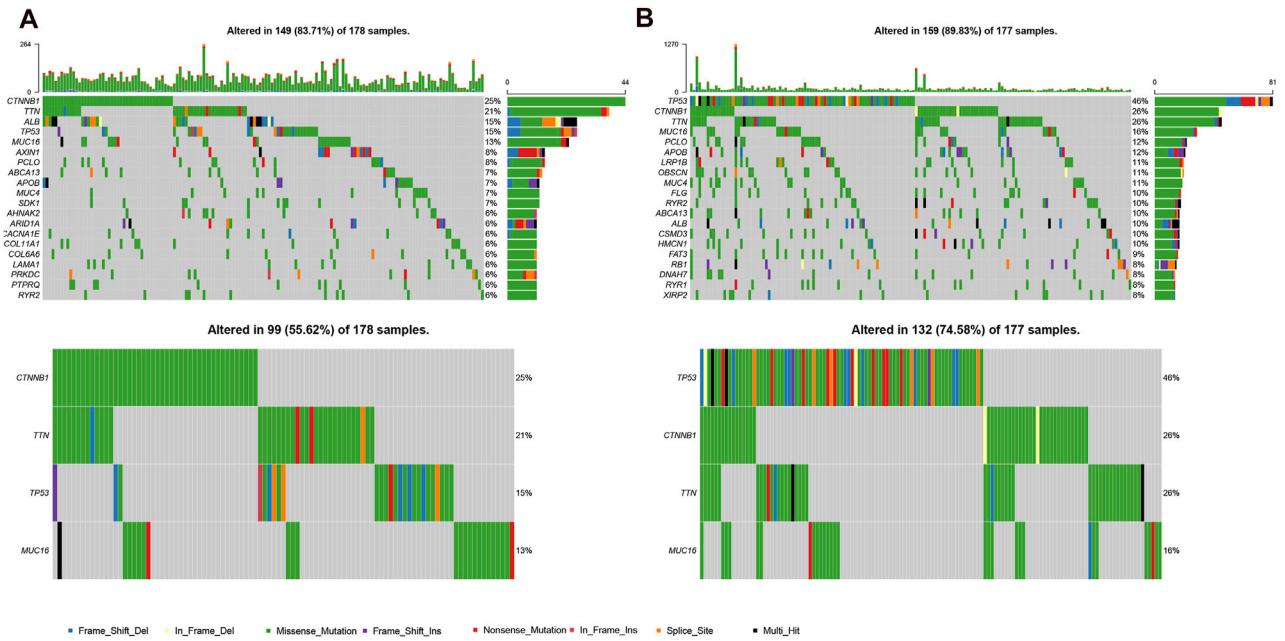

FIGURE 6 | Mutational landscape of two risk subgroups in the TCGA-LIHC. **(A,B)**, genes with high frequency mutation in the HCC samples of low-risk subgroup **(A)** and high-risk subgroup **(B)**.

in the high-risk subgroup, whereas ZC3H13 is upregulated in the low-risk subgroup, serving as a protective m6A regulator. The 1, 3, and 5 years ROC curves in this model showed that the AUC values were moderate. The patients in the low-risk group exhibited a longer survival time than those in the high-risk group ($p < 0.001$; **Figure 5A**). Similarly, in the ICGC cohort, the patients in the high-risk subgroup showed a shorter survival time ($p = 0.007$; **Figure 5B**), and the 1, 3, and 5 years AUC values were also moderate. Hence, the AUC values demonstrated that the four risk signatures were effective for distinguishing HCC patient outcomes. Taken together, our findings demonstrate that the risk score that was obtained based on the four m6A-associated genes might have a high accuracy and precision for predicting the clinical outcome of HCC patients. Next, univariate and multivariate Cox regression analyses were carried out with the TCGA, GEO, and ICGC datasets (**Supplementary Figure S3**). All analyses demonstrated that the risk score was closely linked with the survival time of the patients with information in the TCGA, GEO, and ICGC datasets. The findings confirmed that the risk score based on the four m6A regulators serve as independent prognostic factors in HCC patients.

The Mutational Landscape and Therapeutic Sensitivity of Different Subgroups

Because gene mutation status has been shown to impact the survival time of patients with HCC, we assessed the distribution of somatic variants in HCC driver genes between the two subgroups (**Supplementary Figure S4A**). The analysis demonstrated that missense variations were the most frequent mutation type in HCC. As shown in **Figure 6**, we then identified the top 20 genes with the highest mutation rates in the two risk subgroups. The mutation rates of TP53, CTNNB1, MUC16, ALB, and TTN were higher than 10% in both groups. Mutation of the TP53 gene was more common in the high-risk subgroup, while mutation of the CTNNB1 gene was the most common in the low-risk subgroup. These results might provide innovative insights for elucidating the distinct mechanisms of tumor progression. Genetic mutations can affect the tumor response to chemotherapy and targeted therapy; therefore, we investigated the association between the risk model and the efficacy of chemotherapy and targeted therapy drugs in patients with HCC. As shown in **Figure 7**, we listed 25 common drugs used for HCC, such as sorafenib, mitomycin, and doxorubicin. Significant differences in the estimated IC50 between the two risk groups were observed, which suggest that the risk model might be used to identify potential biomarkers for chemotherapy and targeted therapy sensitivity. Then, we tested the ability of the signature to predict the efficacy of sorafenib treatment in TCGA cohort (**Supplementary Figures S4B,4C**). We found that a weak tendency for progressive disease (PD) patients and high-risk patients to have a poorer OS was observed. Surprisingly, we found that low-risk patients showed a higher response rate to sorafenib compared with high-risk patients.

The Correlation Between the Risk Score and Immune Characteristics in Hepatocellular Carcinoma

Because of the relationship between m6A regulators and immune-related biological pathways, the impact of the risk

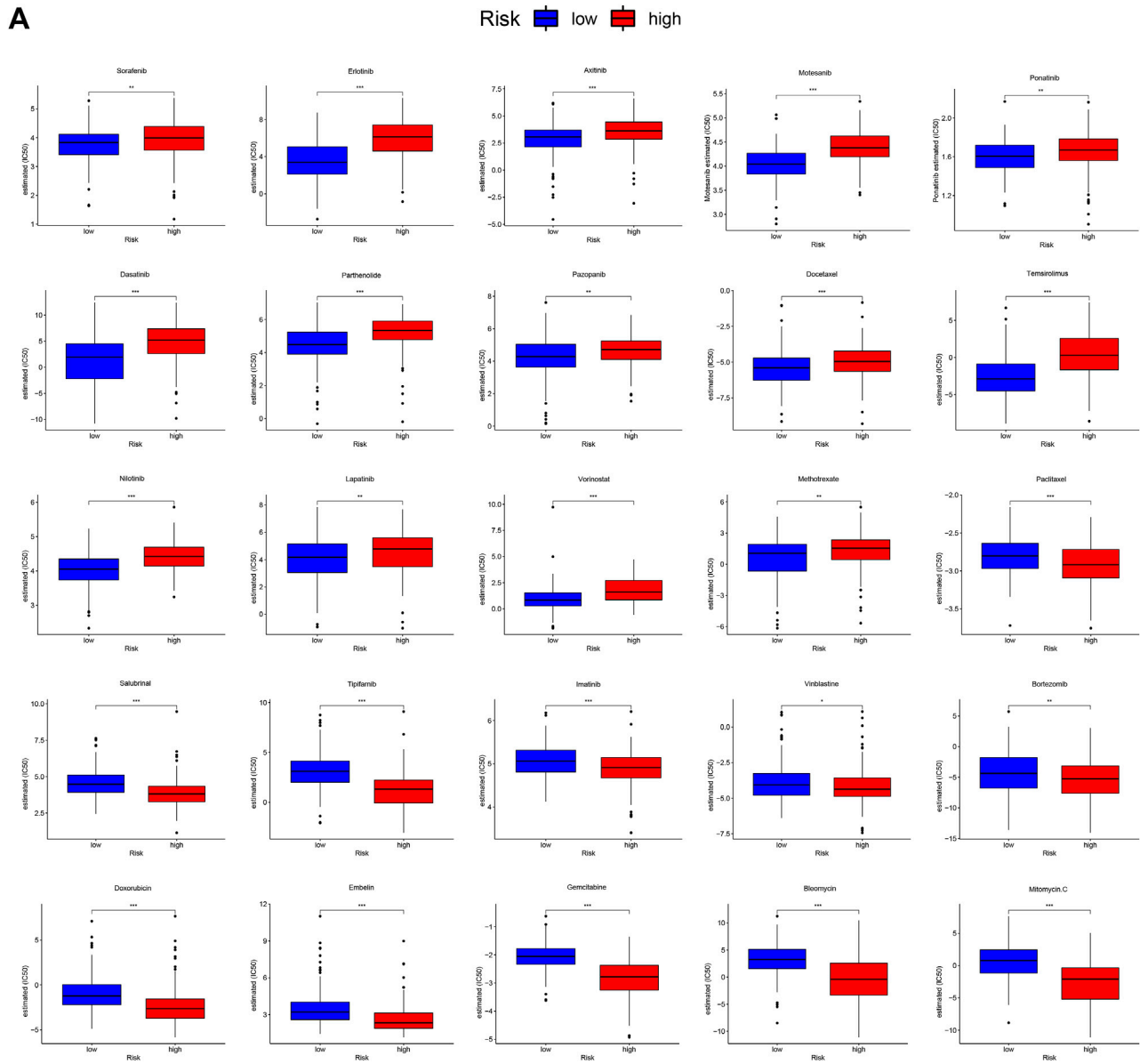

FIGURE 7 | Differential chemotherapy and targeted therapy responses in two risk groups. **(A)**, the high-risk score was related to a higher IC50 for chemotherapy and targeted therapy such as sorafenib, whereas it was related to a lower IC50 for drugs such as mitomycin and doxorubicin.

model on the TIME in HCC was investigated. The risk score had a positive correlation with the infiltration levels of 6 immune cell types ($p < 0.001$, **Figure 8A**). This finding suggested that the risk score is intimately involved in the TIME for patients with HCC. Then, the expression levels of immune checkpoints such as PD-L1, IDO1, PD1, LAG3, CTLA4, and TIM3 between the two risk groups were examined. It is obvious that the high-risk subgroup overexpressed PD-L1, LAG3, IDO1, PD1, CTLA4, and TIM3 (**Figure 8B**). Next, we studied the relationships between the risk score and total mutation burden (TMB), and neoantigens. We found that the TMB and neoantigen counts in the high-risk subgroup were very high (**Figures 8C,D**). Our findings revealed that the risk score is related to vital regulatory functions in the immune microenvironment in HCC and may indicate the extent of a tumor response to immunotherapy, especially ICI treatment.

Genetic Alterations and Expression Levels of Four Predictive m6A-Related Regulators in Hepatocellular Carcinoma

Finally, we analyzed the genetic alterations, expression levels, overall survival, and infiltration levels of immune cells of the four identified genes. We found that ZC3H13 had the most frequent genetic alterations (2.2%) among these four genes in HCC. Furthermore, deep deletion and amplification mutation were the most common alterations among these four genes

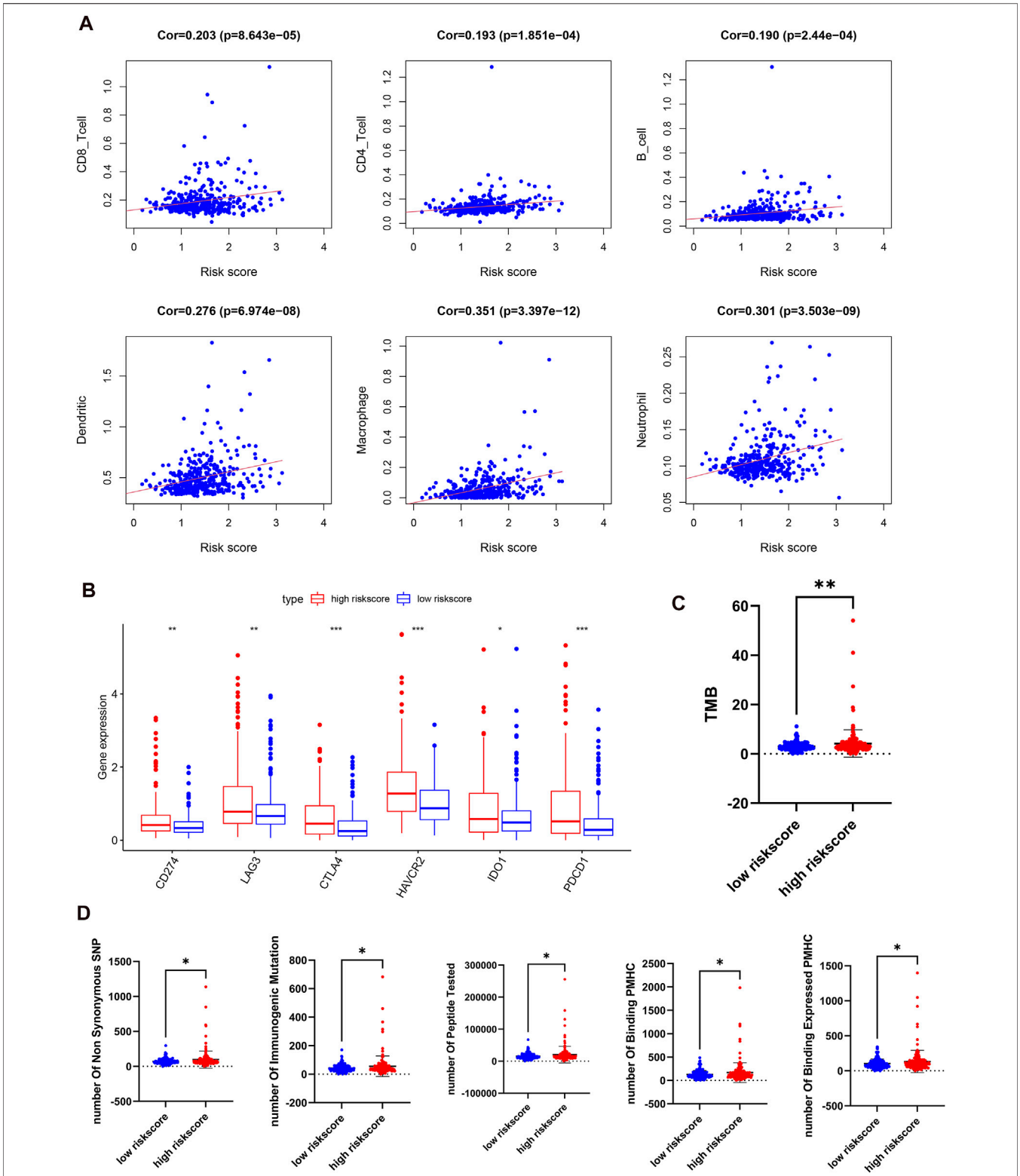

FIGURE 8 | Distant immune features in two risk subgroups in the TCGA-LIHC. **(A)**, the correlation between the risk score and the immune cell infiltration. **(B)**, the expression levels of immune checkpoints in two risk subgroups. **(C,D)**, tumor mutation burden **(C)** and neoantigen **(D)** were compared with the two risk subgroups.

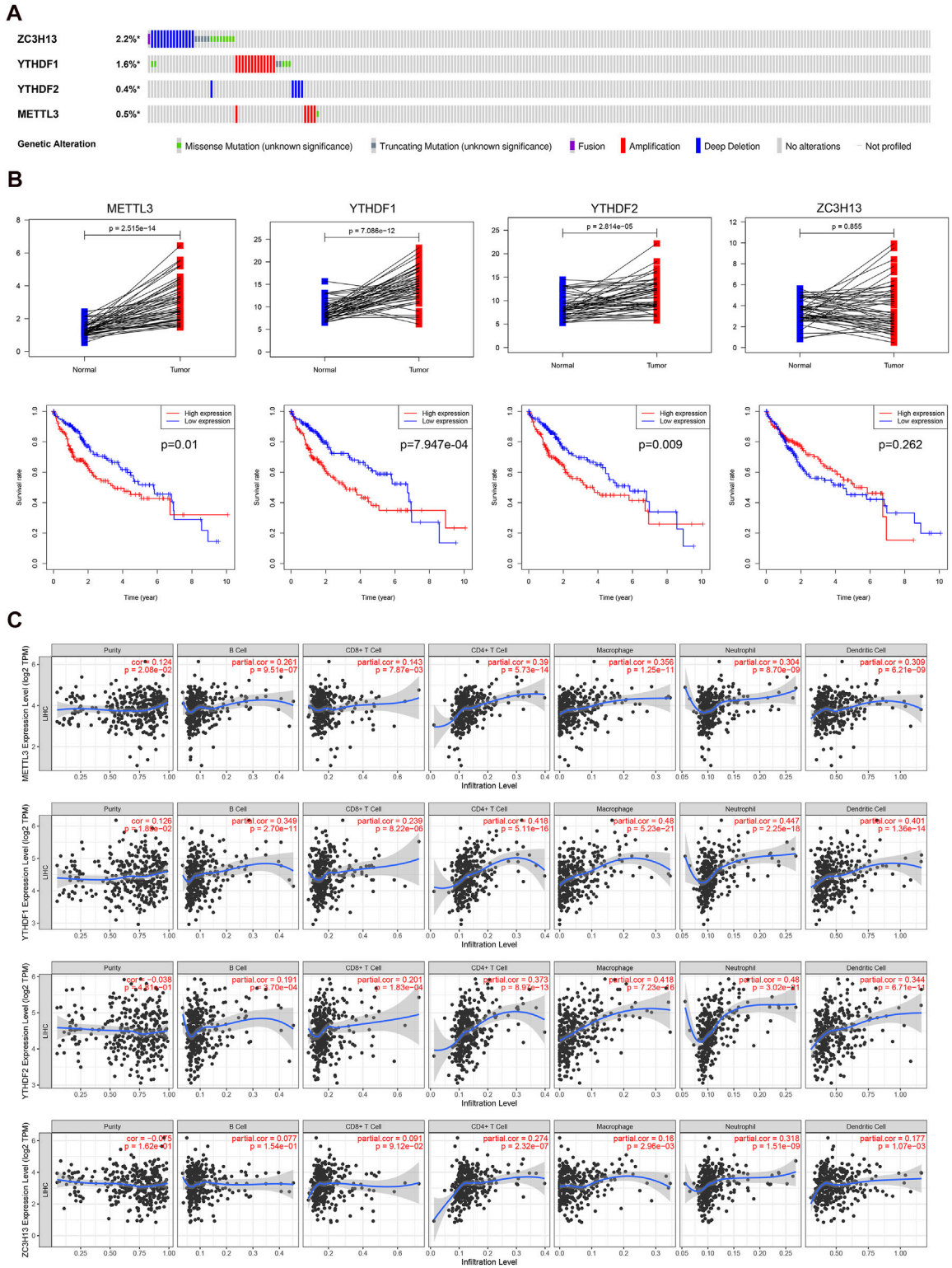

FIGURE 9 | Genetic alterations, expression levels and prognosis, and correlation with immune cells of the four predictive genes. **(A)**, genetic alterations of the four m6A-associated regulators in the TCGA cohort. **(B)**, the expression levels and survival outcomes of the four genes in the TCGA cohort. **(C)**, effects of the expression levels of four m6A-associated regulators on the immune cell infiltration.

(**Figure 9A**). Then, we compared the expression levels and prognosis of the METTL3, YTHDF1, YTHDF2, and ZC3H13 genes (**Figure 9B**). In accordance with our results, METTL3, YTHDF2, and YTHDF1 were found to be considerably overexpressed between tumor and normal adjacent tissues. Moreover, patients with high expression of these three genes exhibited shorter survival times. The effects of the four m6A-related genes on immune cell infiltration were further explored. We discovered that the expression levels of the identified m6A-associated regulators had a great effect on the infiltration levels of the six immune cells in HCC (**Figure 9C**). Our findings suggested that the identified m6A-associated regulators crucially affected the survival time and tumor immune microenvironment of patients with HCC.

DISCUSSION

As one of the most primary and common forms of mRNA modification, N6-methyladenosine has a tremendous effect on posttranscriptional regulation (He, 2010). Numerous studies have confirmed that the dysregulation of m6A methylation regulatory proteins is associated with the development and progression of many tumors (Pan et al., 2018). However, the functions of specific m6A regulators that serve as oncogenes or tumor suppressor genes in different tumor types are overwhelmingly complicated. For instance, several studies found that ALKBH5, a demethylase, plays distinct roles in different tumor types (Kwok et al., 2017; Zhang et al., 2017). Since most studies have made efforts to elucidate how m6A regulators modulate intrinsic tumor carcinogenic signaling pathways, further research focusing on the potential regulatory mechanisms of m6A-associated regulators in the TIME and immune response of HCC is urgently needed.

Specifically, our results found that the expression levels of m6A-associated genes, except ZC3H13 and METTL14, were strikingly overexpressed in HCC cases compared with normal cases. Our study also showed unexpected associations between m6A regulators and immune checkpoints. Next, we identified two different HCC subtypes by consensus clustering. The two cluster subtypes had different prognostic outcomes and clinicopathological features. In addition, the two clusters were also related to the different expression of immune checkpoints and immune cell infiltration levels, which means that there was a significant difference in the TIME between the two clusters. The differences in the tumor immune microenvironment between the two clusters may have contributed to the difference in survival times, with the TIME in cluster 2 characterized by immunosuppressive cells and factors. The immune checkpoint expression levels were highly significant in cluster 2 with respect to cluster 1. That result indicates that immunotherapy such as ICI treatment may function in patients with data in cluster 2. Further analysis demonstrated that the proportions of B cells, CD4+ T cells, CD8+ T cells, neutrophils, macrophages, and dendritic cells in cluster 2 were greatly increased compared with those in cluster 1. The GO analysis suggested that immune-related pathways were mainly enriched in the cluster 2 samples. In addition, we conducted GSEA and found that the functional regulatory pathways of malignant tumors, such as the P53 pathway, Wnt/β-Catenin pathway, and PI3K/AKT/mTOR pathway, were evidently enriched in the cluster 2 samples. A previous study found that depleting m6A methyltransferase had an evident impact on gene expression, leading to the regulation of the p53 signaling pathway (Dominissini et al., 2012). In addition, the expression of p53 is regulated posttranscriptionally by m6A RNA methylation (Ghazi et al., 2020). There is also experimental evidence indicating that mutated YTHDF1 results in the m6A-mediated activation of Wnt/β-Catenin signaling and gastric carcinogenesis (Pi et al., 2020). Additionally, METTL3 exerts an angiogenic role by regulating Wnt signaling (Yao et al., 2020). m6A regulators regulate the AKT signaling activity to promote the development and progression of endometrial cancer (Liu et al., 2018). Similarly, the METTL3 expression level is associated PI3K/AKT/mTOR pathway molecule expression levels and is related to unfavorable outcomes in renal cell carcinoma (Li et al., 2017c). These results suggest that the PI3K/AKT/mTOR pathway, Wnt/β-Catenin pathway, and P53 pathway may act as potential targets for m6A-modified RNA. Therefore, the m6A modification and the P53 pathway, Wnt/β-Catenin pathway, and PI3K/AKT/mTOR pathway may be collectively associated with the modulation of the tumor microenvironment and immune response in different HCC clusters. Next, the prognostic value of the m6A-associated genes in HCC patients was assessed based on four regulators (ZC3H13, METTL3, YTHDF1, and YTHDF2). Among these four m6A-associated genes, METTL3 promotes the development and progression of HCC (Chen et al., 2018), whereas it exerts a tumor-suppressive function in breast cancer (Wang et al., 2017). ZC3H13 works as a cancer inhibitory factor in colorectal cancer (Zhu et al., 2019), but another study indicated that ZC3H13 functions as an oncogene in several types of cancers (Panahi et al., 2016). A study also demonstrated the oncogenic role of YTHDF1 in HCC (Liu et al., 2020a). YTHDF2 can promote liver cancer metastasis (Zhang et al., 2020). Importantly, the model revealed valid prognostic biomarkers for HCC. The risk score derived from four identified m6A-related genes effectively enabled the categorization of the patients with HCC into two subgroups. As expected, cluster 2 had an evidently higher risk score than cluster 1. In addition, compared with the low-risk patients, the high-risk patients in the TCGA dataset had worse overall survival. We also obtained consistent results in the GSE14520 and ICGC external datasets. Univariate and multivariate Cox regression analyses suggested that the prognostic risk model was independent of other clinical factors in HCC. In summary, this m6A regulator-associated risk model can precisely evaluate HCC patient outcomes.

The tumor immune microenvironment, which is regulated by various immune factors, has a critical effect on tumor development and progression. In addition, its dysregulation can result in multiple outcomes, such as different prognosis results and therapeutic responses to immunotherapy (Fridman et al., 2012; Hui and Chen, 2015). As an immunosuppressive disease, HCC consists of a variety of immunocompetent cells and immunosuppressive cells, including DCs, CD4+ T cells, CD8+ T cells, Tregs, and macrophages. However, the effects of m6A-related genes on the TIME in HCC still need to be understood. This study demonstrated that the risk score calculated by the four risk signatures of m6A regulators was evidently connected with the expression levels of immune checkpoints and immune cell infiltration. The risk score was

significantly positively correlated with the abundance of B cells, CD4+ T cells, CD8+ T cells, neutrophils, macrophages, and dendritic cells. There have been a variety of studies focusing on the relationship of m6A regulators and the immune system. For example, a study revealed that METTL3 is closely related to homeostasis and differentiation disorders of T cells (Li et al., 2017a). Similarly, it has been found that both METTL3 and METTL14 may regulate immune responses to immunotherapy (Wang et al., 2020). Another study revealed that YTHDF1 has a negative correlation with the proportion of CD8+ T cells (Han et al., 2019). In addition, FTO plays a crucial role in promoting melanoma anti-PD-1 resistance (Yang et al., 2019). Therefore, these findings indicated that m6A-related genes are more or less associated with the dysregulation of the TIME.

To gain further biological insight into different aspects of the two subgroups, we studied gene mutations, therapeutic sensitivity, TMB, and neoantigens of different subgroups. The largest difference in mutations between these two groups was TP53 mutation, which was more common in the high-risk samples than in the low-risk samples (46% vs. 15%). TP53 mutation is not only the most common single genetic variation in cancer but is also associated with additional unfavorable outcomes in various cancers, particularly HCC (Kandoth et al., 2013; Muller and Vousden, 2014). In contrast, the CTNNB1 mutation was the most frequent mutation in the low-risk subgroup, which may indicate that low-risk HCCs promote proliferation through the Wnt/β-Catenin signaling pathway (Delgado et al., 2015). Therefore, high-risk patients with more TP53 mutations have a worse outcome than low-risk patients with fewer TP53 mutations. Currently, because chemotherapy and targeted therapy are common methods used to treat HCC, we found that there was a significantly different sensitivity between the two risk groups, allowing us to promote a deep understanding of personalized treatments. For example, low-risk HCC patients were more sensitive to sorafenib than high-risk HCC patients. Next, we examined the relationship between this risk score and known predictive biomarkers for immunotherapy, such as TMB and neoantigens. Here, our results revealed that the risk score had an evidently positive correlation with TMB and neoantigens, which indicated that high-risk patients may have an improved response to ICI treatment. Recently, TMB has been assessed as a promising and potential biomarker for predicting the response to ICI therapy in many clinical trials and across different tumor types, including HCC (Samstein et al., 2019). In addition, patients with higher neoantigen loads tend to show a better response to ICI therapy (Liu et al., 2020b). These results indicate that patients with HCC and high-risk scores might profit the most from immunotherapy. In conclusion, because there are significant differences in the tumor immune microenvironment and molecular characteristics, HCC patients with different risk scores may have different survival statuses and experience distinct outcomes from immunotherapy, chemotherapy, and targeted therapy.

It is undeniable that our study has some limitations. First, the proposed risk model, which was derived from four m6A regulators, was only substantiated in the TCGA, GSE14520 and ICGC cohorts. Therefore, further external validation in other external cohorts with sufficiently available information is warranted to test the accuracy and precision of this risk score model. In addition, due to the lack of specific HCC cohorts with ICI treatment, we did not evaluate the correlation between the risk model and the response to immunotherapy. Last, the interactions and regulatory mechanisms of m6A RNA methylation regulators in the tumor immune microenvironment need to be further studied to remodel the tumor immune microenvironment and enhance the efficacy of immunotherapy in HCC. Overall, in our study, we performed a systematic evaluation of the underlying regulatory mechanisms of m6A-related genes and the effects of these genes on prognosis, the expression of immune checkpoints, the infiltration of several major immune cells, the levels of TMB and neoantigens, the gene mutation rate, and therapeutic sensitivity in HCC. The risk model, which has the ability to distinguish immune and molecular characteristics, might become a helpful prognostic indicator of immunotherapy, but further studies are needed to confirm its effectiveness.

DATA AVAILABILITY STATEMENT

The raw data supporting the conclusion of this article will be made available by the authors, without undue reservation.

AUTHOR CONTRIBUTIONS

YD conducted the data analysis and wrote the manuscript. YM and QZ prepared the figures. TL revised the manuscript and provided financial support. YJ helped data discussion. XW and PY conceived and designed the study, and provided financial support for the study. All the authors reviewed and approved the final manuscript.

FUNDING

This work was supported by the National Natural Science Foundation Fund (81772490), National Key R&D Program of China (2020YFC2002705), the Chinese Academy of Medical Sciences (CAMS) Innovation Fund for Medical Sciences (CIFMS) (2019-I2M-1-003), the Science and Technology Planning Project of Guangzhou City (No.201804010493TL), and the Natural Science Foundation of Guangdong Province (No. 2019A1515011934 and 2021A1515011233 TL).

ACKNOWLEDGMENTS

All authors would like to thank the TCGA, GSE14520, and ICGC datasets, which provided data for this study. We also thank the funding sources mentioned above. We sincerely thank Qiongzhu Dong, Lunxiu Qin, and Xiaotian Shen for their assistance in downloading data.

SUPPLEMENTARY MATERIAL

The Supplementary Material for this article can be found online at: https://www.frontiersin.org/articles/10.3389/fphar.2021.707930/full#supplementary-material

REFERENCES

Alarcón, C. R., Lee, H., Goodarzi, H., Halberg, N., and Tavazoie, S. F. (2015). N6-methyladenosine marks Primary microRNAs for Processing. *Nature* 519 (7544), 482–485. doi:10.1038/nature14281

Bellmunt, J., de Wit, R., Vaughn, D. J., Fradet, Y., Lee, J.-L., Fong, L., et al. (2017). Pembrolizumab as Second-Line Therapy for Advanced Urothelial Carcinoma. *N. Engl. J. Med.* 376 (11), 1015–1026. doi:10.1056/nejmoa1613683

Bray, F., Ferlay, J., Soerjomataram, I., Siegel, R. L., Torre, L. A., and Jemal, A. (2018). Global Cancer Statistics 2018: GLOBOCAN Estimates of Incidence and Mortality Worldwide for 36 Cancers in 185 Countries. *CA: A Cancer J. Clinicians* 68 (6), 394–424. doi:10.3322/caac.21492

Chen, M., Wei, L., Law, C.-T., Tsang, F. H.-C., Shen, J., Cheng, C. L.-H., et al. (2018). RNA N6-Methyladenosine Methyltransferase-like 3 Promotes Liver Cancer Progression through YTHDF2-dependent Posttranscriptional Silencing of SOCS2. *Hepatology* 67 (6), 2254–2270. doi:10.1002/hep.29683

Delgado, E., Okabe, H., Preziosi, M., Russell, J. O., Alvarado, T. F., Oertel, M., et al. (2015). Complete Response of Ctnnb1-Mutated Tumours to β-catenin Suppression by Locked Nucleic Acid Antisense in a Mouse Hepatocarcinogenesis Model. *J. Hepatol.* 62 (2), 380–387. doi:10.1016/j.jhep.2014.10.021

Dominissini, D., Moshitch-Moshkovitz, S., Schwartz, S., Salmon-Divon, M., Ungar, L., Osenberg, S., et al. (2012). Topology of the Human and Mouse m6A RNA Methylomes Revealed by m6A-Seq. *Nature* 485 (7397), 201–206. doi:10.1038/nature11112

El-Khoueiry, A. B., Sangro, B., Yau, T., Crocenzi, T. S., Kudo, M., Hsu, C., et al. (2017). Nivolumab in Patients with Advanced Hepatocellular Carcinoma (CheckMate 040): an Open-Label, Non-comparative, Phase 1/2 Dose Escalation and Expansion Trial. *The Lancet* 389 (10088), 2492–2502. doi:10.1016/s0140-6736(17)31046-2

Fang, X., Li, M., Yu, T., Liu, G., and Wang, J. (2020). Reversible N6-Methyladenosine of RNA: The Regulatory Mechanisms on Gene Expression and Implications in Physiology and Pathology. *Genes Dis.* 7 (4), 585–597. doi:10.1016/j.gendis.2020.06.011

Ferris, R. L., Blumenschein, G., Jr., Fayette, J., Guigay, J., Colevas, A. D., Licitra, L., et al. (2016). Nivolumab for Recurrent Squamous-Cell Carcinoma of the Head and Neck. *N. Engl. J. Med.* 375 (19), 1856–1867. doi:10.1056/nejmoa1602252

Fridman, W. H., Pagès, F., Sautès-Fridman, C., and Galon, J. (2012). The Immune Contexture in Human Tumours: Impact on Clinical Outcome. *Nat. Rev. Cancer* 12 (4), 298–306. doi:10.1038/nrc3245

Garassino, M. C., Gadgeel, S., Esteban, E., Felip, E., Speranza, G., Domine, M., et al. (2020). Patient-reported Outcomes Following Pembrolizumab or Placebo Plus Pemetrexed and Platinum in Patients with Previously Untreated, Metastatic, Non-squamous Non-small-cell Lung Cancer (KEYNOTE-189): a Multicentre, Double-Blind, Randomised, Placebo-Controlled, Phase 3 Trial. *Lancet Oncol.* 21 (3), 387–397. doi:10.1016/s1470-2045(19)30801-0

Geula, S., Moshitch-Moshkovitz, S., Dominissini, D., Mansour, A. A., Kol, N., Salmon-Divon, M., et al. (2015). m6A mRNA Methylation Facilitates Resolution of Naïve Pluripotency toward Differentiation. *Science* 347 (6225), 1002–1006. doi:10.1126/science.1261417

Ghazi, T., Nagiah, S., and Chuturgoon, A. A. (2020). Fusaric Acid Decreases P53 Expression by Altering Promoter Methylation and m6A RNA Methylation in Human Hepatocellular Carcinoma (HepG2) Cells. *Epigenetics*, 1–13.

Han, D., Liu, J., Chen, C., Dong, L., Liu, Y., Chang, R., et al. (2019). Anti-tumour Immunity Controlled through mRNA m6A Methylation and YTHDF1 in Dendritic Cells. *Nature* 566 (7743), 270–274. doi:10.1038/s41586-019-0916-x

He, C. (2010). Grand challenge Commentary: RNA Epigenetics? *Nat. Chem. Biol.* 6 (12), 863–865. doi:10.1038/nchembio.482

He, R.-Z., Jiang, J., and Luo, D.-X. (2020). The Functions of N6-Methyladenosine Modification in lncRNAs. *Genes Dis.* 7 (4), 598–605. doi:10.1016/j.gendis.2020.03.005

Hui, L., and Chen, Y. (2015). Tumor Microenvironment: Sanctuary of the Devil. *Cancer Lett.* 368 (1), 7–13. doi:10.1016/j.canlet.2015.07.039

Huo, F. C., Zhu, Z. M., and Pei, D. S. (2020). N(6) -methyladenosine (M(6) A) RNA Modification in Human Cancer. *Cel Prolif.* 53 (11), e12921. doi:10.1111/cpr.12921

Jiang, Y., Zhang, Q., Hu, Y., Li, T., Yu, J., Zhao, L., et al. (2018). ImmunoScore Signature. *Ann. Surg.* 267 (3), 504–513. doi:10.1097/sla.0000000000002116

Kandoth, C., McLellan, M. D., Vandin, F., Ye, K., Niu, B., Lu, C., et al. (2013). Mutational Landscape and Significance across 12 Major Cancer Types. *Nature* 502 (7471), 333–339. doi:10.1038/nature12634

Kwok, C. T., Marshall, A. D., Rasko, J. E., and Wong, J. J. (2017). Genetic Alterations of M(6)A Regulators Predict Poorer Survival in Acute Myeloid Leukemia. *J. Hematol. Oncol.* 10 (1), 39. doi:10.1186/s13045-017-0410-6

Larkin, J., Chiarion-Sileni, V., Gonzalez, R., Grob, J. J., Cowey, C. L., Lao, C. D., et al. (2015). Combined Nivolumab and Ipilimumab or Monotherapy in Untreated Melanoma. *N. Engl. J. Med.* 373 (1), 23–34. doi:10.1056/nejmoa1504030

Li, H.-B., Tong, J., Zhu, S., Batista, P. J., Duffy, E. E., Zhao, J., et al. (2017). m6A mRNA Methylation Controls T Cell Homeostasis by Targeting the IL-7/STAT5/SOCS pathwaysA mRNA Methylation Controls T Cell Homeostasis by Targeting the IL-7/STAT5/SOCS Pathways. *Nature* 548 (7667), 338–342. doi:10.1038/nature23450

Li, T., Fan, J., Wang, B., Traugh, N., Chen, Q., Liu, J. S., et al. (2017). TIMER: A Web Server for Comprehensive Analysis of Tumor-Infiltrating Immune Cells. *Cancer Res.* 77 (21), e108–e110. doi:10.1158/0008-5472.can-17-0307

Li, X., Tang, J., Huang, W., Wang, F., Li, P., Qin, C., et al. (2017). The M6A Methyltransferase METTL3: Acting as a Tumor Suppressor in Renal Cell Carcinoma. *Oncotarget* 8 (56), 96103–96116. doi:10.18632/oncotarget.21726

Lin, X., Chai, G., Wu, Y., Li, J., Chen, F., Liu, J., et al. (2019). RNA M(6)A Methylation Regulates the Epithelial Mesenchymal Transition of Cancer Cells and Translation of Snail. *Nat. Commun.* 10 (1), 2065. doi:10.1038/s41467-019-09865-9

Liu, J., Eckert, M. A., Harada, B. T., Liu, S.-M., Lu, Z., Yu, K., et al. (2018). m6A mRNA Methylation Regulates AKT Activity to Promote the Proliferation and Tumorigenicity of Endometrial cancerA mRNA Methylation Regulates AKT Activity to Promote the Proliferation and Tumorigenicity of Endometrial Cancer. *Nat. Cel Biol* 20 (9), 1074–1083. doi:10.1038/s41556-018-0174-4

Liu, T., Tan, J., Wu, M., Fan, W., Wei, J., Zhu, B., et al. (2020). High-affinity Neoantigens Correlate with Better Prognosis and Trigger Potent Antihepatocellular Carcinoma (HCC) Activity by Activating CD39(+) CD8(+) T Cells. *Gut*.

Liu, X., Qin, J., Gao, T., Li, C., He, B., Pan, B., et al. (2020). YTHDF1 Facilitates the Progression of Hepatocellular Carcinoma by Promoting FZD5 mRNA Translation in an m6A-dependent Manner. *Mol. Ther. - Nucleic Acids* 22, 750–765. doi:10.1016/j.omtn.2020.09.036

Ma, J., Zheng, B., Goswami, S., Meng, L., Zhang, D., Cao, C., et al. (2019). PD1(Hi) CD8(+) T Cells Correlate with Exhausted Signature and Poor Clinical Outcome in Hepatocellular Carcinoma. *J. Immunother. Cancer* 7 (1), 331. doi:10.1186/s40425-019-0814-7

Mayakonda, A., Lin, D.-C., Assenov, Y., Plass, C., and Koeffler, H. P. (2018). Maftools: Efficient and Comprehensive Analysis of Somatic Variants in Cancer. *Genome Res.* 28 (11), 1747–1756. doi:10.1101/gr.239244.118

Muller, P. A. J., and Vousden, K. H. (2014). Mutant P53 in Cancer: New Functions and Therapeutic Opportunities. *Cancer cell* 25 (3), 304–317. doi:10.1016/j.ccr.2014.01.021

Nishino, M., Ramaiya, N. H., Hatabu, H., and Hodi, F. S. (2017). Monitoring Immune-Checkpoint Blockade: Response Evaluation and Biomarker Development. *Nat. Rev. Clin. Oncol.* 14 (11), 655–668. doi:10.1038/nrclinonc.2017.88

Pan, Y., Ma, P., Liu, Y., Li, W., and Shu, Y. (2018). Multiple Functions of M(6)A RNA Methylation in Cancer. *J. Hematol. Oncol.* 11 (1), 48. doi:10.1186/s13045-018-0590-8

Panahi, Y., Darvishi, B., Ghanei, M., Jowzi, N., Beiraghdar, F., and Varnamkhasti, B. S. (2016). Molecular Mechanisms of Curcumins Suppressing Effects on Tumorigenesis, Angiogenesis and Metastasis, Focusing on NF-Kb Pathway. *Cytokine Growth Factor. Rev.* 28, 21–29. doi:10.1016/j.cytogfr.2015.12.004

Pi, J., Wang, W., Ji, M., Wang, X., Wei, X., Jin, J., et al. (2020). *YTHDF1 Promotes Gastric Carcinogenesis by Controlling Translation of FZD7*. Cancer research.

Rao, X., Lai, L., Li, X., Wang, L., Li, A., and Yang, Q. (2020). N(6) -methyladenosine Modification of Circular RNA Circ-ARL3 Facilitates Hepatitis B Virus-Associated Hepatocellular Carcinoma via Sponging miR-1305. *IUBMB Life*.

Ringelhan, M., Pfister, D., O'Connor, T., Pikarsky, E., and Heikenwalder, M. (2018). The Immunology of Hepatocellular Carcinoma. *Nat. Immunol.* 19 (3), 222–232. doi:10.1038/s41590-018-0044-z

Ruf, B., Heinrich, B., and Greten, T. F. (2020). Immunobiology and Immunotherapy of HCC: Spotlight on Innate and Innate-like Immune Cells. *Cell Mol. Immunol.*

Samstein, R. M., Lee, C.-H., Shoushtari, A. N., Hellmann, M. D., Shen, R., Janjigian, Y. Y., et al. (2019). Tumor Mutational Load Predicts Survival after Immunotherapy across Multiple Cancer Types. *Nat. Genet.* 51 (2), 202–206. doi:10.1038/s41588-018-0312-8

Taketo, K., Konno, M., Asai, A., Koseki, J., Toratani, M., Satoh, T., et al. (2018). The Epitranscriptome m6A Writer METTL3 Promotes Chemo- and Radioresistance in Pancreatic Cancer Cells. *Int. J. Oncol.* 52 (2), 621–629. doi:10.3892/ijo.2017.4219

Thorsson, V., Gibbs, D. L., Brown, S. D., Wolf, D., Bortone, D. S., Ou Yang, T. H., et al. (2018). The Immune Landscape of Cancer. *Immunity* 48 (4), 812–e14. doi:10.1016/j.immuni.2018.03.023

Vassilakopoulou, M., Avgeris, M., Velcheti, V., Kotoula, V., Rampias, T., Chatzopoulos, K., et al. (2016). Evaluation of PD-L1 Expression and Associated Tumor-Infiltrating Lymphocytes in Laryngeal Squamous Cell Carcinoma. *Clin. Cancer Res.* 22 (3), 704–713. doi:10.1158/1078-0432.ccr-15-1543

Wang, L., Hui, H., Agrawal, K., Kang, Y., Li, N., Tang, R., et al. (2020). m(6A RNA Methyltransferases METTL3/14 Regulate Immune Responses to Anti-PD-1 Therapy. *EMBO J.* 39 (20), e104514. doi:10.15252/embj.2020104514

Wang, S., Sun, C., Li, J., Zhang, E., Ma, Z., Xu, W., et al. (2017). Roles of RNA Methylation by Means of N6-Methyladenosine (m6A) in Human Cancers. *Cancer Lett.* 408, 112–120. doi:10.1016/j.canlet.2017.08.030

Weng, H., Huang, H., Wu, H., Qin, X., Zhao, B. S., Dong, L., et al. (2018). METTL14 Inhibits Hematopoietic Stem/Progenitor Differentiation and Promotes Leukemogenesis via mRNA m6A Modification. *Cell stem cell* 22 (2), 191–205. doi:10.1016/j.stem.2017.11.016

Yang, S., Wei, J., Cui, Y. H., Park, G., Shah, P., Deng, Y., et al. (2019). m(6A mRNA Demethylase FTO Regulates Melanoma Tumorigenicity and Response to Anti-PD-1 Blockade. *Nat. Commun.* 10 (1), 2782. doi:10.1038/s41467-019-10669-0

Yang, Y., Hsu, P. J., Chen, Y.-S., and Yang, Y.-G. (2018). Dynamic Transcriptomic m6A Decoration: Writers, Erasers, Readers and Functions in RNA Metabolism. *Cell Res* 28 (6), 616–624. doi:10.1038/s41422-018-0040-8

Yao, M.-D., Jiang, Q., Ma, Y., Liu, C., Zhu, C.-Y., Sun, Y.-N., et al. (2020). Role of METTL3-dependent N6-Methyladenosine mRNA Modification in the Promotion of Angiogenesis. *Mol. Ther.* 28 (10), 2191–2202. doi:10.1016/j.ymthe.2020.07.022

Yoshihara, K., Shahmoradgoli, M., Martínez, E., Vegesna, R., Kim, H., Torres-Garcia, W., et al. (2013). Inferring Tumour Purity and Stromal and Immune Cell Admixture from Expression Data. *Nat. Commun.* 4, 2612. doi:10.1038/ncomms3612

Yu, G., Wang, L.-G., Han, Y., and He, Q.-Y. (2012). clusterProfiler: an R Package for Comparing Biological Themes Among Gene Clusters. *OMICS: A J. Integr. Biol.* 16 (5), 284–287. doi:10.1089/omi.2011.0118

Zeng, D., Zhou, R., Yu, Y., Luo, Y., Zhang, J., Sun, H., et al. (2018). Gene Expression Profiles for a Prognostic Immunoscore in Gastric Cancer. *Br. J. Surg.* 105 (10), 1338–1348. doi:10.1002/bjs.10871

Zhang, C., Huang, S., Zhuang, H., Ruan, S., Zhou, Z., Huang, K., et al. (2020). YTHDF2 Promotes the Liver Cancer Stem Cell Phenotype and Cancer Metastasis by Regulating OCT4 Expression via m6A RNA Methylation. *Oncogene* 39 (23), 4507–4518. doi:10.1038/s41388-020-1303-7

Zhang, S., Zhao, B. S., Zhou, A., Lin, K., Zheng, S., Lu, Z., et al. (2017). m 6 A Demethylase ALKBH5 Maintains Tumorigenicity of Glioblastoma Stem-like Cells by Sustaining FOXM1 Expression and Cell Proliferation ProgramA Demethylase ALKBH5 Maintains Tumorigenicity of Glioblastoma Stem-like Cells by Sustaining FOXM1 Expression and Cell Proliferation Program. *Cancer cell* 31 (4), 591–606. doi:10.1016/j.ccell.2017.02.013

Zheng, C., Zheng, L., Yoo, J.-K., Guo, H., Zhang, Y., Guo, X., et al. (2017). Landscape of Infiltrating T Cells in Liver Cancer Revealed by Single-Cell Sequencing. *Cell* 169 (7), 1342–1356. doi:10.1016/j.cell.2017.05.035

Zhu, A. X., Finn, R. S., Edeline, J., Cattan, S., Ogasawara, S., Palmer, D., et al. (2018). Pembrolizumab in Patients with Advanced Hepatocellular Carcinoma Previously Treated with Sorafenib (KEYNOTE-224): a Non-randomised, Open-Label Phase 2 Trial. *Lancet Oncol.* 19 (7), 940–952.

Zhu, D., Zhou, J., Zhao, J., Jiang, G., Zhang, X., Zhang, Y., et al. (2019). ZC3H13 Suppresses Colorectal Cancer Proliferation and Invasion via Inactivating Ras-ERK Signaling. *J. Cel Physiol* 234 (6), 8899–8907. doi:10.1002/jcp.27551

Conflict of Interest: The authors declare that the research was conducted in the absence of any commercial or financial relationships that could be construed as a potential conflict of interest.

frontiers in Pharmacology

REVIEW
published: 02 July 2021
doi: 10.3389/fphar.2021.695957

Emerging Biological Functions of IL-17A: A New Target in Chronic Obstructive Pulmonary Disease?

Meiling Liu[1†], Kang Wu[2,3†], Jinduan Lin[1†], Qingqiang Xie[1], Yuan Liu[1], Yin Huang[1], Jun Zeng[1], Zhaogang Yang[4], Yifan Wang[5], Shiyan Dong[5], Weiye Deng[5], Mingming Yang[4], Song Wu[2,3], Wen Jiang[5]* and Xuefeng Li[1,2]**

[1]The Sixth Affiliated Hospital of Guangzhou Medical University, Qingyuan People's Hospital; State Key Laboratory of Respiratory Disease, Sino-French Hoffmann Institute, School of Basic Medical Sciences, Guangzhou Medical University, Guangzhou, China, [2]Shenzhen Luohu People's Hospital, The Third Affiliated Hospital of Shenzhen University, Shenzhen, China, [3]South China Hospital, Shenzhen University, Shenzhen, China, [4]Department of Radiation Oncology, The University of Texas Southwestern Medical Center, Dallas, TX, United States, [5]Department of Radiation Oncology, The University of Texas MD Anderson Cancer Center, Houston, TX, United States

Chronic obstructive pulmonary disease (COPD) is a chronic inflammatory disease that causes high rates of disability and mortality worldwide because of severe progressive and irreversible symptoms. During the period of COPD initiation and progression, the immune system triggers the activation of various immune cells, including Regulatory T cells (Tregs), dendritic cells (DCs) and Th17 cells, and also the release of many different cytokines and chemokines, such as IL-17A and TGF-β. In recent years, studies have focused on the role of IL-17A in chronic inflammation process, which was found to play a highly critical role in facilitating COPD. Specially, IL-17A and its downstream regulators are potential therapeutic targets for COPD. We mainly focused on the possibility of IL-17A signaling pathways that involved in the progression of COPD; for instance, how IL-17A promotes airway remodeling in COPD? How IL-17A facilitates neutrophil inflammation in COPD? How IL-17A induces the expression of TSLP to promote the progression of COPD? Whether the mature DCs and Tregs participate in this process and how they cooperate with IL-17A to accelerate the development of COPD? And above associated studies could benefit clinical application of therapeutic targets of the disease. Moreover, four novel efficient therapies targeting IL-17A and other molecules for COPD are also concluded, such as Bufei Yishen formula (BYF), a Traditional Chinese Medicine (TCM), and curcumin, a natural polyphenol extracted from the root of *Curcuma longa*.

Keywords: IL-17A, COPD, inflammation, cytokine, chemokine, treatment

OPEN ACCESS

Edited by:
Vincent Kam Wai Wong, Macau University of Science and Technology, SAR China

Reviewed by:
Wei Gao, Tongji University School of Medicine, China
Bao-ping Tian, Zhejiang University, China

***Correspondence:**
Xuefeng Li
xuefengli@gzhmu.edu.cn
Wen Jiang
WJiang4@mdanderson.org
Song Wu
wusong@szu.edu.cn

[†]These authors have contributed equally to this work.

Specialty section:
This article was submitted to Ethnopharmacology, a section of the journal Frontiers in Pharmacology

Received: *16 April 2021*
Accepted: *23 June 2021*
Published: *02 July 2021*

Citation:
Liu M, Wu K, Lin J, Xie Q, Liu Y, Huang Y, Zeng J, Yang Z, Wang Y, Dong S, Deng W, Yang M, Wu S, Jiang W and Li X (2021) Emerging Biological Functions of IL-17A: A New Target in Chronic Obstructive Pulmonary Disease? Front. Pharmacol. 12:695957. doi: 10.3389/fphar.2021.695957

INTRODUCTION

Chronic obstructive pulmonary disease (COPD), which is characterized by airflow obstruction and gas trapping of chronic bronchitis and emphysema, causes high morbidity and mortality. It can further develop into pulmonary heart diseases and common chronic diseases that result in severe respiratory failure (Adeloye et al., 2015). The common comorbidities of COPD include cardiovascular diseases, metabolic syndromes and lung cancer, leading to a worse health condition (Negewo et al., 2015). The World Health Organization (WHO) predicts that COPD

will become the third leading cause of human death worldwide by 2030, pushing us to focus on the improvement of the treatments and prognosis.

The common clinical symptoms of COPD include chronic cough, sputum production, and dyspnea. The major risk factors are tobacco smoking, air pollution from indoors or outdoors, occupational dust, chemicals like smog, and infections caused by bacteria, viruses, or fungi. Besides environmental exposures, host factors such as abnormal lung development and genetic abnormalities are also important factors for individuals to develop COPD. COPD exacerbation is an important and complex event in COPD development and is a major determinant reflecting health status of COPD patients. According to the Global Initiative for Chronic Obstructive Lung Disease (2021), an COPD exacerbation is defined as an acute worsening of respiratory symptoms which requires additional therapy (Halpin et al., 2021). The common symptoms of COPD exacerbation include increased airway inflammation, increased mucus production and marked gas trapping, which leads to increased dyspnea, a key symptom of COPD exacerbation. Other symptoms include increased sputum purulence and volume, as well as increased cough and wheeze (Anthonisen et al., 1987). COPD exacerbation can be triggered by various factors, among which respiratory viral and bacterial infections are the most common factors. Meanwhile, environmental factors such as pollution and ambient temperature also initiate and/or amplify these events (Woodhead et al., 2005). The increase of bacteria burden in the sputum, eosinophil numbers together with neutrophils and other inflammatory cells are also the pathological features in a proportion of subjects with COPD exacerbation (Boixeda et al., 2015; Kim and Aaron, 2018). Studies conducted in smoking mice have shown that innate immunity plays a major role in the early stage of lung tissue changes, while acquired immune responses are important in the late stages of COPD (Rovina et al., 2013). Airway inflammation, which may induce parenchymal tissue destruction, disruption of defense mechanisms, and host normal repair, is a core feature in patients with COPD (de Nijs et al., 2011). Activating immune cells by stimulating inflammatory cell surface molecules is required to promote the development of lung inflammation in COPD patients (Wang et al., 2018a).

Interleukin-17 A (IL-17A), an essential member of the IL-17 family and known as an important proinflammatory factor in COPD, was cloned from activated cytotoxic T cells and originally named as CTLA8 (Rouvier et al., 1993). IL-17 can be produced by many different cells, such as Th17 cells, γδ T cells, innate lymphoid cells, lymphoid tissue inducer cells, and natural killer T cells (He et al., 2016). IL-17 participates in many important physiological responses (McGeachy et al., 2019). Naive T cells can differentiate into Th17 cells by up-regulating retinoic acid receptor-related orphan nuclear receptor γ (RORγt) mRNA by co-stimulating transforming growth factor-β (TGF-β) plus IL-6; IL-1β and IL-23 strengthen this process (Bettelli et al., 2006; McGeachy et al., 2009). Based on sequence homology, researchers later discovered that the IL-17 family includes six members: IL-17A, IL-17B, IL-17C, IL-17D, IL-17E (also called IL-25), and IL-17F. Till now, IL-17A is the most widely studied molecule in the IL-17 family and was found to have the closest relationship with IL-17F, among all family members. Besides, the receptor family of IL-17 consists of IL-17RA, IL-17RB, IL-17RC, IL-17RD, and IL-17RE. IL-17A shares the same IL-17RA/RC heterodimeric receptor complex with IL-17F and IL-17A/F heterodimers, while IL-17E binds to the heterodimeric receptor complex of IL-17RA and IL-17RB. IL-17C interacts with the heterodimeric receptor complex of IL-17RA and IL-17RE, and the combination of ligands and receptors contributes to passing the signal to the downstream pathways. However, the ligands for the heterodimeric receptor complex of IL-17RA and IL-17RD are not clear, though a study about psoriasis-like skin inflammation showed that IL-17RA/RD directly bound to IL-17A but not IL-17F or IL-17A/F heterodimer to mediate the proinflammatory gene expression downstream of IL-17A (Su et al., 2019). Besides, the receptor for IL-17D and the other component of IL-17RB heterodimeric receptor complex for IL-17B are still unknown (McGeachy et al., 2019). Actually, IL-17 receptor family share the SEFIR domain which is akin to Toll/Il-1 Receptor (TIR) domain, it can mediate SEFIR-SEFIR homotypic interactions by combing with Act1 (Novatchkova et al., 2003), then the combination of IL-17 receptor and Act1 recruits TNF receptor associated factor (TRAF) family members to initiate the pathways of nuclear factor kappa-B (NF-κB) and mitogen-activated protein kinases (MAPKs), resulting in the transcription and expression of target genes (Zhou et al., 2014; Li et al., 2016a; Herjan et al., 2018). Moreover, IL-17RA have the Toll/IL-1R-like loop (Till) and C/EBP-β activating domain (CBAD), which can activate extracellular signal-regulated kinase (Erk), leading to the phosphorylation of C/EBP-β and expression of target genes (Shen et al., 2009) (**Figure 1**).

Under normal condition, IL-17 protects the host against extracellular fungal and bacterial infections (Yang et al., 2018). However, IL-17A can also promote the progression of inflammatory processes, autoimmune diseases, chronic diseases like COPD and cancers, even worsen outcomes. Therefore, IL-17A and its family members are double-edged swords. On one hand, IL-17A can expand the role of the immune response in protecting the body against infections and promote tissue repair; on the other hand, the excessive secretion of IL-17A induces the expression of plenty inflammatory factors, which may result in conditions such as decreased flexibility of tissue and tissue fibrosis (Lei et al., 2019). Given the double effects of IL-17A, exploration the relationship and mechanism between IL-17A and various diseases is of essential importance.

The increased expression of IL-17A in the lung tissues of COPD patients was found to be negatively associated with the clinical evaluation indexes of lung function, such as forced expiratory volume in 1 s (FEV1%), forced vital capacity (FVC %) and FEV1/FVC (Zheng et al., 2018). Since FEV1%, FVC % and FEV1/FVC are negatively correlated with COPD severity (JalusicGluncic, 2011), the expression of IL-17A is positively correlated with the COPD severity. Although both IL-17A and IL-17F share the same receptor, their expression levels are different in COPD, while the affinity of IL-17F to IL-17RA/IL-17RC is far lower than that of IL-17A. Therefore, some researchers agree that IL-17A, rather than IL-17F, regulates the epithelial cell proliferation and apoptosis in central and distal airways to repair the damaged tissue in COPD patients (Eustace et al., 2011; Montalbano

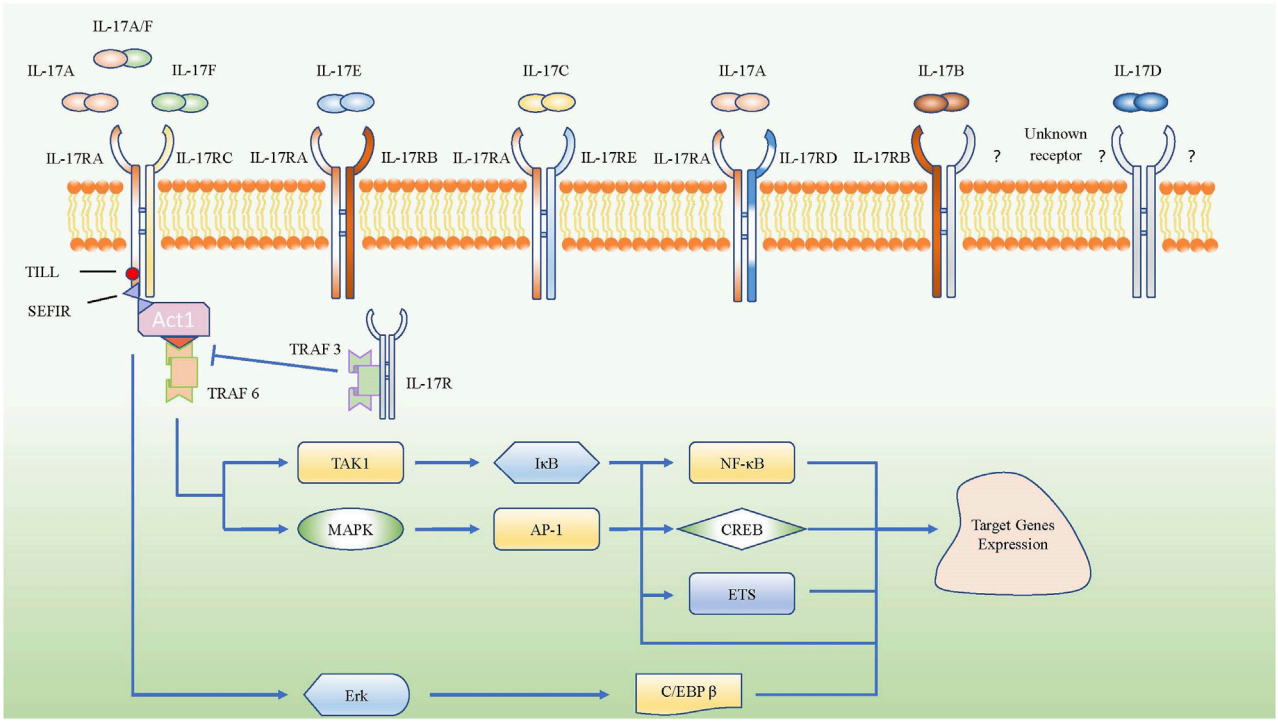

FIGURE 1 | Schematic represent IL-17 family subgroup and their corresponding receptors from IL-17 receptor family. IL-17A, IL-17A/F and IL-17F share the IL-17RA/RC heterodimeric receptor. The intracellular domains of all IL-17R encode conserved SEFIR domains which interact with a corresponding SEFIR motif on the adaptor Act1, then they combine with TRAF6 to activate the pathway of NF-κB and MAPK. However, TRAF3 could inhibit SEFIR- Act1- TRAF6 pathway by competitive binding the IL-17RA directly. Only IL-17RA own the CBAD and TILL, which can promote the target gene expressions *via* C/EBP β pathway.

et al., 2015). Currently, it is generally believed that emphysema and severe airway obstruction are common clinical characteristics of COPD (Huang et al., 2018), and their evolvement and lymphoid neogenesis could be promoted by the up-regulation of IL-17A in COPD (Shan et al., 2012; Roos et al., 2015). Th17 cells, rather than IL-17A-secreting lung γδT cells, act as mediators of smoke-induced lung inflammation and emphysema. Unexpectedly, γδT cells can even hamper Th17 pathological responses in lung changes under certain conditions (Shan et al., 2012). Study has shown that lung inflammation in COPD is characterized by ascending neutrophils, alveolar macrophages, DCs, and T lymphocytes (predominantly TC1, TH1, and Th17 cells, while high level of eosinophils could also be detected in some patients with COPD (Barnes, 2016). Because IL-17A, a well-known pro-inflammatory factor in COPD patients, can promote the infiltration of inflammatory cells in the lung parenchyma and airways, the role of IL-17A in regulating the progression of COPD should be further explored.

IL-17A PROMOTES COPD PROGRESSION

IL-17A Promotes Airway Remodeling in COPD

Airway remodeling which could result in irreversible airflow obstruction is a common change in COPD lung tissue structure (Barnes et al., 2015). In airway remodeling, elevated level of epidermal growth factor (EGF) and increased expression of EGF receptors can be observed in the bronchial epithelial cells (Li and Luan, 2010). Cigarette smoke (CS), acting as an inducement for inflammation in COPD, can activate the EGF receptor through both damaged tissue and augmented epithelial permeability (Wang et al., 2014). The activated EGF receptor could promote the expression of airway mucin5AC and mucin5B, and facilitate goblet cell hyperplasia (Yu et al., 2012; Kato et al., 2020), while EGF could stimulate the proliferation of airway smooth muscle in the bronchi (Song et al., 2000). In fact, increased deposition of extracellular matrix (ECM) is an important structural change in airway remodeling, while fibroblasts are the main source of ECM and play a significant role in airway fibrosis formation, both of which play a key part in COPD airway remodeling (Hogg et al., 2004; Krimmer et al., 2012). In mouse pulmonary inflammation and fibrosis models, IL-17A not only directly regulated the synthesis and secretion of collagen in alveolar epithelial cells in a TGF-β1-dependent manner and facilitated the transition of epithelia to the mesenchyme, but also suppressed autophagy and promoted autophagy-associated cells death in inflammatory lung tissue (Li et al., 2015; Ye et al., 2015; Li et al., 2016b; Zhuang et al., 2016; Wang et al., 2018b). This led to more serious inflammation and possible airway remodeling, because the collagen and inflammation-associated mediators or cells could not be degraded or killed through autophagy (Mi et al., 1950; Xie

et al., 2020). It has been reported that both IL-17A and Histone Deacetylase 2 (HDAC2) are related to the thickened wall and increased collagen deposition of the bronchi in COPD, but they have opposite effects. IL-17A can activate fibroblasts by inducing inflammatory cells to produce pro-fibrosis factor TGF-β1, which aggravates CS-induced airway remodeling, whereas HDACs could inhibit the differentiation of Th17 cells by reversing the high acetylation of core histone proteins. Therefore, the production of IL-17A from Th17 cells was reduced, and the airway remodeling in COPD was attenuated even inhibited (Lai et al., 2018). In all, IL-17A can promote airway remodeling by increasing TGF-β1 and inhibiting inflammation-associated mediator or cell autophagy in inflammatory lung tissue (**Figure 2**).

IL-17A Facilitates Neutrophil Inflammation in COPD

COPD is a chronic inflammatory airway disease dominated by neutrophil infiltration. In COPD, increased neutrophil mobilization and elevated IL-17A were observed. Although CS is regarded as one of the crucial causes for triggering COPD, IL-17A is not significantly reduced after smoking cessation (Hansen et al., 2014). IL-17A, p53, and plasminogen activator inhibitor (PAI)-1 were higher in smokers with COPD than in healthy smokers (HSs) and healthy control subjects (HCs) (Gouda et al., 2018a). P53, a tumor suppressor gene that controls the initiation of the cell cycle, could initiate cell apoptosis if damage to cells is beyond repair. As COPD pulmonary fibrosis injury is associated with damaged alveolar epithelia, research has mostly focused on damaged alveolar epithelia and found higher expression of p53 and PAI-1, as well as the activation of caspase-3, which participates in promoting apoptosis of alveolar epithelial cells (Bhandary et al., 2013). In the experiment of bleomycin-induced alveolar basal epithelial cells to simulate the inflammation *in vitro*, the up-regulation of IL-17A promoted migration of alveolar basal epithelial cells and increased p53 and PAI-1 expression (Gouda et al., 2018b). p53 can induce obvious epithelial cell apoptosis and lung injury, while PAI-1 is a downstream mediator of p53-induced pulmonary inflammation. After serine phosphorylation in the p53 protein, p53 binds to PAI-1 to promote PAI-1 expression, leading to the increase of CXCL1, CXCL2 and CXCR2 in COPD patients (Tiwari et al., 2016), which could induce the influx of neutrophils to infection site. Higher PAI-1 levels can not only promote airway and alveolar epithelial cells apoptosis, but also cause fibrinolysis defects and alveolar fibrin deposition in patients with COPD (Gouda et al., 2018a). Meanwhile, the increased expression of PAI-1 could suppress neutrophil apoptosis and apoptotic neutrophil phagocytosis (Zmijewski et al., 2011),

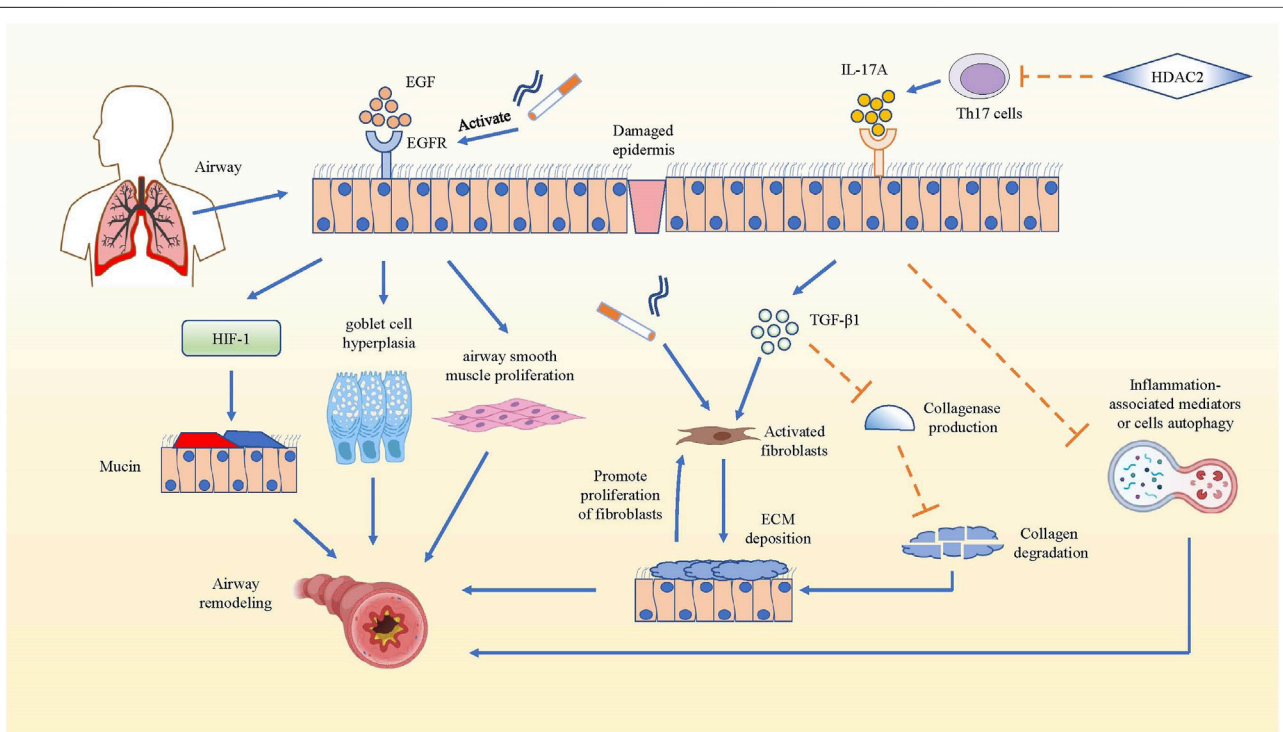

FIGURE 2 | IL-17A promotes airway remodeling in COPD. The mechanism that IL-17A promotes airway remodeling by increasing collagen deposition and inhibiting inflammation-associated mediators or cells autophagy are summarized. In COPD airway remodeling, the activated EGFR facilitates the production of mucin5AC *via* hypoxia inducible factor-1 (HIF-1) pathway, promotes goblet cell hyperplasia and airway smooth muscle proliferation. While IL-17A produced by Th17 cells activates fibroblasts to secrete ECM and inhibit the collagen degradation in TGF-β1-dependent manner, and IL-17A also could hampers the autophagy of inflammation-associated mediators, which promotes development and progression of pulmonary fibrosis. Actually, the deposition of ECM also has positive effect on the proliferation of fibroblasts, which strengthens ECM deposition. However, HDAC2 reverses the above result by inhibiting the differentiation of Th17 cells.

leading to neutrophil accumulation and inflammation in damaged lungs of patients with COPD.

In brief, IL-17A could facilitate neutrophil inflammation in COPD by facilitating the expression of p53 and PAI-1 to increase CXCL1, CXCL2 and CXCR2 to induce the influx of neutrophils. Besides, IL-17A can recruit neutrophils to the inflammation nidus by inducing the expression of neutrophil chemokines, such as IL-8, G-CSF and CXCL2 (Hansen et al., 2014). The increase of neutrophils could secrete more neutrophil elastase (NE) and myeloperoxidase, which can degrade collagen, destroy alveolar wall and cause emphysema (Cohen et al., 1982) (**Figure 3**).

IL-17A Induces TSLP Expression by Activating IKK-α in COPD

Thymic stromal lymphopoiesis (TSLP), a cytokine homologous to IL-7, is expressed in epithelial cells and is involved in the pathogenesis of chronic diseases by combining with its receptor (El-Ghareeb et al., 2019). TSLP can directly promote the differentiation as well as the response of Th2 cells in the lung to promote COPD through an independent pathway without draining lymph nodes (Lai et al., 2020). TSLP-activated DCs primed naïve T(H) cells to produce cytokines such as IL-4, IL-5, IL-13 and TNF-α to facilitate the development of Th2 cell-mediated airway inflammation (Soumelis et al., 2002). Research on TSLP production in COPD patients has shown that serum concentrations of TSLP and IL-17A were higher in patients with COPD than that in HCs. After stimulating a human epithelial cell line (16HBE) with induced sputum supernatants (ISS) from HCs, HSs, or COPD patients, significantly higher levels of TSLP were induced by elevated IL-17A from COPD patients, which could be inhibited by anti-IL-17A Ab(antibody), indicating a direct and specific association between IL-17A and TSLP in the airways. IKKα silencing reduced TSLP synthesis in 16HBE stimulated with IL-17A or with ISs from COPD patients more effectively than in stimulated unsilenced cells (Anzalone et al., 2018). Therefore, IL-17A, TSLP, and IKKα might closely interact. Anzalone et al. reported that IL-17A induced the acetylation of histone H3 (Ac-His H3) (k9) and inflammation by activating IKKα in human lung epithelial cells (Anzalone et al., 2016). In conclusion, the aforementioned studies suggested that IL-17A initiated IKK-α signaling to induce the TSLP production to regulate airway inflammation in COPD.

The specific induction process mentioned earlier may involve CREP-binding protein (CBP), NF-κB, and IκB kinase, so their roles and functions need to be elucidated first. IKK-α is a catalytic subunit of the IκB kinase (also named IKK complex, which consists of IKK-α, IKK-β, and IKK-γ), and NF-κB is a key nuclear transcription factor related to activating immune cells, and also to triggering T and B cells, apoptosis, and stress response (Liu et al., 2012). At rest, NF-κB binds to the IκB kinase, presenting an inactive status. Upon external stimulation, the IKK complex becomes active and NF-κB is released from the complex. Then, the activated NF-κB translocates from the cytoplasm to the nucleus, and acts as a key nuclear

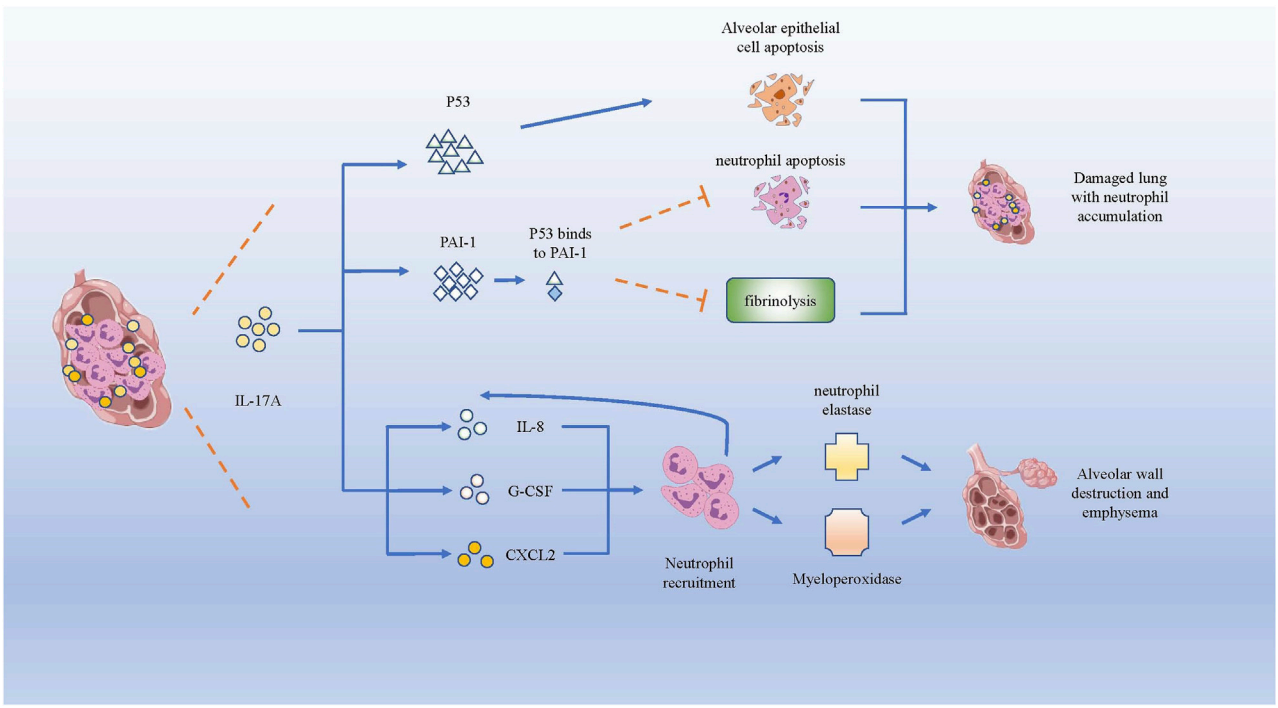

FIGURE 3 | IL-17A promotes neutrophils infiltration and lung destruction by increasing p53 and PAI-1. Both p53 and PAI-1 can induce the apoptosis of alveolar epithelial cells, while PAI-1 inhibits the neutrophil apoptosis and fibrinolysis in lung tissue. Besides, IL-17A induces the expression of IL-8, G-CSF and CXCL2, which recruits neutrophils producing neutrophil elastase and myeloperoxidase, giving rise to the destruction of alveolar wall and emphysema.

transcription factor to regulate the expression of various genes, including those of cytokines and chemokines associated with airway inflammation (Mulero et al., 2019). Interestingly, IKK-β, but not IKK-α, plays a critical role in cytokine-induced IκB activation of the classical pathway to regulate the transcription of various cytokines and chemokines. Nevertheless, IKK-α-deficient mice are defective in their ability to induce NF-κB-dependent transcription. Therefore, a direct key relationship between IKK-α and NF-κB is still unclear. Studies later found that IKK-α can also directly translocates to the nucleus to rapidly regulate the expression of NF-κB response gene by catalyzing phosphorylation of histone H3 to activate NF-κB-directed gene expression (Yamamoto et al., 2003).

Hence, inducing TSLP and other pro-inflammatory mediators by IL-17A-associated IKK-α signaling in patients with COPD can be described as follows. First, elevated IL-17A in COPD patients activates IKK-α. Second, IKK-α catalyzes phosphorylation of Ser10 in histone H3 to activate CBP. Third, the activated CBP that owns activated histone acetyltransferase (HAT) activity acetylates H3 at Lys14, contributing to chromatin modification such as dissociating DNA and histone octamer, so that a variety of transcription factors such as NF-κB can specifically combine with DNA binding sites and activate gene transcription, thereby promoting the expression of pro-inflammatory molecules such as TSLP in patients with COPD (Chung et al., 2010; Anzalone et al., 2018) (**Figure 4**). In brief, IL-17A promotes the expression of TSLP and other pro-inflammatory mediators by activating IKK-α to drive the development of COPD.

DCs Induces the Differentiation of Th17 Cells to Produce More IL-17A to Promote COPD Progression

DCs are functional specialized antigen-presenting cells. Different biomarkers indicate a different maturity DC status. For example, CD1a and CCR6 are used for immature DCs, and CD40, CD80, and CD83 are used for mature DCs.

Zheng et al. confirmed that levels of CD80, Treg, FOXP3, and mature DCs were significantly lower, and levels of CCR6, Th17 cells, IL-17A, and immature DCs were higher in COPD$^+$ patients than in CS$^+$ COPD$^-$ patients and HCs. The acute exacerbation of the COPD (AECOPD) group showed the highest effects on decreasing mature DCs and increasing immature DCs (Zheng et al., 2018). Several studies have indicated that DCs induced CD4$^+$ T cells to differentiate toward a Th17 cell type by up-regulating RORγt mRNA *via* the CD40/CD40L pathway and cooperating with IL-6 and IL-23 that were produced by DCs (Perona-Wright et al., 2009; Iezzi et al., 2009). Higher levels of Th17 cells not only produce more IL-17A to enhance inflammation, but also induce the differentiation and activation of DCs, which, in turn, further induce the differentiation of Th17 cell and strengthen the inflammation response in COPD (Vargas-Rojas et al., 2011; Wang et al.,

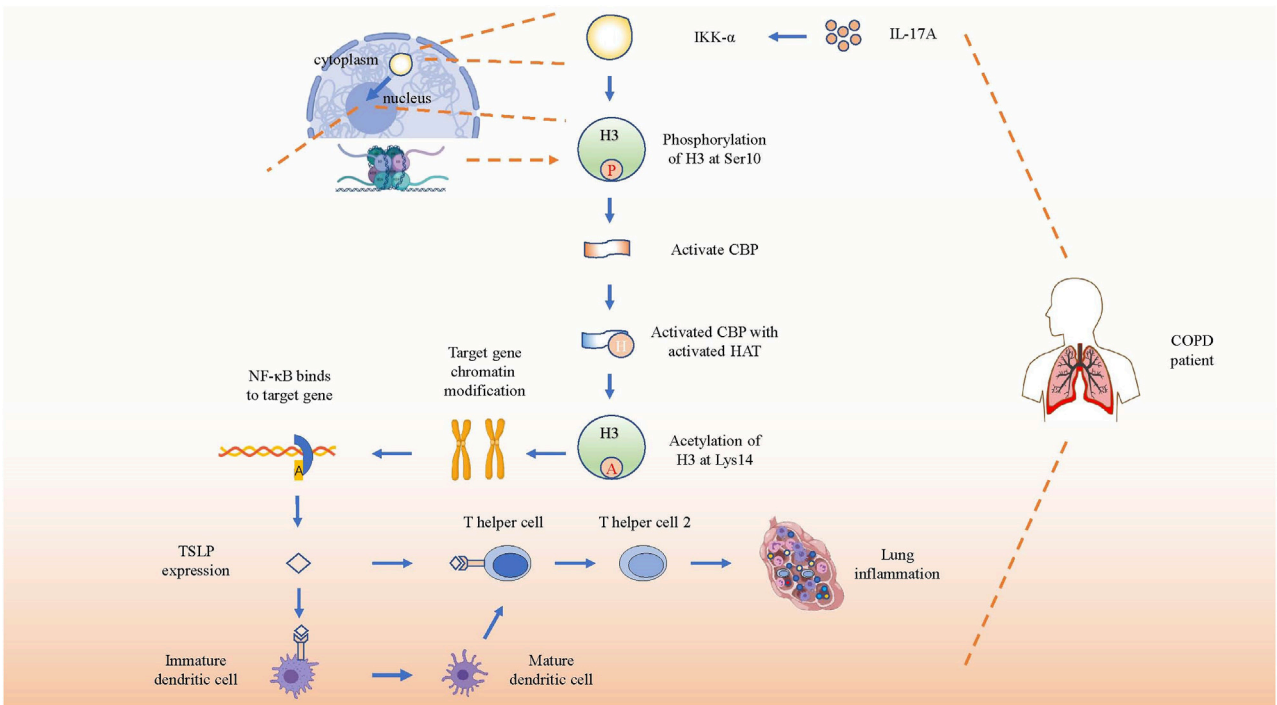

FIGURE 4 | IL-17A induces gene expression by activating IKK-α. Schematic show the pathway of inflammation-associated gene expression directly regulated by activated IKK-α through direct translocation into nucleus after receiving the stimulation of increased IL-17A. After phosphorylation and acetylation of H3, the target genes' chromatin will be recombined and bind to NF-κB to promote TSLP expression. Then TSLP will combine with its receptor on immature dendritic cells and T helper cells to promote the differentiation and immune response of Th2 in COPD lung tissue.

2019). In brief, the increase of IL-17A produced by DCs-induced Th17 cells could promote the progression of COPD, which suggests that the subgroup of DCs plays an important role in promoting COPD development.

Imbalance of Th17/Treg in COPD Progression

Tregs are a subgroup of T cells with strong immunosuppressive functions and Th17 are the T helper cells that could secret IL-17A.

Wang et al. reported that COPD patients had higher levels of circulating Th17 cells, serum IL-1β, IL-6, IL-17A, IL-21, IL-22, IL-23, and TGF-β, but lower levels of Tregs and IL-10, which accounted for the dramatically higher ratio of Th17 to Tregs than that in HCs. Interestingly, they also observed that Tregs counts were remarkable higher in HSs, but lower in patients with COPDs, than in HCs. This phenomenon suggested the participation of Tregs in the normal immune system to sustain physiological homeostasis by functioning in immune-suppression. Simultaneously, the same tendency of fork head/winged helix transcription factor (FOXP3) mRNA and IL-10 levels were also observed in these groups (Wang et al., 2015a). Similarly, Ito et al. used CS-induced COPD mice to prove the increased expression of pro-inflammatory molecules such as TNF-α, IL-6, and IL-17 along with decreased anti-inflammatory molecule and cell levels such as IL-10 and FOXP3. These changes were linked to higher alveolar enlargement and impaired lung function in CS-induced COPD mice than healthy control mice (Ito et al., 2019).

Despite increased IL-2 and TGF-β (also considered to be a type of anti-inflammatory chemokine that promotes Tregs expression) in patients with COPD and elevated Tregs frequencies in AECOPD (Jin et al., 2014), higher levels of pro-inflammatory molecule such as IL-1β, IL-6, and IL-23 were predominant in patients with COPD. Because IL-1β, IL-6, and IL-23 can strongly promote the expression of Th17 cells but inhibit FOXP3 and Tregs (Morishima et al., 2009), we can easily account for the increased Th17 and decreased Tregs in COPD. Besides, elevated levels of IL-21 also down-regulated Tregs differentiation (Nguyen et al., 2012) and regulated Th17 development in a critical autocrine way (Nurieva et al., 2007). Although IL-22, an essential member of the IL-10 family, promotes tissue repair and host defense by binding to its heterodimeric transmembrane receptor complex composed of IL-22R1 and IL-10R2, it can also cooperate with co-expressed IL-17 to induce secretion of neutrophil chemotactic factors such as GM-CSF and CXCL8, and cytokines such as IL-6 to promote inflammation (Rutz et al., 2013).

Overall, elevated levels of pro-inflammatory molecules, such as IL-1β, IL-6, and IL-23, induced the development of Th17 cells, which, in turn, secreted pro-inflammatory chemokines and cytokines like IL-17A. IL-17A cooperated with other molecules like IL-22 to recruit GM-CSF, CXCL8 and IL-6 to promote inflammation development. In contrast, the suppressive development of Tregs and relative anti-inflammatory molecules certainly like IL-10 damaged their strong immunosuppressive function, thus both changes further promoted inflammation as well as COPD progression. Taking advantage of the imbalanced ratio of Th17 to Tregs, we can learn about the progression of COPD.

RELATIVE IMPORTANT AND COMMON MOLECULES PROMOTING COPD DEVELOPMENT

IL-17A Promotes the Expression of IL-8 in COPD

IL-8, also known as chemokine CXCL8, is secreted by macrophages, epithelial cells, among other cells. It can bind to IL-8RA (also named CXCR1) and IL-8RB (also named CXCR2), which are distributed on the surface of neutrophils, and the combination recruits and activates neutrophils to the damaged site to generate an inflammatory immune response (Lin et al., 2004). IL-8 has been proved to induce the recruitment and activation of neutrophils in the bronchial epithelium of COPD, and plays an important role in persistent airway inflammation of COPD and also reduces steroid sensitivity (Reynolds et al., 2018).

Anzalone et al. found higher levels of both macrophages and neutrophils in HSs, while only higher levels of neutrophils were observed in patients with COPD. The concentrations of IL-17A and IL-8 were dramatically elevated in ISS from patients with COPD. They detected the relative molecule expression in 16HBE after stimulating with ISS from HCs, HSs, and COPD patients, and the control group was untreated 16HBE. The expression of IL-8 mRNA and IL-8 protein were higher in 16HBE stimulated with ISS from HSs and COPD patients than that of 16HBE stimulated with the ISS from HCs or untreated 16HBE. Also, 16HBE stimulated with IL-17A yielded the same results, including increased IL-8, Ac-His H3 (k9), and IKKα, although 16HBE pretreated with anti-IL-17A or tiotropium could reverse this phenomenon (Anzalone et al., 2016).

According to above results, higher IL-17A level have promoted the expression of IL-8 in patients with COPD. A possible mechanism is that IL-17A facilitates the expression of inducible nitric oxide synthase (iNOS), which promotes the production of nitric oxide (NO) (Su et al., 2016). Furthermore, NO promotes the transcription of IL-8 mRNA by NF-κB and AP-1 to express higher IL-8 levels (Seo et al., 2009). These results indicated the positive link between IL-17A and IL-8 in patients with COPD, leading to neutrophil infiltration and airway inflammation.

IL-1β Cooperate With Other Cytokines to Induce IL-17A Expression in COPD

IL-1β is mainly produced by monocytes and macrophages and can work with the IL-1 receptor (IL-1R), distributed on the surface of most nucleated cells, to promote monocytes to directionally migrate toward inflammatory lesions. Therefore, it is considered to be a potent pro-inflammatory cytokine that is crucial for host-defense responses to infection and injury

(Dinarello, 1996). IL-1β can also promote the development of Th17 cells that produce IL-17A by cooperating with TGF-β, IL-6, and IL-23, contributing to the production of IL-17A in COPD progression when infections taking place (Revu et al., 2018).

PREVENTION AND PRESENT TREATMENT

In order to prevent and improve the symptoms of COPD, individuals are recommended to stop smoking (van Eerd et al., 2016), perform pharmacological therapy, make use of inhaler technique, undergo pulmonary rehabilitation or/and inject influenza vaccination (Poole et al., 2006). For stable COPD, patients are long to alleviate the symptoms, reduce the frequency and severity of exacerbations, and improve exercise tolerance.

The American College of Physicians (ACP), American College of Chest Physicians (ACCP), American Thoracic Society (ATS), and European Respiratory Society (ERS) aim at managing patients with COPD, according to the following guidelines: *1*) Patients with respiratory symptoms and 60–80% FEV1 can use bronchodilators *via* inhalation. *2*) Patients with respiratory symptoms and FEV1<60% are recommended to use bronchodilators *via* inhalation. *3*) Patients with symptoms and FEV1<60% are recommended to use either long-acting anticholinergics or long-acting β-agonists, both *via* inhalation. *4*) Patients with symptoms and FEV1<60% could use combined therapies *via* inhalation (long-acting anticholinergics, long-acting β-agonists, or corticosteroids) *5*) Patients with symptoms and FEV1<50% are strongly recommended to receive pulmonary rehabilitation, while patients with symptoms or exercise-limitation and FEV1 >50% could use pulmonary rehabilitation. *6*) Patients with severe resting hypoxemia (Pao2 ≤ 55 mm Hg or Spo2 ≤ 88%) are strongly encouraged to receive continuous oxygen therapy (Qaseem et al., 2011).

Tiotropium, a kind of long-acting muscarinic antagonist (LAMA), can inhibit the activation of airway secretory cells and smooth muscle cells, which, in turn, can reduce mucus secretion in the lungs of patients with COPD to improve their function (Coulson and Fryer, 2003). Bronchodilation with LAMAs, such as tiotropium, and long-acting ß2-agonists (LABAs), such as olodaterol, is a highly effective long-term maintenance treatment for COPD. Anzalone et al. showed that pretreating 16HBE cells with tiotropium significantly reduced the expression of IL-8 and Ac-His H3 (k9), and decreased the translocation of nuclear IKKα protein after stimulation with ISS in patients with COPD, which indicated the therapeutic effectiveness of tiotropium in COPD (Anzalone et al., 2016).

Although the therapeutic methods aforementioned improve airflow limitation and suppress the inflammatory responses of COPD to some extent, side effects are still observed. For instance, inhaled corticosteroids may cause dysphonia and moderate to severe bruising, while long-acting inhaled β-agonists can lead to increased cardiovascular events; tiotropium may cause dry mouth in patients (Yohannes et al., 2011; Gershon et al., 2013). These results indicate the need for therapeutic methods with minimum adverse effects in patients with COPD.

Novel and Promising Drug Treatments

As it is urgent for patients with COPD to get some effective and safe treatments, we introduce several novel and promising drug treatments as follows. Studies have shown the effectiveness of the Bufei Yishen formula (BYF), a Traditional Chinese Medicine (TCM) that consists of 12 medicinal herbs, as a potential therapeutic for COPD (Li et al., 2012). BYF can effectively alleviate COPD symptoms by declining exacerbation frequency, delaying acute exacerbation, and improving pulmonary function in patients. Later, Zhao et al. proved that BYF with oral administration could decrease the levels of pro-inflammatory cytokines such as IL-1β, IL-6, TNF-α, and IL-17A secreted by Th17 cells, but increase anti-inflammatory cytokines IL-10 secreted by Tregs in the BAL fluid. BYF treatment dramatically decreased $CD4^+ROR\gamma t^+$ T (Th17) cells and increased $CD4^+CD25^+FOXP3^+$ T (Treg) cells, so that the balance of Th17/Tregs could be restored to slow COPD progression. Moreover, BYF further suppressed phosphorylation of signal transducer and activator of transcription-3 (STAT3) and promoted phosphorylation of STAT5 (Zhao et al., 2018). Similarly, Dong et al. proved that BYF inhibited the lipopolysaccharide - or CS extract -induced expressions of TNF-α, IL-8 in H292 cells, and suppressed the activation of transcription factors like NF-κB and STAT3 to inhibit their correlative pathways (Dong et al., 2020). STAT3 is known to be a critical transcription factor that induces RORγt gene expression to promote Th17 differentiation (Lee et al., 2017). In contrast, STAT5 is regarded as an important transcription factor that induces the development and maintenance of Tregs by binding to the FOXP3 gene (Ma et al., 2018), but inhibits the expression of Th17 cells (Zheng et al., 2015). In brief, BYF could improve COPD by restoring the Th17/Treg balance as well as increasing related anti-inflammatory cytokines, while decreasing pro-inflammatory cytokines. In fact, BYF can treat patients with COPD *via* their multiple components. According to the network pharmacology analysis and molecular docking validation, a study showed that 48 components in BYF might act on 65 targets to exert the therapeutic effect, and the therapeutic process involved IL-17, Toll-like receptor (TLR) and TNF pathways (Wu et al., 2020). Therefore, more attention should be drawn to BYF for therapeutic use in COPD.

Curcumin, a natural polyphenol extracted from the root of *Curcuma longa* (turmeric plant), is a safe and bioactive phytochemical component with many molecular targets and high pharmacological activity. Curcumin plays a key role in decreasing serum lipids, suppressing inflammation, promoting antitumor activities, and improving the development of COPD (Khorasani et al., 2019). A study showed that administrations of bleomycin and IL-17A to the alveolar epithelial cells could result in significant down-regulation of Akt expression, a proliferation biomarker for cell, while this phenomenon could be reversed by treatment with Curcumin (Gouda et al., 2018c). Another study indicated Curcumin alleviated IL-17A-mediated p53-PAI-1 expression in bleomycin-induced alveolar basal epithelial cells (Gouda et al., 2018b). Both of these two studies showed pulmonary inflammation mediated by bleomycin and IL-17A was intervened effectively by curcumin. Chen et al. further proved

that Curcumin decreased the inflammation of acute lung injury not only by promoting the expression of IL-35, increasing STAT5 proportion, but also by decreasing IL-17A in lung tissue (Chen et al., 2020). Curcumin can significantly decrease the number of neutrophils and macrophages in the BAL fluid, and reduce the apoptosis index of alveolar epithelial cells to attenuate alveolar epithelial damage in COPD, and may be associated with down-regulating the expression of p66Shc (Zhang et al., 2016). Curcumin can also suppress chemokine expression by restoring HDAC2 expression and function on histone modification to attenuate COPD development (Gan et al., 2016). Also, curcumin effectively reduced CS-induced inflammation responses and improved pulmonary function, presumably by up-regulating peroxisome proliferators-activated receptor γ (PPARγ) and inhibiting NF-κB activation (Li et al., 2019). Therefore, curcumin is a safe and natural drug with promising therapeutic value for improving the life quality of patients with COPD (**Figure 5**).

MLN4924, a potent and selective inhibitor of NEDD8-activating enzyme (NAE), mediates cell cycle by deregulating the S-phase of DNA synthesis (Soucy et al., 2009). MLN4924 could significantly inhibit the expression of proinflammatory cytokines and chemokines such as IL-1β, IL-6, and CXCL-1 in IL-17A-inducing pulmonary inflammation. Mechanistically, MLN4924 inhibited TRAF6 ubiquitination by interfering the interaction between ACT1 of IL-17A and TRAFs, leading to significant inhibition of MAPK and NF-κB pathways (Hao et al., 2019). The other study also showed that MLN4924 acted against bleomycin-induced pulmonary fibrosis mainly at the early inflammatory stage, during which it inhibited MAPK and NF-κB pathways to decrease the expression of proinflammatory cytokines and chemokines. And the study indicated the potential therapeutic role of MLN4924 against other inflammation-associated diseases like COPD (Deng et al., 2017). However, although MLN4924 might be a novel and promising drug treatment for COPD, there are very few correlative studies at present, which needs our more attentions to study them.

Simvastatin, belonging to Statins, certainly has anti-inflammatory, anti-oxidant function *in vitro* and *in vivo*. Maneechotesuwan et al. showed that Simvastatin reversed the IL-17A/IL-10 imbalance in the airways of COPD. Compared with placebo treatment, IL-17A, IL-22, IL-6, and CXCL8 concentrations in sputum significantly reduced at 4 wk, whereas IL-10 were markedly increased during Simvastatin treatment (Maneechotesuwan et al., 2015). Another study proved that in rat COPD model, Simvastatin decreased the levels of IL-8, IL-17 and TNF-α in bronchoalveolar lavage fluid (BALF) and inhibit the expression of NF-κB and MUC5AC in airway and lung tissue. Simvastatin plays preventive and therapeutic roles by reducing airway inflammation and airway mucus hypersecretion (Wang et al., 2015b). Murphy et al. showed that IL-17 upregulated IL-8, IL-6, G-CSF and GM-CSF, whereas TGF-β increased IL-6 and GM-CSF. Simvastatin attenuated effects of both IL-17 and TGF-β. Their study has demonstrated the ability of Simvastatin to alleviate neutrophilic airway inflammation and remodeling by inhibiting the upregulation of various pro-inflammatory cytokines induced by IL-17A and TGF-β (Murphy et al., 2008). There are less associated studies about Simvastatin, targeting IL-17A, for COPD at present, which needs to be studied further.

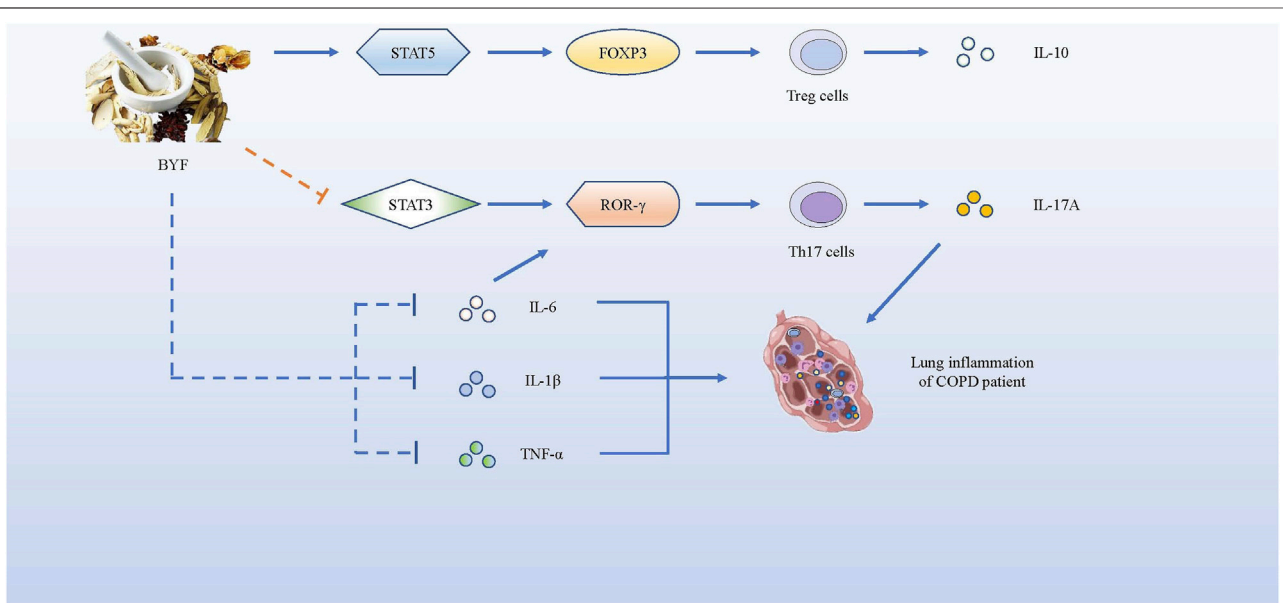

FIGURE 5 | BYF alleviates COPD symptoms by promoting the expression of pro-inflammatory factors and suppressing the production of anti-inflammatory cytokines. BYF induces T naïve cells towards Tregs, producing IL-10, by up-regulating the FOXP3 expression *via* STAT5 pathway, while it inhibits the differentiation of Th17 cells, producing IL-17A, by down-regulating the RORγt gene *via* STAT3 pathway. Meanwhile, BYF also decrease the levels of pro-inflammatory cytokines such as IL-1β, IL-6 and TNF-α, which could alleviate the inflammation development of COPD.

Recently, Christenson et al. discovered a new COPD subgroup characterized by a markedly enhanced IL-17 signature that decreased in response to corticosteroids. This subgroup was irrelevant to airway eosinophilic or type 2 inflammation. Hence, more attention should be focused on exploring the relative specific mechanism of this COPD subgroup, so that we can improve personalized therapy to improve the life quality of patients with COPD (Christenson et al., 2019).

CONCLUSION

COPD is a chronic inflammatory disease that leads to high rates of disability and mortality worldwide. Increased expression of IL-17A promotes the progression of COPD, but some specific underlying mechanisms which promote the development of this disease is still unknown. Hence, we looked into the relationship between IL-17A and immune cells, chemokines, cytokines, and transcription factors to explore and discuss several possible mechanisms of IL-17A in promoting COPD progression. We discussed some specific mechanisms of IL-17A in facilitating the progression of COPD, and introduced some promising effective therapies to improve the symptom of COPD. Further, in order to encourage more studies on the novel therapeutic targets for COPD, we provided some useful novel viewpoint for clinical applications of COPD therapy.

Based on all kinds of inducements for COPD, IL-17A can exert important function to promote the inflammation in patients with COPD. Firstly, IL-17A can promote airway remodeling by increasing TGF-β1 expression and inhibiting inflammation-associated mediators or cells autophagy in inflammatory lung tissue, while HDACs can inhibit the differentiation of Th17 cells by reversing the high acetylation of core histone proteins to reduce IL-17A from TH17 cells to alleviate airway remodeling. Secondly, IL-17A can facilitate neutrophil inflammation in COPD by facilitating the expression of p53 and PAI-1 to increase CXCL1, CXCL2 and CXCR2 to induce the influx of neutrophils towards nidus. Thirdly, IL-17A promotes the expression of TSLP and other pro-inflammatory mediators by activating IKK-α to drive the development of COPD. Fourthly, DCs induces $CD4^+$ T cells to differentiate toward Th17 cells to produce more IL-17A to promote inflammation, which in turn further induces the differentiation and activation of DCs, leading to enhanced inflammation response in COPD. Last but not least, elevated levels of pro-inflammatory molecules such as IL-1β, IL-6, and IL-23, induce the development of Th17 cells, which, in turn, secrete pro-inflammatory chemokines and cytokines like IL-17A. IL-17A cooperated with other molecules like IL-22 to recruit GM-CSF, CXCL8 and IL-6 to promote inflammation development. In contrast, the suppressive development of Tregs and relative anti-inflammatory molecules certainly like IL-10 damaged their strong immunosuppressive function, thus both changes further promoted inflammation as well as COPD progression. Overall, we can focus on above pathways to inhibit the inflammation of COPD.

When it comes to novel and promising drug treatments for COPD with minimum side effects, we found Bufei Yishen formula and Curcumin very potential. 48 components in BYF might act on 65 targets to exert the therapeutic effect, and the therapeutic process involved IL-17 and TNF pathways. BYF inhibited the inflammation of COPD by the way of suppressing the phosphorylation of STAT3 and promoting phosphorylation of STAT5 to promote the differentiation of Tregs but inhibit the differentiation of Th17 cells. Hence, BYF decreased the levels of pro-inflammatory cytokines such as IL-1β, IL-6, TNF-α, and IL-17A secreted by Th17 cells, but increased anti-inflammatory cytokines IL-10 secreted by Tregs in the BAL fluid. As for Curcumin, it decreased the inflammation of acute lung injury not only by promoting the expression of IL-35, increasing STAT5 proportion, but also by decreasing IL-17A in lung tissue. In conclusion, both of Bufei Yishen formula and Curcumin are novel and promising drug treatments for COPD with minimum side effects, which deserve more attentions to study.

AUTHOR CONTRIBUTIONS

XL, WJ, and SW contributed to conception and design of the study. ML, KW, and JL wrote the first draft of the manuscript. QX, YL, YH, JZ, ZY, YW, SD, WD, and MY wrote sections of the manuscript. All authors contributed to manuscript revision, read, and approved the submitted version.

FUNDING

This work was supported by National Natural Science Foundation of China (81972204), Natural Science Foundation of Guangdong Province (2019A1515011097), Innovation Program of Shenzhen (Grant No. JCYJ20180508165208399), Science and Technology Planning Project of Guangzhou (201904010089), the grant from the State Key Lab of Respiratory Disease, Guangzhou Medical University (SKLRD-Z-202002), the 111 Project (D18010) from the Ministry of Education of China, and Medical Science and Technology Research Foundation of Guangdong Province (A201944). We also thank Dr. Damiana Chiavolini for editing the manuscript.

REFERENCES

Adeloye, D., Chua, S., Lee, C., Basquill, C., Papana, A., Theodoratou, E., et al. (2015). Global and Regional Estimates of COPD Prevalence: Systematic Review and Meta-Analysis. *J. Glob. Health* 5 (2), 020415. doi:10.7189/jogh.05.020415

Anthonisen, N. R., Manfreda, J., Warren, C. P., Hershfield, E. S., Harding, G. K., and Nelson, N. A. (1987). Antibiotic Therapy in Exacerbations of Chronic Obstructive Pulmonary Disease. *Ann. Intern. Med.* 106 (2), 196–204. doi:10.7326/0003-4819-106-2-196

Anzalone, G., Albano, G. D., Montalbano, A. M., Riccobono, L., Bonanno, A., Gagliardo, R., et al. (2018). IL-17A-associated IKK-α Signaling Induced TSLP

Production in Epithelial Cells of COPD Patients. *Exp. Mol. Med.* 50 (10), 1–12. doi:10.1038/s12276-018-0158-2

Anzalone, G., Gagliardo, R., Bucchieri, F., Albano, G. D., Siena, L., Montalbano, A. M., et al. (2016). IL-17A Induces Chromatin Remodeling Promoting IL-8 Release in Bronchial Epithelial Cells: Effect of Tiotropium. *Life Sci.* 152, 107–116. doi:10.1016/j.lfs.2016.03.031

Barnes, P. J., Burney, P. G., Silverman, E. K., Celli, B. R., Vestbo, J., Wedzicha, J. A., et al. (2015). Chronic Obstructive Pulmonary Disease. *Nat. Rev. Dis. primers* 1, 15076. doi:10.1038/nrdp.2015.76

Barnes, P. J. (2016). Inflammatory Mechanisms in Patients with Chronic Obstructive Pulmonary Disease. *J. Allergy Clin. Immunol.* 138 (1), 16–27. doi:10.1016/j.jaci.2016.05.011

Bettelli, E., Carrier, Y., Gao, W., Korn, T., Strom, T. B., Oukka, M., et al. (2006). Reciprocal Developmental Pathways for the Generation of Pathogenic Effector TH17 and Regulatory T Cells. *Nature* 441 (7090), 235–238. doi:10.1038/nature04753

Bhandary, Y. P., Shetty, S. K., Marudamuthu, A. S., Ji, H. L., Neuenschwander, P. F., Boggaram, V., et al. (2013). Regulation of Lung Injury and Fibrosis by P53-Mediated Changes in Urokinase and Plasminogen Activator Inhibitor-1. *Am. J. Pathol.* 183 (1), 131–143. doi:10.1016/j.ajpath.2013.03.022

Boixeda, R., Almagro, P., Díez-Manglano, J., Cabrera, F., Recio, J., Martin-Garrido, I., et al. (2015). Bacterial Flora in the Sputum and Comorbidity In Patients With Acute Exacerbations of COPD. *Int. J. Chron. Obstruct. Pulmon. Dis.* 10, 2581–2591. doi:10.2147/copd.s88702

Chen, Y.-q., Chai, Y.-s., Xie, K., Yu, F., Wang, C.-j., Lin, S.-h., et al. (2020). Curcumin Promotes the Expression of IL-35 by Regulating Regulatory T Cell Differentiation and Restrains Uncontrolled Inflammation and Lung Injury in Mice. *Inflammation* 43 (5), 1913–1924. doi:10.1007/s10753-020-01265-2

Christenson, S. A., van den Berge, M., Faiz, A., Inkamp, K., Bhakta, N., Bonser, L. R., et al. (2019). An Airway Epithelial IL-17A Response Signature Identifies a Steroid-Unresponsive COPD Patient Subgroup. *J. Clin. Invest.* 129 (1), 169–181. doi:10.1172/JCI121087

Chung, S., Sundar, I. K., Yao, H., Ho, Y.-S., and Rahman, I. (2010). Glutaredoxin 1 Regulates Cigarette Smoke-Mediated Lung Inflammation Through Differential Modulation of IκB Kinases in Mice: Impact on Histone Acetylation. *Am. J. Physiology-Lung Cell Mol. Physiol.* 299 (2), L192–L203. doi:10.1152/ajplung.00426.2009

Cohen, A. B., Chenoweth, D. E., and Hugli, T. E. (1982). The Release of Elastase, Myeloperoxidase, and Lysozyme from Human Alveolar Macrophages. *Am. Rev. Respir. Dis.* 126 (2), 241–247. doi:10.1164/arrd.1982.126.2.241

Coulson, F. R., and Fryer, A. D. (2003). Muscarinic Acetylcholine Receptors and Airway Diseases. *Pharmacol. Ther.* 98 (1), 59–69. doi:10.1016/s0163-7258(03)00004-4

de Nijs, S. B., Fens, N., Lutter, R., Dijkers, E., Krouwels, F. H., Smids-Dierdorp, B. S., et al. (2011). Airway Inflammation and Mannitol Challenge Test in COPD. *Respir. Res.* 12 (1), 11. doi:10.1186/1465-9921-12-11

Deng, Q., Zhang, J., Gao, Y., She, X., Wang, Y., Wang, Y., et al. (2017). MLN4924 Protects Against Bleomycin-Induced Pulmonary Fibrosis by Inhibiting the Early Inflammatory Process. *Am. J. Transl. Res.* 9 (4), 1810–1821.

Dinarello, C. (1996). Biologic Basis for Interleukin-1 in Disease. *Blood* 87 (6), 2095–2147. doi:10.1182/blood.v87.6.2095.bloodjournal8762095

Dong, H., Liu, X., Zheng, W., Feng, S., Li, J., Qin, Y., et al. (2020). Three Tiaobu Feishen Formulae Reduces Cigarette Smoke-Induced Inflammation in Human Airway Epithelial Cells. *J. Tradit Chin. Med.* 40 (3), 386–392. doi:10.19852/j.cnki.jtcm.2020.03.004

El-Ghareeb, M. I., Helmy, A., Al Kazzaz, S., and Samir, H. (2019). Serum TSLP Is a Potential Biomarker of Psoriasis Vulgaris Activity. *Psoriasis (Auckl).* 9, 59–63. doi:10.2147/ptt.s212774

Eustace, A., Smyth, L. J. C., Mitchell, L., Williamson, K., Plumb, J., and Singh, D. (2011). Identification of Cells Expressing IL-17A and IL-17F in the Lungs of Patients with COPD. *Chest* 139 (5), 1089–1100. doi:10.1378/chest.10-0779

Gan, X., Li, C., Wang, J., and Guo, X. (2016). Curcumin Modulates the Effect of Histone Modification on the Expression of Chemokines by Type II Alveolar Epithelial Cells in a Rat COPD Model. *Int. J. Chron. Obstruct. Pulmon. Dis.* 11, 2765–2773. doi:10.2147/copd.s113978

Gershon, A., Croxford, R., Calzavara, A., To, T., Stanbrook, M. B., Upshur, R., et al. (2013). Cardiovascular Safety of Inhaled Long-Acting Bronchodilators in Individuals with Chronic Obstructive Pulmonary Disease. *JAMA Intern. Med.* 173 (13), 1175–1185. doi:10.1001/jamainternmed.2013.1016

Gouda, M. M., Prabhu, A., and Bhandary, Y. P. (2018a). Curcumin Alleviates IL-17A-mediated p53-PAI-1 Expression in Bleomycin-induced Alveolar Basal Epithelial Cells. *J. Cel. Biochem.* 119 (2), 2222–2230. doi:10.1002/jcb.26384

Gouda, M. M., Prabhu, A., and Bhandary, Y. P. (2018b). IL-17A Suppresses and Curcumin Up-Regulates Akt Expression Upon Bleomycin Exposure. *Mol. Biol. Rep.* 45 (4), 645–650. doi:10.1007/s11033-018-4199-3

Gouda, M. M., Shaikh, S. B., Chengappa, D., Kandhal, I., Shetty, A., and Bhandary, Y. (2018c). Changes in the Expression Level of IL-17A and P53-Fibrinolytic System in Smokers With or Without COPD. *Mol. Biol. Rep.* 45 (6), 2835–2841. doi:10.1007/s11033-018-4398-y

Halpin, D. M. G., Criner, G. J., Papi, A., Singh, D., Anzueto, A., Martinez, F. J., et al. (2021). GLOBAL STRATEGY FOR THE DIAGNOSIS, MANAGEMENT, AND PREVENTION OF CHRONIC OBSTRUCTIVE PULMONARY DISEASE (2021 REPORT). *Am. J. Respir. Crit. Care Med.* 203 (1), 24–36. Available at: https://www.dxy.cn/bbs/newweb/pc/post/44953965?replyId=45141809&page=1 (Accessed June 12, 2021). doi:10.1164/rccm.202009-3533SO

Hansen, M. J., Chan, S. P., Langenbach, S. Y., Dousha, L. F., Jones, J. E., Yatmaz, S., et al. (2014). IL-17A and Serum Amyloid A Are Elevated in a Cigarette Smoke Cessation Model Associated with the Persistence of Pigmented Macrophages, Neutrophils and Activated NK Cells. *PLoS One* 9 (11), e113180. doi:10.1371/journal.pone.0113180

Hao, R., Song, Y., Li, R., Wu, Y., Yang, X., Li, X., et al. (2019). MLN4924 Protects Against Interleukin-17a-Induced Pulmonary Inflammation by Disrupting ACT1-Mediated Signaling. *Am. J. Physiology-Lung Cell Mol. Physiol.* 316 (6), L1070–l1080. doi:10.1152/ajplung.00349.2018

He, S., Li, X., Li, R., Fang, L., Sun, L., Wang, Y., et al. (2016). Annexin A2 Modulates ROS and Impacts Inflammatory Response via IL-17 Signaling in Polymicrobial Sepsis Mice. *PLoS Pathog.* 12 (7), e1005743. doi:10.1371/journal.ppat.1005743

Herjan, T., Hong, L., Bubenik, J., Bulek, K., Qian, W., Liu, C., et al. (2018). IL-17-receptor-associated Adaptor Act1 Directly Stabilizes mRNAs to Mediate IL-17 Inflammatory Signaling. *Nat. Immunol.* 19 (4), 354–365. doi:10.1038/s41590-018-0071-9

Hogg, J. C., Chu, F., Utokaparch, S., Woods, R., Elliott, W. M., Buzatu, L., et al. (2004). The Nature of Small-Airway Obstruction in Chronic Obstructive Pulmonary Disease. *N. Engl. J. Med.* 350 (26), 2645–2653. doi:10.1056/nejmoa032158

Huang, F., Zhang, J. S., Yang, D. Y., Zhang, Y. L., Huang, J. X., Yuan, Y. C., et al. (2018). MicroRNA Expression Profile of Whole Blood Is Altered in Adenovirus-Infected Pneumonia Children. *Mediators Inflamm.* 2018, 2320640. doi:10.1155/2018/2320640

Iezzi, G., Sonderegger, I., Ampenberger, F., Schmitz, N., Marsland, B. J., and Kopf, M. (2009). CD40-CD40L Cross-Talk Integrates Strong Antigenic Signals and Microbial Stimuli to Induce Development of IL-17-producing CD4+ T Cells. *Proc. Natl. Acad. Sci. U S A.* 106 (3), 876–881. doi:10.1073/pnas.0810769106

Ito, J. T., Cervilha, D. A. B., Lourenço, J. D., Gonçalves, N. G., Volpini, R. A., Caldini, E. G., et al. (2019). Th17/Treg Imbalance in COPD Progression: A Temporal Analysis Using a CS-Induced Model. *PLoS One* 14 (1), e0209351. doi:10.1371/journal.pone.0209351

JalusicGluncic, T. (2011). What Happens With Airway Resistance (RAW) in Asthma and COPD Exacerbation. *Acta Inform. Med.* 65 (5), 270–273. doi:10.5455/medarh.2011.65.270-273

Jin, Y., Wan, Y., Chen, G., Chen, L., Zhang, M. Q., Deng, L., et al. (2014). Treg/IL-17 Ratio and Treg Differentiation in Patients with COPD. *PLoS One* 9 (10), e111044. doi:10.1371/journal.pone.0111044

Kato, K., Chang, E. H., Chen, Y., Lu, W., Kim, M. M., Niihori, M., et al. (2020). MUC1 Contributes to Goblet Cell Metaplasia and MUC5AC Expression in Response to Cigarette Smoke In Vivo. *Am. J. Physiology-Lung Cell Mol. Physiol.* 319 (1), L82–l90. doi:10.1152/ajplung.00049.2019

Khorasani, M. Y., Langari, H., Sany, S. B. T., Rezayi, M., and Sahebkar, A. (2019). The Role of Curcumin and its Derivatives in Sensory Applications. *Mater. Sci. Eng. C.* 103, 109792. doi:10.1016/j.msec.2019.109792

Kim, V., and Aaron, S. D. (2018). What Is a COPD Exacerbation? Current Definitions, Pitfalls, Challenges and Opportunities for Improvement. *Eur. Respir. J.* 52 (5), 1801261. doi:10.1183/13993003.01261-2018

Krimmer, D. I., Burgess, J. K., Wooi, T. K., Black, J. L., and Oliver, B. G. G. (2012). Matrix Proteins from Smoke-Exposed Fibroblasts Are Pro-proliferative. *Am. J. Respir. Cell Mol. Biol.* 46 (1), 34–39. doi:10.1165/rcmb.2010-0426oc

Lai, J-F., Thompson, L. J., and Ziegler, S. F. (2020). TSLP Drives Acute TH2-Cell Differentiation in Lungs. *J. Allergy Clin. Immunol.* 146 (6), 1406–1418.e7. doi:10.1016/j.jaci.2020.03.032

Lai, T., Tian, B., Cao, C., Hu, Y., Zhou, J., Wang, Y., et al. (2018). HDAC2 Suppresses IL17A-Mediated Airway Remodeling in Human and Experimental Modeling of COPD. *Chest* 153 (4), 863–875. doi:10.1016/j.chest.2017.10.031

Lee, P. W., Smith, A. J., Yang, Y., Selhorst, A. J., Liu, Y., Racke, M. K., et al. (2017). IL-23R-activated STAT3/STAT4 Is Essential for Th1/Th17-Mediated CNS Autoimmunity. *JCI Insight* 2 (17), e91663. doi:10.1172/jci.insight.91663

Lei, Y., Wang, K., Li, X., Li, Y., Feng, X., Zhou, J., et al. (2019). Cell-surface Translocation of Annexin A2 Contributes to Bleomycin-Induced Pulmonary Fibrosis by Mediating Inflammatory Response in Mice. *Clin. Sci.* 133 (7), 789–804. doi:10.1042/cs20180687

Li, Q., Sun, J., Mohammadtursun, N., Wu, J., Dong, J., and Li, L. (2019). Curcumin Inhibits Cigarette Smoke-Induced Inflammation via Modulating the PPARγ-NF-Kb Signaling Pathway. *Food Funct.* 10 (12), 7983–7994. doi:10.1039/c9fo02159k

Li, S. Y., Li, J. S., Wang, M. H., Xie, Y., Yu, X. Q., Sun, Z. K., et al. (2012). Effects of Comprehensive Therapy Based on Traditional Chinese Medicine Patterns in Stable Chronic Obstructive Pulmonary Disease: A Four-center, Open-Label, Randomized, Controlled Study. *BMC Complement. Altern. Med.* 12, 197. doi:10.1186/1472-6882-12-197

Li, X., Ye, Y., Zhou, X., Huang, C., and Wu, M. (2015). Atg7 Enhances Host Defense against Infection via Downregulation of Superoxide But Upregulation of Nitric Oxide. *J Immunol.* 194 (3), 1112–1121. doi:10.4049/jimmunol.1401958

Li, X. F., He, S. S., Li, R. P., Zhou, X. K., Zhang, S., Yu, M., et al. (2016a). *Pseudomonas aeruginosa* Infection Augments Inflammation Through miR-301b Repression of C-Myb-Mediated Immune Activation and Infiltration. *Nat. Microbiol.* 1 (10), 16132. doi:10.1038/nmicrobiol.2016.132

Li, X. F., He, S. S., Zhou, X. K., Ye, Y., Tan, S. R., Zhang, S., et al. (2016b). Lyn Delivers Bacteria to Lysosomes for Eradication through TLR2-Initiated Autophagy Related Phagocytosis. *PLoS Pathog.* 12 (1), e1005363. doi:10.1371/journal.ppat.1005363

Li, X. H., and Luan, B. (2010). Effect of Epidermal Growth Factor Receptor on Airway Remodeling in Asthmatic Mice and its Mechanism. *Zhongguo Dang Dai Er Ke Za Zhi* 12 (2), 137–140. doi:10.7666/d.y1834191

Lin, F., Nguyen, C. M.-C., Wang, S.-J., Saadi, W., Gross, S. P., and Jeon, N. L. (2004). Effective Neutrophil Chemotaxis Is Strongly Influenced by Mean IL-8 Concentration. *Biochem. Biophysical Res. Commun.* 319 (2), 576–581. doi:10.1016/j.bbrc.2004.05.029

Liu, F., Xia, Y., Parker, A. S., and Verma, I. M. (2012). IKK Biology. *Immunological Rev.* 246 (1), 239–253. doi:10.1111/j.1600-065x.2012.01107.x

Ma, H., Gao, W., Sun, X., and Wang, W. (2018). STAT5 and TET2 Cooperate to Regulate FOXP3-TSDR Demethylation in CD4(+) T Cells of Patients with Colorectal Cancer. *J. Immunol. Res.* 2018, 6985031. doi:10.1155/2018/6985031

Maneechotesuwan, K., Wongkajornsilp, A., Adcock, I. M., and Barnes, P. J. (2015). Simvastatin Suppresses Airway IL-17 and Upregulates IL-10 in Patients with Stable COPD. *Chest*. 148 (5), 1164–1176. doi:10.1378/chest.14-3138

McGeachy, M. J., Chen, Y., Tato, C. M., Laurence, A., Joyce-Shaikh, B., Blumenschein, W. M., et al. (2009). The Interleukin 23 Receptor Is Essential for the Terminal Differentiation of Interleukin 17-producing Effector T Helper Cells In Vivo. *Nat. Immunol.* 10 (3), 314–324. doi:10.1038/ni.1698

McGeachy, M. J., Cua, D. J., and Gaffen, S. L. (2019). The IL-17 Family of Cytokines in Health and Disease. *Immunity* 50 (4), 892–906. doi:10.1016/j.immuni.2019.03.021

Mi, S., Li, Z., Yang, H. Z., Liu, H., Wang, J. P., Ma, Y. G., et al. (1950). Blocking IL-17A Promotes the Resolution of Pulmonary Inflammation and Fibrosis via TGF-beta1-dependent and -independent Mechanisms. *J. Immunol.* 187 (6), 3003–3014. doi:10.4049/jimmunol.1004081

Montalbano, A. M., Riccobono, L., Siena, L., Chiappara, G., Di Sano, C., Anzalone, G., et al. (2015). Cigarette Smoke Affects IL-17A, IL-17F and IL-17 Receptor Expression in the Lung Tissue: Ex Vivo and In Vitro Studies. *Cytokine* 76 (2), 391–402. doi:10.1016/j.cyto.2015.07.013

Morishima, N., Mizoguchi, I., Takeda, K., Mizuguchi, J., and Yoshimoto, T. (2009). TGF-β Is Necessary for Induction of IL-23R and Th17 Differentiation by IL-6 and IL-23. *Biochem. biophysical Res. Commun.* 386 (1), 105–110. doi:10.1016/j.bbrc.2009.05.140

Mulero, M. C., Huxford, T., and Ghosh, G. (2019). NF-κB, IκB, and IKK: Integral Components of Immune System Signaling. *Adv. Exp. Med. Biol.* 1172, 207–226. doi:10.1007/978-981-13-9367-9_10

Murphy, D. M., Forrest, I. A., Corris, P. A., Johnson, G. E., Small, T., Jones, D., et al. (2008). Simvastatin Attenuates Release of Neutrophilic and Remodeling Factors from Primary Bronchial Epithelial Cells Derived from Stable Lung Transplant Recipients. *Am. J. Physiology-Lung Cell Mol. Physiol.* 294 (3), L592–L599. doi:10.1152/ajplung.00386.2007

Negewo, N. A., Gibson, P. G., and McDonald, V. M. (2015). COPD and its Comorbidities: Impact, Measurement and Mechanisms. *Respirology* 20 (8), 1160–1171. doi:10.1111/resp.12642

Nguyen, V., Luzina, I., Rus, H., Tegla, C., Chen, C., and Rus, V. (2012). IL-21 Promotes Lupus-like Disease in Chronic Graft-Versus-Host Disease Through Both CD4 T Cell- and B Cell-Intrinsic Mechanisms. *J. Immunol. (Baltimore, Md: 1950)* 189 (2), 1081–1093. doi:10.4049/jimmunol.1200318

Novatchkova, M., Leibbrandt, A., Werzowa, J., Neubüser, A., and Eisenhaber, F. (2003). The STIR-Domain Superfamily in Signal Transduction, Development and Immunity. *Trends Biochemical Sciences* 28 (5), 226–229. doi:10.1016/s0968-0004(03)00067-7

Nurieva, R., Yang, X. O., Martinez, G., Zhang, Y., Panopoulos, A. D., Ma, L., et al. (2007). Essential Autocrine Regulation by IL-21 in the Generation of Inflammatory T Cells. *Nature* 448 (7152), 480–483. doi:10.1038/nature05969

Perona-Wright, G., Jenkins, S. J., O'Connor, R. A., Zienkiewicz, D., McSorley, H. J., Maizels, R. M., et al. (2009). A Pivotal Role for CD40-Mediated IL-6 Production by Dendritic Cells during IL-17 Induction In Vivo. *J. Immunol.* 182, 2808–2815. doi:10.4049/jimmunol.0803553

Poole, P. J., Chacko, E., Wood-Baker, R. W., and Cates, C. J. (2006). Influenza Vaccine for Patients with Chronic Obstructive Pulmonary Disease. *Cochrane database Syst. Rev.* 1, Cd002733. doi:10.1002/14651858.CD002733.pub2

Qaseem, A., Wilt, T. J., Weinberger, S. E., Hanania, N. A., Criner, G., van der Molen, T., et al. (2011). Diagnosis and Management of Stable Chronic Obstructive Pulmonary Disease: a Clinical Practice Guideline Update from the American College of Physicians, American College of Chest Physicians, American Thoracic Society, and European Respiratory Society. *Ann. Intern. Med.* 155 (3), 179–191. doi:10.7326/0003-4819-155-3-201108020-00008

Revu, S., Wu, J., Henkel, M., Rittenhouse, N., Menk, A., Delgoffe, G. M., et al. (2018). IL-23 and IL-1β Drive Human Th17 Cell Differentiation and Metabolic Reprogramming in Absence of CD28 Costimulation. *Cel Rep.* 22 (10), 2642–2653. doi:10.1016/j.celrep.2018.02.044

Reynolds, C. J., Quigley, K., Cheng, X., Suresh, A., Tahir, S., Ahmed-Jushuf, F., et al. (2018). Lung Defense Through IL-8 Carries a Cost of Chronic Lung Remodeling and Impaired Function. *Am. J. Respir. Cell Mol. Biol.* 59 (5), 557–571. doi:10.1165/rcmb.2018-0007oc

Roos, A. B., Sandén, C., Mori, M., Bjermer, L., Stampfli, M. R., and Erjefält, J. S. (2015). IL-17A Is Elevated in End-Stage Chronic Obstructive Pulmonary Disease and Contributes to Cigarette Smoke-Induced Lymphoid Neogenesis. *Am. J. Respir. Crit. Care Med.* 191 (11), 1232–1241. doi:10.1164/rccm.201410-1861oc

Rouvier, E., Luciani, M. F., Mattéi, M. G., Denizot, F., and Golstein, P. (1993). CTLA-8, Cloned from an Activated T Cell, Bearing AU-Rich Messenger RNA Instability Sequences, and Homologous to a Herpesvirus saimiri Gene. *J. Immunol. (Baltimore, Md: 1950)* 150 (12), 5445–5456.

Rovina, N., Koutsoukou, A., and Koulouris, N. G. (2013). Inflammation and Immune Response in COPD: Where Do We Stand? *Mediators Inflamm.* 2013, 413735. doi:10.1155/2013/413735

Rutz, S., Eidenschenk, C., and Ouyang, W. (2013). IL-22, Not Simply a Th17 Cytokine. *Immunol. Rev.* 252 (1), 116–132. doi:10.1111/imr.12027

Seo, J. Y., Yu, J. H., Lim, J. W., Mukaida, N., and Kim, H. (2009). Nitric Oxide-Induced IL-8 Expression Is Mediated by NF-kappaB and AP-1 in Gastric Epithelial AGS Cells. *J. Physiol. Pharmacol. official J. Polish Physiol. Soc.* 60 (Suppl. 7), 101–106.

Shan, M., Yuan, X., Song, L.-z., Roberts, L., Zarinkamar, N., Seryshev, A., et al. (2012). Cigarette Smoke Induction of Osteopontin (SPP1) Mediates TH17 Inflammation in Human and Experimental Emphysema. *Sci. Translational Med.* 4 (117), 117ra9. doi:10.1126/scitranslmed.3003041

Shen, F., Li, N., Gade, P., Kalvakolanu, D. V., Weibley, T., Doble, B., et al. (2009). IL-17 Receptor Signaling Inhibits C/EBP by Sequential Phosphorylation of the Regulatory 2 Domain. *Sci. Signaling* 2 (59), ra8. doi:10.1126/scisignal.2000066

Song, Y., Cui, D., and Mao, P. (2000). The Potential Role of Growth Factor in the Airway wall Remodeling of a Chronic Obstructive Pulmonary Disease Rat Model and the Effects of Drugs on Them. *Zhonghua nei ke za zhi* 39 (11), 751–754. doi:10.3760/j.issn:0578-1426.2000.11.010

Soucy, T. A., Smith, P. G., Milhollen, M. A., Berger, A. J., Gavin, J. M., Adhikari, S., et al. (2009). An Inhibitor of NEDD8-Activating Enzyme as a New Approach to Treat Cancer. *Nature* 458 (7239), 732–736. doi:10.1038/nature07884

Soumelis, V., Reche, P. A., Kanzler, H., Yuan, W., Edward, G., Homey, B., et al. (2002). Human Epithelial Cells Trigger Dendritic Cell-Mediated Allergic Inflammation by Producing TSLP. *Nat. Immunol.* 3 (7), 673–680. doi:10.1038/ni805

Su, S.-a., Yang, D., Zhu, W., Cai, Z., Zhang, N., Zhao, L., et al. (2016). Interleukin-17A Mediates Cardiomyocyte Apoptosis Through Stat3-iNOS Pathway. *Biochim. Biophys. Acta (Bba) - Mol. Cel Res.* 1863 (11), 2784–2794. doi:10.1016/j.bbamcr.2016.08.013

Su, Y., Huang, J., Zhao, X., Lu, H., Wang, W., Yang, X. O., et al. (2019). Interleukin-17 Receptor D Constitutes an Alternative Receptor for interleukin-17A Important in Psoriasis-like Skin Inflammation. *Sci. Immunol.* 4 (36), eaau9657. doi:10.1126/sciimmunol.aau9657

Tiwari, N., Marudamuthu, A. S., Tsukasaki, Y., Ikebe, M., Fu, J., and Shetty, S. (2016). p53- and PAI-1-Mediated Induction of C-X-C Chemokines and CXCR2: Importance in Pulmonary Inflammation Due to Cigarette Smoke Exposure. *Am. J. Physiology-Lung Cell Mol. Physiol.* 310 (6), L496–L506. doi:10.1152/ajplung.00290.2015

van Eerd, E. A., van der Meer, R. M., van Schayck, O. C., and Kotz, D. (2016). Smoking Cessation for People with Chronic Obstructive Pulmonary Disease. *Cochrane Database Syst. Rev.* 2016 (8), CD010744. doi:10.1002/14651858.CD010744.pub2

Vargas-Rojas, M. I., Ramírez-Venegas, A., Limón-Camacho, L., Ochoa, L., Hernández-Zenteno, R., and Sansores, R. H. (2011). Increase of Th17 Cells in Peripheral Blood of Patients with Chronic Obstructive Pulmonary Disease. *Respir. Med.* 105 (11), 1648–1654. doi:10.1016/j.rmed.2011.05.017

Wang, H., Ying, H., Wang, S., Gu, X., Weng, Y., Peng, W., et al. (2015a). Imbalance of Peripheral Blood Th17 and Treg Responses in Patients with Chronic Obstructive Pulmonary Disease. *Clin. Respir. J.* 9 (3), 330–341. doi:10.1111/crj.12147

Wang, S., Xiong, L., Deng, X., Ren, W., Zhu, C., Li, C., et al. (2015b). Effects of Simvastatin on Airway Inflammation and Airway Mucus Hypersecretion in Rats with Chronic Obstructive Pulmonary Disease. *Zhonghua yi xue za zhi* 95 (22), 1726–1730. doi:10.3760/cma.j.issn.0376-2491.2015.22.005

Wang, J., Sun, W., Bond, A., Xu, C., Li, K., Ren, D., et al. (2019). A Positive Feedback Loop Between Th17 Cells and Dendritic Cells in Patients with Endplate Inflammation. *Immunological Invest.* 48 (1), 39–51. doi:10.1080/08820139.2018.1496097

Wang, K., Zhang, T., Lei, Y., Li, X., Jiang, J., Lan, J., et al. (2018a). Identification of ANXA2 (Annexin A2) as a Specific Bleomycin Target to Induce Pulmonary Fibrosis by Impeding TFEB-Mediated Autophagic Flux. *Autophagy* 14 (2), 269–282. doi:10.1080/15548627.2017.1409405

Wang, Y., Xu, J., Meng, Y., Adcock, I. M., and Yao, X. (2018b). Role of Inflammatory Cells in Airway Remodeling in COPD. *Int. J. Chron. Obstruct. Pulmon. Dis.* 13, 3341–3348. doi:10.2147/copd.s176122

Wang, W., Ye, Y., Li, J., Li, X., Zhou, X., Tan, D., et al. (2014). Lyn Regulates Cytotoxicity in Respiratory Epithelial Cells Challenged by Cigarette Smoke Extracts. *Curr. Mol. Med.* 14 (5), 663–672. doi:10.2174/1566524014666140603095027

Woodhead, M., Blasi, F., Ewig, S., Huchon, G., Ieven, M., Ortqvist, A., et al. (2005). Guidelines for the Management of Adult Lower Respiratory Tract Infections. *Eur. Respir. J.* 26 (6), 1138–1180. doi:10.1183/09031936.05.00055705

Wu, L., Chen, Y., Yi, J., Zhuang, Y., Cui, L., and Ye, C. (2020). Mechanism of Action of Bu-Fei-Yi-Shen Formula in Treating Chronic Obstructive Pulmonary Disease Based on Network Pharmacology Analysis and Molecular Docking Validation. *Biomed. Research International* 2020, 9105972. doi:10.1155/2020/9105972

Xie, Q. Q., Liu, Y., and Li, X. F. (2020). The Interaction Mechanism between Autophagy and Apoptosis in colon Cancer. *Transl. Oncol.* 13 (12), 100871. doi:10.1016/j.tranon.2020.100871

Yamamoto, Y., Verma, U. N., Prajapati, S., Kwak, Y.-T., and Gaynor, R. B. (2003). Histone H3 Phosphorylation by IKK-α Is Critical for Cytokine-Induced Gene Expression. *Nature* 423 (6940), 655–659. doi:10.1038/nature01576

Yang, C., Xue, B., Song, W., Kan, B., Zhang, D., Yu, H., et al. (2018). Reducing the Toxicity of Amphotericin B by Encapsulation Using Methoxy Poly(ethylene Glycol)-B-poly(L-Glutamic Acid-Co-L-Phenylalanine). *Biomater. Sci.* 6 (8), 2189–2196. doi:10.1039/c8bm00506k

Ye, Y., Tan, S., Zhou, X., Li, X., Jundt, M. C., Lichter, N., et al. (2015). Inhibition of P-Iκbα Ubiquitylation by Autophagy-Related Gene 7 to Regulate Inflammatory Responses to Bacterial Infection. *J. Infect. Dis.* 212 (11), 1816–1826. doi:10.1093/infdis/jiv301

Yohannes, A. M., Willgoss, T. G., and Vestbo, J. (2011). Tiotropium for Treatment of Stable COPD: A Meta-Analysis of Clinically Relevant Outcomes. *Respir. Care* 56 (4), 477–487. doi:10.4187/respcare.00852

Yu, H., Li, Q., Kolosov, V. P., Perelman, J. M., and Zhou, X. (2012). Regulation of Cigarette Smoke-Mediated Mucin Expression by Hypoxia-Inducible Factor-1α via Epidermal Growth Factor Receptor-Mediated Signaling Pathways. *J. Appl. Toxicol.* 32 (4), 282–292. doi:10.1002/jat.1679

Zhang, M., Xie, Y., Yan, R., Shan, H., Tang, J., Cai, Y., et al. (2016). Curcumin Ameliorates Alveolar Epithelial Injury in a Rat Model of Chronic Obstructive Pulmonary Disease. *Life Sci.* 164, 1–8. doi:10.1016/j.lfs.2016.09.001

Zhao, P., Li, J., Tian, Y., Mao, J., Liu, X., Feng, S., et al. (2018). Restoring Th17/Treg Balance via Modulation of STAT3 and STAT5 Activation Contributes to the Amelioration of Chronic Obstructive Pulmonary Disease by Bufei Yishen Formula. *J. Ethnopharmacology* 217, 152–162. doi:10.1016/j.jep.2018.02.023

Zheng, X., Zhang, L., Chen, J., Gu, Y., Xu, J., and Ouyang, Y. (2018). Dendritic Cells and Th17/Treg Ratio Play Critical Roles in Pathogenic Process of Chronic Obstructive Pulmonary Disease. *Biomed. Pharmacother.* 108, 1141–1151. doi:10.1016/j.biopha.2018.09.113

Zheng, Y., Wang, Z., Deng, L., Zhang, G., Yuan, X., Huang, L., et al. (2015). Modulation of STAT3 and STAT5 Activity Rectifies the Imbalance of Th17 and Treg Cells in Patients with Acute Coronary Syndrome. *Clin. Immunol.* 157 (1), 65–77. doi:10.1016/j.clim.2014.12.012

Zhou, X., Li, X., Ye, Y., Zhao, K., Zhuang, Y., Li, Y., et al. (2014). MicroRNA-302b Augments Host Defense to Bacteria by Regulating Inflammatory Responses via Feedback to TLR/IRAK4 Circuits. *Nat. Commun.* 5, 3619. doi:10.1038/ncomms4619

Zhuang, Y., Li, Y., Li, X. F., Xie, Q., and Wu, M. (2016). Atg7 Knockdown Augments Concanavalin A-Induced Acute Hepatitis through an ROS-Mediated P38/MAPK Pathway. *PloS One* 11 (3), e0149754. doi:10.1371/journal.pone.0149754

Zmijewski, J. W., Bae, H.-B., Deshane, J. S., Peterson, C. B., Chaplin, D. D., and Abraham, E. (2011). Inhibition of Neutrophil Apoptosis by PAI-1. *Am. J. Physiology-Lung Cell Mol. Physiol.* 301 (2), L247–L254. doi:10.1152/ajplung.00075.2011

Conflict of Interest: The authors declare that the research was conducted in the absence of any commercial or financial relationships that could be construed as a potential conflict of interest.

GLOSSARY

COPD Chronic obstructive pulmonary disease
BYF Bufei Yishen formula
TCM Traditional Chinese Medicine
WHO World Health Organization
IL-17A Interleukin-17 A
RORγ retinoic acid receptor-related orphan nuclear receptor γ
TIR Toll/Il-1 Receptor
TRAF TNF receptor associated factor
NF-κB nuclear factor kappa-B
MAPKs mitogen-activated protein kinases
Till Toll/IL-11R-like loop
CBAD C/EBP-β activating domain
Erk extracellular signal-regulated kinase
FEV1 forced expiratory volume in 1 s
FVC forced vital capacity
DCs dendritic cells
EGF epidermal growth factor
CS cigarette smoke
ECM extracellular matrix
HDAC Histone Deacetylase
PAI plasminogen activator inhibitor
HSs healthy smokers
HCs healthy control subjects
G-CSF Granulocyte Colony-Stimulating Factor
NE neutrophil elastase
TSLP Thymic stromal lymphopoiesis
ISS induced sputum supernatants
Ab antibody
Ac-His H3 acetylation of histone H3
CBP CREP-binding protein
HAT histone acetyltransferase
FOXP fork head/winged helix transcription factor
iNOS inducible nitric oxide synthase
NO inducible nitric oxide synthaseNOnitric oxide
MIP macrophage inflammatory protein
ACP American College of Physicians
ACCP American College of Chest Physicians
ATS American Thoracic Society
ERS European Respiratory Society
LAMAs long-acting muscarinic antagonists
LABAs long-acting β2-agonists
STAT3 signal transducer and activator of transcription-3
PPARγ peroxisome proliferators-activated receptor γ
NAE NEDD8-activating enzyme
BALF bronchoalveolar lavage fluid

frontiers in Pharmacology

ORIGINAL RESEARCH
published: 30 July 2021
doi: 10.3389/fphar.2021.719785

EGFR-IL-6 Signaling Axis Mediated the Inhibitory Effect of Methylseleninic Acid on Esophageal Squamous Cell Carcinoma

Yu Wang, Xianghe Liu, Guanghui Hu, Chenfei Hu, Yang Gao, Miaomiao Huo, Hongxia Zhu, Mei Liu and Ningzhi Xu**

Laboratory of Cell and Molecular Biology and State Key Laboratory of Molecular Oncology, National Cancer Center/National Clinical Research Center for Cancer/Cancer Hospital, Chinese Academy of Medical Sciences and Peking Union Medical College, Beijing, China

OPEN ACCESS

Edited by:
Zhaogang Yang,
University of Texas MD Anderson Cancer Center, United States

Reviewed by:
Shiyan Dong,
Jilin University, China
Yifan Ma,
The Ohio State University, United States

***Correspondence:**
Mei Liu
liumei@cicams.ac.cn
Ningzhi Xu
xuningzhi@cicams.ac.cn

Specialty section:
This article was submitted to Inflammation Pharmacology, a section of the journal Frontiers in Pharmacology

Received: *03 June 2021*
Accepted: *13 July 2021*
Published: *30 July 2021*

Citation:
Wang Y, Liu X, Hu G, Hu C, Gao Y, Huo M, Zhu H, Liu M and Xu N (2021) EGFR-IL-6 Signaling Axis Mediated the Inhibitory Effect of Methylseleninic Acid on Esophageal Squamous Cell Carcinoma. Front. Pharmacol. 12:719785. doi: 10.3389/fphar.2021.719785

Epidemiological and experimental evidence indicate that selenium is associated with a reduced risk of some cancers, including esophageal cancer. However, the exact mechanism is still unclear. In the present study, we used esophageal squamous cell carcinoma (ESCC) cell lines and animal models to explore the anti-cancer mechanism of methylseleninic acid (MSA). Firstly, MSA treatment dramatically attenuated Epidermal Growth Factor Receptor (EGFR) protein expression but did not alter mRNA levels in ESCC cells. On the contrary, EGFR overexpression partly abolished the inhibitory effect of MSA. With a microRNA-array, we found MSA up-regulated miR-146a which directly targeted EGFR, whereas miR-146a inhibitor antagonized MSA-induced decrease of EGFR protein. We further used 4-nitroquinoline-1-oxide (4NQO)-induced esophageal tumor mice model to evaluate the inhibitory effect of MSA *in vivo*. MSA treatment significantly decreased the tumor burden and EGFR protein expression in tumor specimens. Furthermore, MSA treatment inhibited EGFR pathway and subsequntly reduced Interleukin-6 (IL-6) secretion in the supernatant of cancer cell lines. MSA-induced IL-6 suppression was EGFR-dependent. To further evaluate the association of IL-6 and the anti-tumor effect of MSA on esophageal cancer, we established the 4NQO-induced esophageal tumor model in IL-6 knock-out (IL-6 KO) mice. The results showed that IL-6 deficiency did not affect esophageal tumorigenesis in mice, but the inhibitory effect of MSA was abolished in IL-6 KO mice. In conclusion, our study demonstrated that MSA upregulated miR-146a which directly targeted EGFR, and inhibited EGFR protein expression and pathway activity, subsequently decreased IL-6 secretion. The inhibitory effect of MSA on esophageal cancer was IL-6 dependent. These results suggested that MSA may serve as a potential drug treating esophageal cancer.

Keywords: MSA, ESCC, EGFR, miR-146a, IL-6

INTRODUCTIONS

Selenium (Se), an essential and unique trace element, plays a key role in human health and disease. Schwartz and Foltz found selenium prevented liver necrosis in rats in 1950s (Schwarz and Foltz, 1958), thereafter, benefits of selenium in human health have been rapidly recognized. Epidemiologic studies suggested that serum selenium levels inversely correlated with cancer risk (Willett et al., 1983). A significantly inverse correlation was reported between serum selenium levels and the incidence of esophageal squamous cell carcinoma (ESCC) in Linxian, China, an area with high incidence of esophageal cancer (Mark et al., 2000). Furthermore, selenomethionine possessed a protective effect among subjects with mild esophageal squamous dysplasia at baseline (Limburg et al., 2005).

Several selenium compounds have been shown to selectively target tumour cells (Ghose et al., 2001; Nilsonne et al., 2006), thus making selenium promising to be an antitumour drug. Chemical forms and doses are key factors affected selenium effectiveness as anti-cancer agents. Among these forms, Monomethylselenol is a highly reactive species and probabaly the most efficient compound to induce apoptosis in malignant cells. Methylseleninic acid (MSA) is a synthetic selenium compound acting as an immediate precursor of methylselenol (Ip et al., 2000; Wallenberg et al., 2014). The anticancer effects of MSA have been evident in human lung (Poerschke et al., 2008), prostate (Jiang et al., 2001; Jiang et al., 2002; Lee et al., 2006; Li et al., 2007), breast cancer (Jariwalla et al., 2009). Moreover, MSA considerably reduced tumor growth in prostate and colon cancer xenograft models, but did not induce animal weight loss or other signs of systemic toxicity (Lee et al., 2006; Wang et al., 2009; Zeng and Wu, 2015). However, the exact mechanism of MSA in the prevention of esophageal carcinogenesis is still unclear.

Epidermal growth factor receptor (EGFR), a tyrosine kinases receptor (RTK) of ErbB family, is over-expressed in some cancers (Salomon et al., 1995; Mendelsohn and Baselga, 2000), including esophageal squamous cell carcinoma (ESCC) (Hanawa et al., 2006; Wang et al., 2013; Shang et al., 2014). High EGFR expression was associated with invasion, metastasis and poor prognosis (Wang et al., 2013). EGFR activation stimulates several pathways as RAS/RAF/MEK/ERK, PI3K/AKT, Src kinases, and STAT signaling (Lemmon and Schlessinger, 2010). Interleukin-6 (IL-6) is a key inflammatory cytokine participating in inflammation-associated carcinogenesis. IL-6 is also a target of STAT3, which serves as an important component of EGFR downstream signaling (Schafer and Brugge, 2007; Heikkilä et al., 2008). IL-6 was reported to positively associate with angiogenesis, EMT, and poor prognosis in esophageal cancer (Chen et al., 2013; Chen et al., 2014). Rooprai *et al* reported that selenium downregulated EGFR mRNA levels in human biopsy-derived glima cells (Rooprai et al., 2007). Seleno-L-methionine (SeMet) reduced EGFR transcription and protein stability in human lung cancer cell lines (Shin et al., 2007). These two studies provided clues that selenium may affect EGFR expression, but the mechanism is unclear. Recent studies implied that inhibiting EGFR pathway in cancer cells modulated cytokine secretion (Zhang et al., 2016; Suh et al., 2017). Our previous studies have demonstrated that MSA inhibited cell growth and induced apoptosis in ESCC cells by attenuating β-catenin/TCF pathway and modulating HDAC activity (Zhang et al., 2010; Hu et al., 2015). Whether EGFR was involved in the inhibitory effect of MSA have not been studied.

In the present study, we firstly verified that MSA decreased the incidence of esophageal tumor formation in 4NQO-induced mice model. We further the mechanism and found that MSA downregulated EGFR by inducing miR-146a and subsequently inhibited activation of EGFR pathway. MSA decreased the secretion of IL-6. These results indicated that the inhibitory effect of MSA in ESCC was IL-6 dependent.

MATERIALS AND METHODS

Cell Culture and Transfections

The KYSE series was kindly provided by Dr. Yutaka Shimada (Kyoto University, Kyoto, Japan). KYSE150, KYSE510 were cultured in RPMI1640 (Bioroc™, China) containing 10% fetal bovine serum (FBS) and supplemented with 1% penicillin/streptomycin at 37°C with 5% CO_2. Lipofectamine 3000 transfection reagent (Invitrogen, Carlsbad, CA, United States) was used for transfection according to the protocol provided by the manufacturer. Antagomir-146a was synthesized from Ribo Biotechnology (Guangzhou, China). pcDNA6-EGFR plasmid was provided by Mien-Chie Hung (Addgene plasmid # 42665) (Hsu and Hung, 2007). EGFR small interfering RNA (siRNA) (NM_005228, sequence: 5'AGCUAUGAGAUGGAGGAAGACGGCG3') was purchased from Integrated DNA Technologies (IDT, Coralville, IA, United States).

Cell Viability Analysis

Cells were seeded into 96-well plate by 2×10^3 per well, incubated overnight, and then treated with MSA (541281, Sigma) at indicated concentrations. Cell viability was assessed every 24 h for 3 days using the CCK8 assay (Dojindo, Kumamoto, Japan). The detailed procedure was described previously (Pan et al., 2018).

Colony Formation

KYSE 150 and KYSE 510 cells were seeded into six-well plates by 500 per well, respectively. The experiment was performed as previously decribed (Liu et al., 2018).

TaqMan Real-Time PCR microRNA Array

The differentially expressed miRNAs in KYSE 150 cells treated with or without MSA were identified by TaqMan Real-time PCR microRNA Array A (V2.0) (Applied Biosystems, CA). All reactions were performed according to the manufactures' protocol as described previously (Wang et al., 2015). The data was analyzed by using the SDS 2.0.1 software (automatic baseline, threshold 0.2) and Data Assist v2.0 software (Applied Biosystems, CA). U6 was used as endogenous control for miRNA expression analysis.

Quantitative Real-Time PCR

The expression of EGFR, IL-6 mRNAs was measured by using qRT-PCR. Total RNA extraction and reverse transcription were performed as described (Yang et al., 2020). qPCR was performed with SYBR Green PCR reagents (Applied Biosystems). GAPDH was used as the control gene. The primers used were as follows: GAPDH, 5'GCTCCTCCTGTTCGACAGTCA3'/5'ACCTTC CCCATGGTGTCTGA3'; EGFR, 5'AGGCACGAGTAACAA GCTCAC3'/5'ATGAGGACATAACCAGCCACC3'; IL-6, 5'ACTCACCTCTTCAGAACGAATTG3'/5' CCATCTTTG GAAGGTTCAGGTTG3'.

For miRNA analysis, reverse transcription and stem-loop real-time RT-PCR were performed as described (Chen et al., 2005). For normalization, U6 was used as endogenous control.

All the quantitative real-time PCR of each sample was performed in triplicate on StepOnePlus™ Real-Time PCR System (Applied Biosystems, Carlsbad, CA, United States) and analyzed with StepOne Software.

Western Blot

Cells were harvested and washed in PBS and lysed in RIPA buffer (9806, Cell Signaling Technology). Western blot analysis was performed by using the conventional protocols as described previously (Ma et al., 2016). Primary antibodies were used including EGFR (sc-03, Santa Cruz Biotechnology), phospho-EGFR (Tyr1068) (3777, Cell Signaling Technology), phospho-Stat3 (Tyr705) (9145, Cell Signaling Technology), Stat3 (9132, Cell Signaling Technology), phospho-Akt (Ser473) (9271, Cell Signaling Technology), Akt (9272, Cell Signaling Technology), GAPDH (60004-1-Ig, Proteintech). After extensively washed, the membranes were then incubated with secondary antibodies (Zhongshan Golden Bridge Biotechnology Company, Beijing, China) for 1 h at room temperature. Signals were detected using enhanced chemiluminescence (Engreen, Beijing, China). The bands intensities were analyzed using ImageJ software.

Animal Experiments

IL-6^{tm1Kopf} mice, which are IL-6 gene-knockout (IL-6 KO) mice, were purchased from Model Animal Research Center of Nanjing University. 6-week-old C57BL/6 J mice and IL-6 KO mice were used for establishing the 4-nitroquinoline 1-oxide (4NQO)-induced esophageal tumor model. The carcinogen 4NQO (N8141-5G, Sigma) stock solution was prepared in propylene glycol at 5 mg/ml and stored at 4°C and added to the drinking water at a concentration of 100 μg/ml (Tang et al., 2004). After 12 weeks of the carcinogen treatment, mice were randomly divided into the experimental group and the control group and received drinking water with or without MSA, respectively. The MSA stock solution was prepared in ddH_2O at 0.04 g/ml and added to the drinking water for the mice at the concentration of 0.02 mg/ml. With MSA treatment or not for 12 weeks, mice were sacrificed and whole esophagi were opened longitudinally, and tumors were counted and tumor volumes were calculated according to the formula Length×Width^2×0.5. Tissues were fixed overnight in 4% paraformaldehyde, paraffinembedded and sectioned. All animal experiments were approved by the Institutional Animal Care and Use Committee (IACUC) of the Cancer Hospital, Chinese Academy of Medical Science.

Cytokine Antibody Array and ELISA Analysis

KYSE150 and KYSE510 were treated with MSA (2 and 5 μM, respectively) for 24 h, then cells were digested and reseeded in 100 mm dish (1.2×10^6 cells/dish) with the same volume medium without fetal bovine serum, 24 h later, collected the conditioned media for the cytokine antibody array. Cytokine antibody array (Raybiotech) was performed according to manufacturer's protocol. The complete array maps (AAH-CYT-G5 Array 5) can be found at https://www.raybiotech.com/human-cytokine-array-g5-4/.

According to the manufacturer's protocols, human IL-6 levels in the supernatant and mouse IL-6 levels in the serum were measured by ELISA Kits (#D6050 and #M6000B, R&D Systems), respectively.

Immunohistochemistry

Sections of 5 μm thickness were deparaffinized in xylene and rehydrated in graded ethanol. Antigen retrieval was carried out in 10 mM sodium citrate buffer (pH 6.0). The endogenous peroxidase activity was quenched by 3% hydrogen peroxide for 20 min, and then the slides was blocked by 5% BSA for 1 h to avoid nonspecific staining. The subsequent immunostaining were performed as described previously (Wang et al., 2016). The primary antibody against EGFR (sc-03-G, 1:1,000, Santa Cruz Biotechnology), PCNA (sc-7907, 1:1,000, Santa Cruz Biotechnology) CD31 (77699, 1:1,000, Santa Cruz Biotechnology) was used. We also performed histological analyses by using H&E staining.

Statistical Analysis

Data with error bars were shown as mean ± SD. The two-tailed Student's *t*-test was performed to analyze the significance of differences between treatment and control group. $p < 0.05$ was designated statistically significant. GraphPad Prism software was used to do the calculations.

REAULTS

EGFR Mediated the Inhibitory Effect of MSA in ESCC Cells

We found MSA significantly supressed the growth of KYSE150 and KYSE510 cells (**Figure 1A**), consistant with our previous reports (Zhang et al., 2010; Hu et al., 2015). To better understand the molecular mechanisms by which MSA inhibits tumor cell growth, we performed RNA sequencing (RNA-seq) on KYSE150 and KYSE510 cells treated with or without MSA, respectively. The results revealed 465 commonly differentially expressed genes (Fold change ≥ 2, false discovery rate (FDR) < 0.001) (**Supplementary Figure S1A**). KEGG pathway analysis reported a number of enriched terms, such as PI3K-Akt signaling pathway, MAPK signaling pathway and Ras signaling pathway (**Supplementary Figure S1B**). Results indicated that MSA may affect the EGFR pathway. To determine whether EGFR could be supressed by MSA treatment, Western blotting were

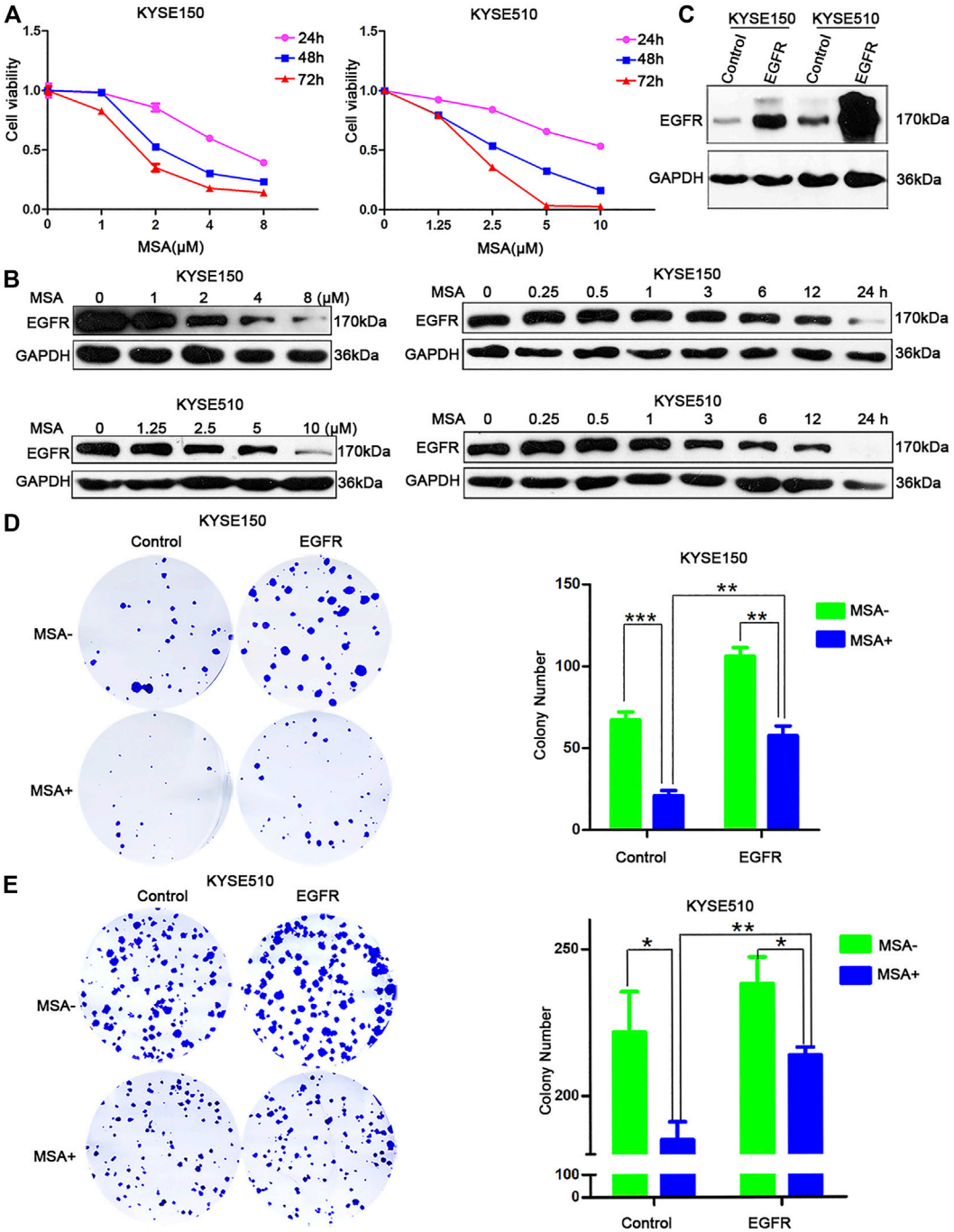

FIGURE 1 | EGFR mediated the inhibitory effect of MSA in ESCC cells. **(A)** Growth inhibition of MSA were measured by CCK8 assay in KYSE150 and KYSE510 cells. Cells were treated with the indicated concentration of MSA for 24, 48 and 72 h, respectively. Data are represented as mean ± SD, *n* = 3. **(B)** KYSE150 and KYSE510 cells were treated with MSA at different concentrations for 24 h (left), or treated with a fixed concentration (2 μM for KYSE150, 5 μM MSA for KYSE510) at different time points (right) and harvested. EGFR protein levels were evaluated by western blotting. GAPDH was used as internal control. **(C)** KYSE150 and KYSE510 cells were transfected with EGFR expression plasmid or the empty control plasmid, and then treated with or without MSA for 24 h, respectively. EGFR protein levels were evaluated by western blotting. GAPDH was used as internal control. **(D,E)** Colony formation assay of KYSE150 **(D)** and KYSE510 **(E)** transfected with EGFR expression plasmid or the empty control plasmid, 12 h afer transfection, the cells were digested, reseeded and treated with or without MSA (1 μM for KYSE150, 2.5 μM for KYSE510) for 9 days, respectively. Results are shown as mean ± SD, *n* = 3.

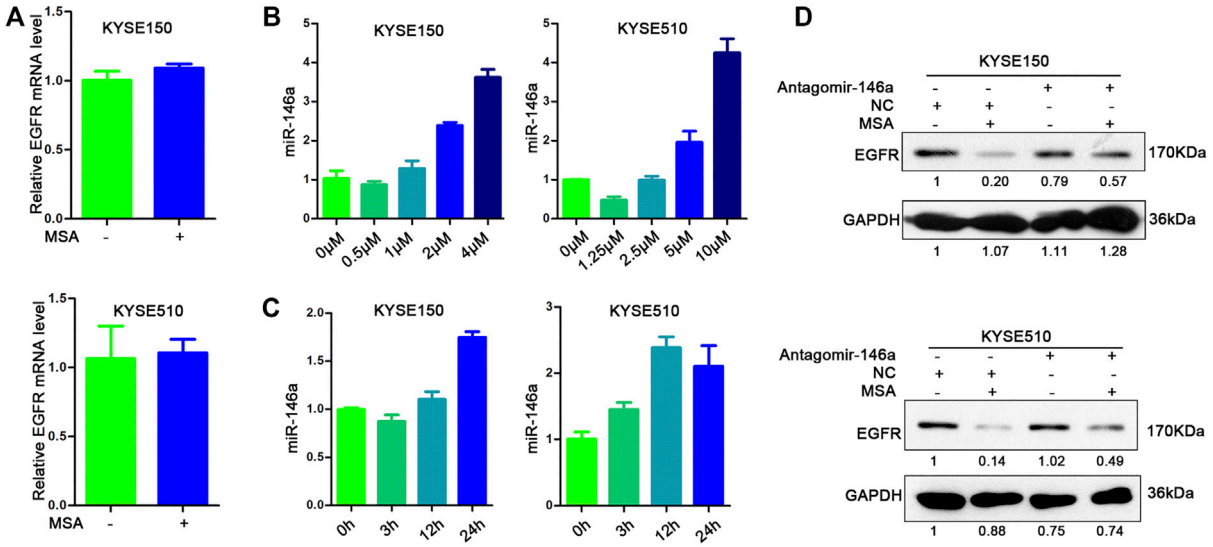

FIGURE 2 | MSA down-regulated EGFR via up-regulating miR-146a. **(A)** KYSE150 and KYSE510 cells were treated with MSA for 24 h (2 and 5 μM, respectively); EGFR mRNA was determined by quantitative real-time PCR. Values are normalized to the untreated cells. **(B,C)** miR-146a expression was detected by TaqMan Real-time PCR in KYSE150 and KYSE510 cells treated with MSA at different concentration for 24 h **(B)** or treated with a fixed concentration (2 μM for KYSE150, 5 μM for KYSE510) at different time points as indicated. **(C)**. U6 was used as the endogenous control. Values are normalized to the corresponding untreated cells, respectively. Bars represent the mean ± SD ($n = 3$) for each treatment. **(D)** KYSE150 and KYSE510 cells transfected with a negative control (NC) or antagomir-146a with or without MSA treatment for 24 h (2 μM for KYSE150 and 5 μM for KYSE510) were harvested and EGFR levels were determined by western blotting. GAPDH was used as internal control.

performed in KYSE150 and KYSE510 cells treated with or without MSA, respectively. Interestingly, we found MSA reduced EGFR protein level in a dose- and time-dependent manner (**Figure 1B**).

Furthermore, to examine whether MSA suppressed cell growth by downregulating EGFR in ESCC cells, KYSE150 and KYSE510 cells were transfected with EGFR expression plasmid or the empty control plasmid (**Figure 1C**), and then treated with or without MSA, respectively. The results revealed that EGFR overexpression could promote colony formation of ESCC cells and partly abolish the inhibitory effect of MSA (**Figures 1D,E**).

MSA Down-Regulated EGFR Via Up-Regulating miR-146a

As mentioned above, MSA treatment could downregulate EGFR protein, but didn't influence the mRNA level of EGFR in both KYSE150 and KYSE510 cells (**Figure 2A**). Next, we compared the expression of microRNAs in KYESE150 cells treated with or without MSA by TaqMan Real-time PCR microRNA array. The Analysis of the array data showed that 21 microRNAs changed more than 2-fold in expression between the two samples (**Supplementary Table 1**). Among these 21 miRNAs, we found miR-146a could directly target EGFR, which have been reported (Li et al., 2010; Kogo et al., 2011). So we chose miR-146a to further detected. As showed in **Figures 2B,C**, miR-146a showed a dose- and time-dependent increase with MSA treatment. And, antagomir-146a could attenuate MSA-induced EGFR down-regulation (**Figure 2D**). These findings demonstrated that MSA could down-regulate EGFR via inducing miR-146a.

MSA Inhibited Tumor Growth of Esophageal Cancer *In Vivo*

To explore the anti-tumor activity of MSA *in vivo*, we constructed a 4NQO-induced esophageal tumor mice model using C57 mice (Tang et al., 2004). After 12 weeks of carcinogen exposure, the mice were subjected to MSA treatment for another 12 weeks (**Figure 3A**). The results showed that the MSA-treated mice had almost the same body weight, less tumors and lower tumor burden compared with the 4NQO group without MSA treatment (**Figures 3B,C**). To assess whether MSA could decrease the expression of EGFR *in vivo*, we investigated EGFR expression in tumor tissues by IHC staining. As shown in **Figure 3D**, MSA treatment indeed supressed EGFR expression *in vivo*. We also detected the expression of Proliferating Cell Nuclear Antigen (PCNA). As expected, MSA could attenuate the expression of PCNA in MSA treated mice compared with the control mice.

MSA Inhibited IL-6 Production

As shown above, MSA could down-regulate EGFR protein. Next, we examined the downstream signaling molecules of EGFR pathway. As **Figure 4A** showed, the phosphorylation of STAT3, AKT were down-regulated upon MSA treatment. All these indicated that MSA could inhibit the activation of EGFR pathway in ESCC cells. We wonder whether MSA could affect the cytokine secretory. To this end, KYSE150 and KYSE510 cells were treated with MSA or not for 24 h, then the cells were digested and reseeded at the same amount in RPMI1640 without fetal bovine serum, another 24 h later, the supernatant was harvested and tested by the cytokine array. Among the 80

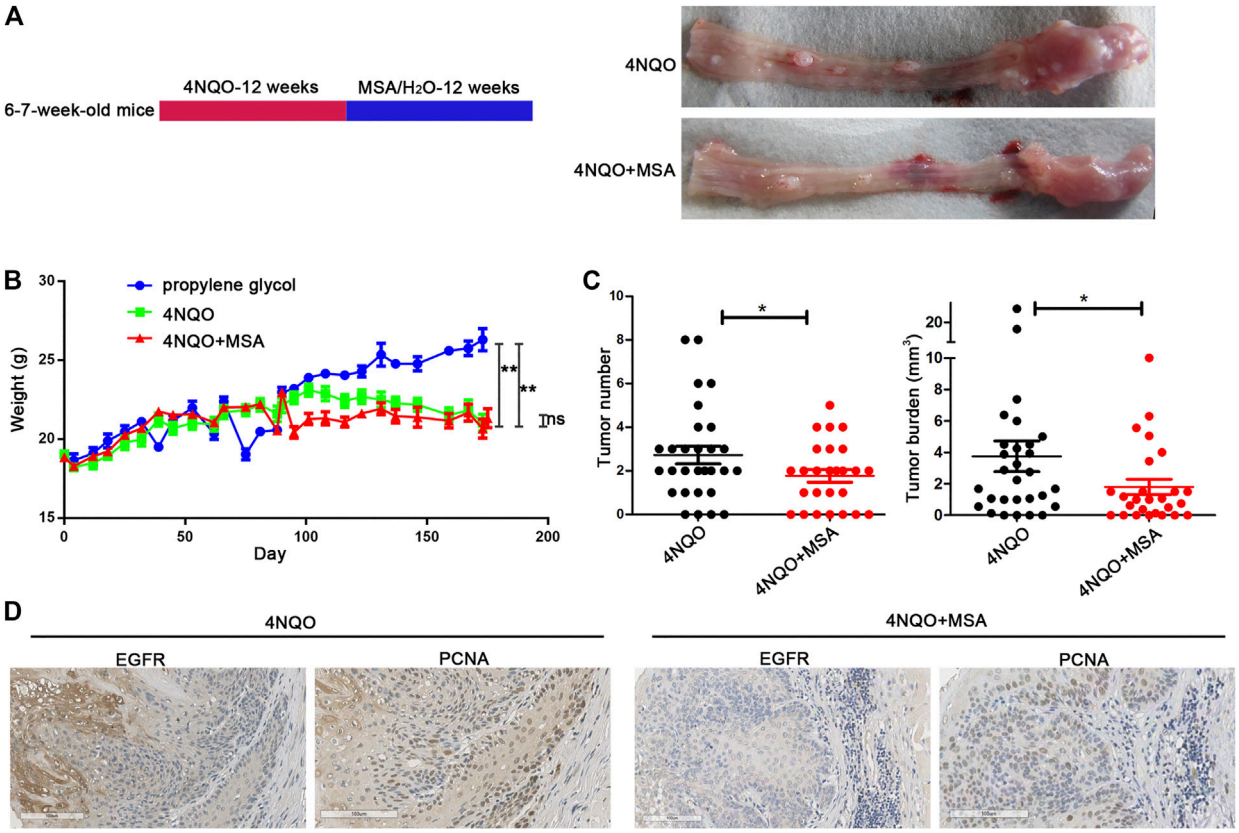

FIGURE 3 | MSA inhibited esophageal tumor growth *in vivo*. **(A)** Schematic representation of 4NQO mice model. 6–7 week-old mice were given drinking water containing 4NQO (100 μg/ml) for 12 weeks. Then mice were randomly divided into two group with treatment of drinking water containing MSA (0.02 mg/ml) or pure water. Twelve weeks later, the mice were sacrificed for esophageal tumor analysis. **(B)** Body weight of mice were measured. Data are expressed as mean ± SD. $^{**}p < 0.01$; ns, non significant. **(C)** Tumor number and tumor budern in the mice esophagi. C57+4NQO ($n = 29$), C57+4NQO + MSA (n = 26), bars represent the mean ± SD for each group. $^{*}p < 0.05$. **(D)** Representative photomicrographs of immunostaining of EGFR and PCNA in the mice esophageal tissue.

cytokines, 7 cytokines displayed a significant difference with more than 1.5-fold in expression both in the two cell lines treated with or without MSA, respectively. The levels of IL-1a and MIP-3a were higher and IL-6, FGF9, GDNF, NT3, and BLC were lower in the supernatant of MSA-treated cells than that of the untreated cells (**Figure 4B**). It was already well known that IL-6 regulates immune and inflammatory responses and is involved in tumor progression (Hodge et al., 2005; Iliopoulos et al., 2009). So we firstly chose IL-6 to further study. We evaluated the levels of IL-6 at transcription levels. As shown in **Figure 4C**, IL-6 mRNA levels were down-regulated in the cells treated with MSA. In accord with the cytokine array, ELISA results also showed a significant decrease of IL-6 in the supernant of ESCC cells with MSA treatment (**Figure 4D**). Furthermore, we also measured the IL-6 level in the mouse serum by the ELISA Kit (#M6000B, R&D Systems). Although the serum level of IL-6 in 4NQO-induced mice was a little lower than the minimum detectable amount (7.8 pg/ml), it was higher than the levels of IL-6 in the serum of 4NQO-induced mice with MSA treatment and normal C57 mice (data not shown). Even so, our results may provide clues to imply that MSA could inhibit IL-6 production both *in vitro* and *in vivo*.

EGFR Involved in MSA-Induced IL-6 Downregulation

We next examined whether MSA-induced IL-6 downregulation by depending on EGFR-mediated signal transduction. After transfection with pcDNA6, pcDNA6-EGFR or EGFR siRNA for 48 h in KYSE150 and KYSE510 cells, EGFR mRNA and protein were detected. The results revealed that EGFR expression plasmid could significantly upregulate EGFR mRNA and protein levels, and EGFR siRNA could efficaciously downregulate EGFR mRNA and protein, compared to the control cells, respectively (**Figures 5A,B**). Overexpression of EGFR increased IL-6 mRNA expression in both KYSE150 and KYSE510 cells, *vice versa* (**Figure 5C**).

EGFR overexpression increased the phosphorylation of EGFR, Akt, and STAT3 signaling proteins and could partly restored the inhitory effect of MSA treatment, including the phosphorylation of EGFR, Akt, STAT3 (**Figure 5D**) and IL-6 mRNA levels in both KYSE150 and KYSE 510 cells (**Figure 5E**). We also detected the levels of IL-6 in the supernant of KYSE510 cells that overexpressed EGFR accompanied with MSA treatment or not, the result showed that EGFR overexpression indeed upregulated

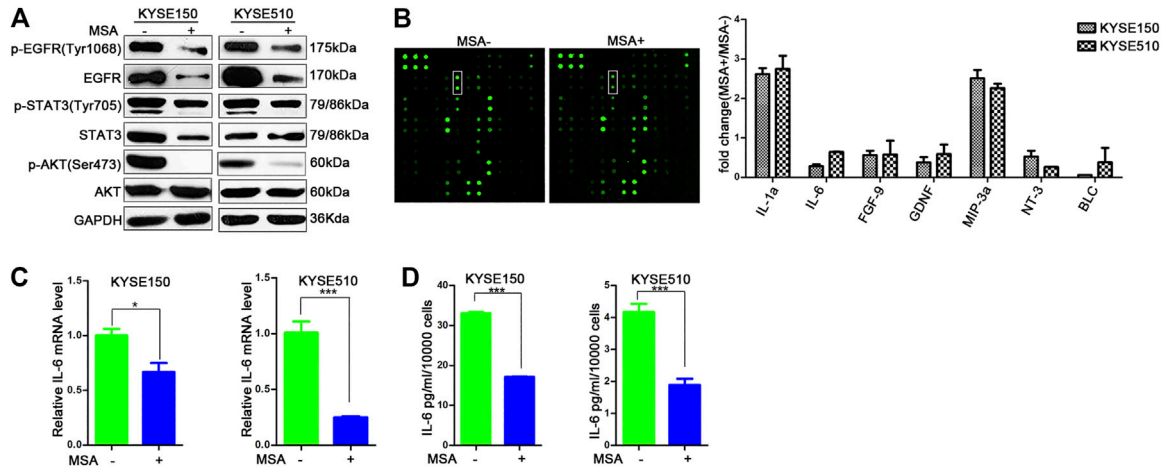

FIGURE 4 | MSA inhibits IL-6 production. **(A)** KYSE150 and KYSE510 cells were treated with MSA for 24 h (2 μM for KYSE150 and 5 μM for KYSE510), then cells were harvested and analyzed by western blotting. GAPDH was used as internal control. **(B)** Conditional media were collected and analyzed by cytokine antibody array. The value represented the average signal density ratio of MSA treatment condition media (MSA+) to the control condition media (MSA-). Mean ± SD (n = 2). **(C)** KYSE150 and KYSE510 cells were treated with or without MSA for 24 h, and the IL-6 mRNA levels were determined by q-RT-PCR. Bars represent the mean ± SD (n = 3) for each treatment. **(D)** KYSE150 and KYSE510 cells were treated with MSA for 24 h (2 μM for KYSE150 and 5 μM for KYSE510), then cells were digested and equal count of cells were reseeded with the same volume medium, 24 h later, collected the conditional media and IL-6 levels were determined by ELISA. Bars represent the mean ± SD (n = 2) for each treatment. *p < 0.05; ***p < 0.001.

IL-6 secretion and partly abolished the inhibitory effect of MSA treatment (**Figure 5F**). In addition, when we used EGF stimulation to active the EGFR pathway (**Figure 5G**), IL-6 secretion was higher in EGF-stimulated KYSE510 cells than the control cells that did not receive the EGF stimulation both in the groups with or without MSA treatment, respectively (**Figure 5H**).

IL-6 Deficiency Attenuated the Tumor Inhibitory Effect of MSA

To determine the role of IL-6 in tumorigenesis of esophageal cancer, we used IL-6 KO mice to generate esophageal cancer that induced by 4NQO. Our data showed that 4NQO-induced IL-6 KO mice formed almost the same tumors as 4NQO-induced IL-6 WT mice, indicating that lack of IL-6 may not affect tumorigenesis of esophageal cancer (**Figure 6A**). To further test the role of IL-6 in MSA-mediated inhibition of esophageal tumor growth, IL-6 KO mice were induced by 4NQO and then treated with MSA for 12 weeks. Interestingly, MSA treatment didn't reduced the tumor number of 4NQO-induced IL-6 KO mice, MSA-mediated tumor suppression was abolished (**Figures 6A,B**). However, EGFR expression still could be down-regulated in 4NQO-induced IL-6 KO mice when treated with MSA (**Figure 6C**). To test whether MSA could inhibit EGFR-IL-6 axis and subsequently affect tumor angiogenesis, the tumor tissues were evaluated the expression of the endothelial staining marker CD31 by immunohistochemistry. As shown in **Figure 6D**, MSA treatment could obviously reduce vessel density and IL-6 deficiency could attenuate the effect. All these implicated that the anti-tumor effect of MSA was at least partly dependent on IL-6.

DISCUSSION

Selenium has been recognized as a chemotherapeutic agent in human beings for more than 100 years. One of the most exciting results demonstrated that intravenous injection of colloidal suspension of erythro-selenium beta resulted in significantly improvement in carcinoma of the alimentary tract (Watson-Williams, 1919). Previous studies showed that selenium treatment could downregulate EGFR mRNA levels in human biopsy-derived glima cells (Rooprai et al., 2007) and lung cancer cell lines (Shin et al., 2007). Sun *et al* reported Se-(methyl) selenocysteine hydrochloride (MSC) could inhibit pro-inflammatory responses by inducing miR-146a in *Staphylococcus* aureus-infected mouse mastitis model (Sun et al., 2017). miR-146a have been demonstrated to target EGFR directly (Li et al., 2010; Kogo et al., 2011). Consistent with these, we found MSA could up-regulate miR-146a at a dose- and time-dependent manner in ESCC cells; when we inhibited miR-146a with antagomir-146a, MSA-induced EGFR decrease was partly reverted, indicating that MSA-induced EGFR down-regualtion was dependent on miR-146a.

As a tyrosine kinase receptor, EGFR is capable to induce STAT3 phosphorylation (Levy and Darnell, 2002). STAT3 is also a transcriptional factor of IL-6. In the present study, we found MSA treatment could decrease the phosphorylation of STAT3, and the secretion of IL-6 in ESCC cells (**Figure 4**). Previous studies have already indicated the negative correlation between selenium and IL-6. For example, Zhou *et al* reported Selenium deficiency was present in Kashin–Beck disease (KBD), a chronic joint disease with chondral destruction, and IL-6 expression was elevated in the cartilages of KBD children (Zhou et al., 2014). Pei *et al* reported that sodium selenite pretreatment blocked the transcriptional factor NF-κB activation and inhibited IL-6 production in LPS-

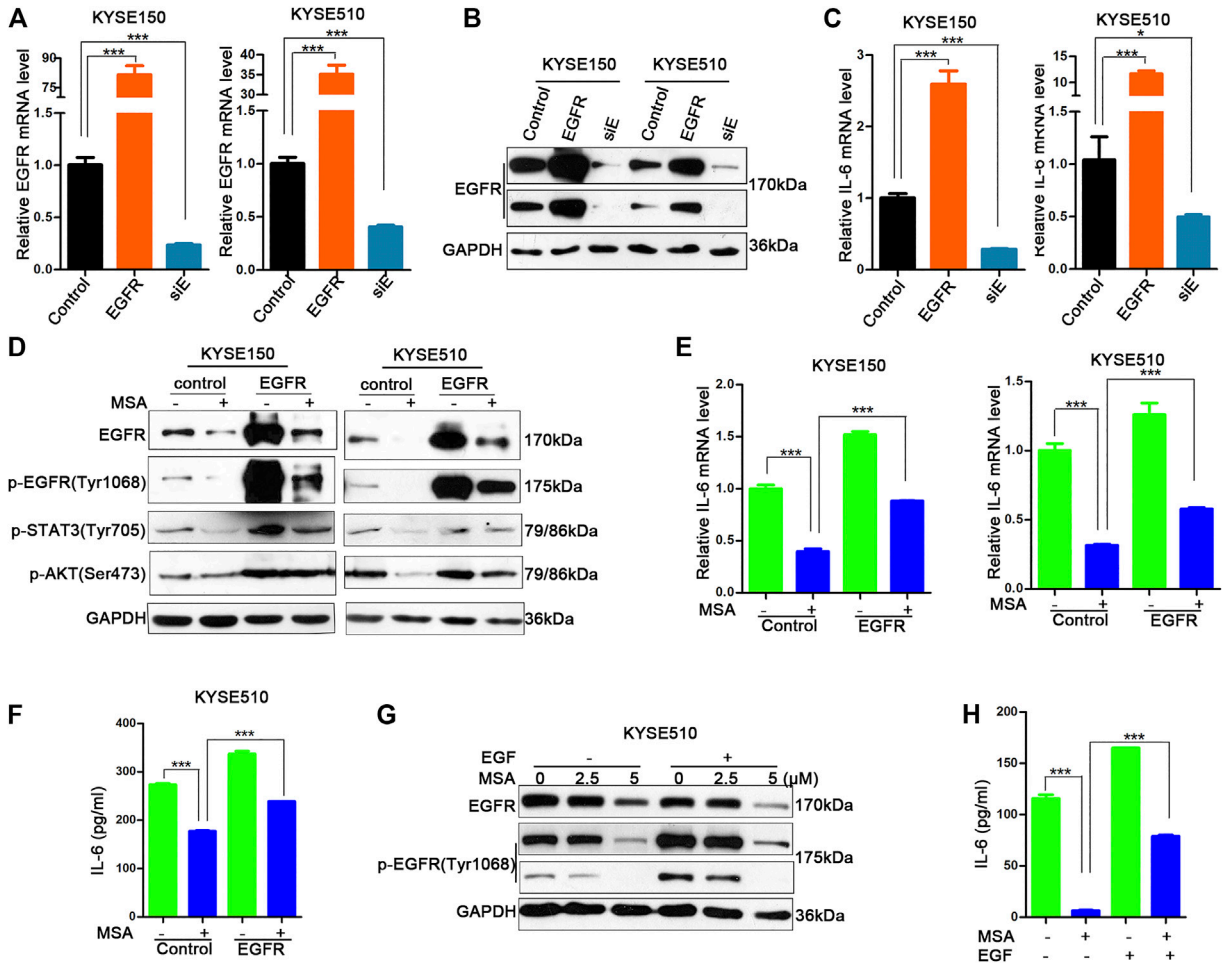

FIGURE 5 | EGFR involved in MSA-induced IL-6 downregulation. **(A–C)** KYSE150 and KYSE510 cells were transfected with pcDNA6 (control), pcDNA6-EGFR (EGFR), or EGFR siRNA (siE), respectively. The cells were harvested after 48 h and EGFR mRNA **(A)** and EGFR protein **(B)** were detected. IL-6 mRNA levels were also detected by Real-time PCR **(C)**. **(D–F)** KYSE150 and KYSE510 cells were transfected with the pcDNA6, or pcDNA6-EGFR, and then treated with or without MSA (2 μM for KYSE150, 5 μM for KYSE510), respectively. EGFR, *p*-EGFR, *p*-Akt, p-STAT3 were detected by western blotting. IL-6 mRNA was detected by real-time PCR **(E)** and IL-6 protein in the supernant of KYSE510 was deceted by ELISA **(F)**. **(G,H)** EGF (25 ng/ml) was added in the supernant of KYSE510 cells for 12 h, EGFR, *p*-EGFR (short and long exposure) were detected by western blotting **(G)**. IL-6 protein in the supernant was detected in the supernant of KYSE510 cells treated with or without MSA (5 μM) by ELISA **(H)**. Bars represent the mean ± SD (n = 3) for each treatment. ***$p < 0.001$. Control: pcDNA6; EGFR: pcDNA6-EGFR; siE: EGFR siRNA.

stimulated human PC3 cells (Pei et al., 2010). It has also been reported that MSA could inhibit tumor growth in colon cancer xenografts, and this inhibition was associated with a reduction of plasma tumor necrosis factor (TNFα)/IL-6 level (Zeng and Wu, 2015). Our findings showed that MSA treatment could inhibit IL-6 secretion, and EGFR was mediated MSA-induced IL-6 downregulation in ESCC, at least in part.

IL-6 is a cytokine that have extensive effects and its overexpression has been reported in almost all kinds of tumours (Kumari et al., 2016). Previous study showed that IL-6 is markedly associated with aggressive tumor behavior and poor outcomes in ESCC(Chen et al., 2013). The mice with IL-6 stimulation showed significantly increased myeloid derived suppressor cells (MDSCs) levels and an increased incidence of invasive esophageal tumor formation in the 4NQO-induced esophageal tumor animal model; however, blockade of IL-6 prevented induction of MDSCs and the incidence of 4NQO-induced invasive tumors (Chen et al., 2014). These data suggest that IL-6 blockade not only has direct intrinsic inhibitory effect on tumor cells, but also modulates the microenvironment toward an anti-tumor phenotype. In addition, previous study showed that selenium nanoparticles could increase the levels of cellular immunomodulatory components (granzyme B, IL-12, IFN-γ, and IL-2) to boost the immune response in mice bearing tumor exposed to crude antigens of 4T1 cells (Yazdi et al., 2015). Our experimental data showed that STAT3 activity in ESCC cells was markedly reduced when treated with MSA (**Figures 4**, **5**), it is possible that the alteration also affects the antitumor immunity induced by MSA. All these provide hints that Se has potential to be applied to cancer treatment by modulating the immune

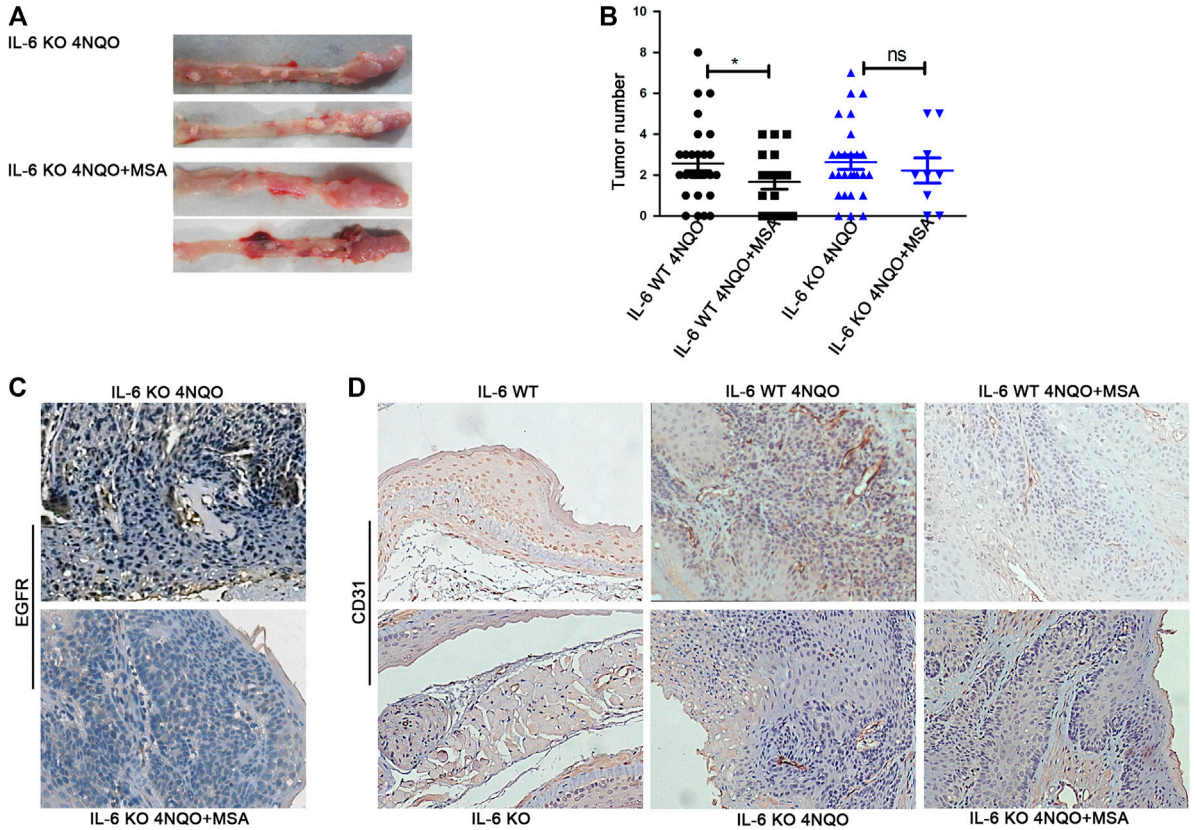

FIGURE 6 | IL-6 deficiency attenuated the tumor inhibitory effect of MSA. **(A)** The esophageal tumors of IL-6^{tm1Kopf} (IL-6 KO) mice knock-out (KO) mice treated with 4NQO (100 μg/ml) in drinking water (4NQO) or the combination of 4NQO and MSA (4NQO + MSA) for 12 weeks. **(B)** Quantification of tumor numbers in 4NQO–treated mice with or without MSA treatment both in IL-6 Wildtype (WT) (normal C57) and IL-6 KO mice. All mice were with 4NQO exposure for 12 weeks, then mice were divided into the control or MSA treatment group. IL-6 WT 4NQO (n = 28), IL-6 WT 4NQO + MSA (n = 18), IL-6 KO-4NQO (n = 27), IL-6 KO 4NQO + MSA (n = 9). Bars represent the mean ± SD for each group. *p < 0.05. **(C)**Representative photomicrographs of immunostaining of EGFR in the esophageal tumor tissues of IL-6 KO mice treated with 4NQO or the combination of 4NQO and MSA (4NQO + MSA). **(D)** IHC staining of CD31 in normal esophageal tissues of IL-6 WT and KO mice, and the tumor tissues of 4NQO mice model treated with or without MSA. Magnification 100×.

microenvironment, but the underlying mechanism needs to be further clarified.

It is well documented that angiogenesis is necessary for the continued growth of tumors. IL-6, as a well-known angiogenic inducer, has been identified to enhance endothelial cell migration directly via IL-6R or through macrophage infiltration (Nilsson et al., 2005; Izumi-Nagai et al., 2007). Coward *et al* reported the therapeutic effect of siltuximab (anti-IL-6 antibody) was accompanied by reductions in angiogenesis in ovarian cancer cells xenograft models (Coward et al., 2011). Shinriki *et al* reported anti-Interleukin-6 receptor antibody suppressed tumor angiogenesis and *in vivo* growth of human oral squamous cell carcinoma (Shinriki et al., 2009). Here, we found MSA treatment could markedly decrease the density of tumor-associated vessels in tumors of 4NQO-induced wildtype mice. Although IL-6 deficiency did not affect esophageal tumorigenesis in mice (**Figure 6**), there are less vessels in the tumor tissue of 4NQO-induced IL-6 KO mice than that in 4NQO-induced wildtype mice. All these data suggest that MSA-induced IL-6 downregulation may impair tumor angiogenesis and then suppressed tumor growth *in vivo*.

In conclusion, we showed the intriguing possibility that MSA may have therapeutic value for the treatment of ESCC. MSA could downregulate EGFR via miR-146a and decrease IL-6 secretion, lead to substantial decrease in tumor angiogenesis to inhibit ESCC cell growth.

DATA AVAILABILITY STATEMENT

The data generated in this article can be found in NCBI SRA using accession PRJNA742425.

ETHICS STATEMENT

The animal study was reviewed and approved by The Institutional Animal Care and Use Committee (IACUC) of the Cancer Hospital, Chinese Academy of Medical Science.

AUTHOR CONTRIBUTIONS

Conception and design: ML, NX. Acquisition of data: YW, XL. Analysis and interpretation of data: YW, ML. Administrative, technical, or material support: GH, CH, YG, MH, and HZ. Project administration: ML, NX. Study supervision: ML, NX. Writing original draft: YW, ML. Writing review and editing: YW, ML, and NX.

FUNDING

The funders had no role in study design, data collection and analysis, interpretation of date, or preparation of the manuscript.

This work was supported by the National Key Research & Development (R&D) Program of China (2016YFC1302103) and National Natural Science Foundation (81472561, 81972767), PR China. The funders had no role in study design, data collection and analysis, interpretation of date, or preparation of the manuscript.

SUPPLEMENTARY MATERIAL

The Supplementary Material for this article can be found online at: https://www.frontiersin.org/articles/10.3389/fphar.2021.719785/full#supplementary-material.

REFERENCES

Chen, C., Ridzon, D. A., Broomer, A. J., Zhou, Z., Lee, D. H., Nguyen, J. T., et al. (2005). Real-time Quantification of microRNAs by Stem-Loop RT-PCR. *Nucleic Acids Res.* 33, e179. doi:10.1093/nar/gni178

Chen, M.-F., Chen, P.-T., Lu, M. S., Lin, P. Y., Chen, W.-C., and Lee, K.-D. (2013). IL-6 Expression Predicts Treatment Response and Outcome in Squamous Cell Carcinoma of the Esophagus. *Mol. Cancer* 12, 26. doi:10.1186/1476-4598-12-26

Chen, M.-F., Kuan, F.-C., Yen, T.-C., Lu, M.-S., Lin, P.-Y., Chung, Y.-H., et al. (2014). IL-6-stimulated CD11b+CD14+HLA-DR− Myeloid-Derived Suppressor Cells, Are Associated with Progression and Poor Prognosis in Squamous Cell Carcinoma of the Esophagus. *Oncotarget* 5, 8716–8728. doi:10.18632/oncotarget.2368

Coward, J., Kulbe, H., Chakravarty, P., Leader, D., Vassileva, V., Leinster, D. A., et al. (2011). Interleukin-6 as a Therapeutic Target in Human Ovarian Cancer. *Clin. Cancer Res.* 17, 6083–6096. doi:10.1158/1078-0432.ccr-11-0945

Ghose, A., Fleming, J., El-Bayoumy, K., and Harrison, P. R. (2001). Enhanced Sensitivity of Human Oral Carcinomas to Induction of Apoptosis by Selenium Compounds: Involvement of Mitogen-Activated Protein Kinase and Fas Pathways. *Cancer Res.* 61, 7479–7487.

Hanawa, M., Suzuki, S., Dobashi, Y., Yamane, T., Kono, K., Enomoto, N., et al. (2006). EGFR Protein Overexpression and Gene Amplification in Squamous Cell Carcinomas of the Esophagus. *Int. J. Cancer* 118, 1173–1180. doi:10.1002/ijc.21454

Heikkilä, K., Ebrahim, S., and Lawlor, D. A. (2008). Systematic Review of the Association between Circulating Interleukin-6 (IL-6) and Cancer. *Eur. J. Cancer* 44, 937–945. doi:10.1016/j.ejca.2008.02.047

Hodge, D. R., Hurt, E. M., and Farrar, W. L. (2005). The Role of IL-6 and STAT3 in Inflammation and Cancer. *Eur. J. Cancer* 41, 2502–2512. doi:10.1016/j.ejca.2005.08.016

Hsu, S.-C., and Hung, M.-C. (2007). Characterization of a Novel Tripartite Nuclear Localization Sequence in the EGFR Family. *J. Biol. Chem.* 282, 10432–10440. doi:10.1074/jbc.m610014200

Hu, C., Liu, M., Zhang, W., Xu, Q., Ma, K., Chen, L., et al. (2015). Upregulation of KLF4 by Methylseleninic Acid in Human Esophageal Squamous Cell Carcinoma Cells: Modification of Histone H3 Acetylation through HAT/HDAC Interplay. *Mol. Carcinog.* 54, 1051–1059. doi:10.1002/mc.22174

Iliopoulos, D., Hirsch, H. A., and Struhl, K. (2009). An Epigenetic Switch Involving NF-κB, Lin28, Let-7 MicroRNA, and IL6 Links Inflammation to Cell Transformation. *Cell* 139, 693–706. doi:10.1016/j.cell.2009.10.014

Ip, C., Thompson, H. J., Zhu, Z., and Ganther, H. E. (2000). *In Vitro* and *In Vivo* Studies of Methylseleninic Acid: Evidence that a Monomethylated Selenium Metabolite Is Critical for Cancer Chemoprevention. *Cancer Res.* 60, 2882–2886.

Izumi-Nagai, K., Nagai, N., Ozawa, Y., Mihara, M., Ohsugi, Y., Kurihara, T., et al. (2007). Interleukin-6 Receptor-Mediated Activation of Signal Transducer and Activator of Transcription-3 (STAT3) Promotes Choroidal Neovascularization. *Am. J. Pathol.* 170, 2149–2158. doi:10.2353/ajpath.2007.061018

Jariwalla, R. J., Gangapurkar, B., and Nakamura, D. (2009). Differential Sensitivity of Various Human Tumour-Derived Cell Types to Apoptosis by Organic Derivatives of Selenium. *Br. J. Nutr.* 101, 182–189. doi:10.1017/S0007114508998305

Jiang, C., Wang, Z., Ganther, H., and Lu, J. (2001). Caspases as Key Executors of Methyl Selenium-Induced Apoptosis (Anoikis) of DU-145 Prostate Cancer Cells. *Cancer Res.* 61, 3062–3070.

Jiang, C., Wang, Z., Ganther, H., and Lü, J. (2002). Distinct Effects of Methylseleninic Acid versus Selenite on Apoptosis, Cell Cycle, and Protein Kinase Pathways in DU145 Human Prostate Cancer Cells. *Mol. Cancer Ther.* 1, 1059–1066.

Kogo, R., Mimori, K., Tanaka, F., Komune, S., and Mori, M. (2011). Clinical Significance of miR-146a in Gastric Cancer Cases. *Clin. Cancer Res.* 17, 4277–4284. doi:10.1158/1078-0432.ccr-10-2866

Kumari, N., Dwarakanath, B. S., Das, A., and Bhatt, A. N. (2016). Role of Interleukin-6 in Cancer Progression and Therapeutic Resistance. *Tumor Biol.* 37, 11553–11572. doi:10.1007/s13277-016-5098-7

Lee, S. O., Yeon Chun, J., Nadiminty, N., Trump, D. L., Ip, C., Dong, Y., et al. (2006). Monomethylated Selenium Inhibits Growth of LNCaP Human Prostate Cancer Xenograft Accompanied by a Decrease in the Expression of Androgen Receptor and Prostate-specific Antigen (PSA). *Prostate* 66, 1070–1075. doi:10.1002/pros.20329

Lemmon, M. A., and Schlessinger, J. (2010). Cell Signaling by Receptor Tyrosine Kinases. *Cell* 141, 1117–1134. doi:10.1016/j.cell.2010.06.011

Levy, D. E., and Darnell, J. E., Jr. (2002). Stats: Transcriptional Control and Biological Impact. *Nat. Rev. Mol. Cel Biol* 3, 651–662. doi:10.1038/nrm909

Li, G.-X., Hu, H., Jiang, C., Schuster, T., and Lü, J. (2007). Differential Involvement of Reactive Oxygen Species in Apoptosis Induced by Two Classes of Selenium Compounds in Human Prostate Cancer Cells. *Int. J. Cancer* 120, 2034–2043. doi:10.1002/ijc.22480

Li, Y., Vandenboom, T. G., 2nd, Wang, Z., Kong, D., Ali, S., Philip, P. A., et al. (2010). miR-146a Suppresses Invasion of Pancreatic Cancer Cells. *Cancer Res.* 70, 1486–1495. doi:10.1158/0008-5472.can-09-2792

Limburg, P. J., Wei, W., Ahnen, D. J., Qiao, Y., Hawk, E. T., Wang, G., et al. (2005). Randomized, Placebo-Controlled, Esophageal Squamous Cell Cancer Chemoprevention Trial of Selenomethionine and Celecoxib. *Gastroenterology* 129, 863–873. doi:10.1053/j.gastro.2005.06.024

Liu, M., An, J., Huang, M., Wang, L., Tu, B., Song, Y., et al. (2018). MicroRNA-492 Overexpression Involves in Cell Proliferation, Migration, and Radiotherapy Response of Cervical Squamous Cell Carcinomas. *Mol. Carcinog* 57, 32–43. doi:10.1002/mc.22717

Ma, K., Xu, Q., Wang, S., Zhang, W., Liu, M., Liang, S., et al. (2016). Nuclear Accumulation of Yes-Associated Protein (YAP) Maintains the Survival of Doxorubicin-Induced Senescent Cells by Promoting Survivin Expression. *Cancer Lett.* 375, 84–91. doi:10.1016/j.canlet.2016.02.045

Mark, S. D., Qiao, Y. L., Dawsey, S. M., Wu, Y. P., Katki, H., Gunter, E. W., et al. (2000). Prospective Study of Serum Selenium Levels and Incident Esophageal and Gastric Cancers. *J. Natl. Cancer Inst.* 92, 1753–1763. doi:10.1093/jnci/92.21.1753

Mendelsohn, J., and Baselga, J. (2000). The EGF Receptor Family as Targets for Cancer Therapy. *Oncogene* 19, 6550–6565. doi:10.1038/sj.onc.1204082

Nilsonne, G., Sun, X., Nyström, C., Rundlöf, A.-K., Potamitou Fernandes, A., Björnstedt, M., et al. (2006). Selenite Induces Apoptosis in Sarcomatoid Malignant Mesothelioma Cells through Oxidative Stress. *Free Radic. Biol. Med.* 41, 874–885. doi:10.1016/j.freeradbiomed.2006.04.031

Nilsson, M. B., Langley, R. R., and Fidler, I. J. (2005). Interleukin-6, Secreted by Human Ovarian Carcinoma Cells, Is a Potent Proangiogenic Cytokine. *Cancer Res.* 65, 10794–10800. doi:10.1158/0008-5472.can-05-0623

Pan, S., Xing, H., Fu, X., Yu, H., Yang, Z., Yang, Y., et al. (2018). The Effect of Photothermal Therapy on Osteosarcoma with Polyacrylic Acid-Coated Gold Nanorods. *Dose-response : a Publ. Int. Hormesis Soc.* 16, 1559325818789841. doi:10.1177/1559325818789841

Pei, Z., Li, H., Guo, Y., Jin, Y., and Lin, D. (2010). Sodium Selenite Inhibits the Expression of VEGF, TGFβ1 and IL-6 Induced by LPS in Human PC3 Cells via TLR4-NF-KB Signaling Blockage. *Int. Immunopharmacology* 10, 50–56. doi:10.1016/j.intimp.2009.09.020

Poerschke, R. L., Franklin, M. R., and Moos, P. J. (2008). Modulation of Redox Status in Human Lung Cell Lines by Organoselenocompounds: Selenazolidines, Selenomethionine, and Methylseleninic Acid. *Toxicol. Vitro* 22, 1761–1767. doi:10.1016/j.tiv.2008.08.003

Rooprai, H. K., Kyriazis, I., Nuttall, R. K., Edwards, D. R., Zicha, D., Aubyn, D., et al. (2007). Inhibition of Invasion and Induction of Apoptosis by Selenium in Human Malignant Brain Tumour Cells *In Vitro*. *Int. J. Oncol.* 30, 1263–1271.

Salomon, D. S., Brandt, R., Ciardiello, F., and Normanno, N. (1995). Epidermal Growth Factor-Related Peptides and Their Receptors in Human Malignancies. *Crit. Rev. Oncology/Hematology* 19, 183–232. doi:10.1016/1040-8428(94)00144-i

Schafer, Z. T., and Brugge, J. S. (2007). IL-6 Involvement in Epithelial Cancers. *J. Clin. Invest.* 117, 3660–3663. doi:10.1172/jci34237

Schwarz, K., and Foltz, C. M. (1958). Factor 3 Activity of Selenium Compounds. *J. Biol. Chem.* 233, 245–251. doi:10.1016/s0021-9258(19)68065-8

Shang, L., Liu, H.-J., Hao, J.-J., Jiang, Y.-Y., Shi, F., Zhang, Y., et al. (2014). A Panel of Overexpressed Proteins for Prognosis in Esophageal Squamous Cell Carcinoma. *PLoS One* 9, e111045. doi:10.1371/journal.pone.0111045

Shin, S. H., Yoon, M. J., Kim, M., Kim, J. I., Lee, S. J., Lee, Y. S., et al. (2007). Enhanced Lung Cancer Cell Killing by the Combination of Selenium and Ionizing Radiation. *Oncol. Rep.* 17, 209–216.

Shinriki, S., Jono, H., Ota, K., Ueda, M., Kudo, M., Ota, T., et al. (2009). Humanized Anti-interleukin-6 Receptor Antibody Suppresses Tumor Angiogenesis and *In Vivo* Growth of Human Oral Squamous Cell Carcinoma. *Clin. Cancer Res.* 15, 5426–5434. doi:10.1158/1078-0432.ccr-09-0287

Suh, K. J., Sung, J. H., Kim, J. W., Han, S.-H., Lee, H. S., Min, A., et al. (2017). EGFR or HER2 Inhibition Modulates the Tumor Microenvironment by Suppression of PD-L1 and Cytokines Release. *Oncotarget* 8, 63901–63910. doi:10.18632/oncotarget.19194

Sun, W., Wang, Q., Guo, Y., Zhao, Y., Wang, X., Zhang, Z., et al. (2017). Selenium Suppresses Inflammation by Inducing microRNA-146a in Staphylococcus Aureus-Infected Mouse Mastitis Model. *Oncotarget* 8, 110949–110964. doi:10.18632/oncotarget.20740

Tang, X.-H., Knudsen, B., Bemis, D., Tickoo, S., and Gudas, L. J. (2004). Oral Cavity and Esophageal Carcinogenesis Modeled in Carcinogen-Treated Mice. *Clin. Cancer Res.* 10, 301–313. doi:10.1158/1078-0432.ccr-0999-3

Wallenberg, M., Misra, S., and Björnstedt, M. (2014). Selenium Cytotoxicity in Cancer. *Basic Clin. Pharmacol. Toxicol.* 114, 377–386. doi:10.1111/bcpt.12207

Wang, L., Bonorden, M. J. L., Li, G.-x., Lee, H.-J., Hu, H., Zhang, Y., et al. (2009). Methyl-selenium Compounds Inhibit Prostate Carcinogenesis in the Transgenic Adenocarcinoma of Mouse Prostate Model with Survival Benefit. *Cancer Prev. Res.* 2, 484–495. doi:10.1158/1940-6207.capr-08-0173

Wang, L., Liu, M., Zhu, H., Rong, W., Wu, F., An, S., et al. (2015). Identification of Recurrence-Related Serum microRNAs in Hepatocellular Carcinoma Following Hepatectomy. *Cancer Biol. Ther.* 16, 1445–1452. doi:10.1080/15384047.2015.1071730

Wang, Q., Zhu, H., Xiao, Z., Zhang, W., Liu, X., Zhang, X., et al. (2013). Expression of Epidermal Growth Factor Receptor Is an Independent Prognostic Factor for Esophageal Squamous Cell Carcinoma. *World J. Surg. Onc* 11, 278. doi:10.1186/1477-7819-11-278

Wang, S., Ma, K., Chen, L., Zhu, H., Liang, S., Liu, M., et al. (2016). TAZ Promotes Cell Growth and Inhibits Celastrol-Induced Cell Apoptosis. *Biosci. Rep.* 36. doi:10.1042/bsr20160135

Watson-Williams, E. (1919). A Preliminary Note on the Treatment of Inoperable Carcinoma with Selenium. *Bmj* 2, 463–464. doi:10.1136/bmj.2.3067.463-a

Willett, W., Steven Morris, J., Pressel, S., Taylor, J., Frank Polk, B., Stampfer, M., et al. (1983). Prediagnostic Serum Selenium and Risk of Cancer. *The Lancet* 322, 130–134. doi:10.1016/s0140-6736(83)90116-2

Yang, Z., Shi, J., Xie, J., Wang, Y., Sun, J., Liu, T., et al. (2020). Large-scale Generation of Functional mRNA-Encapsulating Exosomes via Cellular Nanoporation. *Nat. Biomed. Eng.* 4, 69–83. doi:10.1038/s41551-019-0485-1

Yazdi, M. H., Mahdavi, M., Faghfuri, E., Faramarzi, M. A., Sepehrizadeh, Z., Mohammad Hassan, Z., et al. (2015). Th1 Immune Response Induction by Biogenic Selenium Nanoparticles in Mice with Breast Cancer: Preliminary Vaccine Model. *Iran J. Biotech.* 13, 1–9. doi:10.15171/ijb.1056

Zeng, H., and Wu, M. (2015). The Inhibitory Efficacy of Methylseleninic Acid against Colon Cancer Xenografts in C57BL/6 Mice. *Nutr. Cancer* 67, 831–838. doi:10.1080/01635581.2015.1042547

Zhang, W., Chen, L., Ma, K., Zhao, Y., Liu, X., Wang, Y., et al. (2016). Polarization of Macrophages in the Tumor Microenvironment Is Influenced by EGFR Signaling within colon Cancer Cells. *Oncotarget* 7, 75366–75378. doi:10.18632/oncotarget.12207

Zhang, W., Yan, S., Liu, M., Zhang, G., Yang, S., He, S., et al. (2010). β-Catenin/TCF Pathway Plays a Vital Role in Selenium Induced-Growth Inhibition and Apoptosis in Esophageal Squamous Cell Carcinoma (ESCC) Cells. *Cancer Lett.* 296, 113–122. doi:10.1016/j.canlet.2010.04.001

Zhou, X., Wang, Z., Chen, J., Wang, W., Song, D., Li, S., et al. (2014). Increased Levels of IL-6, IL-1β, and TNF-α in Kashin-Beck Disease and Rats Induced by T-2 Toxin and Selenium Deficiency. *Rheumatol. Int.* 34, 995–1004. doi:10.1007/s00296-013-2862-5

Conflict of Interest: The authors declare that the research was conducted in the absence of any commercial or financial relationships that could be construed as a potential conflict of interest.

Publisher's Note: All claims expressed in this article are solely those of the authors and do not necessarily represent those of their affiliated organizations, or those of the publisher, the editors and the reviewers. Any product that may be evaluated in this article, or claim that may be made by its manufacturer, is not guaranteed or endorsed by the publisher.

frontiers in Pharmacology

ORIGINAL RESEARCH
published: 10 September 2021
doi: 10.3389/fphar.2021.713331

Inhibition of BCL9 Modulates the Cellular Landscape of Tumor-Associated Macrophages in the Tumor Immune Microenvironment of Colorectal Cancer

Zhuang Wei[1,2†], *Mengxuan Yang*[3†], *Mei Feng*[4], *Zhongen Wu*[4], *Rina Rosin-Arbesfeld*[5], *Jibin Dong*[4] *and Di Zhu*[1,6,7*]

[1]Department of Pharmacology, School of Basic Medical Sciences, Fudan University, Shanghai, China, [2]Key Laboratory of Systems Biology, Innovation Center for Cell Signaling Network, CAS Center for Excellence in Molecular Cell Science, Institute of Biochemistry and Cell Biology, Shanghai Institutes for Biological Sciences, Chinese Academy of Sciences, Shanghai, China, [3]Minhang Branch, Zhongshan Hospital, Fudan University, Shanghai, China, [4]Department of Pharmacology, School of Pharmacy, Fudan University, Shanghai, China, [5]Department of Microbiology and Immunology, Sackler Faculty of Medicine, Tel Aviv University, Tel Aviv, Israel, [6]Key Laboratory of Smart Drug Delivery, State Key Laboratory of Molecular Engineering of Polymers, School of Pharmacy, Ministry of Education, Fudan University, Shanghai, China, [7]Shanghai Engineering Research Center of ImmunoTherapeutics, Fudan University, Shanghai, China

OPEN ACCESS

Edited by:
Lesheng Teng,
Jilin University, China

Reviewed by:
Francesca Bianchini,
University of Florence, Italy
Amol Suryawanshi,
AbbVie Inc., United States

***Correspondence:**
Di Zhu
zhudi@fudan.edu.cn

[†]*These authors have contributed equally to this work*

Specialty section:
This article was submitted to Inflammation Pharmacology, a section of the journal Frontiers in Pharmacology

Received: *22 May 2021*
Accepted: *20 August 2021*
Published: *10 September 2021*

Citation:
Wei Z, Yang M, Feng M, Wu Z, Rosin-Arbesfeld R, Dong J and Zhu D (2021) Inhibition of BCL9 Modulates the Cellular Landscape of Tumor-Associated Macrophages in the Tumor Immune Microenvironment of Colorectal Cancer. Front. Pharmacol. 12:713331. doi: 10.3389/fphar.2021.713331

Tumor-associated macrophages (TAMs) are an indispensable part of the tumor microenvironment (TME), and they likely play a negative rather than positive role in cancer treatment. However, the cellular landscape and transcriptional profile regulation of TAMs in the case of tumor gene inactivation or chemical interference remains unclear. The B-cell lymphoma 9/B-cell lymphoma 9-like (BCL9/BCL9L) is a critical transcription co-factor of β-catenin. Suppression of Bcl9 inhibits tumor growth in mouse models of colorectal cancer (CRC). Here, we studied the TAMs of CRC by single-cell sequencing. Bcl9 depletion caused macrophage polarization inhibition from M0 to M2 and changed the CRC TME, which further interferes with the inflammation of M0 and M1. The transcription factor regulating these processes may be related to the Wnt signaling pathway from multiple levels. Furthermore, we also found that the cells delineated from monocyte to NK-like non-functioning cells were significantly different in the BCL9-deprived population. Combining these data, we proposed a TAM-to-NK score to evaluate the dynamic balance in TME of monocyte/TAM cells and NK-like non-functioning cells in The Cancer Genome Atlas (TCGA) clinical samples to verify the clinical significance. We demonstrated that the cell type balance and transcription differences of TAMs regulated by BCL9-driven Wnt signaling affected immune

Abbreviations: CRC, colorectal cancer; DFS, disease-free survival; GSEA, Gene Set Enrichment Analysis; GSVA, Gene Set Variation Analysis; HCC, human hepatocellular carcinoma; HPLC, high-performance liquid chromatography; HR, hazard ratio; hsbcl9, hsBCL9CT-24; KD, Bcl9-shRNA; Maxstat, maximally selected statistical status; MMR, mismatch repair; MS, mass spectrometry; NT, Non-targeting shRNA; OS, overall survival; PCA, Principal component analysis; Per1, Period Circadian Regulator 1; RRID, Research Resource Identifier; TAMs, Tumor-associated macrophages; TFT, transcription factor targets; TME, tumor microenvironment; t-SNE, t-distributed stochastic neighbor embedding; UMAP, Uniform Manifold Approximation and Projection; UMI, unique molecular identifier; Veh, vehicle

surveillance and inflammation of cancer, ultimately affecting patients' prognosis. We thereby highlighted the potential of targeting Wnt signaling pathway through cancer immunotherapy.

Keywords: colorectal cancer, tumor-associated macrophages, wnt signaling, BCL9, tumor immune microenvironment

INTRODUCTION

Tumor-associated macrophages (TAMs) are the most significant cluster of immune cells infiltrating colon cancer (Li et al., 2020). TAMs play a central role in the formation of the tumor microenvironment (TME) by secretion of cytokines and chemokines. The roles and phenotypes of TAMs in colorectal cancer (CRC) are controversial, however, and previous studies have reported opposite results. Inhibition of CRC cell growth was achieved with co-culturing CRC cells with PMA-activated U937 cells (Forssell et al., 2007). In contrast, the proliferation of CT26 colon carcinoma cells was stimulated when the cells were co-cultured with macrophages derived from the peritoneal cavity (Luput et al., 2017). These conflicting observations may stem from the different origins of macrophages and suggest that the *in vitro* experiments do not reproduce the exact features of TAMs in CRC. A previous study revealed that TAMs differentiated from monocytes induced by CRC tumor cells had enhanced the expression of chemokines, antigen presentation, and T-cell co-stimulation molecules, thereby promoting T-cell antitumor responses (Ong et al., 2012). In 2020, a systematic review and meta-analysis summarizing 27 studies with 6,115 patients indicated that the role of TAMs depended on the infiltration location and mismatch repair (MMR) condition (Li et al., 2020). In that study, better 5-year overall survival (OS) was related to a high density of TAMs in the tumor, which was more prominent in MMR-proficient patients (Li et al., 2020). Stratification by TAM infiltration location revealed that a high density of CD68 + TAMs in tumor stroma and tumor islet plus stroma (but not in tumor islet cells) predicted a favorable OS (Li et al., 2020). Other studies supported these results. For example, Forssell and colleagues found a high density of CD68 + macrophages along the tumor front to be a good prognostic marker for colon cancer (Forssell et al., 2007). Waniczek et al. (2017) suggested that intense M2 macrophages (CD68 + iNOS-) infiltration within the tumor stroma was associated with shorter disease-free survival (DFS) and OS. In contrast, intense infiltration at the tumor edge and the surrounding tissues was associated with a lower recurrence rate (Waniczek et al., 2017). In resected colorectal liver metastases stained for CD68, a high density of TAMs correlated with longer DFS (Cavnar et al., 2017).

Macrophages are known to polarize, heading to either the M1 or M2 phenotypes. M1 is a proinflammatory phenotype, whereas M2 is anti-inflammatory. In cancer, several lines of research have suggested that M2 promotes tumor progression, metastasis, and angiogenesis (Ruffell et al., 2012). In most cases, TAMs are thought to be M2 and related to poor prognosis (Hao et al., 2012); however, the scenario is more complex in colon cancer. In addition, M2 also promotes metastasis in various ways, including MMP-9 expression (Vinnakota et al., 2017), miRNA-containing exosome secretion (Lan et al., 2019), and regulation of epithelial–mesenchymal transition (Lee et al., 2020). Immunohistochemistry (IHC) of CRC samples verified these results. Patients with a high CD206/CD68 ratio had significantly poorer DFS and OS (Feng et al., 2019a). Among 232 patients with CRC, Kaplan–Meier analysis revealed that M2/M1 >3 was related to significantly worse DFS and OS (Lee et al., 2020). Nonetheless, the dominant phenotype of TAMs in colon cancer is debatable, and the balance of M1/M2 changes in different periods in sporadic CRC resulting from the adenoma–carcinoma sequence (Isidro and Appleyard, 2016). Edin and colleagues found that when exposed to RKO, SW480, and Caco2 (i.e., CRC cell line–derived conditioned medium), the TAMs resembled the morphology and cell surface phenotype of M2 macrophage populations, but they showed a "mixed" M1/M2 macrophage phenotype with respect to cytokine and chemokine expression patterns (Edin et al., 2013). Following the former results, a study in 2018 reported the differentiation of monocytes into a mixture population of M1/M2 induced by colon cancer–derived conditioned medium (Sawa-Wejksza et al., 2018). Another study analyzed genes expressed by the TAMs and mapped them into biological functions to see whether TAMs were pro- or anti-inflammatory. Those genes were involved in inflammation (18%), differentiation (18%), chemotaxis (8%), MHC class II antigen presentation (3%), and phagocytosis and endocytosis (2%) (Ong et al., 2012), thus revealing a proinflammatory phenotype. These results suggested that TAMs in colon cancer cannot be simply identified as M1 or M2 phenotype. It is still useful, however, to consider that in various functional states, where M1 and M2 are extremes, re-educating TAMs to the M1 phenotype may be an efficient anticancer strategy.

Wnt signaling is essential in the proliferation and innate immune function of macrophages. Combretastatin A-1 phosphate downregulates the Wnt/β-catenin pathway and induces macrophages (Mao et al., 2016). Wnt3a promotes proliferation of macrophages, while blockade of β-catenin signaling reverses the effect (Feng et al., 2018a). The Wnt5a-NF-κB (p65) pathway is normally kept in a homeostatic state to support survival and the innate immune response of macrophages (Naskar et al., 2014). In addition, Wnt5a signaling enhances fz5-dependent internalization of nonpathogenic (Maiti et al., 2012) and pathogenic bacteria (Jati et al., 2018) and killing of the latter (Jati et al., 2018), whereas Wnt7a inhibits phagocytosis (Wallace et al., 2018).

The Wnt pathway is reported to regulate the pro- or anti-inflammatory phenotype alteration of macrophages. Wnt3a (Feng et al., 2018b; Yuan et al., 2020) or Wnt5a (Feng et al., 2018a) treatment could alter cytokine-stimulated macrophage polarization, thereby predisposing macrophages to the M2 phenotype. LPS-induced proinflammatory cytokine expression in macrophages was abolished after β-catenin knockdown (Fang et al., 2018). Wnt5a signaling, to which Fzd5 and camkii contribute,

stimulated the release of proinflammatory cytokines in macrophages (Pereira et al., 2008). Activation of the Wnt5a/JNK1 pathway significantly increased the expression of TNF-α and IL-6 in pulmonary macrophages (Zhu et al., 2018). Wnt7a inhibited classical markers on macrophages in differentiation and polarization, and affected cytokine secretion from MDM (Wallace et al., 2018).

Wnt signaling in TAMs is complex. Macrophages express Wnt protein and frizzled receptors simultaneously (Blumenthal et al., 2006), which means that the Wnt protein is derived from both tumor cells and TAM. Both could trigger the Wnt pathway in TAMs, indicating the existence of a complicated regulation network. The role of Wnt signaling in TAMs has been partly revealed. Wnt signaling was significantly activated in M2-like TAMs (Yang et al., 2018; Sarode et al., 2020), and activation of Wnt/β-catenin signaling drove M2 polarization in TAMs (Raghavan et al., 2019). These results also were verified in human samples. High expression of Wnt5a in the tumor was significantly associated with intense anti-inflammatory CD163 + TAMs, but not with CD68 + TAMs (Bergenfelz et al., 2012). Accumulation of nucleus-located β-catenin was positively correlated with M2-like TAMs in human hepatocellular carcinoma (HCC) samples (Yang et al., 2018). Wnt3A expression was higher in HCC samples strongly stained for CD163 than in CD163-weakly stained samples (Tian et al., 2020). There are still unrevealed mechanisms, however, and it is still unknown how Wnt signaling in TAMs can be modified to benefit antitumor therapy.

The role of BCL9-driven Wnt signaling in macrophage polarization and how suppression of BCL9 affects tumor immune microenvironment remain unclear. In this study, we used single-cell sequencing technology to reveal the changes in TAMs in TME in genetic depletion and pharmacological inhibition of *Bcl9*.

MATERIALS AND METHODS

Chemicals, shRibo Nucliec Acids and Cells

hsBCL9$_{CT}$-24 was produced by AnaSpec, CA, according to previous protocols (Feng et al., 2019b). The synthesis and purification of peptides were evaluated using analytical high-performance liquid chromatography (HPLC) and mass spectrometry (MS). hsBCL9$_{CT}$-24 was dissolved into 10 mmol/L; both were diluted before assay. pGIPZ (inducible with doxycycline)-based lentiviral shRNAs for mouse Bcl9 shRNA#5 (V3LMM_429161) and non-targeting shRNA were obtained from Open Biosystems/GE Dharmacon. The non-targeting (NT) lentiviral shRNA was constructed to be a negative control expressing no substantial homology to any mammalian transcript. Cell line CT26 cells (ATCC) were cultured according to the supplier's recommendations. All cell lines used are listed using the official cell line name and its Research Resource Identifier (RRID) as available in the ExPASy Cellosaurus database [CT26 (RRID:CVCL_7254)]. All experiments were performed with mycoplasma-free cells.

Tumor Specimens

At least four regions in each tumor were sampled. We obtained 12 tumor samples from 12 mice, respectively. Detailed information is presented in Supplementary Table S1. Male, BALB/c mice, 6–8 weeks old, were purchased from Shanghai Lingchang Biotechnology Co., LTD. Animals were housed under specific pathogen-free conditions (22 ± 1°C, 12/12 light/dark cycle) in Fudan University. All the procedures were performed according to protocols approved by the University's animal care committee, along with the guidelines of "The Association for Assessment and Accreditation of Laboratory Animal Care International."

Tumor Size Measurement

Cultured CT26 colon cancer cells (ATCC) were harvested for subcutaneously (s.c.) inoculation (4×10^5 cells in PBS) in the right flank region of BALB/c female mice (purchased from Charles River) at 6–8 weeks of age. Three randomized cohorts ($n = 4$) with tumor size between 30 and 50 mm^3 were administered vehicle control, hsBCL9$_{CT}$-24 (25 mg/kg, i. p., QD) or hsBCL9$_{CT}$-24 (30 mg/kg, sc., QD) for 17 days after inoculation. In the CT26 combination experiment ($n = 4$) model, mice were grouped into four randomized cohorts and given hsBCL9$_{CT}$-24 (25 mg/kg, i. p., QD), anti–PD-1 antibody (10 mg/kg, i. p., BIW), or a combination arm (hsBCL9$_{CT}$-24 + anti–PD-1 antibody) *via* i. p. injection after tumor volume reached 30 mm^3. Colo320-DM (ATCC) were harvested for subcutaneously (s.c.) inoculation (1×10^6 cells in PBS) in the right flank region of BALB/c female nude mice (purchased from B&K Universal Group Limited) at 6–8 weeks of age. Two randomized cohorts ($n = 4$) with tumor size between 30 and 50 mm^3 were administered vehicle control or hsBCL9$_{CT}$-24 (15 mg/kg, i. p., QD) for 20 days after inoculation. Tumor volume was measured every other day using digital calipers and calculated on the basis of the following formula: tumor volume = (length × width^2)/2. Murine body weights were recorded after tumor measurement. Tumor size of >1000 mm^3 was set as the endpoint, and tumor/organ samples were collected from selected mice at the end of the study.

Specimen Processing

Fresh tumors from mice were surgically resected and collected into MACS Tissues storage solution (130-100-008, Miltenyi Biotec). The samples were immediately transferred to the Fudan laboratory. For further processing, tissues were minced into <1 mm^3 on ice, shifted to a C tube (130-093-237, Miltenyi Biotec), and enzymatically digested by MACS Tumor Dissociation Kit (130-095-929, Mitenyi Biotec). The obtained suspension was filtered through a 40 μm cell strainer (Falcon) and washed by RPMI 1640 (C11875500BT, Gibco). Subsequently, erythrocytes were removed using 2 ml the Red Cell Lysis Buffer (555899, BD biosciences) and live cells were enriched by a Dead Cell Removal Kit (130-090-101, Miltenyi Biotec). After re-suspension in RPMI 1640 (C11875500BT, Gibco), a single-cell suspension was obtained. Cell viability, which needs to be >90% for library construction, was checked by Trypan blue (15250061, Gibco) staining.

Samples were sequenced using the BGISEQ-500 platform at The Beijing Genomics Institute (BGI) for Genomics and Bioinformatics. Raw counts were then normalized to fragments per kilobase of transcript per million mapped reads (FPKM). Cells with genes between 500 and 50,000, UMI numbers less than 30,000, and mitochondrial content less than 20% were selected. Cells identified as doublets or multiplets based on gene expression signatures, which had more than one highly expressed cell

population-specific markers, were filtered out. Filtered data were normalized using a scaling factor of 10,000, and data was log transformed. The sequencing coverage and quality statistics for each sample are summarized in Supplementary Table S2.

10 × Library Preparation and Sequencing

A single-cell suspension was prepared and ran on a Chromium Single-Cell Platform (see *Materials and Methods*). Before running on a Chromium Single-Cell Platform (10 × Genomics Chromium™), the cell concentration was adjusted to 700–1200 cells/ul. A 10 × library was generated following the manufacturer's protocol of 10 × genomics Single-Cell 5′ Gel Bead Kit. The clustering was conducted on a cBot Cluster Generation System with TruSeq PE Cluster Kit v3 implemented the clustering. Qubit was used for library quantification. The final library was sequenced on an Illumina HiSeq3000 instrument using 150-base-pair paired-end reads.

Reduce Dimensionality Analysis

The number of unique molecular identifier (UMI) sequences of high-quality per cell was counted and normalized to the median of the total UMI of all cells using the median normalization process. Means of the Principal component analysis (PCA) reduction dimension were used to evaluate the similarity between cells. The expression trend of cellular genes is positively correlated with the sample distance. The largest variance explained results from using t-distributed stochastic neighbor embedding (t-SNE) or Uniform Manifold Approximation and Projection (UMAP) to visualize the single-cell clustering for the PCA's top 10 principal components. In the t-SNE presentation method, the sample distance is recounted to neighbor's conditional probability neighbor fitting according to the Student T-distribution in the high-dimensional space. The sample can display a divided cluster in the low dimensional space.

Pathway and Functional Annotation Analysis

Pathway annotation and enrichment was performed through Gene Set Enrichment Analysis (GSEA) (Subramanian et al., 2005). MsigDB is a database resource for investigating the high-level functions and effects of the biological system (Liberzon et al., 2011). Pathways with a Q value ≤0.05 were considered to be significantly enriched. Based on The Gene Ontology database, we conducted functional annotation, including biological process, cellular component, and molecular function classifications.

Tumor-Associated Macrophages-To-Natural Killer (NK) Score

Use **Eq. 1** to calculate the TAM-to-NK Score of each cell or each patient.

$$\text{TAM} - \text{to} - \text{NK Score} = \frac{\text{GSVA}\left(\text{TAM\_type\_list}\right)}{\text{GSVA}\left(\text{NK\_type\_list}\right)} \quad (1)$$

In the **Eq. 1**, GSVA () indicated Gene Set Variation Analysis; TAM type gene list (TAM_type_list): *APOE, C1QA, C1QB, C1QC, CCL12, CCL6, CCL8, LYZ2, PF4, WFDC17, CSF1R,* and *CXCL14*; NK-like non-functioning type gene list (NK_type_list):. *AW112010, CCL5, CD3E, CD52, GZMA, GZMB, GZMC, IL2RB, LTB,* and *NKG7.*

Gene Set Variation Analysis and Metascape Analysis

Based on cell population expression data, we obtained the average expression of each gene of the corresponding cell in each sample. GSVA analysis was conducted based on the resulting expression data of the above two types of cells. After performing GSVA Z-score analysis by the gene list above, we obtained the GSVA Z-score of each pathway in each sample. The GSVA score data of the above four types of cells were calculated in the limit package in R. Metascape analysis is carried out according to the published method (Zhou et al., 2019).

Gene Prognostic Performance in The Cancer Genome Atlas Sample

Standardized TCGA datasets are derived from Xena Functional Genomics Explorer (https://xenabrowser.net/). Maxstat (maximally selected statistical status) algorithm is used to distinguish the high and low TAMtoNK Score. Kaplan-Meier curve is used to analyze the overall and disease-free survival of the patient population. Log-Rank p value and HR were also established using the same software as survival analysis.

Statistical analysis

Statistical significance was determined using 2 way ANOVA. (GraphPad Prism 8). The p-values were then calculated using Tukey's multiple comparisons test. $p < 0.05$ was considered statistically significant.

RESULTS

The Effect of bcl9 Inhibitors on Tumor Growth

The CT26 tumor cells were implanted s. c. into the right flanks of BALB/c mice; tumor-bearing animals were treated with vehicle control or hsBCL9$_{CT}$-24 (ip., at 25 mg/kg or sc.,30 mg/kg) for 17 days hsBCL9$_{CT}$-24 significantly reduced tumor volume relative to control throughout the study period (**Figure 1A**) and genetic knockdown of Bcl9 in CT26 also significantly reduced tumor growth in compared with non-targeting RNA (NT -shRNA) (**Figure 1B**). CT26 has low response to anti-PD-1 Ab treatment. We therefore examined whether treatment using hsBCL9$_{CT}$-24 could improve this response through immune-editing functions. In CT26 mouse model, combinatory treatment with hsBCL9$_{CT}$-24 and anti–PD-1 Ab markedly reduced tumor growth (**Figure 1C**) And hsBCL9$_{CT}$-24 was assessed in the mouse CRC model established in both immunocompetent (regular BALB/c) and immunodeficient (nude) mice. In nude mice, hsBCL9$_{CT}$-24 exhibited a

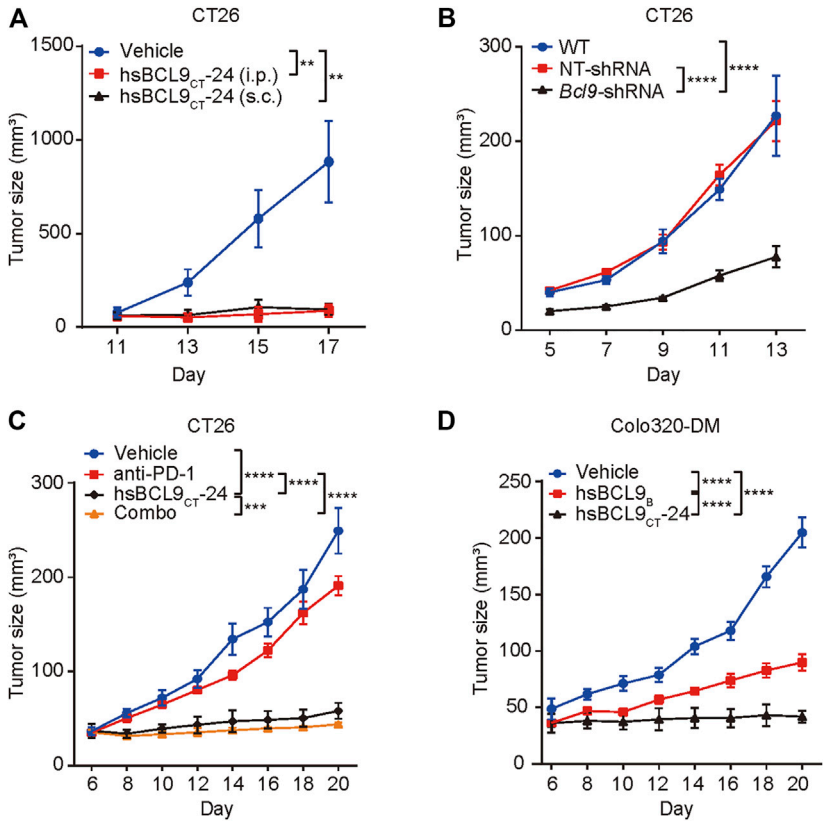

FIGURE 1 | The effect of bcl9 inhibitors on tumor growth. **(A)** BALB/c mice were inoculated with CT26 cells *via* single flank implantation and treated with hsBCL9$_{CT}$-24 (ip., 25 mg/kg, QD) or hsBCL9$_{CT}$-24 (sc.,30 mg/kg, QD) as indicated after tumor volume reached 30 mm^3 (n = 4 per cohort). **(B)** CT26 cells which were transduced with NT-shRNA or *Bcl9*-shRNA were inoculated in BALB/c mice (n = 5 per cohort). **(C)** Combination treatment of hsBCL9$_{CT}$-24 and anti–PD-1 Ab resulted in almost complete regression in the CT26 model. BALB/c mice were inoculated with CT26 cells *via* single flank implantation and treated with hsBCL9$_{CT}$-24 (ip., 25 mg/kg, QD), anti–PD-1 Ab [ip.,10 mg/kg, twice weekly (BIW)], and hsBCL9$_{CT}$-24 + anti–PD-1 Ab as indicated after tumor volume reached 30 mm^3 (n = 4 per cohort). **(D)** Colo320-DM cells were inoculated in BALB/c nude mice before treatment with vehicle control or hsBCL9$_{CT}$-24 (ip.,15 mg/kg, QD) as indicated after tumor volume reached 30 mm^3 (n = 4 per cohort). Significance were tested by 2-way ANOVA for experiments performed in triplicate, and each experiment was repeated three times, $^{**}p \leq 0.01$, $^{***}p \leq 0.001$, $^{****}p \leq 0.0001$.

comparable potency against the growth of Colo320-DM (**Figure 1D**).

Single-Cell RNA-Seq of Mouse CT26 Tumor With Pharmacological Inhibition of Bcl9 and Genetic Depletion of Bcl9

To investigate the heterogeneity of murine CT26 tumor treated with hsBCL9$_{CT}$-24 and genetically depleted *Bcl9*, we conducted single-cell mRNA sequencing in 12 samples (see *Materials and Methods*). After integrating the data from four different groups of treatment, including hsBCL9$_{CT}$-24 (hsbcl9), vehicle (veh), *Bcl9*-shRNA (KD), Non-targeting shRNA (NT), we used an algorithm built in the Seurat package to remove batch effects. After completing the principal component analysis of genes, UMAP, which is a dimensionality reduction method based on manifold analysis, grouped the cells together according to the similarity of gene expression (**Figure 2A**). Through the clustering analysis of all cells, we found that these cells can be divided into eight clusters corresponding to tumor cells, tumor-associated monocytes, TAMs, tumor-associated endothelial cells, fibroblasts, and T cells (**Figure 2A**), these classifications are based on known markers or bioinformatics research (Wei et al., 2020). To study the potential differences in TAMs, we extracted the TAM population based on the cell information we previously reported (Wei et al., 2020), and performed re-clustering analysis (Step 1 re-clustering; **Figures 2B–E**). Most cells showed a notable overlap in the reduced dimension maps between different samples or treatment groups (**Figures 2A–C**) large number of cells continuously distributed topological structure (cells circled by red dashed line; **Figure 2B**). According to the marker gene of these clusters, they could be classified as the main population of TAMs (**Figures 2D,E**) (Shalhoub et al., 2011). The next section includes an analysis of the main population of TAMs.

Macrophage Polarization: Cellular Landscape Difference Between M0, M1, and M2

To further study the classification and biological characteristics of the main population of TAMs, we re-clustered the cells

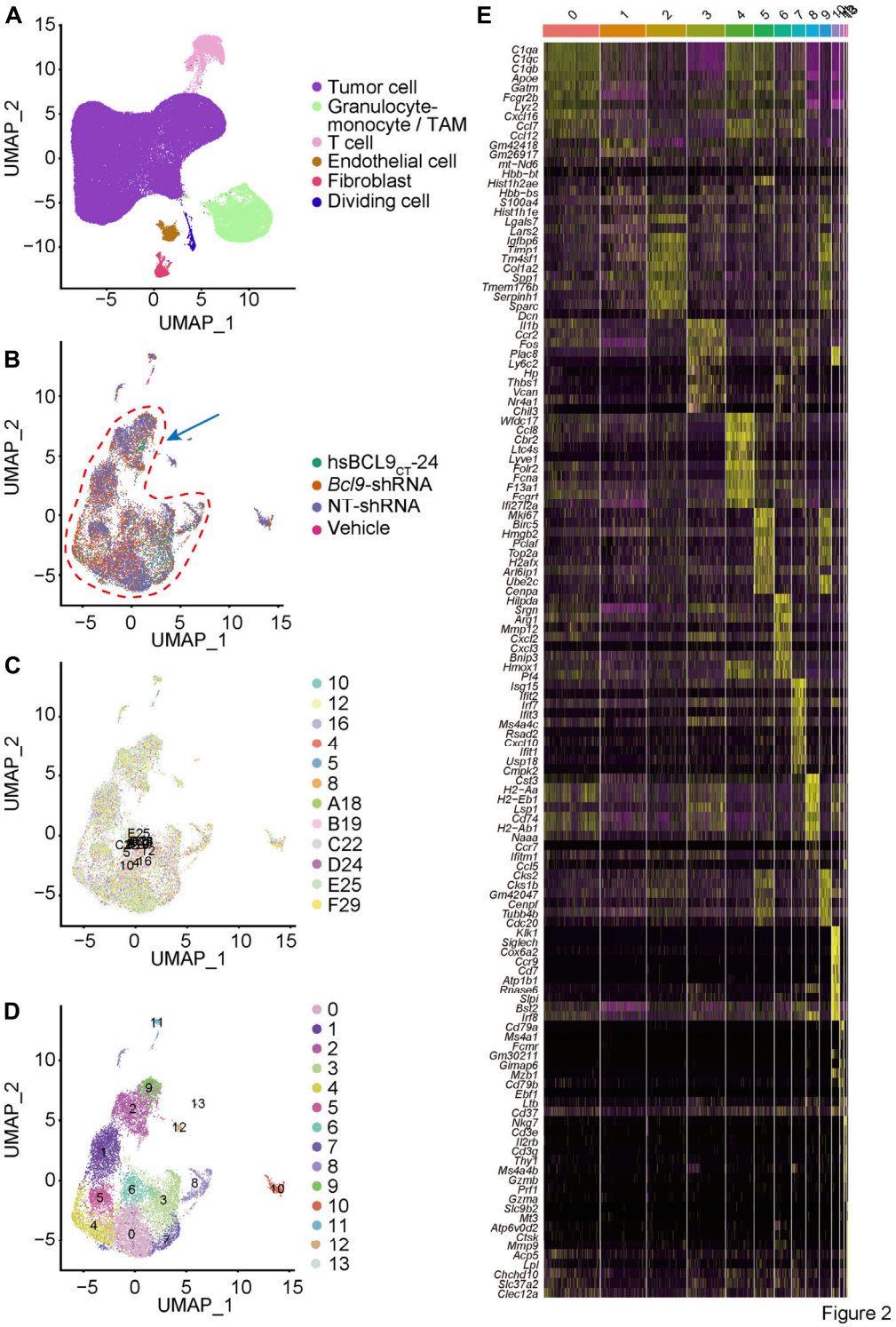

Figure 2

FIGURE 2 | Single cell cluster analysis of BCL9 perturbed CT26 murine tumor. **(A)** UMAP mapping and cell type. Re-cluster analysis of Granulocyte-monocyte (Step 1 re-clustering). **(B)** UMAP mapping and groups (vehicle, hsBCL9$_{CT}$-24, NT-shRNA, *Bcl9*-shRNA), the arrow shows the cell populations with difference. **(C)** UMAP mapping and clusters. **(D)** UMAP mapping and three clusters (clusters 2, 9 and 12) with differences (Used for Step 2 re-clustering). **(E)** Heatmap of the 13 clusters from Step 1 re-clustering. Columns, individual cells; rows, genes (Top10).

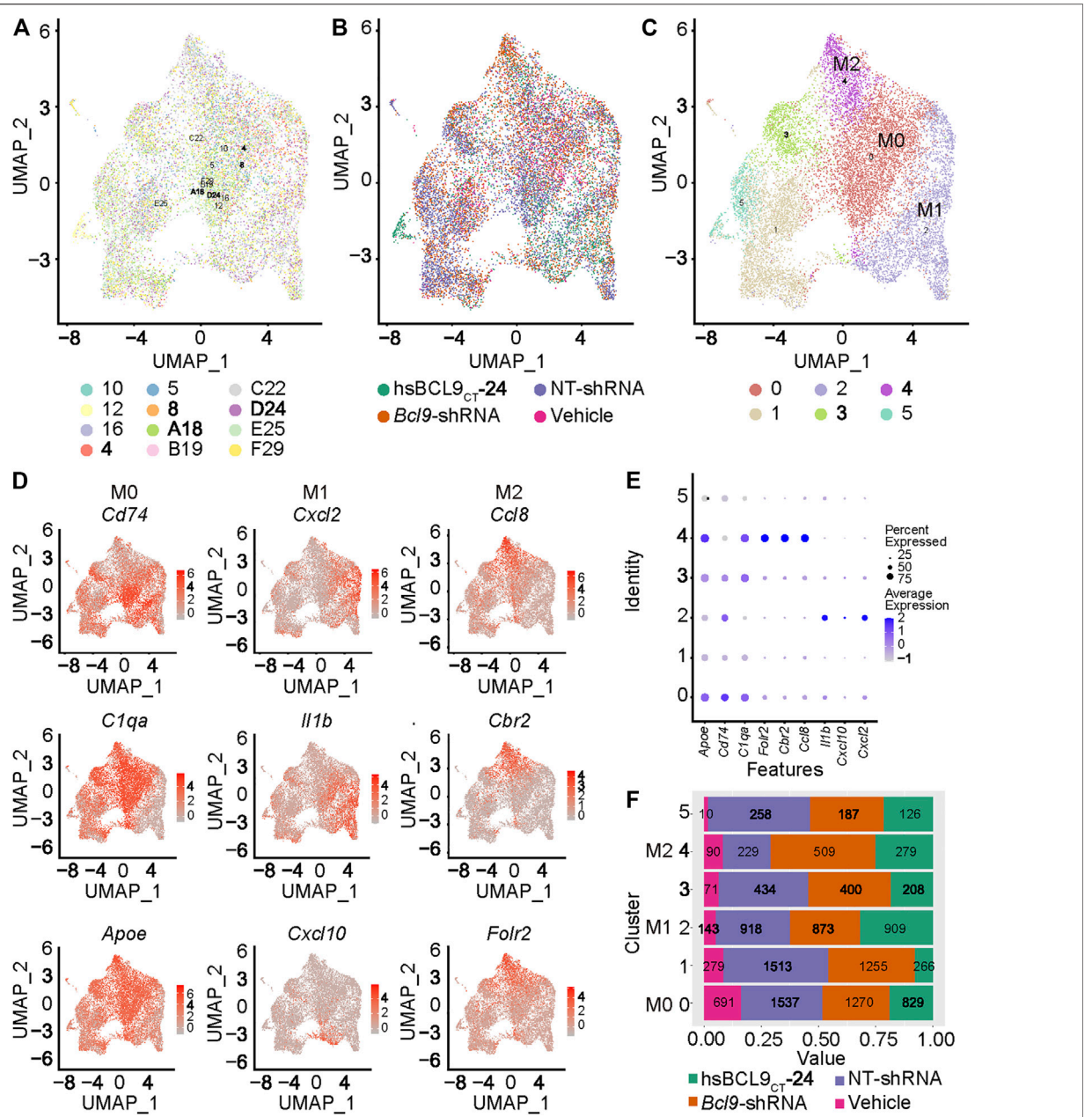

FIGURE 3 | Population of M0, M1 and M2 in the TAM of mouse CT26 tumor. Re-cluster (Step 2 re-clustering) analysis of TAM (The population circled in red dash in **Figure 2**). **(A)** UMAP mapping and clusters and samples. **(B)** UMAP mapping and groups (vehicle, hsBCL9$_{CT}$-24, NT-shRNA, *Bcl9*-shRNA). **(C)** UMAP mapping and clusters. **(D)** UMAP mapping and M0, M1 and M2 marker Gene expression level. **(E)** Bubble chart of TAM clusters with M0, M1 and M2 marker Gene expression level. **(F)** Barchart of cell proportions of different groups in TAM clusters, the number is the actual number of cells.

circled in red in **Figure 2B**. The results (**Figures 3A,B**) showed that the cells from different samples or treatment groups were all merged together, reflecting the successful removal of batch effects. Furthermore, we used the k-nearest neighbors algorithm to cluster cells based on the difference in gene expression (**Figure 3C**). The main population of TAMs could be classified into six populations, among which the three main populations (0, 2, and 4) were topologically connected and occupied the vast majority of the TAM group (**Figure 3C**). This geometric topological connection implies a potential cell population relationship. Furthermore, the analysis of marker genes of these populations proved that clusters 0, 2, and 4 expressed high amounts of marker genes at different stages of macrophage polarization. For example, cluster 0 expressed the known markers of M0 (*Cd74*, *C1qa*, and *Apoe*), and cluster 2 expressed M1 markers (*Cxcl2*, *Il1b*, and *Cxcl10*), whereas cluster 4 expressed M2 markers (*Ccl8*, *Cbr2*, and *Folr2x*) (**Figures 3D,E**). The differential expression of these genes proved that

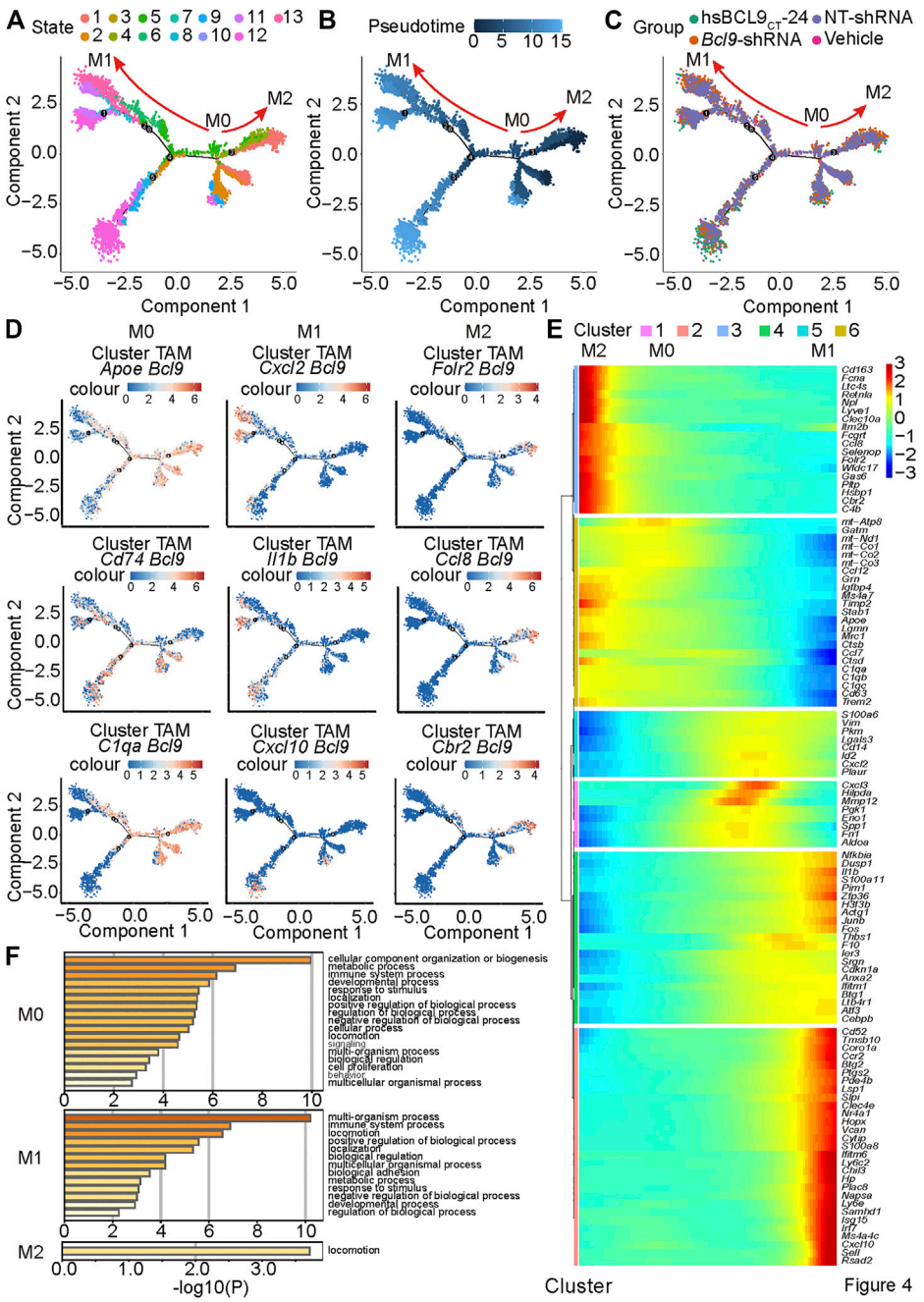

FIGURE 4 | Pseudotime analysis reveals the trajectory of M0, M1 and M2 in mouse CT26 tumor. Pseudotime analysis on the TAM cells of clusters 0, 2 and 4 in **Figure 3C** and **(A)** States; **(B)** Pseudotime; **(C)** groups (vehicle, hsBCL9$_{CT}$-24, NT-shRNA, *Bcl9*-shRNA); **(D)** M0, M1 and M2 marker Gene expression level; **(E)** trend of the gene expression generated by the BEAM function along pseudotime. **(F)** Metascape biological processes enrichment analysis by using gene clusters abtained from BEAM function.

clusters 0, 2, and 4 represented the three states of macrophage polarization.

To further prove the existence and differentiation process of the three states of macrophage polarization (M0, M1, and M2 polarization) in CT26 tumor, we extracted clusters 0, 2, and 4 (from **Figure 3C**) to analyze the trajectory using the DDR-Tree algorithm included in the Monocle package. As shown in **Figures 4A–C**, the cell population was projected on a dendritic structure. State analysis, pseudotime analysis, and classification based on treatment groups are displayed in **Figures 4A–C**. Further analysis showed that classic marker genes of M0, M1, and M2 were obviously polarized on the trajectory (**Figure 4D**). The M0 markers (*Cd74*, *C1qa*, and *Apoe*) tended to be expressed in the middle of the trajectory,

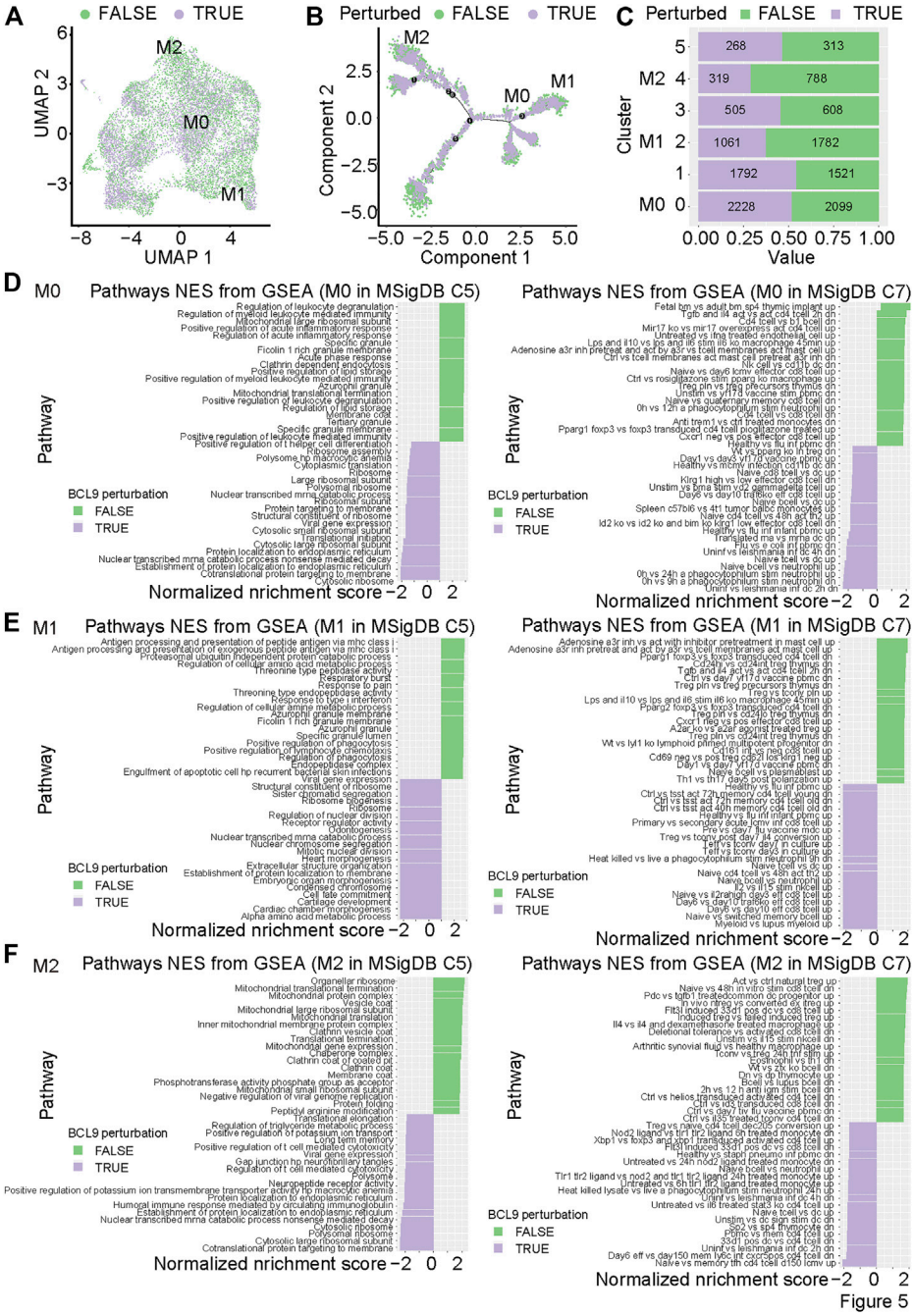

FIGURE 5 | The perturbation of *Bcl9* inhibits the differentiation and function of M0, M1 and M2 in CT26 tumor. **(A)** UMAP mapping of TAM (**Figure 3A**) and perturbation of *Bcl9* or not; **(B)** trajectory of M0, M1 and M2 (**Figure 4A**) and perturbation of *Bcl9* or not; **(C)** Barchart of cell proportions from perturbation of *Bcl9* in TAM clusters, the number is the actual number of cells. GSEA analysis for M0 **(D)**; M1 **(E)**, and M2 **(F)** TAM cells, MsigDB C5 (All gene sets derived from Gene Ontology) is used on the left, and MsigDB C7 (immunologic signature gene sets) is used on the right.

and the M1 markers (*Cxcl2*, *Il1b*, and *Cxcl10*) tended to be expressed in the direction of the right arrow. The M2 markers (*Ccl8*, *Cbr2*, and *Folr2x*) tended to be expressed in the direction of the left arrow (**Figure 4D**). This was consistent with the classic M0, M1, and M2 marker conversion paradigm (Shalhoub et al., 2011; Yuan et al., 2015; Macciò et al., 2020).

To study the overall gene expression trend of the cell population along pseudotime, we used the BEAM function to analyze the differential gene expression along time (**Figure 4E**). The results showed that some different genes were enriched in different stages of the differentiation process (**Figure 4E**). The genes enriched in the middle and right ends may participate in

the biological processes related to M0 and M1, and it is expected that the genes enriched in the left end participate in the biological processes related to M1 and M2. We analyzed these gene sets by Metascape to better understand the associated biological processes (Zhou et al., 2019) (**Figure 4F**). The results showed that gene sets that favored M0, M1, or M2 participated in immune and inflammation-related signal pathways to varying degrees. These conclusions can provide inspiration for further mechanism research.

Differential Gene Expression and Signal Pathway Enrichment Analysis of Mouse CT26 Tumor With Bcl9 Deprivation in the Tumor-Associated Macrophages Subgroups

To further study the effect of *Bcl9* deprivation of M0, M1, and M2 TAMs, we classified the group (hsbcl9, KD) with *Bcl9* deprivation into *Bcl9* perturbed True group, and their controls (veh, NT) into Bc9 perturbed False group. UMAP clustering and trajectory analysis showed no obvious difference between the two groups (**Figures 5A,B**). Comparison of the number of cells in different clusters, however, revealed that the proportion of *Bcl9* perterbed True cells in M2 was significantly lower than that of *Bcl9* perterbed False cells. The decrease in KD in the shRNA group was the most obvious, and the proportions were roughly the same in M0 (**Figure 5C** and **Figure 3F**). This result showed that the deprivation of *Bcl9* may have interfered with the differentiation of M0 to M2. M2 cells are widely regarded as "bad" TAMs, which promote tumor growth (Yuan et al., 2015; Macciò et al., 2020). Nevertheless, there were still many M1 and M2 cells in the *Bcl9* perterbed True group.

To further study the genes that are differentially expressed in M0, M1 and M2, and understand which biological processes are affected by the deprivation of *Bcl9*, we performed Gene Set Enrichment Analysis (GSEA) analysis on TAMs. As shown in **Figures 5D–F**, we performed GSEA analysis on *Bcl9*-deprived and non-deprived cell populations from M0, M1, or M2, using the overall biological process database MsigDB C5 and immune-related signaling pathway database MsigDB C7 (Subramanian et al., 2005; Liberzon et al., 2011). The results showed that the signaling pathways related to immune and inflammatory response in M0 and M1 were significantly enriched in the *Bcl9* perterbed False group, but there was no obvious enrichment in M2. This indicated that *Bcl9* deprivation may have had a strong inhibitory effect on the inflammatory response caused by M0 and M1 cells. Inflammation is one of the most important factors that causes tumor development and prognosis (Coussens and Werb, 2002).

To further clarify the upstream transcription factor regulation mechanism related to these biological processes, we used MsigDB C3 to perform transcription factor analysis. The results are shown in **Supplementary Figure S1**. In the *Bcl9* perterbed True group, Period Circadian Regulator 1 (Per1) target genes were highly enriched in M0, M2, and M2, and the function of Per1 was in circadian regulation (Ono et al., 2017). This result showed that the deprivation of *Bcl9* may disrupt the circadian rhythms of M0, M2, and M2.

Depletion of Bcl9 Inhibits the Delineation From Tumor-Associated Monocytes to NK Cells

To further study the changes of TAMs to discover new cell populations, we again checked the cell classification from **Figure 2B**. Although most cells from different treatment groups (hsbcl9, veh, KD, NT) were merged together, the clusters 2, 9, and 12 shown in **Figure 2B** were not merged well. Topologically, some cells from cluster 12 were strongly related to cells from cluster 2 and were located at the junction of these two clusters (**Figure 2B**, indicated by blue arrow). We showed that these cells were the most responsive and sensitive to *Bcl9* deprivation. According to the difference in genes from **Figure 2E**, we confirmed that most clusters shown in **Figure 2D** highly expressed the markers of monocytes (*C1qb*, *C1qc*, and *C1qa*), which are the precursor cells of TAMs (Tran et al., 2017), whereas cluster 12 highly expressed the markers of natural killer cells and NK cells (*Nkg7*, *Il2rb*, and *Cd3e*). Coupled with the topological correlation of these cell populations, we inferred that cluster 12 belonged to the NK cells delineated from monocytes (Chen et al., 2015).

To further verify that cluster 12 was indeed a delineated NK cell population, we performed the secondary re-clustering analysis to clarify the whole process of cell delineation. We extracted the TAM cells from Step 1 re-clustering (clusters 2, 9, and 12) shown in **Figure 2D**, and performed the second step of re-clustering (Step 2 re-clustering). As shown in **Figures 6A–C**, Step 2 re-clustering divided the cells into several clusters. Clusters 4, 5, and 7 were topologically relevant, which indicated their potential delineation relationship. Further differential expression analysis showed that cluster 5 contained only the NK cell markers (*Nkg7*, *Il2rb*, and *Cd3e*), and cluster 2 contained two kinds of markers, both of monocytes and NK cells (*Nkg7*, *Il2rb*, *Cd3e*, *C1qb*, *C1qc*, and *C1qa*; **Figures 6D–G**), which could be regarded as a transition state of this delineation process. Further quantitative analysis (**Figure 6H**) proved that the populations of the cells of the deprived *Bcl9* group were enriched in clusters 4 and 7. This result showed that during the process of delineation from monocytes to NK-like non-functioning cells, it is very likely that cluster 4 and 7 are the blocking stages because of *Bcl9* deprivation.

Depletion of Bcl9 Inhibits the Delineation From Tumor-Associated Monocytes to NK Cells, Which Depends on Transcriptional Regulation

To further study how *Bcl9* depletion inhibits the delineation from tumor-associated monocytes to NK-like non-functioning cells, we performed pseudotime analysis on the cells from Step 1 re-clustering (clusters 2, 9, and 12; **Figure 6A**). According to the results in **Figures 7A–D**, along pseudotime, cells delineated from state 1 to states 2 and 3.

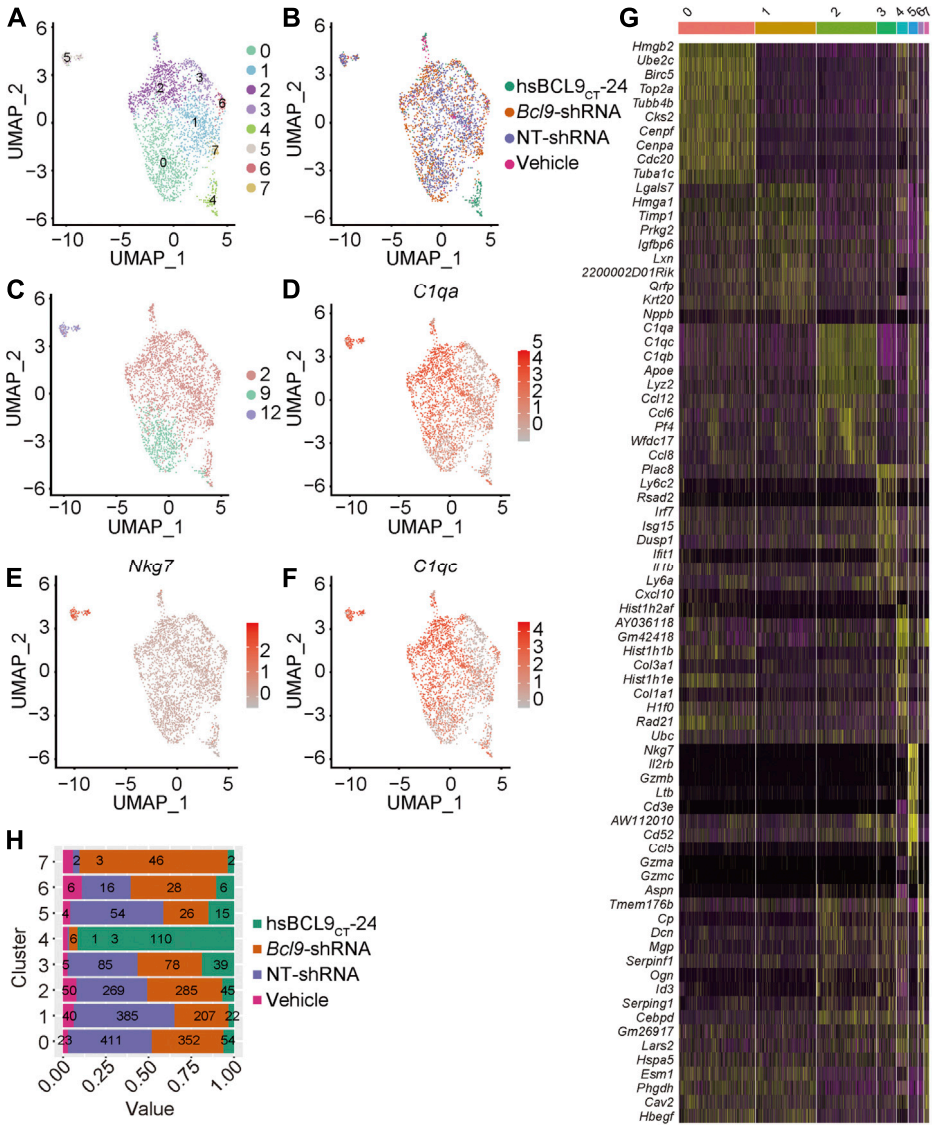

FIGURE 6 | Re-cluster (Step 2 re-clustering) analysis of TAM (monocytes) and delineated NK-like non-functioning cell. **(A)** UMAP mapping and clusters. **(B)** UMAP mapping and groups (vehicle, hsBCL9$_{CT}$-24, NT-shRNA, *Bcl9*-shRNA). **(C)** UMAP mapping and Step 1 re-clustering clusters labeling. **(D–F)** UMAP mapping and monocytes and NK cell marker gene expression level (C1qa, C1qc and Nkg7). **(G)** Barchart of cell proportions of different groups in Step 2 re-clustering, the number is the actual number of cells. **(H)** Heatmap of the 7 clusters from Step 2 re-clustering. Columns, individual cells; rows, genes (Top10).

Displaying clusters from **Figure 6** on delineation trajectory, the un-delineated clusters (Step 2 re-clustering clusters 2 or Step 2 re-clustering clusters 4, 5, and 7) were in the more primitive stage of delineation (State 1)—that is, in the stage of monocytes—while cells at delineated clusters (Step 2 re-clustering clusters 12 or Step 2 re-clustering rest clusters) were at the stage (States 2 and 3) close to NK cells (**Figures 7C,D**). Nkg7 are C1qb were shown as two-stage markers at the two ends of the trajectory (**Figures 7E,F**). To further study the change in trend of gene expression in this process, we used the BEAM function to analyze the difference of the cell population along the pseudotime (**Figure 7G**). The results showed that the expression of NK cell markers (cluster 5) gradually increased, whereas the expression of other genes decreased (cluster 1) or first decreased and then increased (cluster 4). It is not clear to which signaling pathways two clusters of genes other than NK cell markers were related, but according to transcription factor analysis, the gene cluster with decreasing expression (cluster 1) was controlled mainly by the transcription factor PSMB5. The gene cluster that first decreased and then increased (cluster 4) was controlled mainly by the transcription factor PSMB5 and HOXB6.

Low Tumor-Associated Macrophages-To-NK Score Predicts Poor Prognosis in Cancer Patients

Previous results suggested dynamic balance between the infiltrating monocytes and NK-like non-functioning cells in

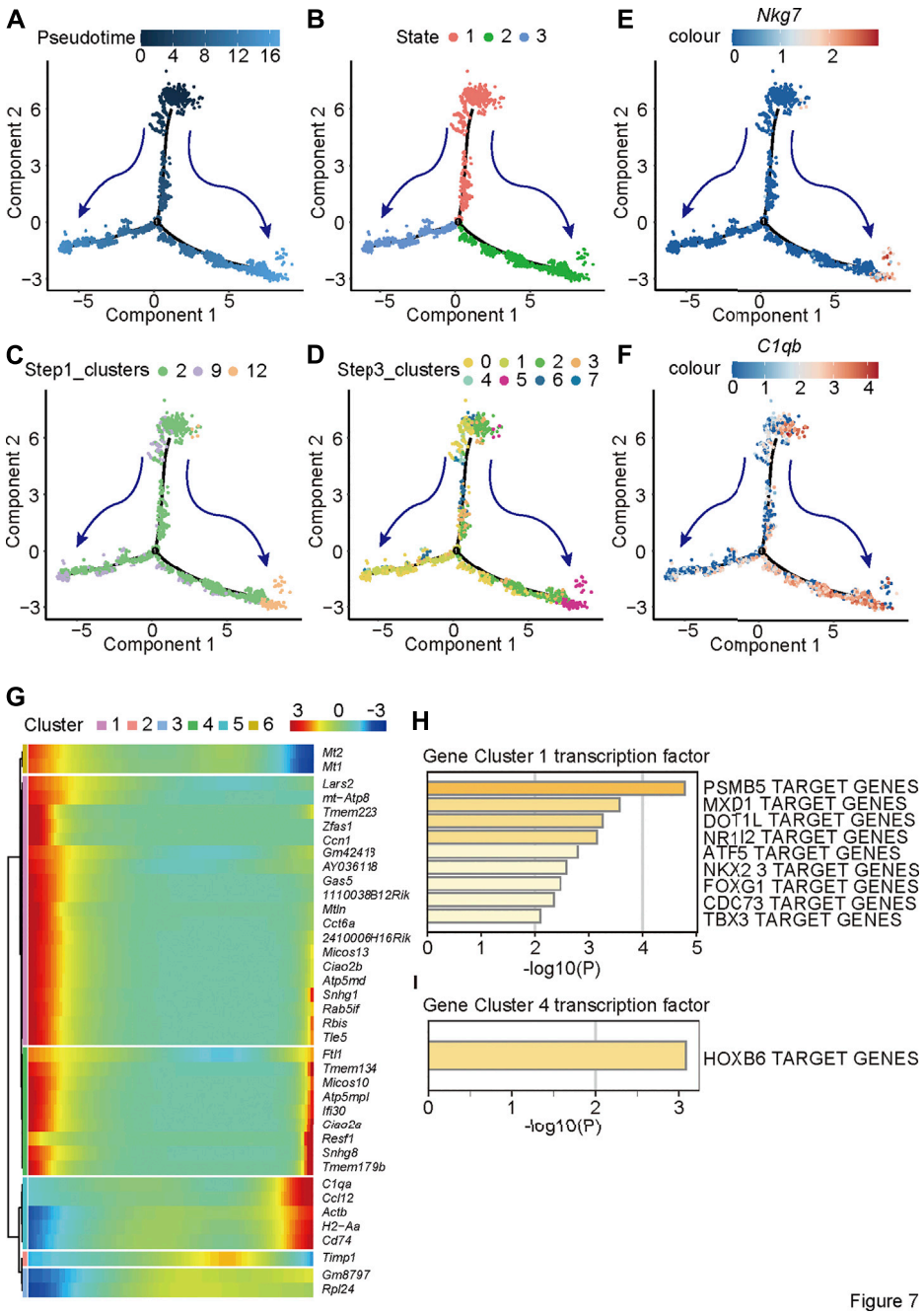

Figure 7

FIGURE 7 | Pseudotime analysis reveals the trajectory of delineation from tumor-associated monocytes to NK-like non-functioning cells. Pseudotime analysis on the TAM cells of Step1 re-clustering (clusters 2, 9 and 12) and **(A)** Pseudotime; **(B)** States; **(C)** labeling by Step 1 re-clustering clusters **(D)** labeling by Step 2 re-clustering clusters; **(E,F)** monocytes and NK cell marker gene expression level (*C1qb* and *Nkg7*). **(G)** The trend of the gene expression generated by the BEAM function along pseudotime of Step1 re-clustering (clusters 2, 9 and 12) TAM population. **(H)** Metascape biological processes enrichment analysis by using gene clusters abtained from BEAM function.

the tumor. To study the clinical significance of the transition between monocytes and NK-like non-functioning cells in tumors, we constructed a TAM-to-NK score to quantify the homeostasis between monocytes and NK-like non-functioning cells in tumors. The TAM-to-NK score quantified the degree of enrichment of the identified key marker genes in monocytes and NK-like non-functioning cells. To further verify that this score could predict the prognosis of cancer patients, we used it in the TCGA pan-cancer data set to estimate the TAM-to-NK scores of different patients. Next, we grouped the patients according to the TAM-to-NK scores, and conducted survival analysis to calculate the hazard ratio (HR). The results showed that low TAM-to-NK

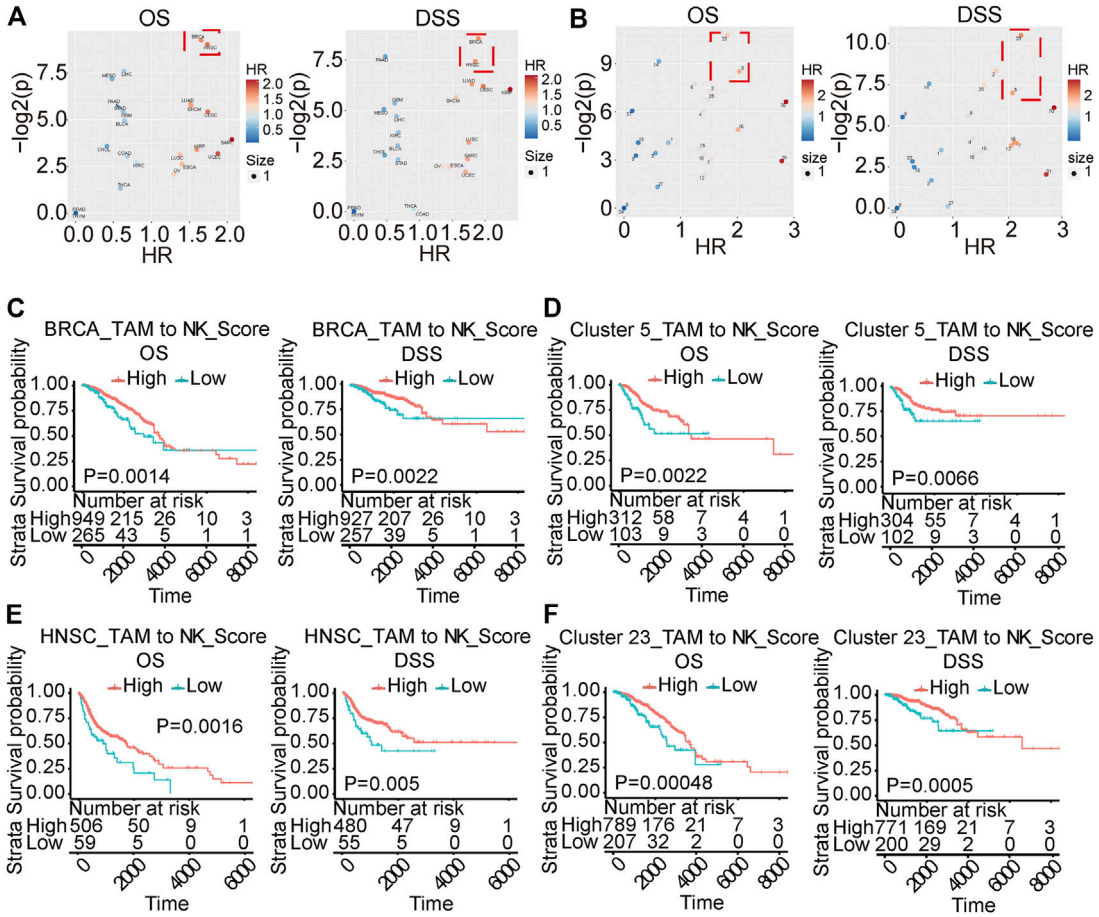

FIGURE 8 | TAMtoNK Score predicts the prognosis of TCGA tumor patients. **(A,B)** Volcano chart of hazard ratio based on TAM-to-NK Score grouping of patients with different types of cancer or different clusters. **(C–F)** Survival analysis of TCGA tumor type or clusters with significant High hazard ratio. OS and DSS respectively represent overall survival and disease-specific survival rate.

score predicted the poor prognosis of certain kinds of patients (**Figures 8A,B**). Among them, Breast invasive carcinoma (BRCA) and Head and Neck squamous cell carcinoma (HNSC) were the most prominent (**Figures 8C,E**). Because tumors classified according to their location of incidence have large gene expression pattern unpredictability, we previously reported a method to cluster the samples of the TCGA pan-cancer dataset according to their gene expression patterns (Wei et al., 2020). The advantage of this method is that it can eliminate the differences between the samples as much as possible, so that the comparison of specific gene sets or clinical prognosis are based on a highly consistent population. Then we used TAM-to-NK score to group patients in each cluster and conducted survival analysis. Low TAM-to-NK score predicted poor prognosis of patients from cluster 5 and cluster 23 with high significance (**Figures 8D,F**). Among them, cluster 23 was composed mainly of BRCA, and cluster 5 was composed mainly of BRCA, Uterine Corpus Endometrial Carcinoma (UCEC), and Cervical squamous cell carcinoma and endocervical adenocarcinoma (CESC). According to our previous reports, cluster 5 had marker genes *TYR* and *MLANA* (Wei et al., 2020). These results suggested that *TYR* and *MLANA* may be used as pathological criteria for prognostic prediction with TAM-to-NK score.

Ligand-Receptor Interactions Analysis Between Tumor-Associated Macrophages and T Cells in the Tumor Microenvironment

To identify potential cell–cell interactions that are conserved across the two synergic tumor models, we scored potential ligand–receptor interactions across the cell types present within the TME. The interaction was determined by calculating the average expression of receptors and ligands. After calculating the score for each ligand and receptor, we averaged the interaction score of the tumor model to determine the conservative interaction. The macrophages interacted with T cells through the CCL3-CCR5, CAF1R-CSF1, and ICAM1-ITGAL to change the T-cell functions in hsBCL9$_{CT}$-24 treated group compared with the vehicle (**Supplementary Figure S2A**). Similar to *Bcl9* pharmacological inhibition, the *Bcl9* depletion also affected the interaction of macrophages and T cells, where CSF1R-CSF1 and CCL4-CCR5 were significantly regulated (**Supplementary Figure S2B**). Our data showed that targeting Wnt pathway through

hsBCL9$_{CT}$-24 treatment very likely inhibit macrophages and enhance T-cell activity (**Supplementary Figures S2C,D**).

Immunohistochemical Analysis of Tumor-Associated Macrophages Markers of CSF1R and Cxcl14 Genes in Colorectal Cancer

We re-analyzed the human CRC immunohistochemical pictures downloaded from the public database the human protein atlas (https://www.proteinatlas.org/). The results showed that the *CSF1R* as the M2 marker gene was highly expressed in CRC. The survival curve data indicated that the prognosis in the high *GSF1R* expression group was poorer than that of the low expression group (**Supplementary Figures S3A–C**). The *CSCL14* gene as a marker of M1 was moderately or weakly expressed in CRC. The survival curve data showed better prognosis in group with high expression of *CXCL14* than in low *CXCL14* expressing groups (**Supplementary Figures S3D–F**).

DISCUSSION

Tumor microenvironment is an important factor affecting tumor treatment and prognosis. Because of its dramatic impact on tumor occurrence and development, as well as heterogeneity, it has attracted growing interest in oncology, especially in consideration of new targets for tumor therapy. TAMs are one of the major cellular components of most cancer microenvironments; more than 50% of tumor-infiltrating cells are TAMs. In this study, we demonstrated that the cellular landscape and transcription differences of TAMs after BCL9 suppression affected cancer and immune surveillance.

TAMs are an extremely heterogeneous population in CRC, and their characteristics are strongly dependent on the TME. Patients with infiltrating TAMs in CRC LMs have poorer prognosis than patients without TAM infiltration in LMs (Cortese et al., 2019). TAMs play an immunosuppressive role by secreting cytokines and chemokines and also can activate the expression of immune regulatory proteins in T cells (Cortese et al., 2019). We found that *Bcl9* suppression changed macrophages polarization into the subtype M1 and M2. Macrophage polarization is increasingly understood as an essential pathogenetic factor in inflammatory and neoplastic diseases.

Macrophages are abundant in CRC (Yahaya et al., 2019), where they are recruited from and where they may mediate metastasis-promoting communication. Their interactions with cancer cells as well as their crosstalk with the TME have not yet been elucidated. CRC is the most common cancer in the world, so fighting this disease presents an enormous therapeutic challenge. Traditional treatment (i.e., surgery, radiotherapy, and chemotherapy combined with targeted drugs) has advanced the treatment for early-stage CRC over the years. Metastases, however, are the leading cause of death and remain poorly understood (Tauriello et al., 2017). Recent reports have demonstrated that Wnt signaling pathway activation induces primary resistance to immunotherapy. Macrophages can interact with the Wnt signaling pathway (Malsin et al., 2019).

After undergoing cluster analysis (**Figure 2** and **Figure 3**), pseudotime analysis (**Figure 4**), signal pathway enrichment analysis (**Figure 4**), and transcription factor analysis (**Supplementary Figure S1**), we found that *Bcl9* deprivation in TME inhibited the differentiation of M0 to M2, and inhibited the inflammatory response caused by TAMs.

The downstream genes of the circadian rhythms-regulated transcription factor Per1 may have important contributions to these biological processes. The circadian clock in mammals is controlled by three cell-autonomous feedback loops. The first loop includes two activators (*CLOCK* and *BMAL1*) and four repressors (*PER1*, *PER2*, *CRY1*, and *CRY2*). PER1 is downregulated in many types of cancers in the Cancer Genome Atlas. Heterozygous deletion of *PER1* also has been observed in cancer (Wu et al., 2019). Circadian disruption was found to change tumor-immune microenvironment, favoring tumor cell proliferation (Aiello et al., 2020). In profile 2 of cardiac dysfunction, the Wnt/beta-catenin pathway was identified with activation (Lecarpentier et al., 2014). Our finding of negative regulation of *Per1* in TIME of colon tumor provided evidence for BCL9-driven Wnt signaling role in circadian disruption.

Delineation of immune cells and their dynamic balance are a growing research field [61]. Their existence and role in tumors, however, are rarely reported. We found TAM-derived NK-like non-functioning cells in our samples, and this type of cells showed significant differences in the BCL9-deprived cell population. Changes in markers on the surface of these cells and their cell biological functions may significantly affect the TME, which in turn affects the growth and metastasis of tumors and the prognosis in patients. To evaluate the impact of this dynamic balance on tumor prognosis, we proposed TAM-to-NK score, which can evaluate the homeostasis of TAM and NK-like non-functioning cell populations in tumors at the level of gene expression. As shown in **Figure 8**, TAM-to-NK score can indeed predict the prognosis of patients in some specific cancers. In the future, further experimental research on NK-like non-functioning cells in the tumor microenvironment is very necessary. This will focus on using specific antibodies to stain newly discovered markers or perform mRNA *in situ* hybridization.

Although targeted TME has great potential for tumor treatment, the treatment of advanced metastatic CRCs remains challenging; therefore, exploring new target molecules and therapeutic strategies is of paramount importance. M2-like TAMs are believed to induce tumor-supporting, angiogenic, and immunosuppressive effects and also may induce failure of immunotherapy (Mantovani et al., 2017). Defining the biology of macrophages present in the CRC-specific environment could allow the introduction of innovative diagnostic and therapeutic strategies. TAMs affect many aspects of tumor biology, including stem cells, metabolism, angiogenesis, invasion, and metastasis virtually. The research progress of Wnt/β-catenin signaling pathway mechanisms accelerates the discovery of new therapeutic methods targeting the Wnt/β-catenin pathway in CRC. Although most drugs are still in early stages of research, there is hope that drugs to cure intractable CRC are on the horizon. Our findings have highlighted the potential of targeting the BCL9-driven Wnt signaling pathway in TMAs in cancer immunotherapy.

NOVELTY AND IMPACT

Changes in the BCL9-mediated signaling pathway caused changes in the balance of cell populations in the tumor microenvironment to affect the prognosis of cancer patients.

DATA AVAILABILITY STATEMENT

The datasets presented in this study can be found in online repositories. The names of the repository/repositories and accession number(s) can be found in the article/**Supplementary Material**.

ETHICS STATEMENT

The animal study was reviewed and approved by the Fudan University's animal care committee.

AUTHOR CONTRIBUTIONS

DZ contributed the idea, oversaw the project, analyzed the data and prepared the manuscript. ZW performed bioinformatics analysis and participated in manuscript writing. MF collected tumor samples, analyzed the data and edited the manuscript. MY participated in data analysis and edited the manuscript. ZW prepared the figures. JD and RR edited the manuscript.

FUNDING

This study was partially supported by grants from National Natural Science Foundation of China (81872895 and 82073881 to DZ), Shanghai Science and Technology Commission (18ZR1403900, 20430713600 and 18JC1413800 to DZ) and Fudan-SIMM Joint Research Fund (FU-SIMM20181010 to DZ), Fudan School of Pharmacy and Pudong hospital Joint Research Fund (RHJJ 2018-03 to DZ), Fudan School of Pharmacy and Minhang hospital Joint Research Fund (RO-MY201712 to DZ).

ACKNOWLEDGMENTS

We thanked Shuru Shen for assistance in sample preparation.

SUPPLEMENTARY MATERIAL

The Supplementary Material for this article can be found online at: https://www.frontiersin.org/articles/10.3389/fphar.2021.713331/full#supplementary-material

Supplementary Figure S1 | GSVA analysis of M0, M1 and M2. Transcription factor analysis for M0 **(A)**; M1 **(B)**, and M2 **(C)** TAM cells classified by perturbation of BCL9 or not, MsigDB C3 (TFT: transcription factor targets) is used.

Supplementary Figure S2 | Cell-cell Interaction between macrophage cells and T cells in the colorectal microenvironment. **(A)** Interaction analysis between CD8 + T and CT26 cells in NT-shRNA group. **(B)** Interaction analysis between CD8 + T and CT26 cells in hsBCL9CT-24 treated group. **(C)** Circos plots of all of the putative ligand–receptor interactions in NT-shRNA and Bcl9-shRNA groups. The solid line represents the interaction of Bcl9-shRNA group, and the dotted line represents the interaction of the NT-shRNA group. **(D)** Circos plots of all of the putative ligand–receptor interactions in vehicle and hsBCL9CT-24 treated groups. The color of the line represents the average expression of the ligand receptor pair in the pair of cells, and the thickness of the line represents the significance of the ligand receptor enrichment in the pair of cells. The solid line represents the interaction of the hsbcl9CT-24 group, and the dotted line represents the interaction of the vehicle group.

Supplementary Figure S3 | Immunohistochemistry analysis of TAM marker of CSF1R and Cxcl14 gene in colorectal cancer. Immunohistochemistry was carried in human colorectal cancer. **(A–C)** CSF1R express in colorectal cancer and survival analysis. **(D,E)** Cxcl14 express and survival analysis in human colorectal cancer. The data were derived from https://www.proteinatlas.org/ENSG00000145824-CXCL14/pathology/liver+cancer#imid_7374796

REFERENCES

Aiello, I., Fedele, M. L. M., Román, F., Marpegan, L., Caldart, C., Chiesa, J. J., et al. (2020). Circadian Disruption Promotes Tumor-Immune Microenvironment Remodeling Favoring Tumor Cell Proliferation. *Sci. Adv.* 6, eaaz4530. doi:10.1126/sciadv.aaz4530

Bergenfelz, C., Medrek, C., Ekström, E., Jirström, K., Janols, H., Wullt, M., et al. (2012). Wnt5a Induces a Tolerogenic Phenotype of Macrophages in Sepsis and Breast Cancer Patients. *J. Immunol.* 188, 5448–5458. doi:10.4049/jimmunol.1103378

Blumenthal, A., Ehlers, S., Lauber, J., Buer, J., Lange, C., Goldmann, T., et al. (2006). The Wingless Homolog WNT5A and its Receptor Frizzled-5 Regulate Inflammatory Responses of Human Mononuclear Cells Induced by Microbial Stimulation. *Blood* 108, 965–973. doi:10.1182/blood-2005-12-5046

Cavnar, M. J., Turcotte, S., Katz, S. C., Kuk, D., Gönen, M., Shia, J., et al. (2017). Tumor-Associated Macrophage Infiltration in Colorectal Cancer Liver Metastases Is Associated with Better Outcome. *Ann. Surg. Oncol.* 24, 1835–1842. doi:10.1245/s10434-017-5812-8

Chen, Q., Ye, W., Jian Tan, W., Mei Yong, K. S., Liu, M., Qi Tan, S., et al. (2015). Delineation of Natural Killer Cell Differentiation from Myeloid Progenitors in Human. *Sci. Rep.* 5, 15118. doi:10.1038/srep15118

Cortese, N., Soldani, C., Franceschini, B., Barbagallo, M., Marchesi, F., Torzilli, G., et al. (2019). Macrophages in Colorectal Cancer Liver Metastases. *Cancers (Basel)* 11, 633. doi:10.3390/cancers11050633

Coussens, L. M., and Werb, Z. (2002). Inflammation and Cancer. *Nature* 420, 860–867. doi:10.1038/nature01322

Edin, S., Wikberg, M. L., Rutegård, J., Oldenborg, P. A., and Palmqvist, R. (2013). Phenotypic Skewing of Macrophages *In Vitro* by Secreted Factors from Colorectal Cancer Cells. *PLoS One* 8, e74982. doi:10.1371/journal.pone.0074982

Fang, Y., Kang, Y., Zou, H., Cheng, X., Xie, T., Shi, L., et al. (2018). β-Elemene Attenuates Macrophage Activation and Proinflammatory Factor Production via Crosstalk with Wnt/β-Catenin Signaling Pathway. *Fitoterapia* 124, 92–102. doi:10.1016/j.fitote.2017.10.015

Feng, M., Jin, J. Q., Xia, L., Xiao, T., Mei, S., Wang, X., et al. (2019). Pharmacological Inhibition of β-catenin/BCL9 Interaction Overcomes Resistance to Immune Checkpoint Blockades by Modulating Treg Cells. *Sci. Adv.* 5, eaau5240. doi:10.1126/sciadv.aau5240

Feng, Q., Chang, W., Mao, Y., He, G., Zheng, P., Tang, W., et al. (2019). Tumor-associated Macrophages as Prognostic and Predictive Biomarkers for Postoperative Adjuvant Chemotherapy in Patients with Stage II Colon Cancer. *Clin. Cancer Res.* 25, 3896–3907. doi:10.1158/1078-0432.CCR-18-2076

Feng, Y., Liang, Y., Ren, J., and Dai, C. (2018). Canonical Wnt Signaling Promotes Macrophage Proliferation during Kidney Fibrosis. *Kidney Dis. (Basel)* 4, 95–103. doi:10.1159/000488984

Feng, Y., Ren, J., Gui, Y., Wei, W., Shu, B., Lu, Q., et al. (2018). Wnt/β-Catenin-Promoted Macrophage Alternative Activation Contributes to Kidney Fibrosis. *J. Am. Soc. Nephrol.* 29, 182–193. doi:10.1681/ASN.2017040391

Forssell, J., Oberg, A., Henriksson, M. L., Stenling, R., Jung, A., and Palmqvist, R. (2007). High Macrophage Infiltration along the Tumor Front Correlates with Improved Survival in colon Cancer. *Clin. Cancer Res.* 13, 1472–1479. doi:10.1158/1078-0432.CCR-06-2073

Hao, N. B., Lü, M. H., Fan, Y. H., Cao, Y. L., Zhang, Z. R., and Yang, S. M. (2012). Macrophages in Tumor Microenvironments and the Progression of Tumors. *Clin. Dev. Immunol.* 2012, 948098. doi:10.1155/2012/948098

Isidro, R. A., and Appleyard, C. B. (2016). Colonic Macrophage Polarization in Homeostasis, Inflammation, and Cancer. *Am. J. Physiol. Gastrointest. Liver Physiol.* 311, G59–G73. doi:10.1152/ajpgi.00123.2016

Jati, S., Kundu, S., Chakraborty, A., Mahata, S. K., Nizet, V., and Sen, M. (2018). Wnt5A Signaling Promotes Defense against Bacterial Pathogens by Activating a Host Autophagy Circuit. *Front. Immunol.* 9, 679. doi:10.3389/fimmu.2018.00679

Lan, J., Sun, L., Xu, F., Liu, L., Hu, F., Song, D., et al. (2019). M2 Macrophage-Derived Exosomes Promote Cell Migration and Invasion in Colon Cancer. *Cancer Res.* 79, 146–158. doi:10.1158/0008-5472.CAN-18-0014

Lecarpentier, Y., Claes, V., Duthoit, G., and Hébert, J. L. (2014). Circadian Rhythms, Wnt/beta-Catenin Pathway and PPAR Alpha/gamma Profiles in Diseases with Primary or Secondary Cardiac Dysfunction. *Front. Physiol.* 5, 429. doi:10.3389/fphys.2014.00429

Lee, Y. S., Song, S. J., Hong, H. K., Oh, B. Y., Lee, W. Y., and Cho, Y. B. (2020). The FBW7-MCL-1 axis Is Key in M1 and M2 Macrophage-Related colon Cancer Cell Progression: Validating the Immunotherapeutic Value of Targeting PI3Kγ. *Exp. Mol. Med.* 52, 815–831. doi:10.1038/s12276-020-0436-7

Li, J., Li, L., Li, Y., Long, Y., Zhao, Q., Ouyang, Y., et al. (2020). Tumor-associated Macrophage Infiltration and Prognosis in Colorectal Cancer: Systematic Review and Meta-Analysis. *Int. J. Colorectal Dis.* 35, 1203–1210. doi:10.1007/s00384-020-03593-z

Liberzon, A., Subramanian, A., Pinchback, R., Thorvaldsdóttir, H., Tamayo, P., and Mesirov, J. P. (2011). Molecular Signatures Database (MSigDB) 3.0. *Bioinformatics* 27, 1739–1740. doi:10.1093/bioinformatics/btr260

Luput, L., Licarete, E., Sesarman, A., Patras, L., Alupei, M. C., and Banciu, M. (2017). Tumor-associated Macrophages Favor C26 Murine colon Carcinoma Cell Proliferation in an Oxidative Stress-dependent Manner. *Oncol. Rep.* 37, 2472–2480. doi:10.3892/or.2017.5466

Macciò, A., Gramignano, G., Cherchi, M. C., Tanca, L., Melis, L., and Madeddu, C. (2020). Role of M1-Polarized Tumor-Associated Macrophages in the Prognosis of Advanced Ovarian Cancer Patients. *Sci. Rep.* 10, 6096. doi:10.1038/s41598-020-63276-1

Maiti, G., Naskar, D., and Sen, M. (2012). The Wingless Homolog Wnt5a Stimulates Phagocytosis but Not Bacterial Killing. *Proc. Natl. Acad. Sci. U S A.* 109, 16600–16605. doi:10.1073/pnas.1207789109

Malsin, E. S., Kim, S., Lam, A. P., and Gottardi, C. J. (2019). Macrophages as a Source and Recipient of Wnt Signals. *Front. Immunol.* 10, 1813. doi:10.3389/fimmu.2019.01813

Mantovani, A., Marchesi, F., Malesci, A., Laghi, L., and Allavena, P. (2017). Tumour-associated Macrophages as Treatment Targets in Oncology. *Nat. Rev. Clin. Oncol.* 14, 399–416. doi:10.1038/nrclinonc.2016.217

Mao, J., Wang, D., Wang, Z., Tian, W., Li, X., Duan, J., et al. (2016). Combretastatin A-1 Phosphate, a Microtubule Inhibitor, Acts on Both Hepatocellular Carcinoma Cells and Tumor-Associated Macrophages by Inhibiting the Wnt/β-Catenin Pathway. *Cancer Lett.* 380, 134–143. doi:10.1016/j.canlet.2016.06.020

Naskar, D., Maiti, G., Chakraborty, A., Roy, A., Chattopadhyay, D., and Sen, M. (2014). Wnt5a-Rac1-NF-κB Homeostatic Circuitry Sustains Innate Immune Functions in Macrophages. *J. Immunol.* 192, 4386–4397. doi:10.4049/jimmunol.1302817

Ong, S. M., Tan, Y. C., Beretta, O., Jiang, D., Yeap, W. H., Tai, J. J., et al. (2012). Macrophages in Human Colorectal Cancer Are Pro-inflammatory and Prime T Cells towards an Anti-tumour Type-1 Inflammatory Response. *Eur. J. Immunol.* 42, 89–100. doi:10.1002/eji.201141825

Ono, D., Honma, S., Nakajima, Y., Kuroda, S., Enoki, R., and Honma, K. I. (2017). Dissociation of Per1 and Bmal1 Circadian Rhythms in the Suprachiasmatic Nucleus in Parallel with Behavioral Outputs. *Proc. Natl. Acad. Sci. U S A.* 114, E3699–E3708. doi:10.1073/pnas.1613374114

Pereira, C., Schaer, D. J., Bachli, E. B., Kurrer, M. O., and Schoedon, G. (2008). Wnt5A/CaMKII Signaling Contributes to the Inflammatory Response of Macrophages and Is a Target for the Antiinflammatory Action of Activated Protein C and Interleukin-10. *Arterioscler Thromb. Vasc. Biol.* 28, 504–510. doi:10.1161/ATVBAHA.107.157438

Raghavan, S., Mehta, P., Xie, Y., Lei, Y. L., and Mehta, G. (2019). Ovarian Cancer Stem Cells and Macrophages Reciprocally Interact through the WNT Pathway to Promote Pro-tumoral and Malignant Phenotypes in 3D Engineered Microenvironments. *J. Immunother. Cancer* 7, 190. doi:10.1186/s40425-019-0666-1

Ruffell, B., Affara, N. I., and Coussens, L. M. (2012). Differential Macrophage Programming in the Tumor Microenvironment. *Trends Immunol.* 33, 119–126. doi:10.1016/j.it.2011.12.001

Sarode, P., Zheng, X., Giotopoulou, G. A., Weigert, A., Kuenne, C., Günther, S., et al. (2020). Reprogramming of Tumor-Associated Macrophages by Targeting β-catenin/FOSL2/ARID5A Signaling: A Potential Treatment of Lung Cancer. *Sci. Adv.* 6, eaaz6105. doi:10.1126/sciadv.aaz6105

Sawa-Wejksza, K., Dudek, A., Lemieszek, M., Kaławaj, K., and Kandefer-Szerszeń, M. (2018). Colon Cancer-Derived Conditioned Medium Induces Differentiation of THP-1 Monocytes into a Mixed Population of M1/M2 Cells. *Tumour Biol.* 40, 1010428318797880. doi:10.1177/1010428318797880

Shalhoub, J., Falck-Hansen, M. A., Davies, A. H., and Monaco, C. (2011). Innate Immunity and Monocyte-Macrophage Activation in Atherosclerosis. *J. Inflamm. (Lond)* 8, 9. doi:10.1186/1476-9255-8-9

Subramanian, A., Tamayo, P., Mootha, V. K., Mukherjee, S., Ebert, B. L., Gillette, M. A., et al. (2005). Gene Set Enrichment Analysis: a Knowledge-Based Approach for Interpreting Genome-wide Expression Profiles. *Proc. Natl. Acad. Sci. U S A.* 102, 15545–15550. doi:10.1073/pnas.0506580102

Tauriello, D. V., Calon, A., Lonardo, E., and Batlle, E. (2017). Determinants of Metastatic Competency in Colorectal Cancer. *Mol. Oncol.* 11, 97–119. doi:10.1002/1878-0261.12018

Tian, X., Wu, Y., Yang, Y., Wang, J., Niu, M., Gao, S., et al. (2020). Long Noncoding RNA LINC00662 Promotes M2 Macrophage Polarization and Hepatocellular Carcinoma Progression via Activating Wnt/β-Catenin Signaling. *Mol. Oncol.* 14, 462–483. doi:10.1002/1878-0261.12606

Tran, M. T. N., Hamada, M., Jeon, H., Shiraishi, R., Asano, K., Hattori, M., et al. (2017). MafB Is a Critical Regulator of Complement Component C1q. *Nat. Commun.* 8, 1700. doi:10.1038/s41467-017-01711-0

Vinnakota, K., Zhang, Y., Selvanesan, B. C., Topi, G., Salim, T., Sand-Dejmek, J., et al. (2017). M2-like Macrophages Induce colon Cancer Cell Invasion via Matrix Metalloproteinases. *J. Cel Physiol* 232, 3468–3480. doi:10.1002/jcp.25808

Wallace, J., Lutgen, V., Avasarala, S., St Croix, B., Winn, R. A., and Al-Harthi, L. (2018). Wnt7a Induces a Unique Phenotype of Monocyte-Derived Macrophages with Lower Phagocytic Capacity and Differential Expression of Pro- and Anti-inflammatory Cytokines. *Immunology* 153, 203–213. doi:10.1111/imm.12830

Waniczek, D., Lorenc, Z., Śnietura, M., Wesecki, M., Kopec, A., and Muc-Wierzgoń, M. (2017). Tumor-Associated Macrophages and Regulatory T Cells Infiltration and the Clinical Outcome in Colorectal Cancer. *Arch. Immunol. Ther. Exp. (Warsz)* 65, 445–454. doi:10.1007/s00005-017-0463-9

Wei, Z., Feng, M., Wu, Z., Shen, S., and Zhu, D. (2020). Bcl9 Depletion Modulates Endothelial Cell in Tumor Immune Microenvironment in Colorectal Cancer Tumor. *Front. Oncol.* 10, 603702. doi:10.3389/fonc.2020.603702

Wu, Y., Tao, B., Zhang, T., Fan, Y., and Mao, R. (2019). Pan-Cancer Analysis Reveals Disrupted Circadian Clock Associates with T Cell Exhaustion. *Front. Immunol.* 10, 2451. doi:10.3389/fimmu.2019.02451

Yahaya, M. A. F., Lila, M. A. M., Ismail, S., Zainol, M., and Afizan, N. A. R. N. M. (2019). Tumour-Associated Macrophages (TAMs) in Colon Cancer and How to Reeducate Them. *J. Immunol. Res.* 2019, 2368249. doi:10.1155/2019/2368249

Yang, Y., Ye, Y. C., Chen, Y., Zhao, J. L., Gao, C. C., Han, H., et al. (2018). Crosstalk between Hepatic Tumor Cells and Macrophages via Wnt/β-Catenin Signaling

Promotes M2-like Macrophage Polarization and Reinforces Tumor Malignant Behaviors. *Cell Death Dis* 9, 793. doi:10.1038/s41419-018-0818-0

Yuan, A., Hsiao, Y. J., Chen, H. Y., Chen, H. W., Ho, C. C., Chen, Y. Y., et al. (2015). Opposite Effects of M1 and M2 Macrophage Subtypes on Lung Cancer Progression. *Sci. Rep.* 5, 14273. doi:10.1038/srep14273

Yuan, C., Yang, D., Ma, J., Yang, J., Xue, J., Song, F., et al. (2020). Modulation of Wnt/β-Catenin Signaling in IL-17A-mediated Macrophage Polarization of RAW264.7 Cells. *Braz. J. Med. Biol. Res.* 53, e9488. doi:10.1590/1414-431X20209488

Zhou, Y., Zhou, B., Pache, L., Chang, M., Khodabakhshi, A. H., Tanaseichuk, O., et al. (2019). Metascape Provides a Biologist-Oriented Resource for the Analysis of Systems-Level Datasets. *Nat. Commun.* 10, 1523. doi:10.1038/s41467-019-09234-6

Zhu, Z., Yin, S., Wu, K., Lee, A., Liu, Y., Li, H., et al. (2018). Downregulation of Sfrp5 in Insulin Resistant Rats Promotes Macrophage-Mediated Pulmonary Inflammation through Activation of Wnt5a/JNK1 Signaling. *Biochem. Biophys. Res. Commun.* 505, 498–504. doi:10.1016/j.bbrc.2018.09.070

Conflict of Interest: The authors declare that the research was conducted in the absence of any commercial or financial relationships that could be construed as a potential conflict of interest.

Publisher's Note: All claims expressed in this article are solely those of the authors and do not necessarily represent those of their affiliated organizations, or those of the publisher, the editors and the reviewers. Any product that may be evaluated in this article, or claim that may be made by its manufacturer, is not guaranteed or endorsed by the publisher.

frontiers in Pharmacology

ORIGINAL RESEARCH
published: 08 October 2021
doi: 10.3389/fphar.2021.749134

FDX1 can Impact the Prognosis and Mediate the Metabolism of Lung Adenocarcinoma

Zeyu Zhang[1†], Yarui Ma[2†], Xiaolei Guo[3], Yingxi Du[4], Qing Zhu[5], Xiaobing Wang[4]* and Changzhu Duan[6]**

[1]Department of the First Clinical Medicine, Chongqing Medical University, Chongqing, China, [2]Department of Medical Oncology, Beijing Hospital, National Center of Gerontology, Institute of Geriatric Medicine, Chinese Academy of Medical Sciences, Beijing, China, [3]Binzhou Polytechnic, Binzhou, China, [4]State Key Lab of Molecular Oncology, National Cancer Center/National Clinical Research Center for Cancer/Cancer Hospital, Chinese Academy of Medical Sciences and Peking Union Medical College, Beijing, China, [5]Department of Clinical Laboratory, Beijing Friendship Hospital, Capital Medical University, Beijing, China, [6]Department of Cell Biology and Genetics, Medicine and Cancer Research Center, Chongqing Medical University, Chongqing, China

OPEN ACCESS

Edited by:
Lesheng Teng,
Jilin University, China

Reviewed by:
Yifan Ma,
The Ohio State University, United States
Shiyan Dong,
Jilin University, China

***Correspondence:**
Qing Zhu
qzhu0608@126.com
Xiaobing Wang
wangxb@cicams.ac.cn
Changzhu Duan
duanchzhu@cqmu.edu.cn

†These authors have contributed equally to this work

Specialty section:
This article was submitted to Inflammation Pharmacology, a section of the journal Frontiers in Pharmacology

Received: 29 July 2021
Accepted: 08 September 2021
Published: 08 October 2021

Citation:
Zhang Z, Ma Y, Guo X, Du Y, Zhu Q, Wang X and Duan C (2021) FDX1 can Impact the Prognosis and Mediate the Metabolism of Lung Adenocarcinoma. Front. Pharmacol. 12:749134. doi: 10.3389/fphar.2021.749134

Background: Lung cancer has emerged as one of the most common cancers in recent years. The mitochondrial electron transport chain (ETC) is closely connected with metabolic pathways and inflammatory response. However, the influence of ETC-associated genes on the tumor immune response and the pathogenesis of lung cancer is not clear and needs further exploration.

Methods: The RNA-sequencing transcriptome and clinical characteristic data of LUAD were downloaded from the Cancer Genome Atlas (TCGA) database. The LASSO algorithm was used to build the risk signature, and the prediction model was evaluated by the survival analysis and receiver operating characteristic curve. We explored the function of FDX1 through flow cytometry, molecular biological methods, and liquid chromatography–tandem mass spectrometry/mass spectrometry (LC–MS/MS).

Results: 12 genes (*FDX1*, *FDX2*, *LOXL2*, *ASPH*, *GLRX2*, *ALDH2*, *CYCS*, *AKR1A1*, *MAOB*, *RDH16*, *CYBB*, and *CYB5A*) were selected to build the risk signature, and the risk score was calculated with the coefficients from the LASSO algorithm. The 1-year, 3-year, and 5-year area under the curve (AUC) of ROC curves of the dataset were 0.7, 0.674, and 0.692, respectively. Univariate Cox analysis and multivariate Cox regression analysis indicated that the risk signature is an independent risk factor for LUAD patients. Among these genes, we focused on the *FDX1* gene, and we found that knockdown of FDX1 neither inhibited tumor cell growth nor did it induce apoptosis or abnormal cell cycle distribution. But FDX1 could promote the ATP production. Furthermore, our study showed that FDX1 was closely related to the glucose metabolism, fatty acid oxidation, and amino acid metabolism.

Abbreviations: AUC, area under curve; ETC, electron transport chain; FAO, fatty acid oxidation; FDX1, ferredoxin 1; LC–MS/MS, liquid chromatography–tandem mass spectrometry/mass spectrometry; LUAD, lung adenocarcinoma; NSCLC, non–small-cell lung carcinoma; ROC, receiver operating characteristic; SD, standard deviation.

Conclusion: Collectively, this study provides new clues about carcinogenesis induced by ETC-associated genes in LUAD and paves the way for finding potential targets of LUAD.

Keywords: lung cancer, inflammatory response, mitochondria electron transport chain, risk signature, metabolism

INTRODUCTION

There have been an increasing number of new cancer cases every year. Lung cancer is one of the most morbidity diseases among all cancers, with a proportion as high as 11.6% (Bray et al., 2018; Barta et al., 2019). Lung cancer has a poor prognosis and is one of the deadly cancers in humans; over one-half of patients die within 1 year of diagnosis (Zappa and Mousa, 2016; Kimura et al., 2018; Duma et al., 2019). Non–small-cell lung carcinoma (NSCLC) accounts for 80–85% of all lung cancers (Sher et al., 2008). Lung adenocarcinoma (LUAD) is the most common histological type of NSCLC, accounting for 50% of NSCLCs (Bi et al., 2020; Zhang et al., 2020).

Metabolism plays an important role in carcinogenesis, and in recent years, it has been leveraged for tumor treatments (Biswas, 2015; Vander Heiden and DeBerardinis, 2017; Kumar and Misra, 2019). Multiple studies have shown that metabolism and cancer are closely related; currently, metabolites are important targets in the treatment of cancer (Chae and Kim, 2018; Dinges et al., 2019; Huang et al., 2021). The mitochondria electron transport chain locates in the inner membrane of the mitochondria and is composed of four complexes, including complexes I, II, III, and ATP synthase (Chen and Butow, 2005). Mutations in mitochondria DNA (mDNA) have been identified in several tumor types (Larman et al., 2012; Bonora et al., 2021; Kopinski et al., 2021). For example, mitochondrial fission regulator 2 (MTFR2) was a biomarker for diagnosis and poor prognosis in LUAD (Chen et al., 2021).

The mitochondria in tumor cells contain the rich protein network, and the interaction between these proteins is very important for initiating an antitumor immune response. Studies have reported that the enzyme RIPK3 can regulate the activity of mitochondrial enzyme PGAM5 and trigger the expression of inflammatory cytokines in NKT cells, thus playing a dual role in the development of autoimmune diseases and the destruction of tumor cells (Kang et al., 2015). The intensity of the inflammatory response and multiple metabolic processes in patients with lung cancer activate each other and jointly promote the progression of the disease. As the inflammatory response intensifies, the metabolic dysfunction becomes more obvious. Studies have found that the serum levels of PCT and IL-6 after lung cancer surgery are higher than those before surgery. Combined detection of PCT and IL-6 can be an effective means to identify complications after lung cancer surgery (Zhu et al., 2019). Therefore, exploring mitochondrial metabolism has important practical significance for tumor progression, tumor prognosis, tumor treatment, and many other aspects.

In this study, we investigated the role of the ETC genes in the overall survival of LUAD using LUAD transcriptome expression data from the TCGA database. Next, we constructed cells with FDX1 knocked down and explored the changes in cellular biological functions, including the proliferation and apoptosis rates, the cell cycle distribution, and cellular metabolism.

METHODS

Dataset Analysis

The RNA-sequencing transcriptome and clinical characteristic data of the LUAD cohort which contained 535 LUAD patients and 59 normal samples were downloaded from the TCGA database (https://cancergenome.nih.gov/). Mitochondria ETC genes were reported (**Supplementary Table S1**).

Prognostic Risk Signature Prediction and Calculation

Univariate Cox analysis was performed to evaluate the correlation between ETC genes and overall survival (OS). A risk score for each patient was calculated as the sum of each gene's score, which was obtained by multiplying the expression of each gene and its coefficient. The cohort was divided into high- and low-risk groups based on the median value of the risk scores. The difference of OS between high- and low-risk groups was calculated by the Kaplan–Meier method with a two-sided log-rank test. The receiver operating characteristic (ROC) curve was constructed to evaluate the prediction accuracy of the prognostic model.

The chi-square test was performed to compare the distribution of clinicopathological parameters between high- and low-risk groups. Heatmaps were used to visualize the difference with heatmap R package. Univariate and multivariate Cox regression analyses were used to identify the independent prognostic factors for the cohort. The survival difference between high-risk and low-risk groups stratified by age, gender, stage, and TNM was further evaluated.

Single Gene Bioinformatics Analysis

The survival curve was plotted through the online tool PrognoScan (http://dna00.bio.kyutech.ac.jp/PrognoScan/index.html). The Go enrichment analysis was performed using clusterProfiler package in R environment. GSEA was carried out using the curated gene sets "c2.cp.kegg.v7.4.symbols.gmt" to illustrate the different enriched terms between the high and low FDX1 expression groups.

Cell Culture

A549 cell line was obtained from the National Infrastructure of Cell Line Resource (Shanghai, China). The A549 cell line was cultured in RPMI 1640 containing 10% fetal bovine serum and penicillin (100 U/mL)/streptomycin (0.1 mg/ml), and cultured at 37°C in a humidified atmosphere containing 5% CO_2.

RNA Interference

Small interfering RNA was purchased from GenePharma (Suzhou, China). A549 cells were transfected with 50 nm FDX1 siRNAs using Lipofectamine RNAiMAX (Invitrogen/ Thermo Fisher Scientific, Cat# 13778030). The knockdown efficiency was evaluated by quantitative RT-PCR after 72 h of transfection. The following siRNA sequences were used: FDX1-1-F, CAUCUUUGAAGAUCACAUAtt; FDX1-1-R, UAUGUG AUCUUCAAAGAUGag; FDX1-2-F, GCAUAUGGACUAACA GACAtt; and FDX1-2-R, UGUCUGUUAGUCCAUAUGCca.

RT-PCR

Total RNA was extracted from the cells using TRIzol reagent (Thermo Scientific, Cat# 15596018). Then, the RNA was quantified using Nanodrop. The RNA was reverse-transcribed into DNA using a PrimeScript RT Reagent Kit (Takara, Cat# RR036A) according to the manufacturer's protocol. The primers were as follows: FDX1-F, TTCAACCTGTCACCTCATCTTTG; FDX1-R, TGCCAGATCGAGCATGTCATT; GAPDH-F, GGA GCGAGATCCCTCCAAAAT; and GAPDH-R, GGCTGTTGT CATACTTCTCATGG.

Cell Growth Assays

The CCK-8 agent (Dojindo, Cat# CK04) was used to detect cell viability. A549 cells were plated in 96-well plates at 2000 cells per well. Then, CCK-8 was added to each well every 24 h for 5 days according to the manufacturer's protocol. The absorbance value was detected using a microplate reader (Bio-Rad Laboratories; Hercules, CA, USA) at 450 nm.

Flow Cytometry

Both apoptosis and cell cycle analysis were analyzed on a flow cytometer (Beckman Coulter) according to the manufacturer's instructions. Apoptosis was determined using the Apoptosis Detection Kit (Dojindo, Kumamoto, Japan) and analyzed with FlowJo v10 (FlowJo, LLC). Cell cycle analysis was performed using the Cell Cycle and Apoptosis Analysis Kit (Beyotime; Jiangsu, China) and analyzed by Modfit LT 3.2 software (Verity Software House; www.vsh.com; Topsham, ME).

ATP Measurement

ATP levels were measured with an ATP assay kit (Beyotime Biotechnology, Cat# S0027) according to the manufacturer's instructions. In brief, 20 μl cell sample was mixed with 100 μl ATP detection working fluid; the luminescence was measured using a multi-scan spectrum (BioTEK H1MFD). The concentration of ATP in the sample was calculated according to the standard curve. In order to eliminate the error caused by the difference of the protein amount in sample preparation, the concentration of ATP is converted to nmol/mg.

Metabolic Profiling

SiFDX1 cells and control cells were cultured in 10-cm plates. The metabolites were extracted using prechilled 80% (v/v) HPLC-grade methanol after culturing for 72 h and then incubated overnight at −80°C. The tubes were centrifuged for 20 min at 14,000 g, and the supernatant was transferred to new tubes. Then, the protein precipitation was used to be quantified by the BCA method. The supernatant was concentrated by a vacuum centrifugal concentrator for 1 h. Furthermore, the metabolites were redissolved according to the protein concentrations. The polar metabolites were detected by liquid chromatography–tandem mass spectrometry/mass spectrometry (LC–MS/MS). Data were acquired in both positive (ESI+) and negative (ESI-) modes. All the data were used for the statistical analysis. T-test results were evaluated with Excel. MetaboAnalyst (www.metaboanalyst.ca) was used to determine the heatmap and differential metabolic pathways.

Statistical Analysis

All statistical analyses were performed using R software (version 3.5.1). Wilcoxon's test was used to compare the expression of ETC genes between LUAD and adjacent normal tissues. The relationship between ETC genes and the clinicopathological characteristics of LUAD patients was analyzed using the Kolmogorov–Smirnov test. Using the "km" method in the R package "ConsensusClusterPlus," we classified 535 LUAD patients into different subtypes. The median risk score was used as a cutoff value to classify patients into a high-risk group and a low-risk group, and the Kaplan–Meier method was used to analyze the difference in overall survival (OS) between the high- and low-risk groups. The chi-square test was used to compare the relationship between the risk score and clinicopathological variables. Cox univariate and multivariate analyses of the relationship between clinicopathological variables and risk scores were performed. $p < 0.05$ was considered to indicate a statistically significant difference.

RESULTS

Expression Pattern and Risk Signature of ETC Genes in LUAD.

Mitochondrial ETC plays a pivotal role in cell energy metabolism. The occurrence and development of lung adenocarcinoma are closely linked to cell metabolism, and we hope to explore the impact of mitochondrial ETC gene expression in LUAD. We downloaded the ETC genes from online database AmiGO2 (http://amigo.geneontology.org/amigo). LUAD cancer tissues and normal lung tissues were compared to explore the expression level of mitochondria ETC genes (**Supplementary Table S2**). A total of 47 differential expression genes (DEGs) were identified with high expression of 34 genes and low expression of 13 genes in LUAD tissues (**Supplementary Figure S1**, **Supplementary Table S2**).

To better explore the relationship between mitochondria ETC genes and clinical outcomes in LUAD patients, univariate Cox regression analysis was performed to evaluate the prognostic role of ETC genes in LUAD (**Supplementary Table S3**). In order to predict the clinical outcomes of LUAD with ETC genes, we applied the least absolute shrinkage and selection operator (LASSO) Cox regression algorithm to the differential expression ETC genes to construct the prognostic signature.

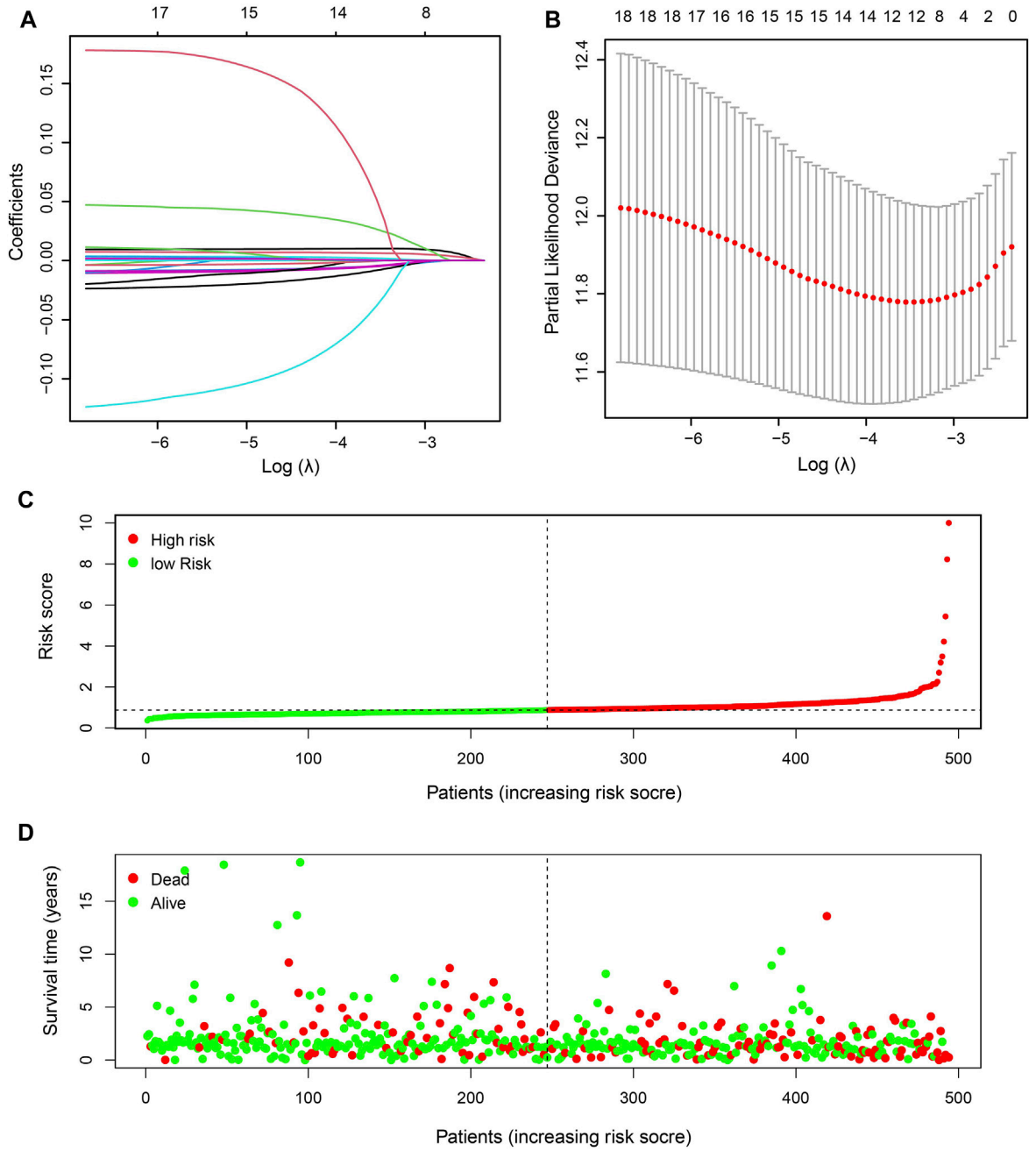

FIGURE 1 | Identification of prognostic ETC-associated genes. **(A)**. The LASSO coefficient distribution map of the 12 ETC genes in LUAD patients. **(B)**. The partial likelihood deviance plot based on the LASSO model. **(C)**. The risk score distribution of the 12-gene risk signature model in LUAD patients. **(D)**. The survival status of patients in high-risk and low-risk groups of LUAD patients.

According to the partial likelihood deviance and lambda values, 12 genes (*FDX1*, *FDX2*, *LOXL2*, *ASPH*, *GLRX2*, *ALDH2*, *CYCS*, *AKR1A1*, *MAOB*, *RDH16*, *CYBB*, and *CYB5A*) were selected to build the risk signature, and the risk score was calculated with the coefficients from the LASSO algorithm (**Figures 1A,B**) (**Supplementary Table S4**). According to the median risk score, LUAD patients were divided into low- and high-risk groups to investigate the prognostic role of the risk signature (**Figures 1C,D**). The results indicated that the high-risk group had a worse survival (**Figure 2A**). Moreover, a receiver operating characteristic (ROC) curve was generated to assess the predictive value of the constructed model. The 1-year, 3-year, and 5-year area under the curve (AUC) of ROC curves of the TCGA-LUAD dataset were 0.7, 0.674, and 0.692, respectively (**Figures 2B–D**).

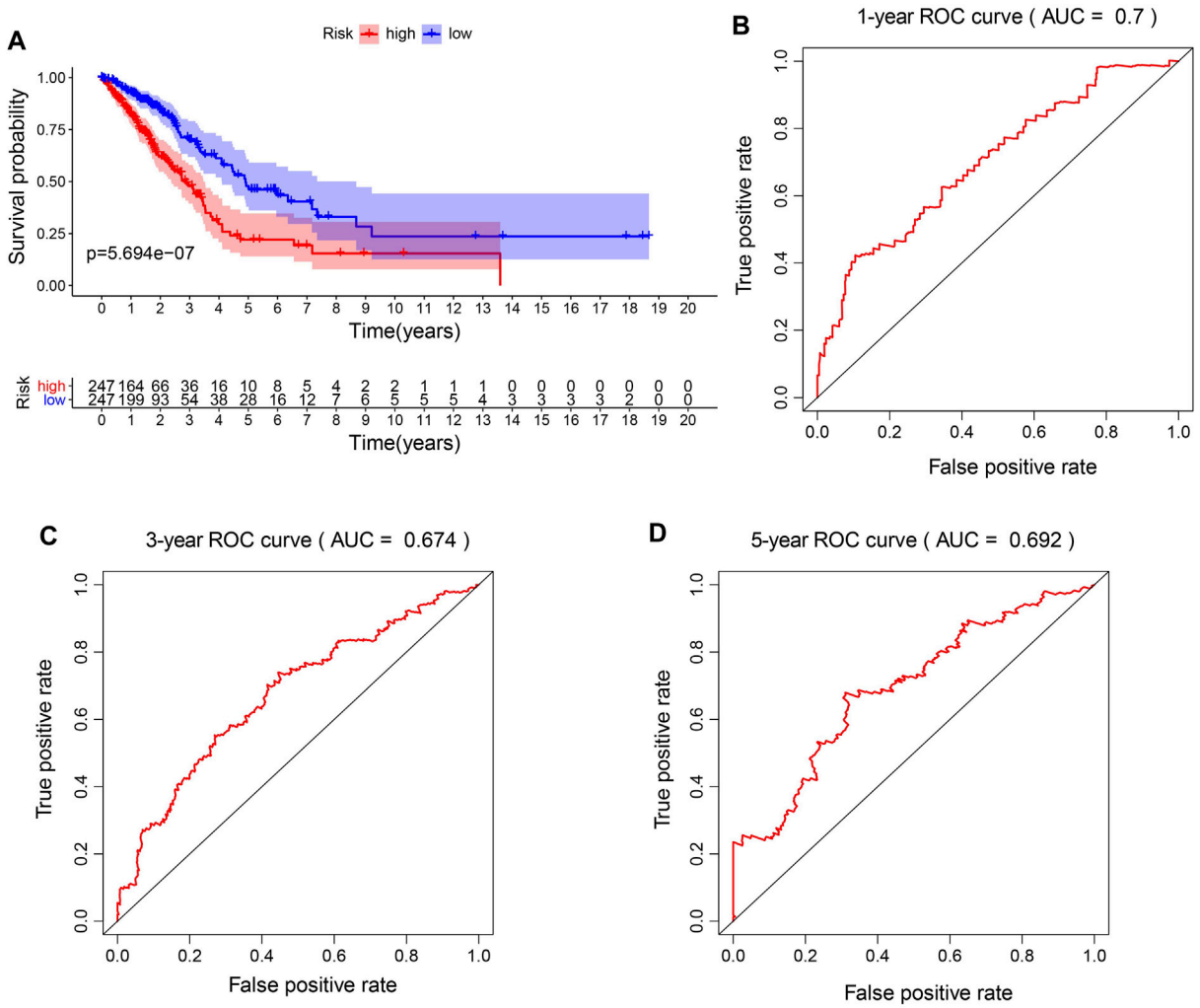

FIGURE 2 | Prognostic accuracy of the risk model. **(A)**. The survival analysis of high-risk signature and low-risk signature in LUAD patients. **(B–D)**. The 1-year, 3-year, and 5-year area under the curve (AUC) of ROC curves.

The Risk Score was an Independent Prognostic Factor in LUAD.

Next, the associations of the risk signature and clinicopathological features were evaluated, and we discovered that significant difference was observed of N stage, T stage, stage, age, and survival status between the two risk groups, while no significant difference was found of M and gender between the two risk groups (**Figure 3A**). Furthermore, we performed univariate and multivariate Cox regression analyses to determine whether the risk signature was an independent prognostic indicator. Univariate Cox analysis showed that the risk score, stage, and T and N status were correlated with the OS (**Figure 3B**). Multivariate Cox regression analysis indicated that the risk score was correlated with the OS (**Figure 3C**). These results suggested that the risk signature is an independent risk factor for LUAD patients.

FDX1 Plays a Pivotal Role in LUAD.

FDX1 encodes a small iron–sulfur protein that participates in the reduction in mitochondrial cytochrome and the synthesis of various steroid hormones (Sheftel et al., 2010; Strushkevich et al., 2011). Also, FDX1 can augment the copper-dependent cell death induced by elesclomol and may provide a new idea for increasing the efficacy of several cancer-targeting agents (Tsvetkov et al., 2019). Next, we focused on *FDX1* and explored its function in LUAD. The mRNA expression level was significantly decreased in the tumor tissues compared to adjacent normal tissues in the TCGA-LUAD dataset (**Figure 4A**). Also, we discovered that LUAD patients with the lower expression of FDX1 had a worse prognosis using the online analysis tool PrognoScan (http://dna00.bio.kyutech.ac.jp/PrognoScan/index.html) (**Figure 4B**), which suggested that FDX1 played a pivotal role in LUAD patients. Moreover, the GO enrichment analyses revealed that FDX1 was mainly associated with oxidative phosphorylation, respiratory electron transport chain, and mitochondrial protein

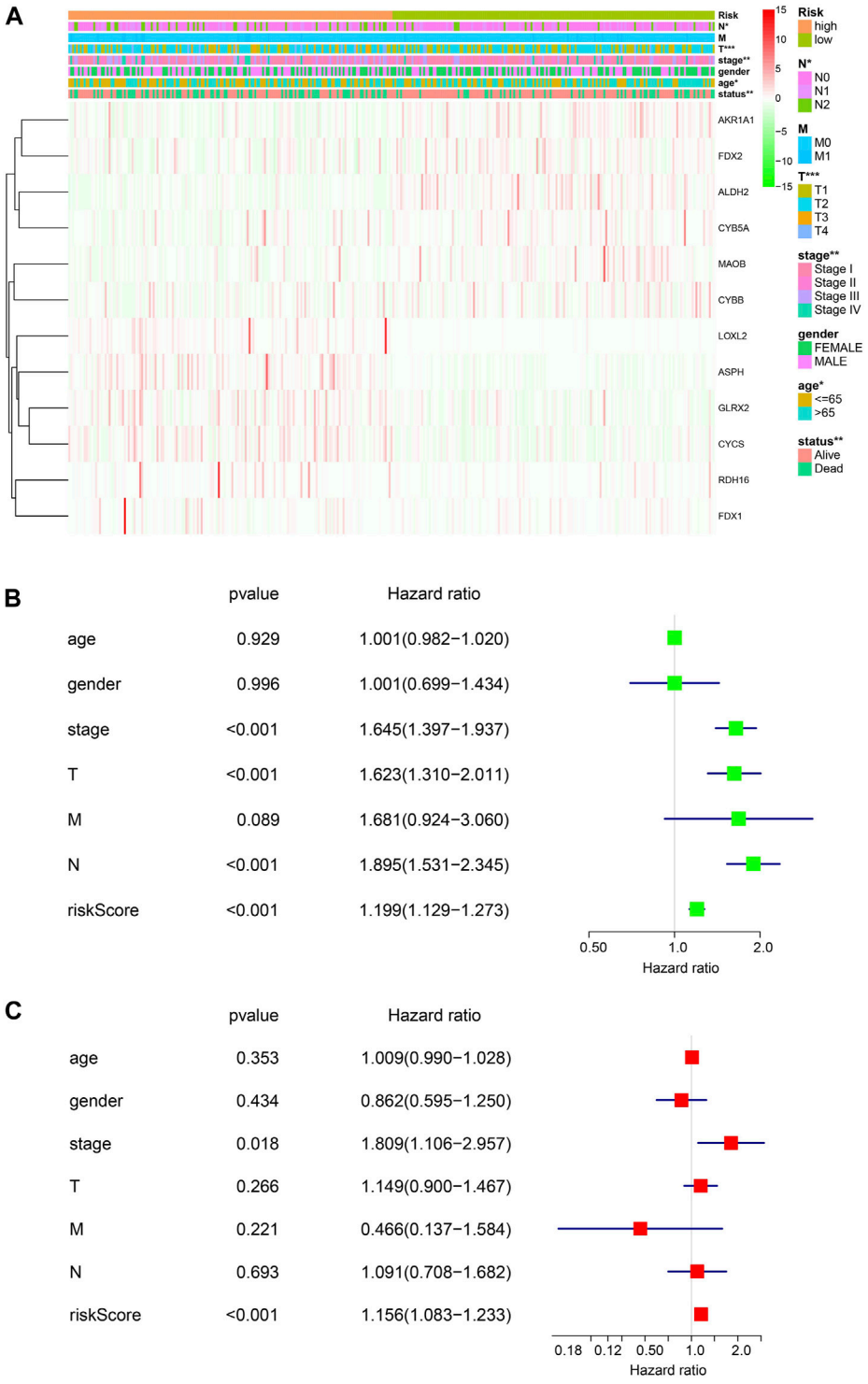

FIGURE 3 | Risk signature of ETC genes in LUAD. **(A)**. The associations of risk signature and clinicopathological features (T, N, M, tumor stage, gender, age, and the survival status). **(B, C)**. Univariate and multivariate Cox analyses of the clinicopathological features (age, gender, stage, T, N, and M) and risk signature of overall survival in LUAD patients.

complex (**Figure 4C**). In addition, GSEA enrichment analysis was performed to explore the underlying mechanism of FDX1, and the analysis suggested that low expressed FDX1 was correlated with fatty acid metabolism and oxidative phosphorylation metabolism (**Figures 4D,E**). Furthermore, we investigated the function of FDX1 in the online database (http://bioinfo.life.hust.edu.cn/

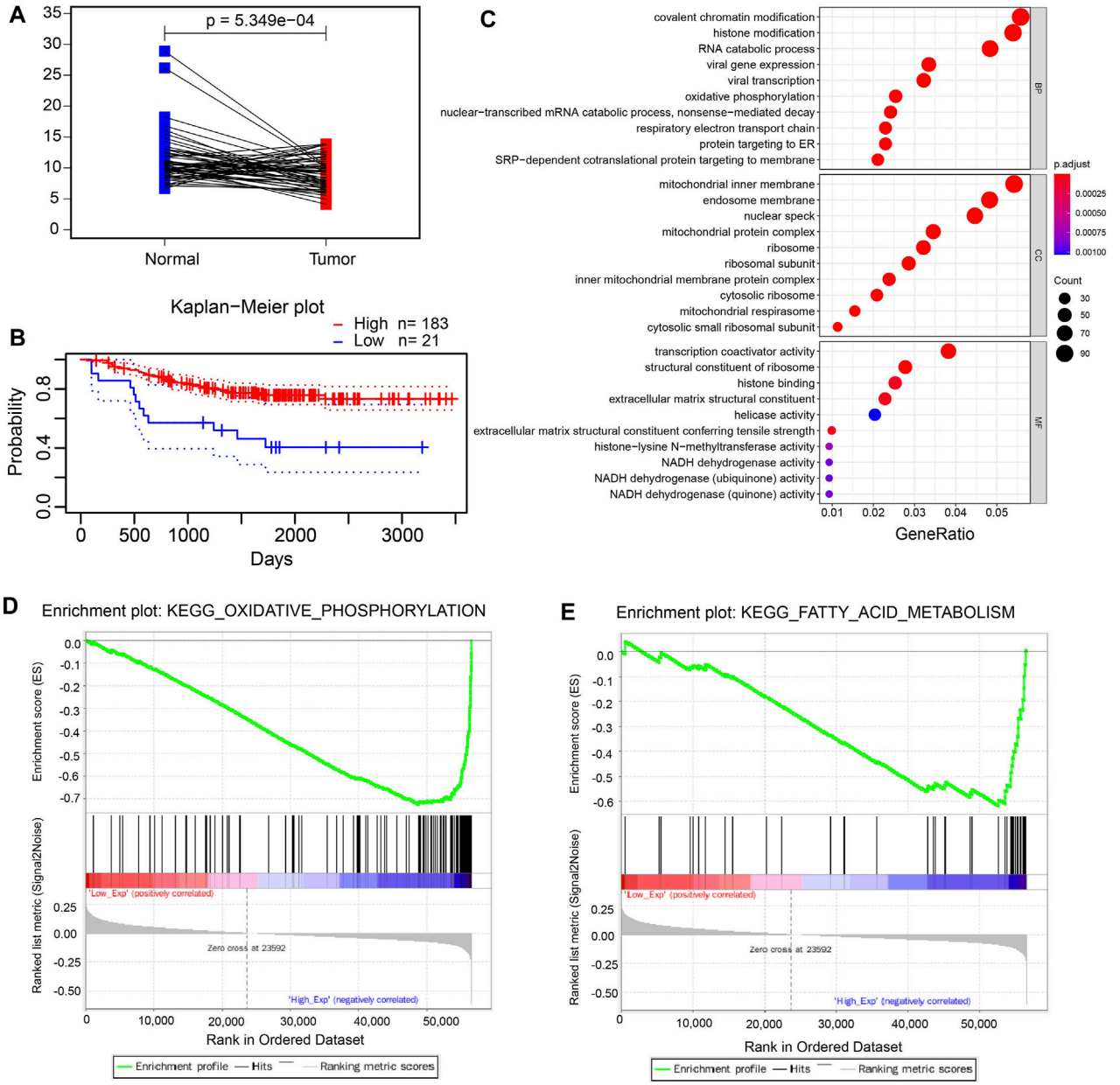

FIGURE 4 | FDX1 plays a pivotal role in LUAD. **(A)**. The mRNA level of paired LUAD tumor tissues and adjacent normal tissues in the TCGA-LUAD dataset. **(B)**. The Kaplan–Meier plot of low expression and high expression of FDX1 in LUAD patients using the ProgScan online tool. c. The GO enrichment analysis of FDX1. **(D, E)**. The GSEA analysis of low expression of FDX1.

GSCA/#/) and found that FDX1 had significant effect on immune-associated cells, such as dendritic cells, macrophage, and iTreg cells (**Supplementary Figure S3**).

Knockdown of FDX1 Neither Inhibited Tumor Cell Growth Nor Did It Induce Apoptosis or Cell Cycle Arrest.

To investigate whether FDX1 deficiency affects the growth of tumor cells, we constructed the FDX1-deficient cells using small interference RNA and determined the knockdown efficiency through qPCR. We found that the siRNAs significantly inhibited the expression of FDX1 (**Figure 5A**). However, knockdown of FDX1 did not change the cell viability through assay (**Figure 5B**). We further investigated the influence of FDX1 on apoptosis, and the effects of two siRNA groups were not significantly different (**Figure 5C**). Next, we determined the cell cycle changes in FDX1-deficient cells (KD-FDX1) and FDX1 wild-type cells (WT-FDX1). Knocking down of FDX1 did not induce G2/M cell cycle arrest significantly (**Figures**

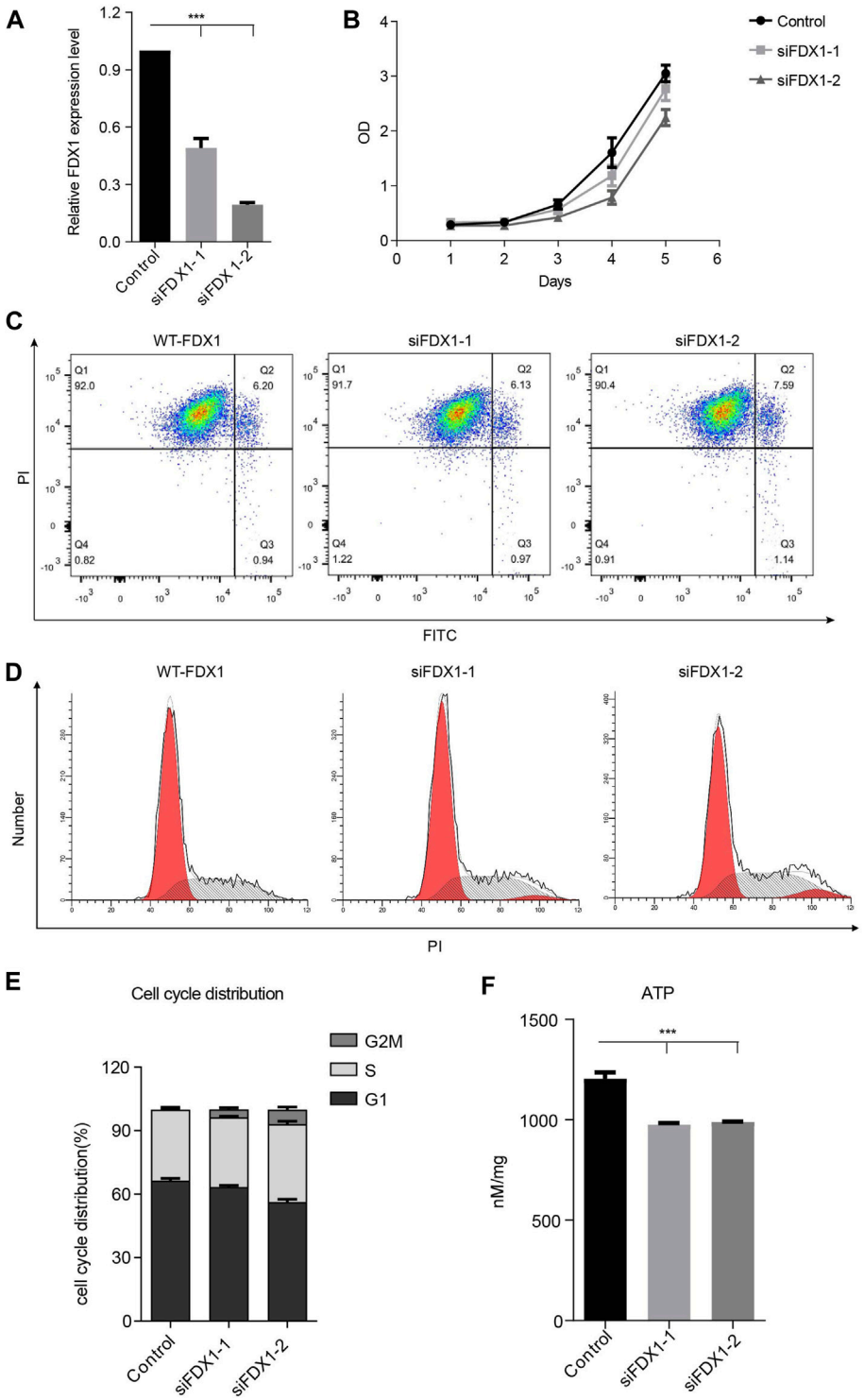

FIGURE 5 | Biological function of FDX1 in A549 cells. **(A)**. Expression of FDX1 in A549 cells transfected with si-FDX1. **(B)**. The cell growth of the FDX1 deficiency group and control group was assessed by the CCK-8 assay. **(C)**. The apoptotic rate of the control group and FDX1 deficient group. **(D)**. PI staining was used to detect the cell cycle distribution of the control group and FDX1-deficient group. **(E)**. The cell cycle distribution of FDX1-knockdown cells and FDX1-wild-type cells. **(F)**. ATP levels of FDX1-deficient cells and wild-type A549 cells.

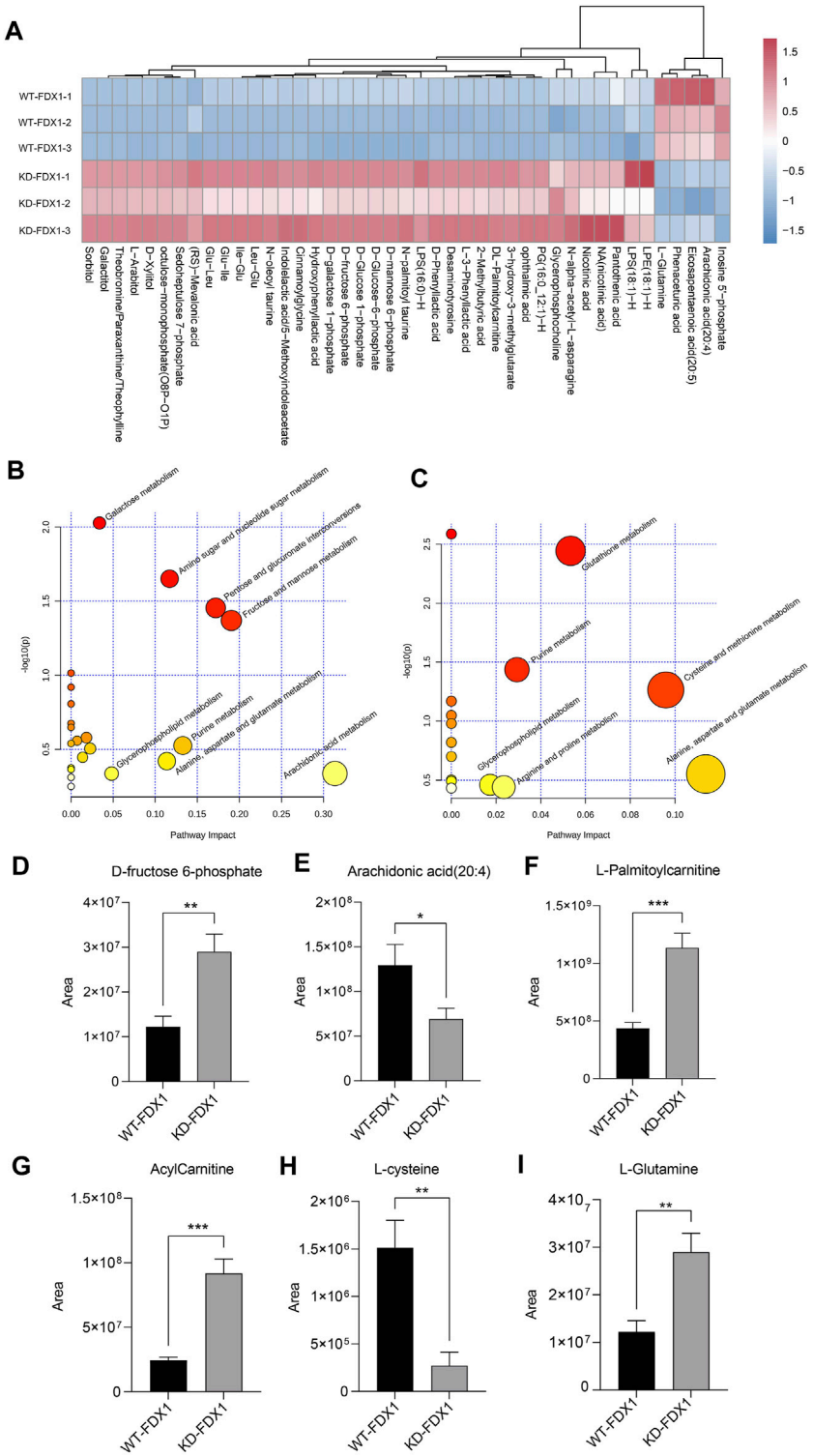

FIGURE 6 | Metabolic profiling of tumor cells with FDX1 deficiency. **(A)**. The heatmap of differential metabolites in WT-FDX1 and KD-FDX1 cells in the negative ion mode. **(B, C)**. Pathway enrichment analysis of the differential metabolites in both the negative and positive ion modes. **(D–I)**. The levels of D-fructose 6-phosphate, arachidonic acid (20:4), L-palmitoylcarnitine, acylcarnitine, L-cysteine, and L-glutamine in WT-FDX1 and KO-FDX1 cells. The data are presented as the mean ± SD. *$p < 0.01$, **$p < 0.001$ and ***$p < 0.0001$ (*t*-test).

5D,E). These data confirmed that knockdown of FDX1 neither affected cell growth nor did it induce apoptosis or cell cycle arrest. To confirm the effect of FDX1 deficiency on ATP levels, we measured the production of ATP in FDX1-wild-type cells and FDX1-knockdown cells, and the results showed that the ATP concentration of the FDX1 deficiency group was lower than that of the control group (**Figure 5F**). These data inspired us to explore more about the aberrant metabolism caused by FDX1 deficiency.

Metabolic Profiling of Tumor Cells With FDX1 Deficiency.

To further explore the metabolic changes caused by FDX1 deficiency, we performed nontargeted metabolomic analysis on WT-FDX1 cells and KD-FDX1 cells. The data showed that 10 metabolites and 5 metabolites were downregulated in positive and negative modes, respectively, with a threshold value of $p < 0.05$ and a ratio of WT-FDX1 cells to KD-FDX1 cells <0.6 (**Supplementary Figure S2**, **Figure 6A**). In addition, 79 metabolites and 38 metabolites were upregulated in positive and negative modes, respectively, with a threshold value of $p < 0.05$ and a ratio of WT-FDX1 cells to KD-FDX1 cells >2 (**Supplementary Figure S2**, **Figure 6A**). Differential metabolite levels were further analyzed using MetaboAnalyst (www.metaboanalyst.ca). Several pathways were identified in the negative mode, including amino sugar and nucleotide sugar metabolism, fructose and mannose metabolism, fatty acid degradation, and alanine, aspartate, and glutamate metabolism (**Figure 6B**). Thiamine metabolism, glutathione metabolism, and fatty acid degradation pathways were changed dramatically in the positive mode (**Figure 6C**).

Among these metabolites, fructose 6-phosphate was increased dramatically after FDX1 knockdown, one of the intermediate metabolites of glucose that affect downstream factors in the glycolysis and the pentose phosphate pathways (**Figures 6D,E**). In addition, long-chain fatty acids, including arachidonic acid (20:4), were decreased in FDX1-knockdown cells. In addition, acylcarnitine and L-palmitoylcarnitine were increased significantly in cells with FDX1 deficiency (**Figures 6F,G**). These data suggested that knockdown of FDX1 promoted fatty acid oxidation. Moreover, L-cysteine and L-glutamine metabolites involved in amino acid metabolism were affected by FDX1 deficiency (**Figures 6H,I**). Taken together, these data suggested that FDX1 deficiency led to metabolic changes, especially in glucose metabolism, fatty acid oxidation, and amino acid metabolism.

DISCUSSION

Over the years, the most prevalent causes of death have changed. Several studies have reported that cancer is the leading cause of death (Heron and Anderson, 2016), and lung cancer is one of the most common causes of death by cancer (Bray et al., 2018). For this reason, researchers have carried out a variety of studies on LUAD to obtain a better understanding of it. In this study, we identified the ETC genes that correlated closely to the overall survival of LUAD patients. The prognostic model was constructed by the Lasso Cox regression model. The LUAD patients were classified into two groups: low-risk group and high-risk group, and the high-risk group was associated with poor prognosis. Moreover, the univariate and multivariate Cox analyses suggested that the ETC-associated gene signature was an independent prognostic factor for predicting the outcome of LUAD patients.

We constructed the risk signature using the 12 genes. Among them, aspartate β-hydroxylase (*ASPH*) plays a pivotal role in the malignant transformation of solid tumors by enhancing cell proliferation, migration, invasion and stimulation of angiogenesis, and immunosuppression (Ince et al., 2000; Huyan et al., 2014; Kanwal et al., 2020). A previous study showed that repression of aldehyde dehydrogenase 2 family (*ALDH2*) promotes lung tumor progression through accumulated acetaldehyde and DNA damage (Li et al., 2019). *CYBB*, a gene related to ETC and ferroptosis, associated signature could predict the 1-, 3-, and 5-year survival rates of LUAD patients (Wang et al., 2021). Also, mutation of the *CYBB* gene selectively affects macrophages and is associated with immune changes (Bustamante et al., 2011). *FDX1* and *FDX2*, the important metabolism-related genes, are closely related to mitochondrial cytochrome (Sheftel et al., 2010; Strushkevich et al., 2011; Shi et al., 2012). These data suggested those genes were associated with the changes of the inflammatory response/immune microenvironment and the prognosis of LUAD patients.

Furthermore, we explored the function of FDX1 in LUAD cell lines. To our knowledge, the detailed function of FDX1 has not yet been elucidated in LUAD. In this study, our data showed that KD-FDX1 cells and WT-FDX1 cells had no difference in terms of growth, apoptosis rate, and cell cycle distribution, while it was involved in other cellular aspects, including aberrant energetics, tumor-associated inflammation, and changes in the immune microenvironment (Hanahan and Weinberg, 2011; Boroughs and DeBerardinis, 2015).

Aberrant metabolism links closely to the immune microenvironment in tumor development. Also, an increasing amount of evidence suggests that the metabolism plays an important role in the development and progression of cancer (Garon et al., 2014; La Vecchia and Sebastián, 2020). We have identified that KD-FDX1 cells have a significant influence on glucose metabolism, fatty acid oxidation (FAO), and amino acid metabolism. Glucose and lactic acid metabolism were reported to be common abnormalities in lung cancer (Hensley et al., 2016; Chen et al., 2019). Our data revealed that KD-FDX1 cells had higher D-fructose 6-phosphate levels. A recent research work has shown that D-fructose 6-phosphate associated with PFKP may be a prognostic factor for lung cancer (Ganapathy-Kanniappan, 2020). In addition, several studies have suggested that fatty acid oxidation is abnormal in lung cancer cells, and FAO may regulate immune suppression through enabling lymph node

metastasis formation (Liu et al., 2020; Li et al., 2021). In our study, we found that KD-FDX1 cells have higher L-palmitoylcarnitine and acylcarnitine levels at the same arachidonic acid (20:4) concentration. In other words, this finding suggested that FDX1 knockdown promotes FAO. Increasing evidence has shown that glutamine can fulfill the metabolic needs of lung cancer cells. This is the first time to reveal the association of FDX1 with fatty acid oxidation (FAO) and amino acid metabolism in LUAD using nontargeted metabolomics. There are still some limitations in our article. For example, the number of cell lines we have verified is limited, and further expansion of cell lines can increase the credibility of the article. In addition, the molecular mechanism of FDX1's regulation of metabolism still needs to be further explored. Overall, in our results, we found that FDX1 knockdown may decrease glutamine, and we speculated that FDX1 was likely to be a potential target in lung cancer treatment (Vanhove et al., 2019).

CONCLUSION

Taken together, we constructed an accurate prognosis model of LUAD patients. Moreover, we explored the effect of FDX1 knockdown in LUAD cells. Although there was no obvious effect on cell growth, apoptosis, or cell cycle distribution in the KD-FDX1 and WT-FDX1 cells, knockdown of FDX1 may significantly affect the metabolism. Our results indicated that knockdown of FDX1 mainly promoted glycolysis and fatty acid oxidation, and changed amino acid metabolism. This study provides new clues about the carcinogenesis induced by FDX1 in LUAD and paves the way for finding potential targets of LUAD.

DATA AVAILABILITY STATEMENT

The original contributions presented in the study are included in the article/**Supplementary Material**; further inquiries can be directed to the corresponding authors.

AUTHOR CONTRIBUTIONS

Conceptualization, ZZ and YM; funding acquisition, CD; supervision, QZ, XW, and CD; data curation, ZZ and XG; writing—original draft, ZZ, YD, and YM; writing—review and editing, QZ, XW, and CD. All authors have read and agreed to the published version of the manuscript.

FUNDING

This work was supported by the National Natural Science Foundation of China (No. 81772178).

SUPPLEMENTARY MATERIAL

The Supplementary Material for this article can be found online at: https://www.frontiersin.org/articles/10.3389/fphar.2021.749134/full#supplementary-material

Supplementary Figure S1 | Volcano plot of the mRNA expression of ETC-associated genes in the TCGA-LUAD dataset.

Supplementary Figure S2 | Heatmap of differential metabolites in WT-FDX1 and KD-FDX1 cells in the positive ion mode.

Supplementary Figure S3 | Correlation between FDX1 expression and immune infiltrates in LUAD.

REFERENCES

Barta, J. A., Powell, C. A., and Wisnivesky, J. P. (2019). Global Epidemiology of Lung Cancer. *Ann. Glob. Health* 85. 8. doi:10.5334/aogh.2419

Bi, K. W., Wei, X. G., Qin, X. X., and Li, B. (2020). BTK Has Potential to Be a Prognostic Factor for Lung Adenocarcinoma and an Indicator for Tumor Microenvironment Remodeling: A Study Based on TCGA Data Mining. *Front. Oncol.* 10, 424. doi:10.3389/fonc.2020.00424

Biswas, S. K. (2015). Metabolic Reprogramming of Immune Cells in Cancer Progression. *Immunity* 43, 435–449. doi:10.1016/j.immuni.2015.09.001

Bonora, M., Missiroli, S., Perrone, M., Fiorica, F., Pinton, P., and Giorgi, C. (2021). Mitochondrial Control of Genomic Instability in Cancer. *Cancers (Basel)* 13. 1914. doi:10.3390/cancers13081914

Boroughs, L. K., and DeBerardinis, R. J. (2015). Metabolic Pathways Promoting Cancer Cell Survival and Growth. *Nat. Cel Biol* 17, 351–359. doi:10.1038/ncb3124

Bray, F., Ferlay, J., Soerjomataram, I., Siegel, R. L., Torre, L. A., and Jemal, A. (2018). Global Cancer Statistics 2018: GLOBOCAN Estimates of Incidence and Mortality Worldwide for 36 Cancers in 185 Countries. *CA Cancer J. Clin.* 68, 394–424. doi:10.3322/caac.21492

Bustamante, J., Arias, A. A., Vogt, G., Picard, C., Galicia, L. B., Prando, C., et al. (2011). Germline CYBB Mutations that Selectively Affect Macrophages in Kindreds with X-Linked Predisposition to Tuberculous Mycobacterial Disease. *Nat. Immunol.* 12, 213–221. doi:10.1038/ni.1992

Chae, Y. C., and Kim, J. H. (2018). Cancer Stem Cell Metabolism: Target for Cancer Therapy. *BMB Rep.* 51, 319–326. doi:10.5483/bmbrep.2018.51.7.112

Chen, C., Tang, Y., Qu, W.-D., Han, X., Zuo, J.-B., Cai, Q.-Y., et al. (2021). Evaluation of Clinical Value and Potential Mechanism of MTFR2 in Lung Adenocarcinoma via Bioinformatics. *BMC Cancer* 21, 619. doi:10.1186/s12885-021-08378-3

Chen, P. H., Cai, L., Huffman, K., Yang, C., Kim, J., Faubert, B., et al. (2019). Metabolic Diversity in Human Non-small Cell Lung Cancer Cells. *Mol. Cel* 76, 838–e5. doi:10.1016/j.molcel.2019.08.028

Chen, X. J., and Butow, R. A. (2005). The Organization and Inheritance of the Mitochondrial Genome. *Nat. Rev. Genet.* 6, 815–825. doi:10.1038/nrg1708

Dinges, S. S., Hohm, A., Vandergrift, L. A., Nowak, J., Habbel, P., Kaltashov, I. A., et al. (2019). Cancer Metabolomic Markers in Urine: Evidence, Techniques and Recommendations. *Nat. Rev. Urol.* 16, 339–362. doi:10.1038/s41585-019-0185-3

Duma, N., Santana-Davila, R., and Molina, J. R. (2019). Non-Small Cell Lung Cancer: Epidemiology, Screening, Diagnosis, and Treatment. *Mayo Clin. Proc.* 94, 1623–1640. doi:10.1016/j.mayocp.2019.01.013

Ganapathy-Kanniappan, S. (2020). PFKP Phenotype in Lung Cancer: Prognostic Potential and beyond. *Mol. Biol. Rep.* 47, 8271–8272. doi:10.1007/s11033-020-05805-9

Garon, E. B., Christofk, H. R., Hosmer, W., Britten, C. D., Bahng, A., Crabtree, M. J., et al. (2014). Dichloroacetate Should Be Considered with Platinum-Based Chemotherapy in Hypoxic Tumors rather Than as a Single Agent in Advanced Non-small Cell Lung Cancer. *J. Cancer Res. Clin. Oncol.* 140, 443–452. doi:10.1007/s00432-014-1583-9

Hanahan, D., and Weinberg, R. A. (2011). Hallmarks of Cancer: the Next Generation. *Cell* 144, 646–674. doi:10.1016/j.cell.2011.02.013

Hensley, C. T., Faubert, B., Yuan, Q., Lev-Cohain, N., Jin, E., Kim, J., et al. (2016). Metabolic Heterogeneity in Human Lung Tumors. *Cell* 164, 681–694. doi:10.1016/j.cell.2015.12.034

Heron, M., and Anderson, R. N. (2016). *Changes in the Leading Cause of Death: Recent Patterns in Heart Disease and Cancer Mortality*. Hyattsville, MD: National Center for Health Statistics, 1–8.

Huang, J., Liu, D., Wang, Y., Liu, L., Li, J., Yuan, J., et al. (2021). Ginseng Polysaccharides Alter the Gut Microbiota and Kynurenine/tryptophan Ratio, Potentiating the Antitumour Effect of Antiprogrammed Cell Death 1/programmed Cell Death Ligand 1 (Anti-PD-1/pd-L1) Immunotherapy. *Gut* 0, 1–12. doi:10.1136/gutjnl-2020-321031

Huyan, T., Li, Q., Ye, L. J., Yang, H., Xue, X. P., Zhang, M. J., et al. (2014). Inhibition of Human Natural Killer Cell Functional Activity by Human Aspartyl β-hydroxylase. *Int. Immunopharmacol* 23, 452–459. doi:10.1016/j.intimp.2014.09.018

Ince, N., de la Monte, S. M., and Wands, J. R. (2000). Overexpression of Human Aspartyl (Asparaginyl) Beta-Hydroxylase Is Associated with Malignant Transformation. *Cancer Res.* 60, 1261–1266.

Kang, Y. J., Bang, B. R., Han, K. H., Hong, L., Shim, E. J., Ma, J., et al. (2015). Regulation of NKT Cell-Mediated Immune Responses to Tumours and Liver Inflammation by Mitochondrial PGAM5-Drp1 Signalling. *Nat. Commun.* 6, 8371. doi:10.1038/ncomms9371

Kanwal, M., Smahel, M., Olsen, M., Smahelova, J., and Tachezy, R. (2020). Aspartate β-hydroxylase as a Target for Cancer Therapy. *J. Exp. Clin. Cancer Res.* 39, 163. doi:10.1186/s13046-020-01669-w

Kimura, M., Yasue, F., Usami, E., Kawachi, S., Iwai, M., Go, M., et al. (2018). Cost-effectiveness and Safety of the Molecular Targeted Drugs Afatinib, Gefitinib and Erlotinib as First-Line Treatments for Patients with Advanced EGFR Mutation-Positive Non-small-cell Lung Cancer. *Mol. Clin. Oncol.* 9, 201–206. doi:10.3892/mco.2018.1640

Kopinski, P. K., Singh, L. N., Zhang, S., Lott, M. T., and Wallace, D. C. (2021). Mitochondrial DNA Variation and Cancer. *Nat. Rev. Cancer* 21(7):431–445. doi:10.1038/s41568-021-00358-w

Kumar, A., and Misra, B. B. (2019). Challenges and Opportunities in Cancer Metabolomics. *Proteomics* 19, e1900042. doi:10.1002/pmic.201900042

La Vecchia, S., and Sebastián, C. (2020). Metabolic Pathways Regulating Colorectal Cancer Initiation and Progression. *Semin. Cel Dev Biol* 98, 63–70. doi:10.1016/j.semcdb.2019.05.018

Larman, T. C., DePalma, S. R., Hadjipanayis, A. G., Cancer Genome Atlas Research, N., Protopopov, A., Zhang, J., et al. (2012). Spectrum of Somatic Mitochondrial Mutations in Five Cancers. *Proc. Natl. Acad. Sci. U S A.* 109, 14087–14091. doi:10.1073/pnas.1211502109

Li, K., Guo, W., Li, Z., Wang, Y., Sun, B., Xu, D., et al. (2019). ALDH2 Repression Promotes Lung Tumor Progression via Accumulated Acetaldehyde and DNA Damage. *Neoplasia* 21, 602–614. doi:10.1016/j.neo.2019.03.008

Li, M., Xian, H. C., Tang, Y. J., Liang, X. H., and Tang, Y. L. (2021). Fatty Acid Oxidation: Driver of Lymph Node Metastasis. *Cancer Cel Int* 21, 339. doi:10.1186/s12935-021-02057-w

Liu, X., Lu, Y., Chen, Z., Liu, X., Hu, W., Zheng, L., et al. (2020). The Ubiquitin Specific Protease USP18 Promotes Lipolysis, Fatty Acid Oxidation and Lung Cancer Growth. *Mol. Cancer Res.* 19(4):667-677. doi:10.1158/1541-7786.MCR-20-0579

Sheftel, A. D., Stehling, O., Pierik, A. J., Elsässer, H. P., Mühlenhoff, U., Webert, H., et al. (2010). Humans Possess Two Mitochondrial Ferredoxins, Fdx1 and Fdx2, with Distinct Roles in Steroidogenesis, Heme, and Fe/S Cluster Biosynthesis. *Proc. Natl. Acad. Sci. U S A.* 107, 11775–11780. doi:10.1073/pnas.1004250107

Sher, T., Dy, G. K., and Adjei, A. A. (2008). Small Cell Lung Cancer. *Mayo Clin. Proc.* 83, 355–367. doi:10.4065/83.3.355

Shi, Y., Ghosh, M., Kovtunovych, G., Crooks, D. R., and Rouault, T. A. (2012). Both human Ferredoxins 1 and 2 and Ferredoxin Reductase Are Important for Iron-Sulfur Cluster Biogenesis. *Biochim. Biophys. Acta* 1823, 484–492. doi:10.1016/j.bbamcr.2011.11.002

Strushkevich, N., MacKenzie, F., Cherkesova, T., Grabovec, I., Usanov, S., and Park, H. W. (2011). Structural Basis for Pregnenolone Biosynthesis by the Mitochondrial Monooxygenase System. *Proc. Natl. Acad. Sci. U S A.* 108, 10139–10143. doi:10.1073/pnas.1019441108

Tsvetkov, P., Detappe, A., Cai, K., Keys, H. R., Brune, Z., Ying, W., et al. (2019). Mitochondrial Metabolism Promotes Adaptation to Proteotoxic Stress. *Nat. Chem. Biol.* 15, 681–689. doi:10.1038/s41589-019-0291-9

Vander Heiden, M. G., and DeBerardinis, R. J. (2017). Understanding the Intersections between Metabolism and Cancer Biology. *Cell* 168, 657–669. doi:10.1016/j.cell.2016.12.039

Vanhove, K., Derveaux, E., Graulus, G. J., Mesotten, L., Thomeer, M., Noben, J. P., et al. (2019). Glutamine Addiction and Therapeutic Strategies in Lung Cancer. *Int. J. Mol. Sci.* 20. 252. doi:10.3390/ijms20020252

Wang, S., Wu, C., Ma, D., and Hu, Q. (2021). Identification of a Ferroptosis-Related Gene Signature (FRGS) for Predicting Clinical Outcome in Lung Adenocarcinoma. *PeerJ* 9, e11233. doi:10.7717/peerj.11233

Zappa, C., and Mousa, S. A. (2016). Non-small Cell Lung Cancer: Current Treatment and Future Advances. *Transl Lung Cancer Res.* 5, 288–300. doi:10.21037/tlcr.2016.06.07

Zhang, Y., Yang, M., Ng, D. M., Haleem, M., Yi, T., Hu, S., et al. (2020). Multi-omics Data Analyses Construct TME and Identify the Immune-Related Prognosis Signatures in Human LUAD. *Mol. Ther. Nucleic Acids* 21, 860–873. doi:10.1016/j.omtn.2020.07.024

Zhu, M., Dai, Y., Gao, F., Xu, C., Chen, L., Xu, Y., et al. (2019). Correlations of Coagulation Indexes and Inflammatory Changes with the Prognosis of Lung Cancer Complicated with Thromboembolic Disease. *J. BUON* 24, 585–590.

Conflict of Interest: The authors declare that the research was conducted in the absence of any commercial or financial relationships that could be construed as a potential conflict of interest.

Publisher's Note: All claims expressed in this article are solely those of the authors and do not necessarily represent those of their affiliated organizations, or those of the publisher, the editors, and the reviewers. Any product that may be evaluated in this article, or claim that may be made by its manufacturer, is not guaranteed or endorsed by the publisher.

frontiers in Pharmacology

ORIGINAL RESEARCH
published: 20 October 2021
doi: 10.3389/fphar.2021.764015

Aberrant ROS Mediate Cell Cycle and Motility in Colorectal Cancer Cells Through an Oncogenic CXCL14 Signaling Pathway

Jun Zeng[1†], Mei Li[1†], Jun-Yu Xu[1], Heng Xiao[2], Xian Yang[1], Jiao-Xiu Fan[1], Kang Wu[3,4] and Shuang Chen[5]**

[1]Department of Genetics and Cell Biology, College of Life Sciences, Chongqing Normal University, Chongqing, China, [2]Department of Hepatobiliary Surgery, the First Affiliated Hospital of Chongqing Medical University, Chongqing, China, [3]Shenzhen Luohu People's Hospital, the Third Affiliated Hospital of Shenzhen University, Shenzhen, China, [4]South China Hospital, Shenzhen University, Shenzhen, China, [5]Department of Dermatovenereology, the First Affiliated Hospital of Chongqing Medical University, Chongqing, China

OPEN ACCESS

Edited by:
Xuefeng Li,
Guangzhou Medical University, China

Reviewed by:
Lei Guo,
University of Texas Southwestern Medical Center, United States
Xuan Liu,
University of Texas MD Anderson Cancer Center, United States

***Correspondence:**
Kang Wu
wukanglaiye@163.com
Shuang Chen
shuangchen07@hotmail.com

†These authors have contributed equally to this work

Specialty section:
This article was submitted to Inflammation Pharmacology, a section of the journal Frontiers in Pharmacology

Received: 24 August 2021
Accepted: 04 October 2021
Published: 20 October 2021

Citation:
Zeng J, Li M, Xu J-Y Xiao H, Yang X, Fan J-X Wu K and Chen S (2021) Aberrant ROS Mediate Cell Cycle and Motility in Colorectal Cancer Cells Through an Oncogenic CXCL14 Signaling Pathway. Front. Pharmacol. 12:764015. doi: 10.3389/fphar.2021.764015

Background: Reactive oxygen species (ROS) act as signal mediators to induce tumorigenesis.

Objective: This study aims to explore whether chemokine CXCL14 is involved in the proliferation and migration of ROS-induced colorectal cancer (CRC) cells.

Methods: The proliferative and migratory capacities of CRC cells treated with or without H_2O_2 were measured by various methods, including the CKK-8 assay, colony formation assay, flow cytometry, wounding healing assay, and migration assay.

Results: The results revealed that H_2O_2 promoted the proliferation and migration of CRC cells by regulating the cell cycle progression and the epithelial to mesenchymal transition (EMT) process. Furthermore, we noted that the expression level of CXCL14 was elevated in both HCT116 cells and SW620 cells treated with H_2O_2. An antioxidant N-Acetyl-L-cysteine (NAC) pretreatment could partially suppress the CXCL14 expression in CRC cells treated with H_2O_2. Next, we constructed CRC cell lines stably expressing CXCL14 (HCT116/CXCL14 and SW620/CXCL14) and CRC cell lines with empty plasmid vectors (HCT116/Control and SW620/Control) separately. We noted that both H_2O_2 treatment and CXCL14 over-expression could up-regulate the expression levels of cell cycle-related and EMT-related proteins. Moreover, the level of phosphorylated ERK (p-ERK) was markedly higher in HCT116/CXCL14 cells when compared with that in HCT116/Control cells. CXCL14-deficiency significantly inhibited the phosphorylation of ERK compared with control (i.e., scrambled shNCs). H_2O_2 treatment could partially restore the expression levels of CXCL14 and p-ERK in HCT116/shCXCL14 cells.

Abbreviations: CAFs, cancer-associated fibroblasts; CCK-8, cell counting kit 8; CDKs, cyclin-dependent kinases; CRC, colorectal cancer; CXCL14, CXC-chemokine ligand 14; DCs, dendritic cells; EMT, epithelial to mesenchymal transition; H2O2, hydrogen peroxide; iDCs, immature dentritic cells; NAC, N-Acetyl-L-cysteine; NK, natural killer; p-ERK, phosphorylated extracellular-regulated kinase; ROS, reactive oxygen species.

Conclusion: Our studies thus suggest that aberrant ROS may promote colorectal cancer cell proliferation and migration through an oncogenic CXCL14 signaling pathway.

Keywords: colorectal cancer, ROS, CXCL14, cell cycle, migration

INTRODUCTION

Colorectal cancer (CRC) is one of the most common fatal malignancies affecting people worldwide (Sung et al., 2021). The incidence of CRC has increased over the years, especially among individuals of age <45 years (Brody, 2015; Siegel et al., 2017). Emerging evidence has suggested CRC cells exhibit elevated reactive oxygen species (ROS) levels than the normal cells (Lei et al., 2011). ROS can regulate the occurrence and development of cancer in an autocrine or paracrine way (Reczek and Chandel, 2018). During intestinal tumorigenesis, myeloid cell-derived ROS triggered oxidative DNA damage in intestinal epithelial cells to stimulate invasive growth in a paracrine manner (Canli et al., 2017). Anti-oxidant treatment can reduce cholangiocellular pre-neoplastic lesions (Yuan et al., 2017). Although accumulating evidence suggests the oncogenic role of ROS, high or excessive levels of ROS can cause damage to the cellular components, leading to cell death (Li et al., 2015; He et al., 2016; Zhuang et al., 2016; Salehi et al., 2018; Ruiz-Torres et al., 2019; Zhang et al., 2019).

Chemokines have been reported to regulate the proliferation and metastasis of tumor cells in an organ-specific manner. CXCL14, a CXC chemokine ligand, chemoattracts proinflammatory cells, such as natural killer (NK) cells and dendritic cells (DCs), to the sites of inflammation or malignancy (Shurin et al., 1950; Starnes et al., 2006). CXCL14 plays a double-sided role in the regulation of tumor development. In head and neck squamous cell carcinoma (HNSCC), CXCL14 could be used as a functional prognosis biomarker for patients' better overall survival rate (Li et al., 2020a; Wu et al., 2021). On the contrary, CXCL14 was reported to promote cancer cell motility by regulating Ca^{2+} release in breast cancer (Pelicano et al., 2009a). Previously, we reported that chemokine CXCL14 was significantly upregulated in the CRC tissues than that in the normal and paracancerous tissues (Zeng et al., 2013a). Whether the contradictory functions of CXCL14 in tumor progression are due to the types of tumors awaits further investigation.

The relationship between ROS and chemokines during carcinogenesis has been studied (Wen et al., 2018; Li et al., 2020b; Dasoveanu et al., 2020; Xian et al., 2020; Alafiatayo et al., 2020; da Ros et al., 2015). A recent study demonstrated that topoisomerase inhibitors could promote the expression and secretion of CXCL1 *via* ROS-mediated activation of JAK2-STAT1 signaling pathway, thereby promoting the motility of cancer cells (Liu et al., 2019). ROS-mediated CXCL8 expression could regulate the development of *H. Pylori*-associated gastric cancer (Kyung et al., 2019). Stromal cells in tumor microenvironment could also secret ROS-mediated chemokine and act on tumor cells in a paracrine manner (Ramírez-Moreno et al., 2020). Despite these recent advances, the oncogenic signaling transduction pathways targeted by aberrant ROS levels and chemokines remain to be fully understood.

The purpose of this present study aims to clarify the association between ROS and chemokine CXCL14 in CRC progression, and demonstrate the oncogenic function of chemokine CXCL14 in CRC cells. Herein, we reported experimental evidence for ROS-induced cell cycle progression and the epithelial to mesenchymal transition (EMT) process via CXCL14/pERK pathway in colorectal cancer cells.

MATERIALS AND METHODS

Cell Culture and Treatment

Human CRC cell line HCT116 and SW620 cells were kind gifts from Prof. Yunlong Lei (Molecular Medicine and Cancer Research Center, Chongqing Medical University). Cells were maintained in DMEM medium (Hyclone) containing 10% fetal calf serum (Hyclone), penicillin and streptomycin at 37°C in a humidified atmosphere with 5% CO_2. The cells were treated without or with H_2O_2 in media, which were changed daily. Cells were pretreated with antioxidant 5 mM or 10 mM N-acetylcysteine (NAC) for 30 min before addition of H_2O_2.

Plasmid Constructions and Cell Transfection

To clone the CXCL14 cDNA, we isolated total RNAs from the HCT116 cell line using Trizol method. The RNA samples were dissolved with TE buffer, and then quantified by measuring OD value. The extracted RNA samples were further reverse transcribed into cDNA, which would be used as PCR template. The primers used for CXCL14 amplification were synthesized (Invitrogen). The primer sequences for amplification were as follows: cxcl14, forward 5′-GATCCC CGCCACCATGTCCCTGCTCCCACGC-3′, reverse 5′-TCG AGCTATTCTTCGTAGACCCTGCGC-3'; *gapdh*, forward 5′-ACCTGACCTGCCGTCTAGAA-3′, reverse 5′-TCCACCACC CTGTTGCTGTA-3'. For CXCL14 stable expression in HCT116 cells, the recombinant plasmid of EX-CXCL14-LV203 and the control plasmid EX-NEG-LV203 were transfected into 293T cells with lentivirus packaging system, separately. Then, the concentrated virus particles were collected and the HCT116 cells were infected with the viruses in their logarithmic growth phase. The stable transfectants were selected in the presence of puromycin and identified by real-time PCR and western blotting. The primers for real-time PCR were as follows: cxcl14, forward 5′-CTACAGCGACGTGAAGAAGC-3′, reverse 5′-TTCTCGTTCCAGGCGTTGTA-3'. The construction of HCT116 cells lacking CXCL14 was also accomplished *via* lentiviral-mediated transduction with a scrambled shNCs or

verified CXCL14-specific shRNA sequence encoded in LVRH1GP. A 21-mer shRNA expressing vector targeting CXCL14 (shCXCL14) and its scrambled sequence-expressing vector as a negative control (shNC) were synthesized (Invitrogen). The sequence for CXCL14 shRNA was forward 5′-GATCCGCACCAAGCGCTTCATCAATTCAAGAGATTG ATGAAGCGCTTGGTGCTTTTTTGG-3′, and reverse 5′-AAT TCCAAAAAAGCACCAAGCGCTTCATCAATCTCTTGA ATTGATGAAGCGCTTGGTGCG-3'.

ROS Measurement

Intracellular ROS were detected by staining cells with 5-(and-6)-chloromethyl-2′,7′-dichlorodihydrofluorescein diacetate (CM-H_2DCF-DA) (Genmed Scientifics Inc., Burlington, MA, United States). Cells after firm adhesion to the wall were treated with H_2O_2 for 6 h. After trypsin digestion and centrifugation, supernatant was removed. 10 μmol/L DCFH-DA dye diluted with serum-free medium was added to cells for incubation at 37°C for 20 min. The CM-H_2DCF-DA signal was then analyzed with the BD Biosciences FACSCalibur Flow Cytometer (Mountain View, CA).

Cell Proliferation and Colony Formation Assay

Cell proliferation was determined by using the Cell Counting Kit-8 (CCK-8) Assay (Boster). The cancer cells (5000 cells per well) were seeded in the 96-well plates and treated with different concentrations of H_2O_2 for 48 h. The cells were incubated with 10 μL of CCK-8 per well and the optical density (OD) value at 450 nm was determined by microplate reader. The experiment was repeated in triplicate. The formula of promotion rate of cell proliferation (P%) is as follows:

$$P\% = \frac{OD(sample) - OD(control)}{OD(control) - OD(blank)} \times 100\% \quad (1)$$

For colony formation assay, the cancer cells (1000 cells per well) were resuspended in DMEM supplemented with 10% FBS without or with H_2O_2 in 6-well plates. The cultures were maintained for 14 days and stained with 0.1% crystal violet and estimated under the microscope. Each experiment was performed in triplicate.

Wound Healing and Cell Migration Assay

Confluent HCT116 cells were wounded with a micropipette tip (200 μL) and immediately placed in 1% serum-containing medium supplemented with or without H_2O_2. Bright-field images of wounded monolayers were obtained immediately after wounding (0 h) and at various times thereafter as indicated. The extent of wound closure was quantified by obtaining three wound measurements for each of three random fields (× 100) per wound, and all wound conditions were performed in triplicate.

The cell migration assay was performed in chambers with 8-μm-porosity polycarbonate filter membranes according to the manufacturer's instructions (Becton Dickinson Labware). Cells (1 × 10^5 cells per well) treated without or with H_2O_2 in serum-free medium were added to the upper chamber and incubated for 20 h. The bottom chamber was prepared with 20% FBS as a chemoattractant. Nonmigrating cells on the upper surface of the membrane were removed. Cells that invaded to the lower surface were fixed with 4% paraformaldehyde stained with crystal violet, and photographed under a microscope (Eclipse TS100, Nikon) at × 20 magnification.

Western Blot Analysis

Both adherent and floating cells were harvested. All cell protein was extracted in RIPA lysis buffer (50 mM Tris, 1.0 mM EDTA, 150 mM NaCl, 0.1% SDS, 1% Triton X-100, 1% sodium deoxycholate, 1 mM PMSF). The concentrations of protein were quantified by using the DC Protein Assay Kit (500–0121; Bio-Rad). The cellular lysates were resolved on SDS-PAGE and electrophoretically transferred to polyvinylidene difluoride membranes. The membranes were then blocked with a buffer [composed of 10 mM Tris (Zhu et al., 2018), 150 mM NaCl, 0.1% Tween 20 and 5% bovine serum albumin], and then incubated with the primary antibodies (CXCL14, diluted 1:400, Proteintech, 10468-1-AP; Cyclin A1, diluted 1:1000–2000, Abcam, ab53699; Cyclin B1, diluted 1:1000–2000, Abcam, ab215436; CDK1, diluted 1:1000–2000, Abcam, ab265590; CDK2, diluted 1:1000–2000, Abcam, ab101682; E-cadherin, diluted 1:1000–2000, Abcam, ab238099; N-cadherin, diluted 1:1000–2000, Abcam, ab207608; vimentin, diluted 1:1000–2000, Abcam, ab92547; ERK, diluted 1:1000–2000, Abcam, ab184699; p-ERK, diluted 1:1000–2000, Abcam, ab214036; and GAPDH, diluted 1:1000–2000, Abcam, ab181602) at 4°C for overnight. Then, the membranes were washed and treated with appropriate secondary antibodies conjugated with horseradish peroxidase for (goat anti-rabbit IgG H&L, Abcam, ab7090; goat anti-mouse IgG H&L, Abcam, ab7068) 2 h. The immunoreactivities were determined by using enhanced chemiluminescence reagents (WBKLS0500; Millipore) (Wang et al., 2011). The GAPDH protein was used as an internal control.

Statistical Analysis

Statistical values were defined by using an unpaired Student's *t*-test. Differences among multiple groups were assessed by one-way ANOVA analysis. $p < 0.05$ was considered to be statistically significant.

RESULTS

ROS Promoted the Proliferation and Migration of CRC Cells

Recent studies have demonstrated that cancer cells can be characterized by elevated ROS levels when compared with the normal cells (Maurya and Vinayak, 2015; Prasad et al., 2017; Moloney and Cotter, 2018). Aberrant ROS production is associated with tumor initiation and progression (Yang et al., 2016; Ghanbari Movahed et al., 2019). To determine the role of ROS in CRC cell proliferation and migration, we applied exogenous H_2O_2 to induce cellular ROS stress in HCT116 cells

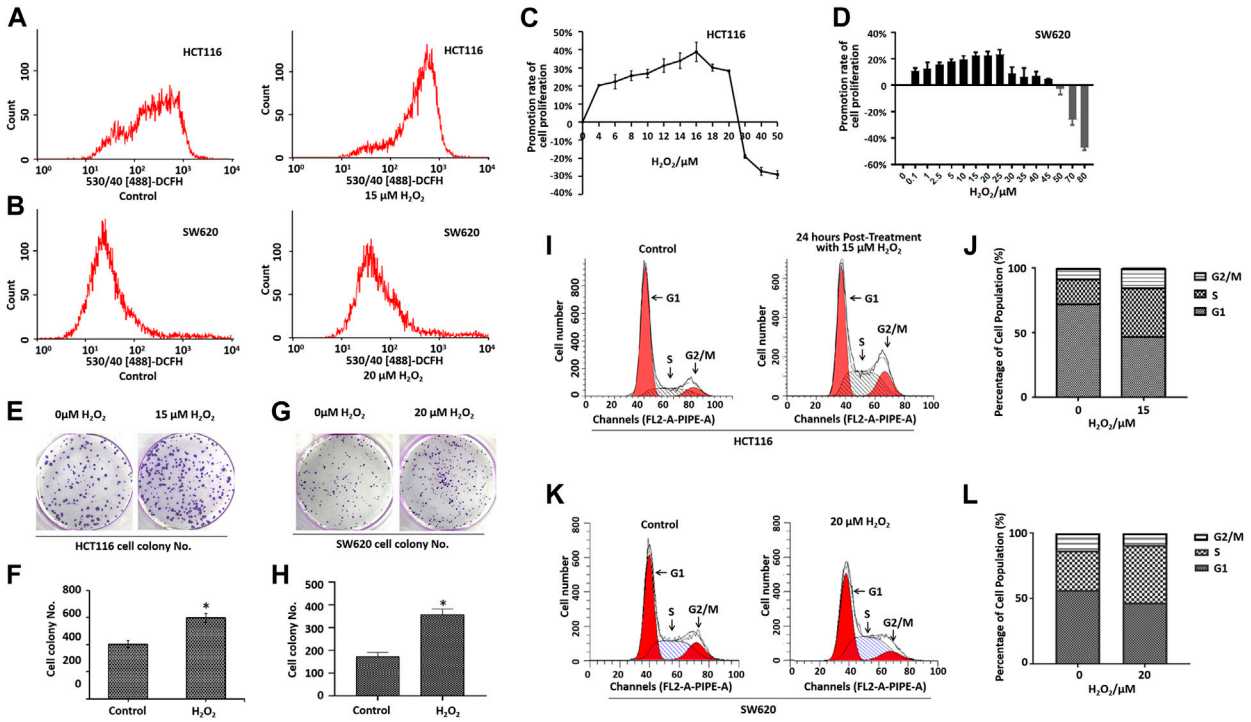

FIGURE 1 | Effects of H_2O_2 on colorectal cancer cell growth and cell cycle. Cells treated with the exogenous H_2O_2 showed an endogenous increase in the oxidative stress level as measured using CM-H_2DCF-DA by flow cytometry in HCT116 cells **(A)** and SW620 cells **(B)**. The HCT116 cells **(C)** and SW620 cells **(D)** were treated with different concentrations of H_2O_2 for 48 h, and the cell proliferation was determined by CCK8 assay. The calculation of promotion rate of cell proliferation has been described in the Materials and Methods section. Representative photographs of colony formation of HCT116 cells **(E)** and SW620 cells **(G)** treated with or without H_2O_2. The statistical analysis of the numbers of cell colonies of HCT116 cells **(F)** and SW620 cells **(H)**. DNA content of HCT116 cells **(I)** and SW620 cells **(K)** treated with or without H2O2 in various phases of the cell cycle measured by flow cytometry. B. Statistical analyses of cell cycle distribution of HCT116 cells **(J)** and SW620 cells **(L)**. The experiments were performed in triplicate (n = 3). Error bars represent mean ± S.D. $p < 0.05$ was considered to be statistically significant. $^*p < 0.05$; $^{**}p < 0.01$.

and SW620 cells. As illustrated in **Figures 1A,B**, the cells treated with the exogenous H_2O_2 showed an endogenous increase in the oxidative stress level when compared with the control cells, as measured by flow cytometry.

Cell proliferation was determined by the CCK-8 assay. As shown in **Figures 1C,D**, treatment with different doses of H_2O_2 induced different biological outcomes. H_2O_2 increased HCT116 cell proliferation at a concentration of <25 μM when compared with the control cells. Adversely, H_2O_2 decreased the cell proliferation at concentration of >25 μM (**Figure 1C**). We found a similar phenomenon in SW620 cells (**Figure 1D**). As expected, the cells treated with H_2O_2 formed a greater number of colonies when compared with the control cells (**Figures 1E–H**). To further characterize the effect of H_2O_2 on the cell cycle progression, we examined the DNA content of HCT116 cells and SW620 cells in various phases of the cell cycle, as measured by flow cytometry (**Figures 1I–L**). Results showed that H_2O_2 increased the cell percentage in the S phase and G2/M phase and decreased the cell percentage in the G1 phase in HCT116 cells (**Figures 1I,J**), and H_2O_2 increased the cell percentage in the S phase in SW620 cells (**Figures 1K,L**).

The migratory capacity of HCT116 cells and SW620 cells treated with or without H_2O_2 was estimated by the wound healing assay. In the wound healing assay, the number of H_2O_2-treated HCT116 and SW620 cells that migrated into the wound area was much greater than the control cells (**Figures 2A–D**), which suggests the role of ROS in mediating the closure of cell wounds. The cells in the wound area may be a direct reflection of migration, or partially due to cell proliferation. To circumvent this difficulty, we further performed cell migration assays in 24-well transwell chambers. Results showed that ROS significantly increased the migration capacity of the HCT116 cells and SW620 cells (**Figures 2E–H**). Taken together, these data strongly suggest that ROS is directly involved in mediating the proliferation and migration of CRC cells.

ROS Promoted Malignant Behaviors in Human CRC Cells *via* Regulation of the Cell Cycle Progression and EMT

In mammalian cells, the cell-cycle progression is highly controlled by cyclins and cyclin-dependent kinases (CDKs). The activity of cyclin A1/CDK2 complex is essential for the cell-cycle G1/S phase transition, and the

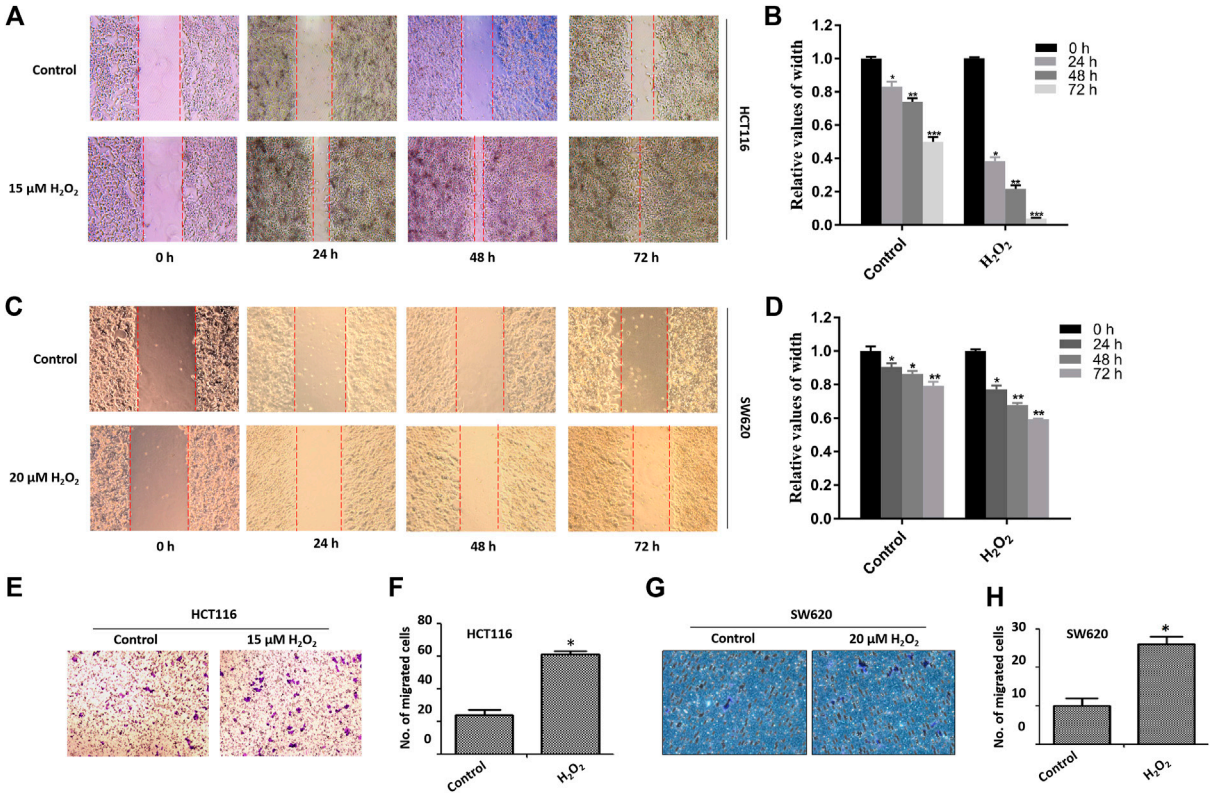

FIGURE 2 | Effects of H_2O_2 on CRC cell migration. The HCT116 cells **(A)** and SW620 cells **(C)** were treated with H_2O_2 for different time, and the cell migration was determined by the wound healing assay. The width of wound area in HCT116 cells **(B)** and SW620 cells **(D)** was quantitatively analyzed. The migration of HCT116 cells **(E)** and SW620 **(F)** cells treated with or without H_2O_2 was measured by the modified Boyden chamber assays. Quantitative results of the numbers of migrated cells in HCT116 cells **(G)** and SW620 cells **(H)**. The experiments were performed in triplicate (n = 3). Error bars represent mean ± S.D. $p < 0.05$ was considered to be statistically significant. *$p < 0.05$; **$p < 0.01$.

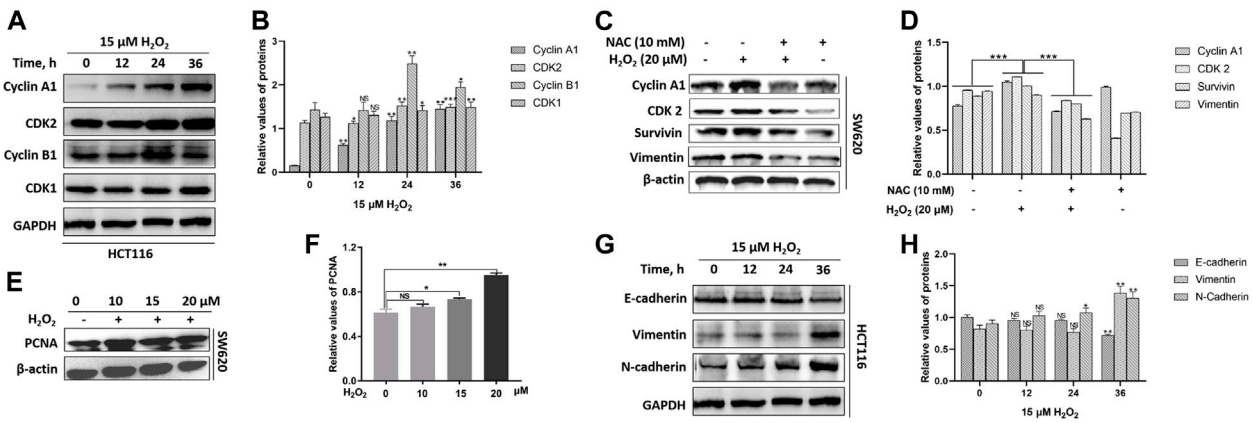

FIGURE 3 | H_2O_2 regulated the expression levels of cell cycle-related and EMT-related proteins. **(A)** The HCT116 cells were treated with or without 15 μM H_2O_2 for different time. The expression levels of Cyclin A1, CDK2, Cyclin B1, CDK1 were measured by western blot. **(B)** Quantitative results of cell cycle-related protein expression levels. **(C)** The SW620 cells treated with or without 20 μM H_2O_2 or pretreated with 10 mM NAC. The expression levels of Cyclin A1, CDK2, surviving and vimentin were measured by western blot, which could be down-regulated by the antioxidant NAC. **(D)** Quantitative results of protein expression. **(E)** The expression of PCNA in SW620 cells treated with different concentration of H_2O_2 was measured by western blot. **(F)** Quantitative results of PCNA expression levels. **(G)** The HCT116 cells treated with or without 15 uM H_2O_2 for different time. The expression levels of E-cadherin, vimentin and N-cadherin were measured by western blot. **(H)** Quantitative results of EMT-related protein expression levels. All experiments were repeated three times or more. Error bars represent ±S.D. $p < 0.05$ was considered to be statistically significant. * $p < 0.05$; ** $p < 0.01$, *** $p < 0.001$.

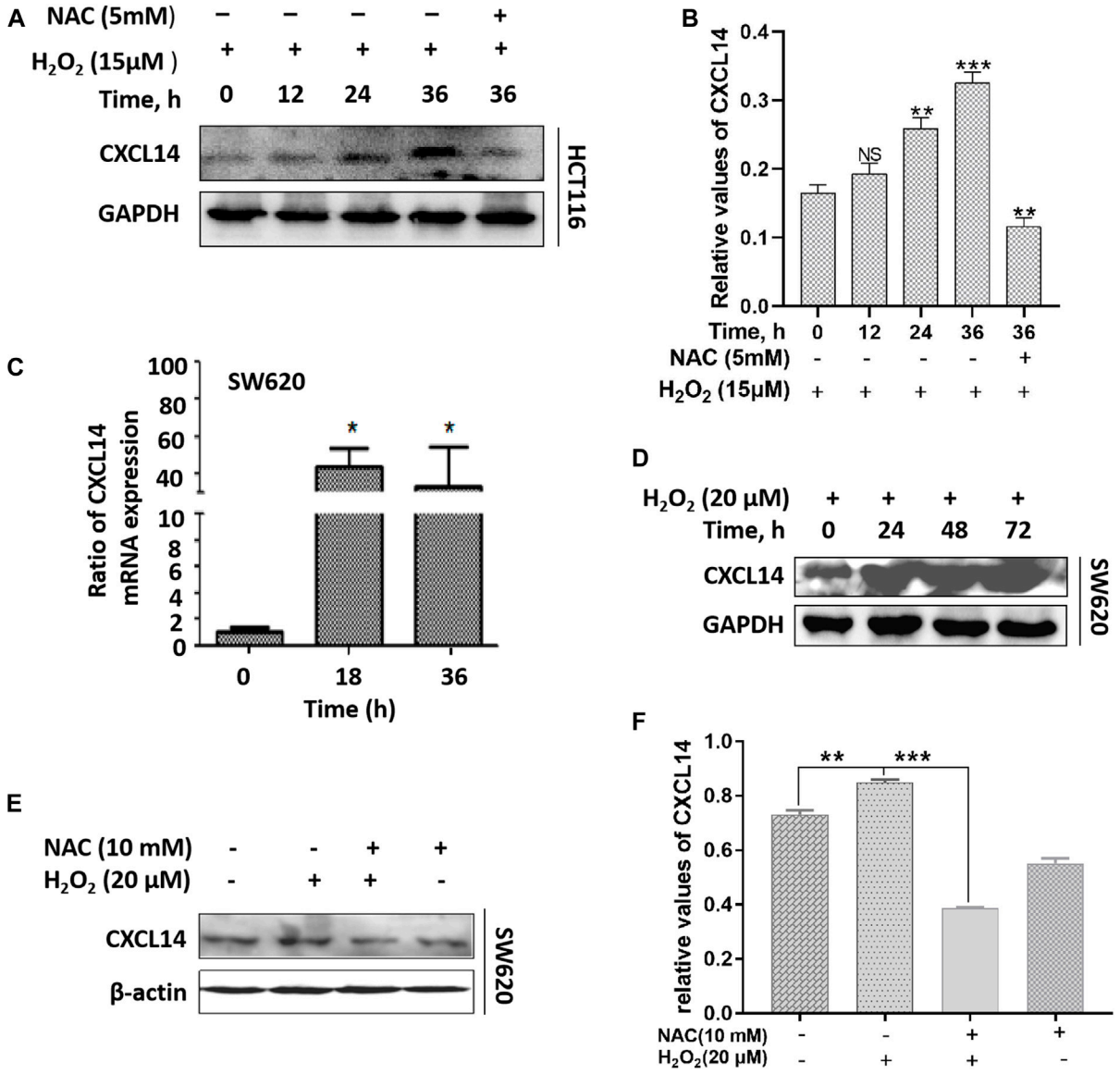

FIGURE 4 | ROS up-regulated the expression of chemokine CXCL14. **(A)** The HCT116 cells were treated with 15 μmol/L H2O2 for different time and/or pretreated with 5 mmol/L NAC. **(B)** Quantitative results of the expression levels of CXCL14. **(C)** The SW620 cells were treated with 20 μmol/L H2O2 for different time. The expression level of CXCL14 mRNA was measured by real-time PCR. **(D)** The SW620 cells were treated with 20 μmol/L H2O2 for different time. The expression level of CXCL14 protein was measured by western blot. **(E)** The SW620 cells were treated with 20 μmol/L H2O2 and/or pretreated with 10 mmol/L NAC. **(F)** Quantitative results of the expression levels of CXCL14. All experiments were repeated three times or more. Error bars represent ± S.D. $p < 0.05$ was considered to be statistically significant. *p <0.05; **p <0.01, ***p <0.001.

cyclin B1/CDK1 complex plays the fundamental role in cell-cycle G2/M transition (Malumbres and Barbacid, 2009; Xie et al., 2020). We noted that H_2O_2 could up-regulate the expression levels of cyclin A1, cyclin B1, CDK1, and CDK2 in a time-dependent manner in HCT116 cells (**Figures 3A,B**). H_2O_2 could up-regulated the expression of cyclin A1, CDK2 and survivin in SW620 cells, which could be partially suppressed by the antioxidant NAC pretreatment (**Figures 3C,D**). We also noted that H_2O_2 could up-regulate the expression of proliferating cell nuclear antigen (PCNA) in SW620 cells (**Figures 3E,F**). These data indicated increased growth capacity for the CRC cells in the presence of H_2O_2 through regulation of the cell cycle progression and cell proliferation.

The epithelial to mesenchymal transition (EMT) endows cancer cells with the properties of invasion and metastasis (Yuan et al., 2020). In solid tumors, EMT occurs at the invasive front and induces migratory cells with downregulated expression of epithelial markers E-cadherin and upregulated expression of the mesenchymal markers vimentin and

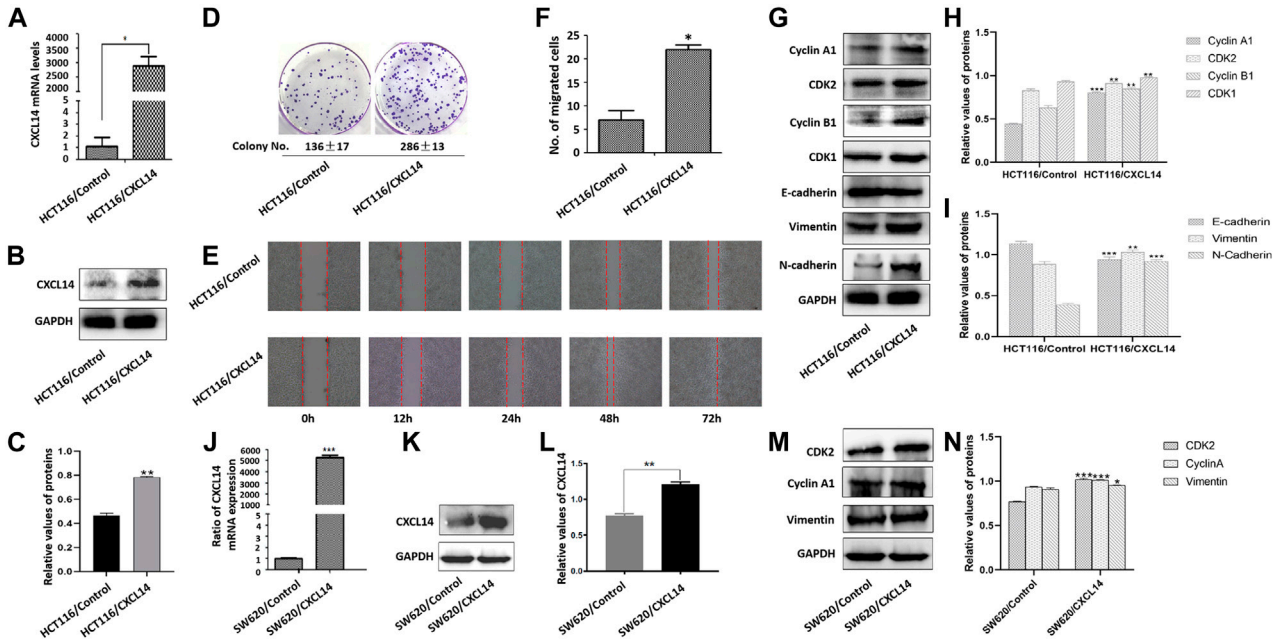

FIGURE 5 | Effects of CXCL14 on cell proliferation and migration of human colorectal cancer cells. CXCL14 was stably over-expressed in the HCT116 cells, as determined by RT-PCR assay **(A)** and western blot assay **(B)**. **(C)** Quantitative results of CXCL14 expression levels. **(D)** The proliferative capacity of HCT116 cells stably expressing CXCL14 (HCT116/CXCL14) was stronger than that of HCT116/Control only transfected with empty vectors, as measured by colony formation assay. **(E)** The migratory capacity of HCT116/CXCL14 was stronger than that of HCT116/control cells, as measured by wound healing assay. **(F)** Quantitative results of cell migration numbers in modified Boyden chamber assays in HCT116/Control cells and HCT116/CXCL14 cells. **(G)** The expression levels of cell cycle-related and EMT-related proteins in HCT116/CXCL14 cells and HCT/Control cells were measured by western blot. **(H)** Quantitative results of cell cycle-related protein expression. **(I)** Quantitative results of EMT-related protein expression. CXCL14 was stably over-expressed in the SW620 cells, as determined by RT-PCR assay **(J)** and western blot assay **(K)**. **(L)** Quantitative results of CXCL14 expression levels. M. The expression levels of CDK2, Cyclin A1, vimentin in HSW620/CXCL14 cells, and SW620/Control cells were measured by western blot. **(H)** Quantitative results of protein expression. The experiments were performed in triplicate ($n = 3$). Error bars represent mean ± S.D. $p < 0.05$ was considered to be statistically significant. * $p < 0.05$; ** $p < 0.01$, *** $p < 0.001$.

N-cadherin (Nieto et al., 2016). By immunoblotting, we observed a substantial decrease in the expression level of E-cadherin and an increase in the expression levels of vimentin and N-cadherin in response to exogenous H_2O_2 in HCT116 cells (**Figures 3G,H**). We also noted that vimentin expression was down-regulated after exposure to H_2O_2, which could be partially restored by the antioxidant NAC in SW620 cells (**Figures 3C,D**).

ROS Up-Regulated the Expression of Chemokine CXCL14

Previous studies have shown that ROS can act as signal transduction molecules and regulate the expression of oncogenic chemokines (Wang et al., 2017). Based on previous reports, we performed immunoblotting to examine the expression level of chemokine CXCL14 after exposure to H_2O_2 in CRC cells. We observed that the CXCL14 expression was significantly elevated in HCT116 cells treated with H_2O_2 when compared with the control cells and in a time-dependent manner (**Figures 4A,B**). We then used the antioxidant NAC to explore whether the CXCL14 expression was affected. Results showed that NAC pretreatment partially suppressed the expression levels of CXCL14, indicating that CXCL14 expression might be regulated by ROS in HCT116 cells (**Figures 4A,B**). Meanwhile, we found that the expression levels of CXCL14 mRNA and protein were elevated after exposure of H_2O_2 in a time-dependent way in SW620 cells (**Figures 4C,D**), which could be partially suppressed by the antioxidant NAC pretreatment (**Figures 4E,F**).

CXCL14 was Required for Oncogenic Signaling in CRC Cells

To gain further insights into the role of CXCL14 in ROS-induced oncogenesis, we first constructed a stably CXCL14-expressing HCT116 cell line (HCT116/CXCL14), as shown in **Figures 5A–C**. The proliferative and migratory capacity of HCT116/CXCL14 cells was determined by using the colony formation assay (**Figure 5D**), wound healing assay (**Figure 5E**) and migration assay (**Figure 5F**). As compared with the control cells (HCT116/Control), HCT116/CXCL14 cells exhibited stronger proliferative and migratory capacities, suggesting that CXCL14 might play an important role in CRC progression, which was consistent with previous data (Zeng et al., 2013a).

We further examined the expression levels of cyclin A1, cyclin B1, CDK1, and CDK2, and found that CXCL14 could up-regulate

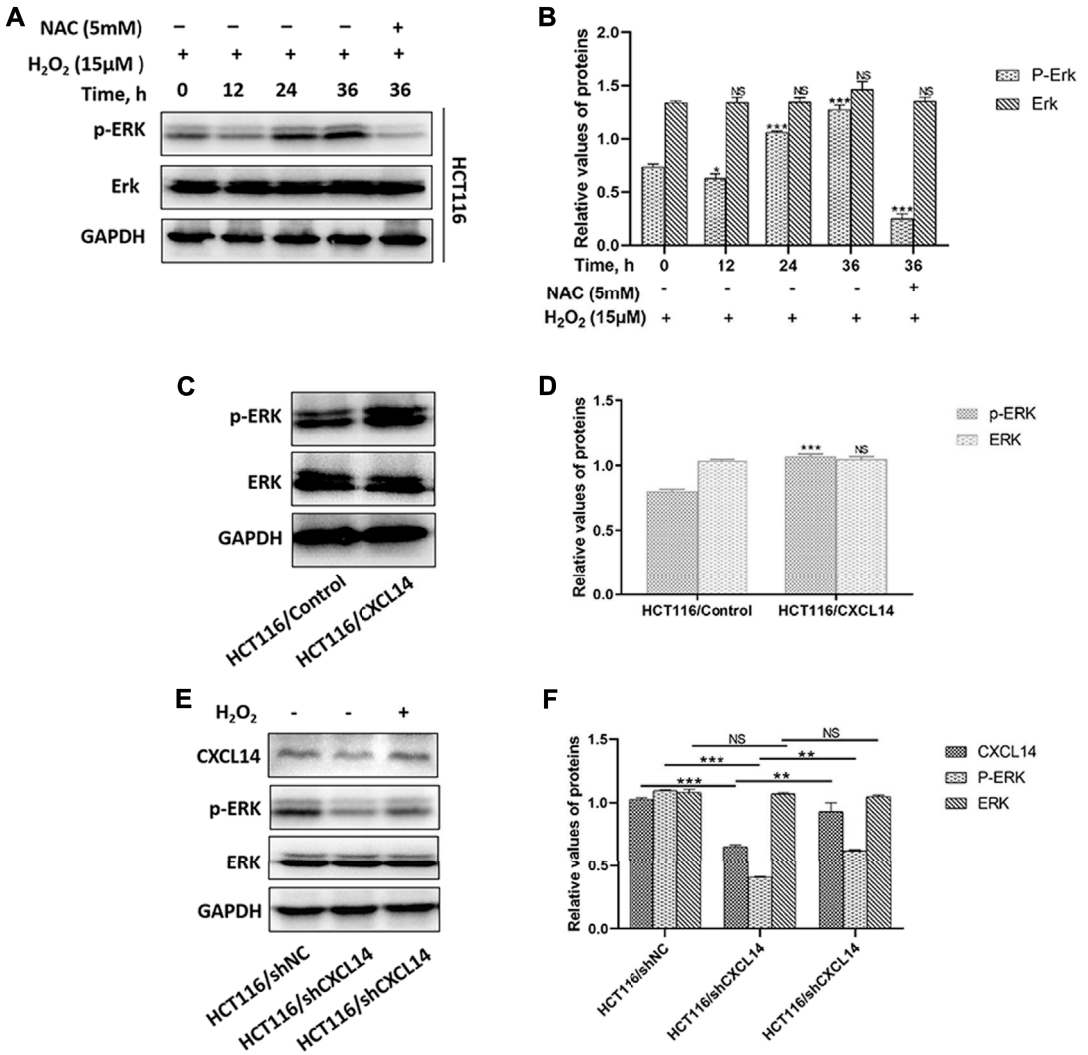

FIGURE 6 | Effects of CXCL14 on the ROS-induced phosphorylation of ERK. **(A)** H_2O_2 increased the expression levels of CXCL14 and p-ERK in HCT116 cells treated without or with 15 μM H_2O_2 or pretreated with 5 mM NAC in a time-dependent manner. **(B)** Quantitative results of the expression levels of p-ERK. **(C)** CXCL14 could up-regulated the phosphorylation level of ERK in HCT116/CXCL14 cells. **(D)** Quantitative results of the p-ERK and total ERK expression levels in the HCT116/CXCL14 cells and HCT/Control cells. **(E)** CXCL14-deficiency markedly inhibited the phosphorylation of ERK in HCT116/shCXCL14 cells when compared with that in HCT116/shNC. **(F)** Quantitative results of the p-ERK and total ERK expression levels in HCT116/shCXCL14 and HCT116/shNC cells. All experiments were repeated three times or more. Error bars represent ±S.D. $p < 0.05$ was considered to be statistically significant. * $p < 0.05$; ** $p < 0.01$, *** $p < 0.001$.

the expression levels of cell cycle-related protein (**Figures 5G,H**). Meanwhile, we also noted that the HCT116/CXCL14 cells were characterized with downregulation of epithelial markers E-cadherin and upregulation of mesenchymal markers vimentin and N-cadherin (**Figures 5G,I**), suggesting that CXCL14 may promote the CRC progression through the regulation the EMT process.

We also constructed a stably CXCL14-expressing SW620 cell line (SW620/CXCL14), as shown in **Figures 5J–L**. We found that the expression levels of CDK2, cyclin B1, and vimentin could be up-regulated by CXCL14 (**Figures 5M,N**).

Taken together, these data strongly suggests that chemokine CXCL14 may be directly involved in CRC cell proliferation and migration.

CXCL14 Regulated the ROS-Induced Phosphorylation of ERK

The typical extracellular-regulated kinase (ERK) cascade is a highly conserved signaling pathway that bridges extracellular signal molecules and intracellular diverse executor proteins, modulating various physiological or pathological processes, including tumor cell proliferation and migration (Maik-Rachline et al., 2019). Aberrant ROS can induce the activation of ERK through different signal cascade reactions in different cancers (Su et al., 2019). In the present study, we found that ROS treatment resulted in a greater accumulation of phosphorylated ERK (p-ERK) in HCT116 cells in a time-dependent manner, which could be partially restored by the antioxidant NAC pretreatment (**Figures**

6A,B). Previous evidence demonstrated that chemokines could induce cancer development through the activation of Erk1/2 (Zhao et al., 2017). To explore whether chemokine CXCL14 could mediate the level of p-ERK in CRC cells, we compared the levels of p-ERK between HCT116/CXCL14 cells and HCT116/Control cells. The results revealed that the level of p-ERK was markedly higher in the HCT116/CXCL14 cells than that in the HCT116/Control cells (**Figures 6C,D**). Furthermore, CXCL14-deficiency markedly inhibited the phosphorylation of ERK when compared with the control cells (i.e., scrambled shRNA), as shown in **Figures 6E,F**. More interestingly, H_2O_2 treatment could partially restore the expression levels of CXCL14 and p-ERK in HCT116/shCXCL14 cells (**Figures 6E,F**).

Taken together, these data suggest that chemokine CXCL14 may stimulate the expression of ROS-induced p-ERK, thereby promoting the CRC progression.

DISCUSSIONS

Accumulating evidence suggests that ROS can function as signaling molecules to participate in various physiological and pathological processes, including tumor cell proliferation and motility (Idelchik et al., 2017). The production of ROS can be induced by chronic inflammation, which may further lead to the development of chronic inflammation (Trivedi and Adams, 2018), which is similar to the roles of chemokines in the pathogenesis of chronic inflammation-associated diseases, including CRC (Coussens and Werb, 2002). Based on these backgrounds, we hypothesized that CXCL14 might be involved in ROS-induced CRC progression. To test the hypothesis, we conducted relevant studies and confirmed an important role of CXCL14 in ROS-induced CRC cell proliferation and migration. (a) Exogenous ROS (H_2O_2) could promote the proliferation and migration of human CRC cells. (b) ROS could promote the malignant behaviors of human CRC cells by regulating the cell cycle progression and EMT process. (c) CXCL14 was required for oncogenic signaling induced by ROS. (d) ROS-induced CXCL14 stimulated the phosphorylation of ERK in human CRC cells.

In the present study, we demonstrated ROS treatment and CXCL14 overexpression could modulate the expression levels of cell cycle-related proteins (Cyclin A1/B1, CDK1/2) and EMT-related proteins (E-cadherin, N-cadherin, vimentin), suggesting that CXCL14 might be involved in ROS-induced cell cycle progression and EMT process, which was consistent with the role of ROS-induced CXCL14 in breast cancer reported by Pelicano et al. (2009b). However, a previous study showed that ROS stimulated angiogenesis and tumor progression by reducing the expression of CXCL14 *via* EGFR/MEK/ERK signaling pathway in HNSCC cells (Maehata et al., 2010). Oncogenic role of ROS is with no doubt, while CXCL14 may have tumor-suppressive or tumor-supportive functions, depending on the type of the tumor. The conflicting biological functions of CXCL14 in tumor biology have been addressed. CXCL14 plays an anti-tumor role in HNSCC and tongue carcinomaa (Sato et al., 2010; Kondo et al., 2016), but a pro-tumor role in some breast cancer, pancreas cancer, and glioblastoma (Wente et al., 2008; Sjöberg et al., 2016). The contradictory results may be related to the type of the tumor, or dosage and treatment of ROS. CXCL14 may play distinct roles even in the same type of tumor. Gu et al. reported that CXCL14 expression was positively correlated to the overall survival of breast cancer patients as well as lymph node metastasis (Gu et al., 2012). However, Sjoberg et al. reported that high stromal CXCL14 expression correlated with shorter recurrence-free survival of breast cancer patients (Sjöberg et al., 2016). Moreover, CXCL14 expression was reported to be up-regulated by ROS and promoted cell motility in breast cancer cell lines (Pelicano et al., 2009b). In colorectal cancer, there are also some seemingly contradictory studies.

We found that CXCL14 modulated ROS-induced cell proliferation and motility in colorectal cancer cells, suggesting an oncogenic role of CXCL14 in CRC, which was consistent with our previous studies (Zeng et al., 2013b). However, the current study contradicted other findings (Lin et al., 2014; Hata et al., 2015). Lin et al. reported that the expression levels of CXCL14 mRNA and protein in CRC tissues were significantly down-regulated compared with levels in normal tissues (Lin et al., 2014). The clinical sample size and the method of evaluation of immunohistochemical staining may have a certain impact on the statistics and analysis of the results. Sjoberg, et al. divided the expression of CXCL14 in breast cancer clinical samples into three categories: epithelial CXCL14 expression, stromal CXCL14 expression, and total CXCL14 expression. They found that CXCL14 was strongly expressed in stromal cells and stromal CXCL14 expression significantly correlated with shorter survival in breast cancer (Sjöberg et al., 2016). Also, we found that CXCL14 was expressed in stromal cells in CRC specimens (data not shown). If software was adopted to calculate the mean optical density of immunohistochemical staining, the value would include CXCL14 expression in both tumor cells/normal epithelial cells and stromal cells. This evaluation method was different from that we used. Hata et al. reported that the incidence of AOM/DSS-induced cancer was suppressed in the CXCL14 transgenic mice due to the enhanced NK cell activity, implying an anti-tumor role of CXCL14 in chronic colitis-associated carcinogenesis (Hata et al., 2015). Accumulating evidence has demonstrated the multifarious roles of CXCL14 in cancer progression and immune responses. Chemoattraction of iDCs and NK cells and functional maturation of dendritic cells by CXCL14 can substantially contribute to anti-tumor immune response (Shurin et al., 1950; Starnes et al., 2006). In addition to normal epithelial cells, some cancer cells and stromal cells such as cancer-associated fibroblasts (CAFs) in the tumor microenvironment can express and secrete CXCL14 (Sjöberg et al., 2016). In the CXCL14 transgenic mice, all cells could highly express CXCL14, which might affect the anti-tumor or pro-tumor effect of CXCL14 from two aspects. First, whether stable expression of CXCL14 in the CXCL14 transgenic mice affects the function of some immune cells or stromal cells remains to be further explored. Second, there is no significant difference in the expression of CXCL14 between tumor tissues and normal tissues in the CXCL14 transgenic mice. In this way, tumor tissues may have no advantage in chemotacxis of DCs, NK cells or other cells to exert anti-tumor or pro-tumor effects.

Western blotting results revealed that the level of pERK1/2 was markedly higher in HCT116/CXCL14 cells when compared with HCT116/control, and CXCL14-deficiency markedly inhibited the phosphorylation of ERK1/2 compared with control (i.e., scrambled shRNA). Furthermore, ROS treatment could partially restore the expression levels of CXCL14 and pERK1/2 inHCT116/shCXCL14 cells. Thus, CXCL14 seems to provide a potent molecular association between oxidative stress and ERK signaling. In HNSCC cells, the level of phosphorylated ERK was up-regulated after ROS treatment (Maehata et al., 2010), which was consistent with our results. It is the difference that CXCL14 acts as a downstream signal molecule of p-ERK in HNSCC cells and CXCL14 acts as an upstream signal, regulating the phosphorylation level of ERK in CRC cells.

In conclusion, our results established the role of CXCL14 in the ROS-induced CRC cell proliferation and migration to facilitate the development of a rationale for the use of CXCL14 blockers in the treatment and prevention of CRC.

DATA AVAILABILITY STATEMENT

The data for this study are available by contacting the corresponding author.

AUTHOR CONTRIBUTIONS

JZ and ML conducted data research and drafted the manuscript. HX, JX, XY, and JF provided assistance on the experiments and statistical analyses. KW and SC provided valuable opinions, evaluation, and assistance during the process of drafting and revision of the manuscript. All authors read and approved the manuscript.

FUNDING

This work was supported by the grants from the National Natural Science Foundation of China (81502131), the Natural Science Foundation of Chongqing (cstc2018jcyjAX0573, cstc2017jcyjAX0165) and the Scientific and Technological Research Program of Chongqing Municipal Education Commission (KJ202000541975044).

ACKNOWLEDGMENTS

We would like to express sincere thanks to Prof. Youquan Bu and Prof. Yunlong Lei of Chongqing Medical University for their help in this study.

REFERENCES

Alafiatayo, A. A., Lai, K. S., Ahmad, S., Mahmood, M., and Shaharuddin, N. A. (2020). RNA-seq Analysis Revealed Genes Associated with UV-Induced Cell Necrosis through MAPK/TNF-α Pathways in Human Dermal Fibroblast Cells as an Inducer of Premature Photoaging. *Genomics* 112 (1), 484–493. doi:10.1016/j.ygeno.2019.03.011

Brody, H. (2015). Colorectal Cancer. *Nature* 521 (7551), S1. doi:10.1038/521S1a

Canli, Ö., Nicolas, A. M., Gupta, J., Finkelmeier, F., Goncharova, O., Pesic, M., et al. (2017). Myeloid Cell-Derived Reactive Oxygen Species Induce Epithelial Mutagenesis. *Cancer cell* 32 (6), 869–e5. doi:10.1016/j.ccell.2017.11.004

Coussens, L. M., and Werb, Z. (2002). Inflammation and Cancer. *Nature* 420 (6917), 860–867. doi:10.1038/nature01322

da Ros, M., Iorio, A. L., Lucchesi, M., Stival, A., de Martino, M., and Sardi, I. (2015). The Use of Anthracyclines for Therapy of CNS Tumors. *Anticancer Agents Med. Chem.* 15 (6), 721–727. doi:10.2174/1871520615666150407155319

Dasoveanu, D. C., Park, H. J., Ly, C. L., Shipman, W. D., Chyou, S., Kumar, V., et al. (2020). Lymph Node Stromal CCL2 Limits Antibody Responses. *Sci. Immunol.* 5 (45), 5. doi:10.1126/sciimmunol.aaw0693

Ghanbari Movahed, Z., Rastegari-Pouyani, M., Mohammadi, M. H., and Mansouri, K. (2019). Cancer Cells Change Their Glucose Metabolism to Overcome Increased ROS: One Step from Cancer Cell to Cancer Stem Cell? *Biomed. Pharmacother.* 112, 108690. doi:10.1016/j.biopha.2019.108690

Gu, X. L., Ou, Z. L., Lin, F. J., Yang, X. L., Luo, J. M., Shen, Z. Z., et al. (2012). Expression of CXCL14 and its Anticancer Role in Breast Cancer. *Breast Cancer Res. Treat.* 135 (3), 725–735. doi:10.1007/s10549-012-2206-2

Hata, R., Izukuri, K., Kato, Y., Sasaki, S., Mukaida, N., Maehata, Y., et al. (2015). Suppressed Rate of Carcinogenesis and Decreases in Tumour Volume and Lung Metastasis in CXCL14/BRAK Transgenic Mice. *Sci. Rep.* 5, 9083. doi:10.1038/srep09083

He, S., Li, X., Li, R., Fang, L., Sun, L., Wang, Y., et al. (2016). Annexin A2 Modulates ROS and Impacts Inflammatory Response via IL-17 Signaling in Polymicrobial Sepsis Mice. *Plos Pathog.* 12 (7), e1005743. doi:10.1371/journal.ppat.1005743

Idelchik, M. D. P. S., Begley, U., Begley, T. J., and Melendez, J. A. (2017). Mitochondrial ROS Control of Cancer. *Semin. Cancer Biol.* 47, 57–66. doi:10.1016/j.semcancer.2017.04.005

Kondo, T., Ozawa, S., Ikoma, T., Yang, X. Y., Kanamori, K., Suzuki, K., et al. (2016). Expression of the Chemokine CXCL14 and Cetuximab-dependent Tumour Suppression in Head and Neck Squamous Cell Carcinoma. *Oncogenesis* 5 (7), e240. doi:10.1038/oncsis.2016.43

Kyung, S., Lim, J. W., and Kim, H. (2019). α-Lipoic Acid Inhibits IL-8 Expression by Activating Nrf2 Signaling in Helicobacter Pylori-Infected Gastric Epithelial Cells. *Nutrients* 11 (10). doi:10.3390/nu11102524

Lei, Y., Huang, K., Gao, C., Lau, Q. C., Pan, H., Xie, K., et al. (2011). Proteomics Identification of ITGB3 as a Key Regulator in Reactive Oxygen Species-Induced Migration and Invasion of Colorectal Cancer Cells. *Mol. Cel ProteomicsMCP* 10 (10), M110–M005397. doi:10.1074/mcp.M110.005397

Li, X., Fang, P., Sun, Y., Shao, Y., Yang, W. Y., Jiang, X., et al. (2020). Anti-inflammatory Cytokines IL-35 and IL-10 Block Atherogenic Lysophosphatidylcholine-Induced, Mitochondrial ROS-Mediated Innate Immune Activation, but Spare Innate Immune Memory Signature in Endothelial Cells. *Redox Biol.* 28, 101373. doi:10.1016/j.redox.2019.101373

Li, X., Ye, Y., Zhou, X., Huang, C., and Wu, M. (2015). Atg7 Enhances Host Defense against Infection via Downregulation of Superoxide but Upregulation of Nitric Oxide. *J. Immunol.* 194 (3), 1112–1121. doi:10.4049/jimmunol.1401958

Li, Y., Wu, T., Gong, S., Zhou, H., Yu, L., Liang, M., et al. (2020). Analysis of the Prognosis and Therapeutic Value of the CXC Chemokine Family in Head and Neck Squamous Cell Carcinoma. *Front. Oncol.* 10, 570736. doi:10.3389/fonc.2020.570736

Lin, K., Zou, R., Lin, F., Zheng, S., Shen, X., and Xue, X. (2014). Expression and Effect of CXCL14 in Colorectal Carcinoma. *Mol. Med. Rep.* 10 (3), 1561–1568. doi:10.3892/mmr.2014.2343

Liu, J., Qu, L., Meng, L., and Shou, C. (2019). Topoisomerase Inhibitors Promote Cancer Cell Motility via ROS-Mediated Activation of JAK2-STAT1-CXCL1 Pathway. *J. Exp. Clin. Cancer Res.* 38 (1), 370. doi:10.1186/s13046-019-1353-2

Maehata, Y., Ozawa, S., Kobayashi, K., Kato, Y., Yoshino, F., Miyamoto, C., et al. (2010). Reactive Oxygen Species (ROS) Reduce the Expression of BRAK/CXCL14 in Human Head and Neck Squamous Cell Carcinoma Cells. *Free Radic. Res.* 44 (8), 913–924. doi:10.3109/10715762.2010.490836

Maik-Rachline, G., Hacohen-Lev-Ran, A., and Seger, R. (2019). Nuclear ERK: Mechanism of Translocation, Substrates, and Role in Cancer. *Int. J. Mol. Sci.* 20 (5). doi:10.3390/ijms20051194

Malumbres, M., and Barbacid, M. (2009). Cell Cycle, CDKs and Cancer: a Changing Paradigm. *Nat. Rev. Cancer* 9 (3), 153–166. doi:10.1038/nrc2602

Maurya, A. K., and Vinayak, M. (2015). Modulation of PKC Signaling and Induction of Apoptosis through Suppression of Reactive Oxygen Species and Tumor Necrosis

Factor Receptor 1 (TNFR1): Key Role of Quercetin in Cancer Prevention. *Tumour Biol.* 36 (11), 8913–8924. doi:10.1007/s13277-015-3634-5

Moloney, J. N., and Cotter, T. G. (2018). ROS Signalling in the Biology of Cancer. *Semin. Cel Dev Biol* 80, 50–64. doi:10.1016/j.semcdb.2017.05.023

Nieto, M. A., Huang, R. Y., Jackson, R. A., and Thiery, J. P. (2016). Emt: 2016. *Cell* 166 (1), 21–45. doi:10.1016/j.cell.2016.06.028

Pelicano, H., Lu, W., Zhou, Y., Zhang, W., Chen, Z., Hu, Y., et al. (2009). Mitochondrial Dysfunction and Reactive Oxygen Species Imbalance Promote Breast Cancer Cell Motility through a CXCL14-Mediated Mechanism. *Cancer Res.* 69 (6), 2375–2383. doi:10.1158/0008-5472.CAN-08-3359

Pelicano, H., Lu, W., Zhou, Y., Zhang, W., Chen, Z., Hu, Y., et al. (2009). Mitochondrial Dysfunction and Reactive Oxygen Species Imbalance Promote Breast Cancer Cell Motility through a CXCL14-Mediated Mechanism. *Cancer Res.* 69 (6), 2375–2383. doi:10.1158/0008-5472.Can-08-3359

Prasad, S., Gupta, S. C., and Tyagi, A. K. (2017). Reactive Oxygen Species (ROS) and Cancer: Role of Antioxidative Nutraceuticals. *Cancer Lett.* 387, 95–105. doi:10.1016/j.canlet.2016.03.042

Ramírez-Moreno, I. G., Ibarra-Sánchez, A., Castillo-Arellano, J. I., Blank, U., and González-Espinosa, C. (2020). Mast Cells Localize in Hypoxic Zones of Tumors and Secrete CCL-2 under Hypoxia through Activation of L-type Calcium Channels. *J. Immunol.* 204 (4), 1056–1068. doi:10.4049/jimmunol.1801430

Reczek, C. R., and Chandel, N. S. (2018). ROS Promotes Cancer Cell Survival through Calcium Signaling. *Cancer cell* 33 (6), 949–951. doi:10.1016/j.ccell.2018.05.010

Ruiz-Torres, V., Rodríguez-Pérez, C., Herranz-López, M., Martín-García, B., Gómez-Caravaca, A. M., Arráez-Román, D., et al. (2019). Marine Invertebrate Extracts Induce Colon Cancer Cell Death via ROS-Mediated DNA Oxidative Damage and Mitochondrial Impairment. *Biomolecules* 9 (12). doi:10.3390/biom9120771

Salehi, F., Behboudi, H., Kavoosi, G., and Ardestani, S. K. (2018). Oxidative DNA Damage Induced by ROS-Modulating Agents with the Ability to Target DNA: A Comparison of the Biological Characteristics of Citrus Pectin and Apple Pectin. *Sci. Rep.* 8 (1), 13902. doi:10.1038/s41598-018-32308-2

Sato, K., Ozawa, S., Izukuri, K., Kato, Y., and Hata, R. (2010). Expression of Tumour-Suppressing Chemokine BRAK/CXCL14 Reduces Cell Migration Rate of HSC-3 Tongue Carcinoma Cells and Stimulates Attachment to Collagen and Formation of Elongated Focal Adhesions *In Vitro*. *Cell Biol Int* 34 (5), 513–522. doi:10.1042/cbi20090108

Shurin, G. V., Ferris, R. L., Ferris, R., Tourkova, I. L., Perez, L., Lokshin, A., et al. (1950).Loss of New Chemokine CXCL14 in Tumor Tissue Is Associated with Low Infiltration by Dendritic Cells (DC), while Restoration of Human CXCL14 Expression in Tumor Cells Causes Attraction of DC Both *In Vitro* and *In Vivo*. *J. Immunol.*, 174, 5490–5498. doi:10.4049/jimmunol.174.9.5490

Siegel, R. L., Miller, K. D., Fedewa, S. A., Ahnen, D. J., Meester, R. G. S., Barzi, A., et al. (2017). Colorectal Cancer Statistics, 2017. *CA Cancer J. Clin.* 67 (3), 177–193. doi:10.3322/caac.21395

Sjöberg, E., Augsten, M., Bergh, J., Jirström, K., and Östman, A. (2016). Expression of the Chemokine CXCL14 in the Tumour Stroma Is an Independent Marker of Survival in Breast Cancer. *Br. J. Cancer* 114 (10), 1117–1124. doi:10.1038/bjc.2016.104

Starnes, T., Rasila, K. K., Robertson, M. J., Brahmi, Z., Dahl, R., Christopherson, K., et al. (2006). The Chemokine CXCL14 (BRAK) Stimulates Activated NK Cell Migration: Implications for the Downregulation of CXCL14 in Malignancy. *Exp. Hematol.* 34 (8), 1101–1105. doi:10.1016/j.exphem.2006.05.015

Su, X., Shen, Z., Yang, Q., Sui, F., Pu, J., Ma, J., et al. (2019). Vitamin C Kills Thyroid Cancer Cells through ROS-dependent Inhibition of MAPK/ERK and PI3K/AKT Pathways via Distinct Mechanisms. *Theranostics* 9 (15), 4461–4473. doi:10.7150/thno.35219

Sung, H., Ferlay, J., Siegel, R. L., Laversanne, M., Soerjomataram, I., Jemal, A., et al. (2021). Global Cancer Statistics 2020: GLOBOCAN Estimates of Incidence and Mortality Worldwide for 36 Cancers in 185 Countries. *CA Cancer J. Clin.* 71 (3), 209–249. doi:10.3322/caac.21660

Trivedi, P. J., and Adams, D. H. (2018). Chemokines and Chemokine Receptors as Therapeutic Targets in Inflammatory Bowel Disease; Pitfalls and Promise. *J. Crohns Colitis* 12 (12), 1508. doi:10.1093/ecco-jcc/jjy130

Wang, K., Liu, R., Li, J., Mao, J., Lei, Y., Wu, J., et al. (2011). Quercetin Induces Protective Autophagy in Gastric Cancer Cells: Involvement of Akt-mTOR- and Hypoxia-Induced Factor 1α-Mediated Signaling. *Autophagy* 7 (9), 966–978. doi:10.4161/auto.7.9.15863

Wang, Y., Xu, M., Ke, Z. J., and Luo, J. (2017).Cellular and Molecular Mechanisms Underlying Alcohol-Induced Aggressiveness of Breast Cancer. *Pharmacol. Res.*, 115, 299–308. doi:10.1016/j.phrs.2016.12.005PMC5205572)

Wen, J., Wang, Y., Gao, C., Zhang, G., You, Q., Zhang, W., et al. (2018). *Helicobacter pylori* Infection Promotes Aquaporin 3 Expression via the ROS-HIF-1α-AQP3-ROS Loop in Stomach Mucosa: a Potential Novel Mechanism for Cancer Pathogenesis. *Oncogene* 37 (26), 3549–3561. doi:10.1038/s41388-018-0208-1

Wente, M. N., Mayer, C., Gaida, M. M., Michalski, C. W., Giese, T., Bergmann, F., et al. (2008). CXCL14 Expression and Potential Function in Pancreatic Cancer. *Cancer Lett.* 259 (2), 209–217. doi:10.1016/j.canlet.2007.10.021

Wu, Z. H., Zhong, Y., Zhou, T., and Xiao, H. J. (2021). miRNA Biomarkers for Predicting Overall Survival Outcomes for Head and Neck Squamous Cell Carcinoma. *Genomics* 113 (1 Pt 1), 135–141. doi:10.1016/j.ygeno.2020.12.002

Xian, Z. Y., Hu, B., Wang, T., Cai, J. L., Zeng, J. Y., Zou, Q., et al. (2020). CircABCB10 Silencing Inhibits the Cell Ferroptosis and Apoptosis by Regulating the miR-326/CCL5 axis in Rectal Cancer. *Neoplasma* 67 (5), 1063–1073. doi:10.4149/neo_2020_191024N1084

Xie, Q., Liu, Y., and Li, X. (2020). The Interaction Mechanism between Autophagy and Apoptosis in colon Cancer. *Transl Oncol.* 13 (12), 100871. doi:10.1016/j.tranon.2020.100871

Yang, Y., Karakhanova, S., Hartwig, W., D'Haese, J. G., Philippov, P. P., Werner, J., et al. (2016). Mitochondria and Mitochondrial ROS in Cancer: Novel Targets for Anticancer Therapy. *J. Cel Physiol* 231 (12), 2570–2581. doi:10.1002/jcp.25349

Yuan, D., Huang, S., Berger, E., Liu, L., Gross, N., Heinzmann, F., et al. (2017). Kupffer Cell-Derived Tnf Triggers Cholangiocellular Tumorigenesis through JNK Due to Chronic Mitochondrial Dysfunction and ROS. *Cancer cell* 31 (6), 771–e6. doi:10.1016/j.ccell.2017.05.006

Yuan, K., Xie, K., Lan, T., Xu, L., Chen, X., Li, X., et al. (2020). TXNDC12 Promotes EMT and Metastasis of Hepatocellular Carcinoma Cells via Activation of β-catenin. *Cell Death Differ* 27 (4), 1355–1368. doi:10.1038/s41418-019-0421-7

Zeng, J., Yang, X., Cheng, L., Liu, R., Lei, Y., Dong, D., et al. (2013). Chemokine CXCL14 Is Associated with Prognosis in Patients with Colorectal Carcinoma after Curative Resection. *J. Transl Med.* 11, 6. doi:10.1186/1479-5876-11-6

Zeng, J., Yang, X., Cheng, L., Liu, R., Lei, Y., Dong, D., et al. (2013). Chemokine CXCL14 Is Associated with Prognosis in Patients with Colorectal Carcinoma after Curative Resection. *J. Transl Med.* 11, 6. doi:10.1186/1479-5876-11-6

Zhang, J., Ahmad, S., Wang, L. Y., Han, Q., Zhang, J. C., and Luo, Y. P. (2019). Cell Death Induced by α-terthienyl via Reactive Oxygen Species-Mediated Mitochondrial Dysfunction and Oxidative Stress in the Midgut of *Aedes aegypti* Larvae. *Free Radic. Biol. Med.* 137, 87–98. doi:10.1016/j.freeradbiomed.2019.04.021

Zhao, J., Ou, B., Han, D., Wang, P., Zong, Y., Zhu, C., et al. (2017). Tumor-derived CXCL5 Promotes Human Colorectal Cancer Metastasis through Activation of the ERK/Elk-1/Snail and AKT/GSK3β/β-catenin Pathways. *Mol. Cancer* 16 (1), 70. doi:10.1186/s12943-017-0629-4

Zhu, X., Yang, J., Zhu, W., Yin, X., Yang, B., Wei, Y., et al. (2018). Combination of Berberine with Resveratrol Improves the Lipid-Lowering Efficacy. *Int. J. Mol. Sci.* 19 (12). doi:10.3390/ijms19123903

Zhuang, Y., Li, Y., Li, X., Xie, Q., and Wu, M. (2016). Atg7 Knockdown Augments Concanavalin A-Induced Acute Hepatitis through an ROS-Mediated P38/MAPK Pathway. *PloS one* 11 (3), e0149754. doi:10.1371/journal.pone.0149754

Conflict of Interest: The authors declare that the research was conducted in the absence of any commercial or financial relationships that could be construed as a potential conflict of interest.

The handling editor declared a past collaboration with several of the authors (JZ, KW).

Publisher's Note: All claims expressed in this article are solely those of the authors and do not necessarily represent those of their affiliated organizations, or those of the publisher, the editors and the reviewers. Any product that may be evaluated in this article, or claim that may be made by its manufacturer, is not guaranteed or endorsed by the publisher.

frontiers in Pharmacology

REVIEW
published: 26 October 2021
doi: 10.3389/fphar.2021.760581

Carnitine Palmitoyltransferase System: A New Target for Anti-Inflammatory and Anticancer Therapy?

Muyun Wang[1†], Kun Wang[1†], Ximing Liao[1], Haiyang Hu[2], Liangzhi Chen[3], Linlin Meng[3], Wei Gao[1] and Qiang Li[1*]*

[1]Department of Pulmonary and Critical Care Medicine, Shanghai East Hospital, Tongji University School of Medicine, Shanghai, China, [2]Department of Vascular Surgery, Shanghai Jiao Tong University Affiliated Sixth People's Hospital, Shanghai, China, [3]Department of Traditional Chinese Medicine, Shandong University of Traditional Chinese Medicine, Jinan, China

Lipid metabolism involves multiple biological processes. As one of the most important lipid metabolic pathways, fatty acid oxidation (FAO) and its key rate-limiting enzyme, the carnitine palmitoyltransferase (CPT) system, regulate host immune responses and thus are of great clinical significance. The effect of the CPT system on different tissues or organs is complex: the deficiency or over-activation of CPT disrupts the immune homeostasis by causing energy metabolism disorder and inflammatory oxidative damage and therefore contributes to the development of various acute and chronic inflammatory disorders and cancer. Accordingly, agonists or antagonists targeting the CPT system may become novel approaches for the treatment of diseases. In this review, we first briefly describe the structure, distribution, and physiological action of the CPT system. We then summarize the pathophysiological role of the CPT system in chronic obstructive pulmonary disease, bronchial asthma, acute lung injury, chronic granulomatous disease, nonalcoholic fatty liver disease, hepatic ischemia–reperfusion injury, kidney fibrosis, acute kidney injury, cardiovascular disorders, and cancer. We are also concerned with the current knowledge in either preclinical or clinical studies of various CPT activators/inhibitors for the management of diseases. These compounds range from traditional Chinese medicines to novel nanodevices. Although great efforts have been made in studying the different kinds of CPT agonists/antagonists, only a few pharmaceuticals have been applied for clinical uses. Nevertheless, research on CPT activation or inhibition highlights the pharmacological modulation of CPT-dependent FAO, especially on different CPT isoforms, as a promising anti-inflammatory/antitumor therapeutic strategy for numerous disorders.

Keywords: carnitine palmitoyltransferase (CPT), fatty acid oxidation (FAO), inflammatory diseases, cancers, CPT activator, CPT inhibitor

OPEN ACCESS

Edited by:
Xuefeng Li,
Guangzhou Medical University, China

Reviewed by:
Xiangling Meng,
Stanford University, United States
Yitian Xu,
Houston Methodist Research Institute, United States
Qiang Qin,
University of Texas MD Anderson Cancer Center, United States
Dandan Zhu,
University of Texas Health Science Center at Houston, United States

***Correspondence:**
Wei Gao
grace19881118@126.com
Qiang Li
liqressh1962@163.com

†These authors have contributed equally to this work

Specialty section:
This article was submitted to Inflammation Pharmacology, a section of the journal Frontiers in Pharmacology

Received: *18 August 2021*
Accepted: *17 September 2021*
Published: *26 October 2021*

Citation:
Wang M, Wang K, Liao X, Hu H, Chen L, Meng L, Gao W and Li Q (2021) Carnitine Palmitoyltransferase System: A New Target for Anti-Inflammatory and Anticancer Therapy? Front. Pharmacol. 12:760581. doi: 10.3389/fphar.2021.760581

1 INTRODUCTION

Lipids, which generally consist of triglycerides, cholesterol, phospholipids, and glycolipids, are hydrophobic molecules that have three basic functions, namely, energy storage, signal transduction, and membrane building. Initially considered as the reserves of static metabolic energy, these are now also considered as important components of various cellular signal transduction pathways. The roles of lipids in modulating host immune response, either in promoting or eliminating inflammation, have been of major clinical interest (Chen et al., 2019). Recently, lipid metabolism has been proved to be associated with various diseases, including acute and chronic inflammatory disorders and cancer. As one of the most important lipid substances *in vivo*, fatty acid (FA) utilization by β-oxidation is a major bioenergetic pathway that could be upregulated with prolonged fasting, exercise, or metabolic stress. FA oxidation (FAO) mainly occurs in the mitochondria and involves a series of reactions that result in the conversion of FA to acetyl-coenzyme A (acetyl-CoA). In the early 20th century, Franz (1904) elucidated the mechanisms underlying FA degradation by successive cyclic removal of two carbon units at a time, which subsequently initiated further studies on FAO (Schlaepfer and Joshi, 2020).

Compared with the transmembrane movement of short-chain and medium-chain FAs, the transport of long-chain FA is more difficult, thus becoming a key step of FAO. In the mid-1950s, Fritz (1955) determined the essential function of carnitine in the oxidation of long-chain FA in mammalian tissues. Subsequent studies by Bremer (1963) and Fritz and Yue (1963) led to a conceptual framework depicting how carnitine enables long-chain FA esterification to CoA in the extramitochondrial compartment to generate enzymes of β-oxidation in the mitochondrial matrix, thus circumventing the permeability issue of the inner membrane to acyl-CoA esters. Generally, the transfer of long-chain FAs into the mitochondria for oxidation occurs in a well-organized and regulated manner. Enzymes that facilitate this transfer are known as L-carnitine acetyltransferases; these catalyze the reversible transfer of acyl groups between L-carnitine and coenzyme A (CoA), resulting in the conversion of acyl-CoA esters into acyl-carnitine esters and vice versa (Schlaepfer and Joshi, 2020). Due to the impermeability of the mitochondrial inner membrane to long-chain CoA FA, this step in CoA and carnitine exchange is essential (McGarry and Brown, 1997). Among the enzymes, carnitine palmitoyltransferase (CPT) plays a rate-limiting role in FAO and thus has been recognized as a pivotal component of cellular metabolic homeostasis. CPT occurs in two isoforms, namely, CPT1 and CPT2, which are localized mainly in the mitochondria (Brosnan et al., 1973; McGarry and Brown, 1997) and play a crucial role in preserving their structural and functional integrity. In addition, CPT also facilitates adaptation to the environment, under both healthy and disease conditions (Roe, 2002). Therefore, intensive studies on CPT may help to understand in depth the pathogenesis of various diseases and explore a promising class of therapeutics.

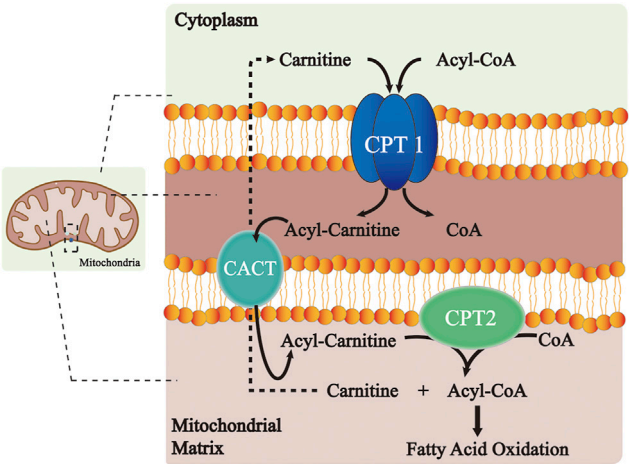

FIGURE 1 | Role of the CPT system in the long-chain FA oxidation. CPT1 at the outer mitochondrial membrane catalyzes the conversion of long-chain acyl-CoA along with carnitine to long-chain acylcarnitine and CoA. The transesterified acylcarnitines are then transferred from cytosol into intermembrane space and the remaining acyl of acylcarnitine is changed back to CoA on the inner membrane catalyzed by CPT2, which is next available for β-oxidation. Meanwhile, the released carnitine is returned to the intermembrane space of the mitochondrion through the CACT and is available for the re-transport of FA. Abbreviations: CPT, carnitine palmitoyltransferase; CACT, carnitine–acylcarnitine–translocase; and CoA, coenzyme A.

2 STRUCTURE, DISTRIBUTION, AND PHYSIOLOGICAL ACTION OF THE CARNITINE PALMITOYLTRANSFERASE SYSTEM

CPT1, CPT2, and carnitine-acylcarnitine translocase (CACT) play vital roles in the transport system for FA esterification in the mitochondrial membrane. The transmembrane protein CPT1 is located at the outer mitochondrial membrane, while CPT2 is in the inner of the mitochondrial membrane (Fraser et al., 1997). Unlike the unique form of CPT2 (Demaugre et al., 1990), three tissue-specific isoforms of CPT1 have been identified: the liver isoform (L-CPT-1, CPT1A), muscle isoform (M-CPT-1, CPT1B), and brain isoform (B-CPT-1, CPT1C) (Britton et al., 1995; Yamazaki et al., 1996; Price et al., 2002). CPT1A, with its full-length cDNA clone isolated from rat liver that predicted a protein of 773 amino acids (Esser et al., 1993), is characterized by tight mitochondrial membrane binding, which would lose activity once removed from the membrane. Compared with CPT1A, CPT1B consists of 772 amino acids (Cox et al., 1998; van der Leij et al., 2000) and has lower affinity for substrate carnitine (McGarry and Brown, 1997). A study has demonstrated that homozygous deletions in CPT1B are lethal in mouse (Ji et al., 2008). The protein primary sequence of CPT1C is larger (798 amino acids) than the two other isoforms. Although CPT1C tends to adopt the same membrane topology as CPT1A, its enzyme activity is extremely low or undetectable (Hada et al., 2014). First identified in 1990 (Woeltje et al., 1990a; Woeltje et al., 1990b), the cDNA sequence of CPT2 predicted a nascent product

of 658 amino acids in both rats and humans. Unlike CPT1, CPT2 does not contain a single polypeptide with both the inhibitor binding and catalytic domains (Bonnefont et al., 2004).

CPT1A is the primary isoform and is found in the liver, spleen, kidneys, lungs, intestines, pancreas, brain, and ovaries (Brown et al., 1997; McGarry and Brown, 1997). CPT1B is predominant in the skeletal muscle, adipose tissue, heart, and testis (Esser et al., 1996), whereas CPT1C is mainly expressed in the brain and is downregulated in the testis, ovaries, small intestine, and colon (Price et al., 2002). Microcosmically, CPT1A and CPT1B are both located in the outer membrane of the mitochondria, whereas CPT1C is localized to both the endoplasmic reticulum and mitochondria (Dai et al., 2007; Sierra et al., 2008). CPT1 isoform switching in the mitochondria has been established during the development of rat heart; although CPT1A represents a minor constituent of the CPT complex in the adult rat heart, its contribution is much greater in newborn animals (Brown et al., 1995). CPT2 is a ubiquitous enzyme in rats and humans (Demaugre et al., 1990; Woeltje et al., 1990a; Woeltje et al., 1990b).

The CPT system is an important intermediate of lipogenesis and a vital mechanism for the homeostasis of FA metabolism (**Figure 1**). CPT1A and CPT1B at the outer mitochondrial membrane catalyze the first transport step of lipid metabolism, in which the long-chain acyl-CoA and carnitine are converted into long-chain acylcarnitine and CoA. The transesterified acylcarnitines are then transferred from the cytosol into the intermembrane space (Eaton et al., 1996; Console et al., 2014) and the remaining acyl of acylcarnitine is converted back to CoA on the inner membrane and catalyzed by CPT2, which is then available for β-oxidation (Joshi and Zierz, 2020). Meanwhile, the released carnitine signal transduction is returned back to the intermembrane space of the mitochondrion through the CACT and available for the re-transport of FA (Joshi and Zierz, 2020). Comparatively, CPT1C does not serve a key role in FAO. However, it shows significant effects on neuronal oxidative metabolism, energy homeostasis, and cell senescence (Lee and Wolfgang, 2012; Reilly and Mak, 2012; Guan et al., 2019). In terms of the underlying molecular pathway, the peroxisome proliferator-activated receptor (PPAR) family is a key transcription factor in the development of FAO. Studies have shown that PPAR activation controls the levels of intracellular free fatty acids (FFAs) (Castaño et al., 2018; Ye et al., 2019). Furthermore, the expression and activity of the CPT system increase with PPAR activation, thus manipulating FA metabolism.

3 IMPLICATIONS OF CARNITINE PALMITOYLTRANSFERASE SYSTEM IN INFLAMMATORY DISEASES AND CANCERS

In recent years, studies have focused on the contribution of lipid metabolic pathways on the pathogenesis of multiple disorders. Considering the modulatory effects and clinical implications of lipid molecules in different tissues or organs, we summarize the pathophysiological role of the CPT system in many diseases of acute and chronic inflammation as well as cancer in this review. These diseases include chronic obstructive pulmonary disease (COPD), bronchial asthma, acute lung injury (ALI), chronic granulomatous disease (CGD), nonalcoholic fatty liver disease (NAFLD), hepatic ischemia–reperfusion (IR) injury, kidney fibrosis, acute kidney injury (AKI), cardiovascular disorders, and cancer (**Figure 2**; **Table 1**). We also concentrate on the current knowledge on pharmacological modulators targeting the CPT system from preclinical evaluation to clinical trials in managing these diseases (**Figure 3**; **Table 2**).

3.1 Pulmonary Diseases

The lung is seldom considered as a metabolic organ. However, active lipid metabolism occurs in lung tissues, especially within the alveolar area, where surfactant homeostasis is exquisitely regulated to ensure continuous optimal function in each respiration cycle. Metabolic disturbance of the lipid profile induces excess inflammation, oxidative stress, and cellular apoptosis, which has been proven to be involved in the occurrence and development of various lung diseases.

3.1.1 Chronic Obstructive Pulmonary Disease

COPD is a major worldwide health problem that is increasing in prevalence and mortality (Rennard and Drummond, 2015). The progressive lung condition is characterized by an irreversible airflow limitation associated with an abnormal inflammatory response in the airway and is mostly attributable to noxious particles or gases (Mizumura et al., 2018; Gong et al., 2019). Among these, cigarette smoke (CS) is the major risk factor for the development of COPD, which accounts for at least 75% of the deaths (Gong et al., 2019). Despite increasing epidemiologic evidence linking lipid metabolism to CS-induced emphysema (Lundström et al., 2011; Zehethofer et al., 2015), the regulatory effects of FAO and CPT on COPD pathogenesis remains unclear (Jiang et al., 2017).

CS exposure has been reported to promote FAO and mitochondrial respiration, along with an increased expression of CPT1 in the airway epithelial cells (EpiCs) (Agarwal et al., 2014; Jiang et al., 2017; Gong et al., 2019). Genome-wide association studies on COPD have demonstrated that FAM13A (family with sequence similarity 13 member A) enhances FAO by upregulating CPT1A expression, while chemical or genetic inhibition of FAO attenuates the accumulation of mitochondrial-derived reactive oxygen species (ROS) and cell death induced by CS exposure *in vitro* and *in vivo* (Jiang et al., 2017). Additionally, CS exposure also disrupts the extracellular matrix during COPD (Shapiro and Ingenito, 2005), which could subsequently promote FAO in EpiC (Schafer et al., 2009). In terms of the specific mechanism, a recent study suggested that the increased FAO and CPT expression by CS challenge in airway EpiC might exploit fat storage in adipose tissues to meet elevated FA demands within the lungs under stress conditions. By metabolic adaptation, the cells are able to generate ATPs to meet their energy needs. However, sustained elevation in

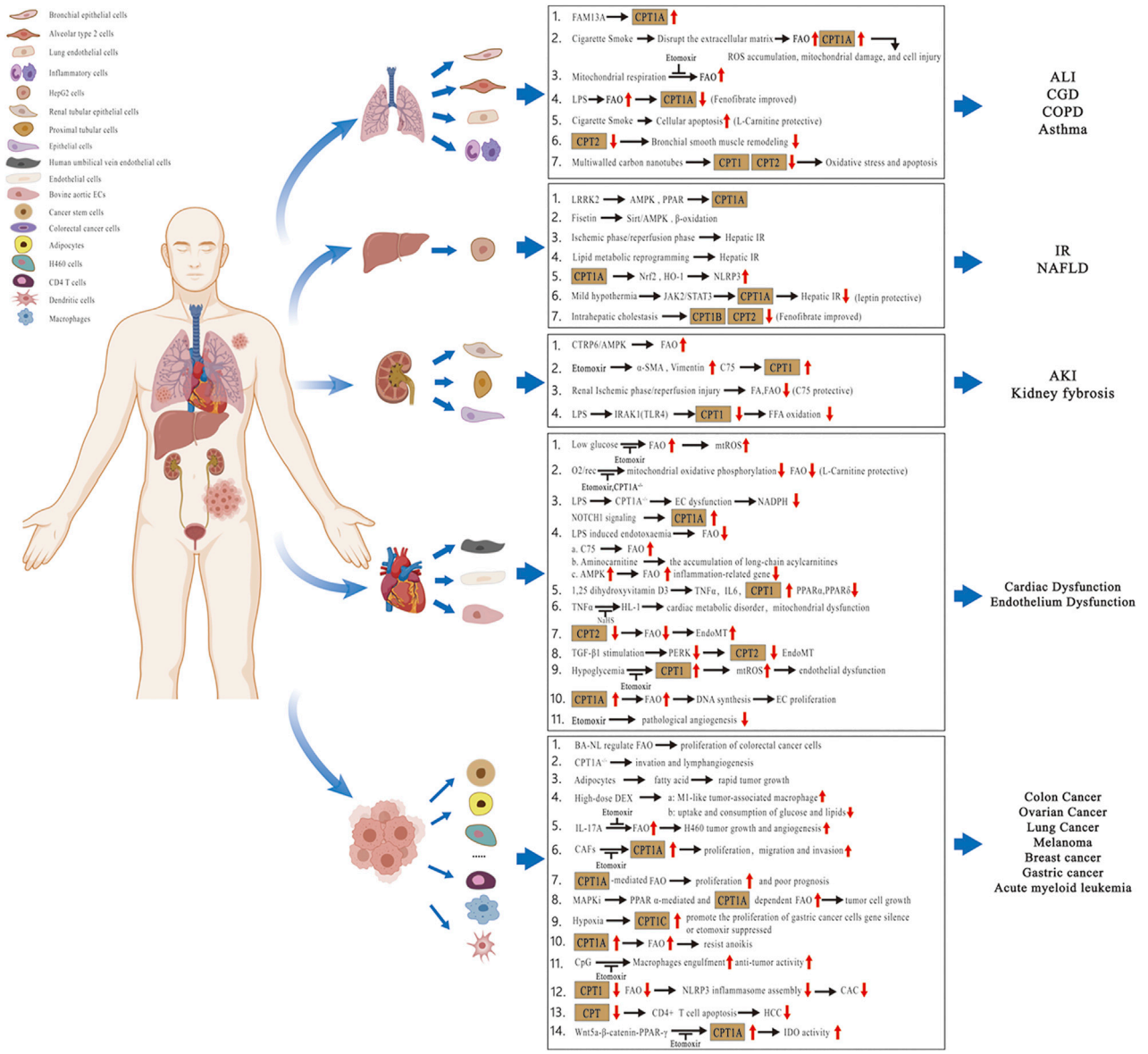

FIGURE 2 | Pathophysiological role of the CPT system in different tissues or organs. Related diseases include COPD, asthma, ALI, CGD, NAFLD, hepatic IR injury, kidney fibrosis, AKI, cardiovascular disorders, and cancer. Abbreviations: COPD, chronic obstructive pulmonary disease; ALI, acute lung injury; CGD, chronic granulomatous disease; NAFLD, nonalcoholic fatty liver disease; IR, ischemia–reperfusion; AKI, acute kidney injury; CPT, carnitine palmitoyltransferase; FA, fatty acid; FFA, free fatty acid; FAO, fatty acid oxidation; FAM13A, family with sequence similarity 13 member A; ROS, reactive oxygen species; mtROS, mitochondrial ROS; LPS, lipopolysaccharide; LRRK2, leucine-rich repeat kinase 2; AMPK, AMP-activated protein kinase; Sirt, sirtuin; PPAR, peroxisome proliferator-activated receptor; Nrf2, nuclear factor erythroid-2–related factor 2; HO-1, heme oxygenase-1; NLRP3, nucleotide-binding oligomerization domain-like receptor protein 3; JAK2/STAT3, Janus kinase 2/Signal transducer and activator of transcription 3; CTRP6, C1q/tumor necrosis factor-related protein 6; α-SMA, α-smooth muscle actin; IRAK1, interleukin-1 receptor–associated kinase 1; TLR4, toll-like receptor 4; O_2/rec, hyperoxia followed by air recovery; ECs, endothelial cells; TNFα, tumor necrosis factor-α; IL6, interleukin 6; NaHS, sodium hydrosulfide; EndoMT, endothelial-to-mesenchymal transition; TGF-β1, transforming growth factor-β1; PERK, protein kinase R-like endoplasmic reticulum kinase; BA-NL, betulinic acid–loaded nanoliposomes; DEX, dexamethasone; IL-17A, interleukin 17A; CAFs, cancer-associated fibroblasts; MAPKis, mitogen-activated protein kinase inhibitors; CAC, colitis-associated cancer; HCC, hepatocellular carcinoma; and IDO, indoleamine 2,3-dioxgenase-1.

FAO and CPT could disturb the metabolic homeostasis of cells and be harmful to their fate and functions. This viewpoint has been supported by observations of reduced mitochondrial ROS production and improved human bronchial EpiC viability with treatment using a CPT1A inhibitor, etomoxir, after CS exposure (Jiang et al., 2017).

However, enhanced FAO and CPT expression by L-carnitine has been proven to be beneficial to emphysema or COPD (Gong et al., 2019). L-carnitine, which is the critical metabolite in the transport of long-chain FAs into the mitochondria for subsequent β-oxidation, is downregulated in the lungs of mice with emphysema (Conlon et al., 2016). L-carnitine is the substrate

TABLE 1 | The role of CPT in inflammatory disease.

Targets	Associated disease	Types of CPT	Major outcome(s)	References
Liver	Liver injury	CPT1B and CPT2	Decreased in intrahepatic cholestasis model	Zhao et al. (2017)
		CPT1A	Promoted oxidative stress	Luo et al. (2021)
		CPT1A	Decreased in HepG2 cells; inhibited inflammation	Wei et al. (2014)
		CPT1A	Suppressed inflammation	Lin et al. (2020)
		CPT1A	JAK2/STAT3-CPT1A–dependent FAO attenuated injury	Wang W. et al. (2020)
		CPT1 and CPT2	L-carnitine elevated its transcription and activity	Karlic et al. (2002)
		CPT	Carnitine ingestion during pregnancy increased liver CPT activity and fetal carnitine concentrations	Xi et al. (2008)
	NAFLD	CPT1	Improved the symptoms of the disease	Liou et al. (2018)
		CPT1	Impaired CPT1 induced hepatic dysfunction and inflammation	Schröder et al. (2016)
	HCC	CPT	Upregulated CPT elevated apoptosis of $CD4^+$ T cells and promoted HCC formation in NAFLD	Brown et al. (2018)
Cardiovascular System	Cardiac dysfunction	CPT1	Downregulated CPT1 induced myocardial dysfunction	Eaton et al. (2003)
		CPT1	Decreased in heart induced by LPS	Fukumoto et al. (2002)
		CPT1	Upregulated in diabetic rats	Lee et al. (2014)
		CPT1	Downregulated CPT1 induced the injury	Lee et al. (2019)
		CPT1 and CPT2	Downregulated CPT induced cardiac injury during endotoxemia	Makrecka-Kuka et al. (2020)
	Endothelium Dysfunction	CPT1A	Loss of CPT1A elevated oxidative stress and promoted endothelial barrier disruption	Kalucka et al. (2018)
		CPT1	Downregulated CPT1 increased atherosclerosis	Fruchart et al. (1999)
		CPT2	Genetic disruption potentiated EndoMT	Xiong J. et al. (2018)
Pulmonary	Asthma	CPT1	Raised in asthmatic mice	Al-Khami et al. (2017)
		CPT2	Increased in asthmatic bronchial SMC	Esteves et al. (2021)
	COPD	CPT1A	CS increased CPT1A and FAO	Jiang et al. (2017)
		CPT1	CS increased CPT1 expression and promote FAO	Agarwal et al. (2014)
	ALI	CPT1B	Decreased CPT1B increased mortality; increased expression and decreased activity in aged ALI mice	Gibbs et al. (2021)
		CPT1A	CPT1A inhibition or depletion aggravated EC apoptosis and lung injury	Yao et al. (2019)
Kidney	Diabetic nephropathy	CPT	Aggravated mitochondrial ROS accumulation in kidney cortical tubules	Rosca et al. (2012)
	Kidney fibrosis	CPT1A	Decreased during the disease	Xie et al. (2021)
		CPT1A	Overexpression of CPT1A showed protective effects	Miguel et al. (2021)
	IR injury	CPT1	Upregulated CPT1 improved renal function	Idrovo et al. (2012)
Colon	Colorectal cancer	CPT1A	Exposure to adipocytes or FA upregulated CPT1A	Xiong et al. (2020)
		CPT1A	CPT1A activation induced anoikis-resist	Wang et al. (2018)
		CPT1A	Low expression in primary tumor tissues while high expression in CAFs	Peng et al. (2021)
	CAC	CPT1	Suppressed CPT1 inhibited NLRP3 assembly in macrophages	Qiao et al. (2020)
Breast	Breast cancer	CPT1A	$CPT1A^{-/-}$ abolished invasion and lymphangiogenesis	Xiong Y. et al. (2018)
		CPT1A	Upregulated in patients; a new biomarker for the diagnosis	Tan et al. (2021)
		CPT1A	Increased in doxorubicin-treated tumours *in vivo*	Petővári et al. (2020)
		CPT1C	Conferred rapamycin resistance on breast cancer cells	Reilly and Mak (2012)
Blood	AML	CPT1A	Overexpression predicted poor clinical outcome	Mao et al. (2021)
	Lymphoblastic leukemia	CPT1 and CPT2	Highly expressed in chronic lymphoblastic leukemia cells	Gugiatti et al. (2018)
	Leukemia	CPT	Downregulated CPT led to death of the leukemic cells	Liu et al. (2016)
Pancreas	Pancreatic cancer	CPT1C	Downregulated CPT1C inducted tumor senescence	Guan et al. (2019)
	Pancreatic ductal adenocarcinoma	CPT1A	Strengthened the antitumor immunity of CpG-treated macrophages	Liu et al. (2019)
Skin	Melanoma	CPT1A	Inhibited CPT1A led to apoptosis in MAPKi-treated cells	Aloia et al. (2019)
			Increased the tumor-mediated immune tolerance	Zhao et al. (2018)
Muscle	Muscle dysfunction	CPT2	A conceptual overview on CPT2 deficiency	Joshi and Zierz (2020)
Nervous	Neuronal dysfunction	CPT1C	Played alternative role in neuronal oxidative metabolism	Lee and Wolfgang (2012)
Gastric	Gastric Cancer	CPT1C	Associated with poor prognosis; promoted proliferation of cancer cells	Chen et al. (2020)

Abbreviation: CPT, carnitine palmitoyltransferase; NAFLD, nonalcoholic fatty liver disease; HCC, hepatocellular carcinoma; JAK2/STAT3, Janus kinase 2/signal transducer and activator of transcription 3; EndoMT, endothelial-to-mesenchymal transition; SMC, smooth muscle cell; CS, cigarette smoke; ALI, acute lung injury; EC, endothelium cells; IR, ischemia–reperfusion; FA, fatty acid; CAC, colitis-associated-cancer; CAFs, cancer-associated fibroblasts; NLRP3, nucleotide-binding oligomerization domain-like receptor protein 3; AML, acute myeloid leukemia; and MAPKi, mitogen-activated protein kinase inhibitors.

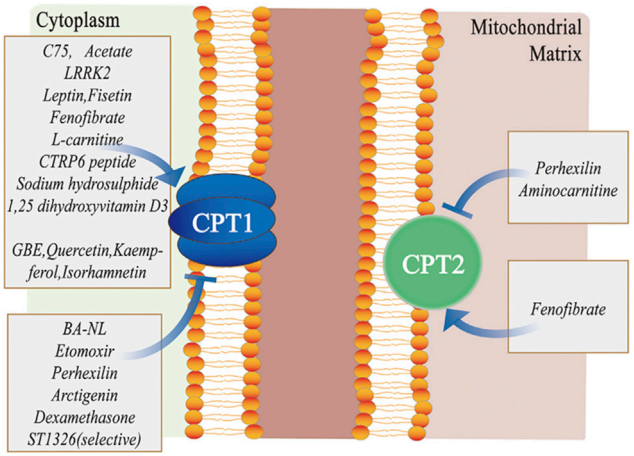

FIGURE 3 | Different pharmacological modulators targeting the CPT system. C75, acetate, LRRK2, leptin, fisetin, fenofibrate, L-carnitine, CTRP6 peptide, sodium hydrosulphide, 1, 25-dihydroxyvitamin D3, GBE, quercetin, kaempferol, and isorhamnetin primarily activate CPT1, whereas BA-NL, etomoxir, perhexilin, dexamethasone and ST1326 mainly inhibit CPT1. Similarly, fenofibrate activates CPT2, while perhexilin and aminocarnitine inhibit CPT2. Abbreviations: LRRK2, leucine-rich repeat kinase 2; CTRP6, C1q/tumor necrosis factor–related protein 6; GBE, ginkgo biloba extract; CPT, carnitine palmitoyltransferase; and BA-NLs, betulinic acid–loaded nanoliposomes.

for CPT1 and can increase its gene and protein expression, thus promoting FAO (Karlic et al., 2002; Xi et al., 2008). Gong et al. (2019) have reported that L-carnitine promotes CPT1A gene expression in lung EpiCs, which in turn imparts a protective effect on CS-induced cellular apoptosis. Furthermore, L-carnitine preserves FAO after CS challenge in lung EpiC, thus preventing lung injury and subsequent emphysema (Petrache et al., 2005; García-Lucio et al., 2018). In an animal emphysema model induced by elastase, L-carnitine also exhibited a significant protective effect (Conlon et al., 2016). In a clinical study, Borghi-Silva et al. (2006) recruited moderate-to-severe COPD patients and conducted oral L-carnitine supplementation for 6 weeks, which showed improved exercise tolerance and inspiratory muscle strength. The exact influence of the CPT system to COPD development and the specific mechanism require further investigation.

3.1.2 Acute Lung Injury

ALI and its severe form, acute respiratory distress syndrome (ARDS), are common respiratory critical syndromes with no effective therapeutic intervention. They are triggered by a variety of direct or indirect pulmonary insults, and their complex pathophysiology is yet to be fully understood. One group of researchers showed that profound impairment in cellular oxygen consumption is one of the pathological hallmarks in the lungs of patients with the pathogen-induced ALI. In the murine model of lipopolysaccharide (LPS)–induced ALI, severely impaired FAO in alveolar EpiCs participated in the inflammatory response and lung injury, which might be attributed to the decreased expression of key mediators involved in FAO, such as CPT1A, and could partly be counteracted by treatment with a PPARα agonist, fenofibrate (Cui et al., 2019). Hyperoxia or positive pressure ventilation induces sustained lung injury in neonates, which is likely due to metabolic dysregulation in pulmonary endothelial cells (ECs). In a hyperoxia-exposed newborn murine model, pharmaceutical inhibition using etomoxir or genetic deletion of *CPT1A* aggravated EC apoptosis and lung injury, while treatment with L-carnitine attenuated the pathological changes (Yao et al., 2019). Elevated age is a risk factor for the poor outcomes of ALI/ARDS. Using an LPS-triggered ALI model in adult and aged mice, Gibbs et al. (2021) assessed age-related alterations in lung inflammation, muscle injury, and metabolism. They observed that etomoxir administration resulted in an increase in the mortality of aged but not adult ALI mice, thereby confirming that the CPT system is essential for survival from severe lung injury and indicating that adult mice have improved resilience to FAO inhibition. Furthermore, CPT1B in the skeletal muscles of aged ALI mice showed a distinct phenotype with its upregulated expression and decreased activity relative to adults, suggesting its correlation to the adverse age-related outcomes of ALI/ARDS.

3.1.3 Bronchial Asthma

As another common chronic respiratory disease, the pathophysiology of bronchial asthma (or asthma) is orchestrated by various inflammatory cells and mediators in close communication with airway structural cells, including EpiCs and smooth muscle cells (SMCs). Increasing evidence has linked energy metabolism to the differentiation, function, and longevity of these inflammatory and structural cells. In allergen-induced murine models, Al-Khami et al. (2017) reported a significant increase in CPT1 expression in the bronchial epithelium and infiltrated inflammatory immune cells of asthma mice. Furthermore, the pharmacologic inhibition of CPT1 by etomoxir decreased airway hyperresponsiveness, inflammatory cell infiltration, and cytokine production associated with the disease. Similarly, Esteves et al. (2021) found a metabolic switch toward mitochondrial β-oxidation with an increased rate of mitochondrial respiration and a higher level of CPT2 in asthmatic bronchial SMC, whereas blocking CPT2 by either etomoxir or perhexiline drastically reduced the proliferation of asthmatic bronchial SMCs and remodeling in bronchial smooth muscles.

3.1.4 Chronic Granulomatous Disease

CGD is a primary immunodeficiency syndrome that is characterized by defects in respiratory burst of phagocytes, leading to serious and life-threatening infections (Squire et al., 2020). Studies have suggested that disrupted lipid metabolism and suppressed mitochondrial FAO contribute to the pathophysiology of granulomatous lung disease (Huizar et al., 2013; Soliman et al., 2020). In a murine model of pulmonary granulomatous inflammation, PPARγ expression and activity in alveolar macrophage were significantly reduced 60 days after multi-walled carbon nanotube (MWCNT) exposure. In macrophage-specific PPARγ knock-out mice, granuloma

TABLE 2 | The development status of CPT inhibitors/activators.

Drugs	Utility	Preclinical/ Clinical Study	Model	Dose	References
Etomoxir	CPT1 inhibitor	Preclinical	Murine model	50 mg/kg	Al-Khami et al. (2017)
		Preclinical	HUVECs, H460 cell line	40 μM	Wang et al. (2019)
		Preclinical	16HBE cell line	50 μM	Jiang et al. (2017)
		Preclinical	Patients' CAFs	50 μM	Peng et al. (2021)
		Preclinical	Murine model, HKC8 cell line	30 mg/kg in mice, 40 μM in cells	Kang et al. (2015)
		Preclinical	Human primary BSM cells	10 nM	Esteves et al. (2021)
		Preclinical	Murine model	5 mg/kg	Wang W. et al. (2020)
		Preclinical	MLE-12, HEK-293T cell line	100 μM	Cui et al. (2019)
		Preclinical	Murine model, human primary HUVEC and EC, mice primary EC	30 mg/kg in mice, 100 μM in cells	Kalucka et al. (2018)
		Preclinical	Mice primary BMDMs	200 μM	Liu et al. (2019)
		Preclinical	Murine model, THP-1 cell line	2 mg/kg in mice, 10 μM in cells	Qiao et al. (2020)
		Preclinical	Murine model, mice primary DCs	25 mg/kg/day in mice, 100 μM in cells	Zhao et al. (2018)
Perhexilin	CPT1 and 2 inhibitor	Preclinical	Human primary BSM cells	10 nM	Esteves et al. (2021)
		Preclinical	Murine model, human primary CLL cells	8 mg/kg in mice, 5–10 μM in cells	Liu et al. (2016)
		Preclinical	Murine model	8 mg/kg	Brown et al. (2018)
ST1326	CPT1A selective inhibitor	Preclinical	Primary AML cells, AML cell line	6 μM or 10 μM	Mao et al. (2021)
Dexamethasone	CPT1A inhibitor	Preclinical	Murine model, LLC cells	50 mg/kg in mice, 1 μM in cells	Xu et al. (2020)
Betulinic acid–loaded nanoliposomes	CPT1A inhibitor	Preclinical	HCT116 cell line	50, 100, or 200 μM	Wang G. et al. (2020)
Arctigenin	CPT1A inhibitor	Preclinical	Murine model, THP-1 cell line, mice primary BMDMs	25, 50 mg/kg in mice; 3, 10, and 30 μM in cells	Qiao et al. (2020)
L-carnitine	CPT activator	Clinical	Patients	1 g/day	Nemati et al. (2019)
				12 g one dose	Evans et al. (2019)
				750 mg/day	Malek et al. (2016)
				1,000 mg/d	Lee et al. (2015)
				12 g one dose	Puskarich et al. (2015)
				20 mg/kg	Savica et al. (2005)
				2 g/day	Borghi-Silva et al. (2006)
Fenofibrate	CPT1B and CPT2 activator	Preclinical	Murine model	200 mg/kg	Zhao et al. (2017)
	CPT1A activator	Preclinical	Murine model	100 mg/kg	Cui et al. (2019)
C75	CPT1 activator	Preclinical	Rat model	3 mg/kg	Idrovo et al. (2012)
		Preclinical	Murine model	15 mg/kg	Kang et al. (2015)
1,25 dihydroxyvitamin D3	CPT1 activator	Preclinical	Rat model	150 ng/kg	Lee et al. (2014)
Sodium hydrosulphide	CPT1 activator	Preclinical	HL-1 cell line	100 μM	Lee et al. (2019)
Fisetin	Increased CPT1, but not CPT2	Preclinical	Murine model, FL83B cell line	20 mg/kg in mice, 3–100 μM in cells	Liou et al. (2018)
Ginkgo biloba extract, quercetin kaempferol, and isorhamnetin	Up-regulate CPT1A	Preclinical	HepG2 cell line	200 μg/ml GBE, 20 μg/ml quercetin, 20 μg/ml kaempferol, or 8 μg/ml isorhamnetin	Wei et al. (2014)
Acetate	CPT1A activator	Preclinical	Murine model, human primary HUVEC and EC, mice primary EC	0.5 M in mice, 500 μM in cells	Kalucka et al. (2018)
CTRP6 peptide	CPT1A activator	Preclinical	HK-2 cell line	2 μg/ml	Xie et al. (2021)

(Continued on following page)

TABLE 2 | (*Continued*) The development status of CPT inhibitors/activators.

Drugs	Utility	Preclinical/ Clinical Study	Model	Dose	References
Leucine-rich repeat kinase 2	CPT1A activator	Preclinical	HepG2 cell line	200 or 400 μM	Lin et al. (2020)
Leptin	CPT1 activator	Preclinical	Murine model	5 mg/kg	Wang W. et al. (2020)

Abbreviation: CPT, carnitine palmitoyltransferase; HUVECs, human umbilical vein endothelial cells; CAFs, cancer-associated fibroblasts; BSM, bronchial smooth muscle; EC, endothelium cells; BMDMs, bone marrow–derived macrophages; DCs, dendritic cells; CLL, chronic lymphocytic leukemia; AML, acute myeloid leukemia; LLC, Lewis lung carcinoma; and CTRP6, C1q/ tumour necrosis factor–related protein 6.

formation was much more extensive than in the wild-type after MWCNT challenge (Soliman et al., 2020). With enhanced mitochondrial FAO and CPT expression mediated by PPARγ activation, Soliman et al. discovered that MWCNT instillation reduced the mRNA expression of CPT1, CPT2, and PPARγ coactivator 1 alpha in permeabilized bronchoalveolar lavage cells, accompanied by elevated oxidative stress in alveolar macrophages and inflammatory injury of murine lung tissues (Huizar et al., 2013).

According to the current evidence, CPT activation can exert either a beneficial or harmful effect during the development of pulmonary diseases. For example, CS exposure could either elevate or decrease FAO and CPT expression of EpiCs in distinct COPD models. This may be explained by the changing metabolic state of injured cells or organs during the pathological process of disease. Inhibition of CPT-dependent FAO impairs the energy metabolism of cells; meanwhile, the continuous activation of the CPT system may also contribute to mitochondrial dysfunction and excess ROS production, which further aggravate cellular damage. Accordingly, it is necessary to identify the basic metabolic profile of certain cells and the pathophysiological condition of the diseases before conducting the experiment.

3.2 Liver Diseases

Mitochondrial FAO is the primary pathway for FA metabolism and performs a key role for energy homeostasis in the liver (Li and Davie, 2010; Singh et al., 2012). Abnormal FAO and CPT1A expression have been shown to participate in the development of NAFLD and hepatic IR injury (Wei et al., 2014). The expression of FAO-relevant genes, including *CPT1B* and *CPT2*, decreased in an intrahepatic cholestasis model. They could partly be counteracted by pretreatment with a PPARα agonist, fenofibrate, which also conferred protection against the cholestatic liver injury (Zhao et al., 2017). In addition, a direct and specific increase of CPT1A in HepG2 cells plays a crucial role in the lipid-lowering and anti-inflammatory effects exerted by Ginkgo biloba extract, quercetin, kaempferol, and isorhamnetin (Wei et al., 2014).

3.2.1 Nonalcoholic Fatty Liver Disease

As a common nexus of a metabolic and hepatic disease, NAFLD is a clinical syndrome that involves lesions in the hepatic lobule, hepatic steatosis, and fat piling pathological features, despite no history of excessive alcohol consumption (Dludla et al., 2020; Ni et al., 2020). Insulin resistance and impaired adipose tissue function are instrumental in promoting hepatic lipid accumulation with metabolic syndrome. In fact, enhanced lipid accumulation, abnormal inflammatory response, and oxidative stress underpinned the development, severity, and the progression of NAFLD (Dludla et al., 2020). Hepatic mitochondrial dysfunction is commonly found in patients with nonalcoholic steatohepatitis. Dysfunction of hepatic mitochondria, altered expression of genes associated with lipid metabolism, and changes in triglycerides, cholesterol, and acyl-carnitines were observed in mice, indicating an impaired mitochondrial carnitine shuttle (Schröder et al., 2016). Using either a Western-style diet or a methionine- and choline-deficient diet, mice with mitochondrial dysfunction developed severe steatohepatitis, which is characterized by lipid accumulation, immune cell infiltration, and hepatocyte ballooning (Schröder et al., 2016).

Since the establishment of the importance of lipid homeostasis and mitochondrial function in NAFLD, much effort has been made to develop therapeutic agents that target the process. One study showed that leucine-rich repeat kinase 2 (LRRK2) participates in the regulation of FAO, and its deficiency might promote inflammation in a palmitic acid-induced NAFLD mouse model. Furthermore, CPT1A, the critical enzyme of FAO, is positively modulated by LRRK2 via the activation of AMP-activated protein kinase (AMPK) and PPARα (Lin et al., 2020). In another study, Liou et al. (2018) reported that fisetin, a naturally abundant flavonoid isolated from various vegetables and fruits, could alleviate hepatic lipid metabolism and improve NAFLD in mice via the activation of the FAO pathway. Recently, Hwangbo et al. (2020) showed that auranofin might have potential as a candidate for improving NAFLD symptoms. Auranofin significantly suppressed lipid peroxidation, inflammatory activity, and hepatic steatosis of liver tissues in NAFLD mice induced by a high-fat diet, which attributed to the decreased expression of NADPH oxidase 4 and PPARγ. Therefore, we hypothesize that regulating mitochondrial FAO and maintaining lipid homeostasis may alleviate NAFLD.

3.2.2 Hepatic Ischemia–Reperfusion Injury

Hepatic IR injury is a severe clinical issue that could lead to poor outcomes; furthermore, no effective therapies have been established (Wang W. et al., 2020; Ibrahim et al., 2021). The

paradigm of hepatic IR follows two apparently separate phases, namely, the ischemic and reperfusion phases. The ischemic phase induces cellular metabolic disturbance due to glycogen consumption, ATP depletion, and lack of oxygen supply, whereas the reperfusion phase results in metabolic disturbance and an unusual immune-inflammatory response that involves both direct and indirect cytotoxic mechanisms (Zhai et al., 2013). Zhang et al. (2018) showed that the pathophysiology of hepatic IR injury is primarily marked by lipid metabolic reprogramming, which results in a secondary effect of inflammation, thereby highlighting the role of lipid metabolism in disease pathogenesis.

In view of the present research, FA metabolism has been attracting considerable interest in hepatic IR injury (Hwangbo et al., 2020), and the role of FAO in the disease is an important research topic (Wang et al., 2020). Luo et al. (2021) reported that CPT1A deficiency mitigated inflammation and oxidative stress in carbon tetrachloride-induced liver injury of mice. They also showed that CPT1A overexpression suppressed the nuclear factor erythroid-2-related factor 2/heme oxygenase-1 and nucleotide-binding oligomerization domain-like receptor protein 3 inflammasome signaling pathways. In a classic IR model with the mice exposed to *in situ* ischemia for 1 h and reperfusion for 6 h, Wang et al. (2020) found that mild hypothermia effectively attenuated hepatic IR injury, which might be attributable to the preservation of mitochondrial FAO and CPT1A expression via the Janus kinase 2/signal transducer and the activator of transcription 3 signaling. In addition, pharmacological interventions of FAO had obvious effects on IR injury, i.e., the activation of CPT1-dependent FAO by leptin significantly attenuated IR-induced injury, which is manifested by reduced hepatic enzyme level, hepatic injury score, hepatocyte apoptosis, and mitochondrial damage, while the inhibition of CPT1 by etomoxir imparted negative effects.

As an essential metabolic and digestive organ, the effect of the CPT system on hepatic disorders is comparatively definite. CPT deficiency and FAO downregulation induce lipid metabolic reprogramming, which leads to a secondary effect on inflammation in diseases. Thus, therapeutic manipulation targeting CPT system to maintain lipid homeostasis may be of great significance to treat multiple liver disorders.

3.3 Kidney Diseases

Kidneys are organs associated with high energy consumption, and they generate large amounts of ATP via FAO. The strongest mitochondrial FAO activity has been observed in the proximal and distal convoluted tubules (Wirthensohn and Guder, 1986). Tubular EpiCs have been confirmed to primarily rely on FAO as their energy source, whereas elevated CPT and FAO aggravated mitochondrial ROS accumulation and cell injury in diabetic nephropathy (Rosca et al., 2012). In human and murine models, reduced FAO contributed to the pathophysiology of kidney fibrosis (Kang et al., 2015). In addition, during the development of AKI, damage to the proximal tubule and medullary thick ascending limb resulted in reduced PPARα expression, which subsequently led to the diminished expression and activity of mitochondrial FAO enzymes, represented by the CPT system.

3.3.1 Kidney Fibrosis

Kidney fibrosis is the major pathological process and common end point of the progression of chronic kidney disease, which eventually leads to end-stage renal disease (Zeisberg and Neilson, 2010). In addition to proper blood pressure and glycemic control, therapeutic options to deter or revert the development of fibrosis are quite limited. In recent years, studies have focused on the metabolic disturbances coexisting with renal fibrosis. Among these, FAO reduction became critical for energy failure in the tubulointerstitial compartment, thus leading to inflammatory cell infiltration and tissue fibrosis (Kang et al., 2015; Chung et al., 2019). In the unilateral ureteral obstruction and transforming growth factor (TGF)-β1–induced kidney fibrosis models, the defective FAO and decreased CPT1A expression occurred during the progression of the disease. C1q/tumor necrosis factor (TNF)–related protein 6 (CTRP6) is a recently identified adiponectin analog, and it has been downregulated in an animal model of kidney fibrosis. The use of human CTRP6 peptide could inhibit extracellular matrix deposition and promote FAO by upregulating CPT1A (Xie et al., 2021). Concerning the critical role of CPT1A in FAO, one study treated tubular EpiCs with the CPT1 inhibitor etomoxir, and the upregulated expression of genes related to fibrosis such as *α-smooth muscle actin* and *vimentin* was observed (Kang et al., 2015). Conversely, a synthetic CPT1 activator, C75, significantly reduced the symptom of kidney fibrosis in an FA-induced murine model (Kang et al., 2015). In addition, Verónica et al. constructed a conditional transgenic mouse model with CPT1A overexpression in tubular EpiCs that was subjected to three models of renal fibrosis. The mice exhibited reduced fibrotic markers expression, attenuated proinflammatory response, and alleviated EpiC damage, which might be mediated by restoring mitochondrial homeostasis (Miguel et al., 2021).

3.3.2 Acute Kidney Injury

Lipid accumulation is related to various kinds of AKI or ischemic renal injury (IRI); however, its underlying causative factors and pathways remain unclear (Scantlebery et al., 2021). Indeed, following the onset of ischemia, the accumulation of cholesterol and triglycerides was apparently protective due to the buffer effect against FA; however, excess lipids during the progression of ischemia, displayed as droplets, could cause renal injury (Erpicum et al., 2018). In an IRI model, Scantlebery et al. (2021) identified a significant accumulation of cholesterol, specific phospholipids, and sphingolipids in the kidneys. Meanwhile, *in silico* analysis revealed that several energy and lipid metabolism pathways, including mitochondrial FAO, were downregulated 24 h after IRI, which could contribute to lipid accumulation. Furthermore, the decrease in CPT1 activity during renal IRI has also been observed, and this led to a reduced FA uptake and defective mitochondrial FAO. Idrovo et al. (2012) subjected rats to renal IRI by bilateral renal pedicle clamping with microvascular clips for 60 min, followed by administration of CPT1 agonist, C75, or vehicle, and they found that C75 recovered

FAO, improved renal function, and attenuated tissue injury in the animal model. Beside IRI, infection is another important etiological factor for AKI. Both metabolic and inflammatory complications have been observed during sepsis or endotoxemia; however, the molecular mechanism responsible for these LPS-modulated metabolic changes remains elusive. In a murine sepsis model, LPS has been shown to suppress FAO by inhibiting the expression of associated genes, including *CPT1*, in kidney and liver tissues. This mechanism might rely on interleukin-1 receptor–associated kinase 1, which is one of the key Toll-like receptor (TLR) 4 intracellular signaling kinases (Maitra et al., 2009).

Existing studies have shown that mitochondrial dysfunction is observed in various nephropathies. Besides, the repairment of damaged renal cells largely depends on the ability of the mitochondria to restore ATP production. Accordingly, the preservation of CPT and FAO may attenuate or reverse renal failure, thus becoming a promising therapeutic target for the kidney diseases.

3.4 Cardiovascular Disorders

FAO serves a pivotal role in myocardial fuel selection, which is a key feature of the function and health of the heart. Recent studies have revealed that abnormal CPT expression or activity and impaired FAO could also contribute to the pathogenesis of multiple cardiovascular disorders.

3.4.1 Cardiac Dysfunction

Energy metabolism suppression is one of the cornerstones of cardiac dysfunction in sepsis/endotoxemia. Systemic inflammatory responses, as well as superoxide, nitric oxide, and peroxynitrite could impair cardiac CPT1 activity *in vivo* and *in vitro*, thus leading to myocardial dysfunction (Eaton et al., 2003). In an LPS-induced rat model of neonatal sepsis, CPT1 activity was significantly decreased in the heart compared to other organs (Fukumoto et al., 2002). Similarly, in another experimental model of murine endotoxemia, excess inflammation markedly reduced cardiac FAO and mechanical function. In addition, aminocarnitine, a CPT2 specific inhibitor, resulted in the accumulation of FAO intermediates in the heart, which further exacerbated inflammatory cardiac dysfunction. By contrast, the activation of CPT1 by C75 could restore both cardiac and mitochondrial FAO without any effects on inflammatory gene expression or cardiac function. The results indicated that impaired CPT-dependent FAO was detrimental to cardiac injury during endotoxemia, but CPT/FAO restoration alone was not sufficient to recover cardiac function (Makrecka-Kuka et al., 2020).

Cardiovascular disease is considered as one of the main causes of mortality for diabetic patients (Stamler et al., 1993). Compared to nondiabetic patients, myocardial dysfunction incidence was much higher in patients with diabetes, which was due to cardiac metabolic disturbance characterized by high FFA and reduced glucose utilization (Herlitz et al., 1988). In an animal model, diabetic rats had higher body weight, larger left ventricular end-diastolic diameter, and longer QT interval, along with increased proinflammatory cytokines and CPT1 expression in the heart than healthy rats. Nevertheless, treatment with 1,25-dihydroxyvitamin D3 dramatically ameliorated cardiac function, inflammatory response, and CPT1-mediated FA metabolism in diabetic hearts (Lee et al., 2014). TNFα is an adipose-derived proinflammatory cytokine that induces myocardial contractile dysfunction of the cardiomyocytes. In TNFα-stimulated mouse cardiac muscle cells, sodium hydrosulfide ameliorated the impaired mitochondrial respiration and ATP production/synthesis, and attenuated excess oxidative stress, which might be due to the enhanced expression of metabolic indices such as CPT1. The study indicated the therapeutic potential of sodium hydrosulfide for inflammation-associated cardiac dysfunctions (Lee et al., 2019).

3.4.2 Endothelial Dysfunction

Most ECs in a healthy person are quiescent, and they maintain barrier function and vasoregulation, and counteract thrombosis and vascular inflammation. EC metabolism has emerged as a novel and promising therapeutic target to block vascular dysregulation associated with various diseases. Glycolysis and FAO are key regulators of EC metabolism, which further influences their function and behavior (Draoui et al., 2017). ROS overproduction in EC plays a critical role in endothelial dysfunction, whereas mitochondrial ROS (mtROS) is essential to the pathogenesis of diabetic vascular complications. In bovine aortic ECs, Kajihara et al. (2017) found that during hypoglycemia, the activation of FAO followed by mtROS generation and vascular cell adhesion molecule-1 expression could induce endothelial dysfunction. Yet, these effects could be suppressed by treatment with the CPT inhibitor etomoxir. Using CPT1A-silenced ECs in the LPS model, Kalucka et al. (2018) demonstrated that the endothelial loss of FAO-controlling CPT1A promoted leukocyte infiltration and barrier disruption by elevating endothelial oxidative stress. More importantly, the supplementation of acetate could counter ROS-mediated EC dysfunction in CPT1A-deficient mice, providing therapeutic opportunities in related disorders. As one of the stimulators for the CPT system, the PPAR family is also present in the endothelium. PPARα regulated lipid metabolism and inhibited inflammatory response in vascular ECs. In the skeletal muscle and heart, PPARα has been shown to increase the mitochondrial FFA uptake and subsequent FAO through the activation of CPT1 (Fruchart et al., 1999).

In healthy adults, blood vessels are lined with a single monolayer of quiescent ECs that remains in this state for years (Eelen et al., 2018). However, upon ischemia or inflammatory injury, quiescent ECs immediately switch to a proliferative/angiogenic state to achieve tissue homeostasis (Kalucka et al., 2018). Draoui et al. (2017) found that CPT1 and FAO-upregulated proliferation in ECs played an essential role in lymphangiogenesis by promoting DNA synthesis. Meanwhile, CPT1 inhibition in blood vessels has also been shown to have potential therapeutic benefits by blocking pathological angiogenesis. Endothelial FAO is also a critical regulator of endothelial-to-mesenchymal transition (EndoMT), which is a cellular process required for normal heart valve development and is often initiated by the TGF-β family of

ligands. However, deregulated EndoMT is associated with a wide range of disorders. Xiong et al. (2018) constructed a conditional mouse model of endothelial CPT2 deletion, and they demonstrated that the disrupted FAO augmented the magnitude of embryonic EndoMT, leading to the thickening of cardiac valves and elevated permeability of multiple vascular beds in adult mice. Soon after that, Shimizu et al. (2020) concentrated on how the TGF-β downstream pathway modulated CPT2 expression. They discovered that the protein kinase R-like endoplasmic reticulum kinase signaling was demanded for cardiac valve formation via CPT2-dependent FAO and EndoMT. Taken together, the results implicated that endothelial CPT and FAO were critical to maintain EC fate, and the therapeutic manipulation targeting EC metabolism might offer the basis for treating various EndoMT-linked disorders.

For the cardiovascular system, enormous quantities of energy are required to maintain the metabolism and physiological function. Current studies implicate the correlation between lipid metabolism reprogramming and cardiovascular disorders and provide evidence that the mitochondrial CPT system is essential for normal cardiac and EC function. Further research is needed to confirm the findings and to develop new effective drugs targeting CPT.

3.5 Cancers

Currently, metabolic rewiring, which supports unrestricted proliferation and metastatic progression of cancer cells, is widely accepted to be an emerging hallmark of cancers (Petővári et al., 2020). As the pivotal energy source and fundamental cellular components in tumor cells, FA is also involved in lipid-dependent metabolic reprogramming. A growing number of studies have pointed out that FAO and CPT are the key regulatory mechanisms underlying the survival, growth, and drug resistance of cancer cells, placing CPT as an emerging target for cancer therapeutics.

3.5.1 Experimental and Preclinical Studies

In the tumor microenvironment, adipocytes served as a metabolic regulator and an energy provider to promote the survival and growth of several cancer cells. One research group reported that adipocytes supplied FA for rapid tumor growth, suggesting a significant role for lipid metabolism in the treatment of cancers (Nieman et al., 2011). Similarly, Wen et al. (2017) isolated adipocytes from tumor tissues of colon cancer patients and found a transfer of FFA from the adipocytes to the cancer cells. Through the absorption of FA, colon cancer cells are resilient to nutrient deprivation conditions as these are capable of upregulating mitochondrial FAO. In addition to colon cancer, Nieman et al. (2011) arrived at a similar conclusion in ovarian cancer. Although studies have confirmed the transfer of FAs from adipocytes to cancer cells, its underlying molecular mechanism remains unclear. In colon cancer patients, abundant adipocytes were correlated with the presence of invasive tumor cells. Xiong et al. (2020) demonstrated that CPT1A is upregulated in colon cancer cells after exposure to adipocytes or FA. Furthermore, three-dimensional culture studies showed that CPT1A is upregulated in tumor cells within adipose tissues compared to that not in direct contact with adipocytes, whereas CPT1A silencing reduces tumor organoid formation and downregulates genes associated with cancer stem cells. In addition, CPT1A-dependent FAO might be a key metabolic pathway that associates adipocytes to colon cancer cells.

Immune cell metabolism in the tumor microenvironment is also important to antitumor immune responses. Macrophages enhance the immunity by phagocyting and killing tumor cells. However, the specific mechanisms have been poorly understood. CpG oligonucleotide, a TLR9 agonist, enhanced the antitumor potential of macrophages by increasing FAO and shunting of acetyl-CoA toward lipid substances synthesis, which needed the involvement of CPT1A and ATP citrate lyase (Liu et al., 2019). Chronic inflammation was considered to participate in the occurrence and development of colon cancer. Arctigenin, the major active constituent of *Fructus arctii*, has been reported to alleviate colitis and protect against colon carcinogenesis in mice models. Mechanistically, Arctigenin downregulated CPT1-mediated FAO, which further inhibited nucleotide-binding oligomerization domain-like receptor protein 3 inflammasome assemblies in macrophages (Qiao et al., 2020). During the development of NAFLD-promoted hepatocellular carcinoma, intrahepatic $CD4^+$ T cells are crucial for antitumor surveillance. In the lipid-rich liver environment, elevated CPT expression and FAO might increase mitochondrial ROS and lead to cell death of $CD4^+$ T cells, thus promoting tumor formation in a murine model, which could be blocked by the CPT inhibitor perhexiline (Brown et al., 2018). Latest evidence has shown a correlation between the toleration of local dendritic cell (DC) in the tumor microenvironment and immune evasion. Zhao et al. (2018) reported a site of immune privilege established by melanomas that drove FAO in DCs via elevating the expression of CPT1A. This FAO shift increased the activity of immunosuppressive enzymes and promoted the generation of regulatory T cells, leading to tumor-mediated immune tolerance. These findings implicate a role for the metabolic reprogramming of local immune cells in the antitumor therapy.

Except for the effects of FA from adipocytes and immune cells, FAO alterations in tumor cells themselves also affect their proliferation and migration. Xu et al. (2020) showed that a high-dose dexamethasone-inhibited tumor progression was associated with the downregulation of FAO genes, including *CPT1A*. It could be decreased by the uptake and consumption of lipids and glucose in cancer cells, thus indicating the orchestration of microenvironmental inherent metabolic pathways related to FAO. Wang et al. (2020) prepared betulinic acid–loaded nanoliposomes and evaluated their anticancer effects on colorectal cancer cell lines. This nanodrug significantly suppressed cell proliferation via modulating potential FA metabolism targets and pathways, such as the CPT system, which might be an effective therapy adjuvant in colorectal cancer. In addition, CPT1 and CPT2 are highly expressed in chronic lymphoblastic leukemia cells (Gugiatti et al., 2018), while the inhibition of CPT by perhexiline led to a decreased FA transport, damaged mitochondrial integrity, and the death of leukemic cells (Liu et al., 2016). Tumor growth is an angiogenesis-dependent process

that requires continuous neovascularization. Wang et al. (2019) demonstrated that interleukin-17 promoted tumor growth of human lung cancer cells *in vivo* and *in vitro*, as well as stimulated angiogenesis by enhancing FAO and the mitochondrial respiration of ECs, which could be blocked by using the CPT inhibitor etomoxir. Furthermore, CPT1A knockdown in breast cancer cells disrupts invasion and lymphangiogenesis of human dermal lymphatic ECs (HDLECs). In addition, CPT1A-null HDLECs showed compromised invasion and lymphangiogenesis relative to the negative control (Xiong Y. et al., 2018).

3.5.2 Clinical Studies

Based on the above information, the CPT system becomes a potential target for the diagnosis and treatment of various cancers, which draws the attention of researchers and clinicians. Tan et al. (2021) collected serum from breast cancer patients, patients with benign breast disease, and healthy controls to estimate the accuracy of CPT1A as a marker in the diagnosis of breast cancer. The results showed that CPT1A levels were higher in patients than in controls, and they were dramatically associated with TNM stage, histological grading, and metastasis. This study suggested a remarkably high diagnostic efficiency of CPT1A that could serve as an indicator for breast cancer monitoring. Malignant melanoma pertains to an aggressive skin tumor with poor prognosis, with approximately 50% of patients harboring gain-of-function mutations in the *BRAF* gene. Treatment of $BRAF^{V600E}$-mutant melanomas using mitogen-activated protein kinase inhibitors (MAPKi) induces tumor regression; however, this eventually results in drug resistance. Aloia et al. (2019) analyzed freshly isolated tumor biopsies from metastatic stage IV melanoma patients with paired pretreatment and early-on treatment and found that melanoma cells treated with MAPKi exhibited increased levels of PPARα-mediated and CPT1A-dependent FAO. In addition, the concomitant inhibition of FAO and glycolysis could induce apoptosis in MAPKi-treated melanoma cells, possibly benefitting patients receiving MAPKi therapies. Research on gastric cancer also proved the relationship between the CPT system and the tumor growth–promoting effect. Chen et al. (2020) showed that hypoxia-induced high expression of CPT1C was closely associated with the poor prognosis of patients with gastric cancer and could promote the proliferation of gastric cancer cells, while gene silencing or etomoxir treatment significantly suppressed cell proliferation and caused cell cycle arrest. In addition, studies on colorectal cancer indicated the possibility of regarding FAO inhibition as a novel approach and clinical strategy against the disease. Through experiments in tissue samples of colorectal patients and human colorectal cancer cell lines, Wang et al. (2018) demonstrated that CPT1A-mediated FAO activation induces cancer cells to resist anoikis, which is a specialized form of apoptosis triggered by the loss of adhesion to the extracellular matrix.

The majority of cancer-related deaths have been attributed to highly aggressive metastases. Colorectal patients with peritoneal metastases have been associated with decreased overall survival. Peng et al. (2021) investigated the primary tumor tissues collected from patients with T4Nx colorectal cancer, and they determined that CPT1A was downregulated in patients with peritoneal metastases. Furthermore, cancer-associated fibroblasts (CAFs) promoted the proliferation, invasion, and migration of colon cancer cells by increasing CPT1A expression. Conversely, disrupting FAO in CAFs with the CPT inhibitor etomoxir results in a decrease in tumor growth and intraperitoneal dissemination. Mao et al. (2021) reported CPT1A expression in 325 cytogenetically normal acute myeloid leukemia (AML) patients, except those with solid tumors. The results revealed that AML patients with upregulated CPT1A expression have a relatively short overall survival than those with downregulated expression. CPT1A-selective inhibitor ST1326 in combination with B-cell lymphoma/leukemia-2 inhibitor ABT199 imparted strong synergistic inhibitory effects on AML cells as well as primary patient blasts.

The development of cancer is a complex pathological process involving multiple cells and mediators. The interaction between cells and microenvironment may induce metabolic reprogramming, thus affecting the prognosis. For the contradictory findings from Peng et al., we speculate that the energy provided by CAFs is sufficient to support distant metastasis of the tumors or there exists competition between primary tumor cells and CAFs for FA utilization. Current studies highlight the importance of lipid metabolic state of single cell type for the proliferation and migration of tumor cells. Novel techniques, such as single-cell sequencing, could be applied to further clarify the metabolic shift in each cell types and patterns of cell–cell cross talk in different cancers.

4 CONCLUSION AND PERSPECTIVES

Lipids are important metabolic energy reserves and crucial components of cellular signal transduction pathways. Dysregulated lipid metabolism is involved in various diseases, including acute and chronic inflammatory disorders and cancers. As one of the most important steps of lipid metabolism, FAO and its key rate-limiting enzyme, the CPT system, regulate host immune responses, which is of great clinical significance. The deficiency or overactivation of the CPT system can ultimately lead to the disruption of immune homeostasis, and therefore elevate the risk for various inflammatory diseases and even cancers. Evidence has shown the involvement of the CPT system and related mitochondrial FAO in the development and progression of these disorders. Accordingly, agonists or inhibitors targeting the CPT system have emerged as novel therapies for these diseases. In addition to experimental therapeutic strategies, there have been several clinical trials on CPT modulators. Oral or intravenous administration of L-carnitine could significantly improve the condition of patients with chronic kidney disease (Nemati et al., 2019), septic shock (Puskarich et al., 2015; Evans et al., 2019), knee osteoarthritis (Malek et al., 2016), coronary artery disease (Lee et al., 2015), and maintenance hemodialysis (Savica et al., 2005). However, the efficacy, stability, and safety of the agents, as well as whether they could disturb local or systemic energy metabolism should be considered comprehensively in future clinical uses.

Besides, due to the uncertain role of the CPT system in several diseases, such as COPD and cancers, new techniques should be applied to seek a breakthrough. For example, single-cell sequencing could be used to identify the expression and influence of the CPT system within each cell type and CRISPR-CAS9 gene editing could be utilized to modify CPT expression in specific cells, thus providing more precise tools to explore its cell-specific role. Furthermore, given the fact that danger signals often change multiple times in lipid metabolism, developing more potent activators/inhibitors that target multiple FAO signaling pathways, including the CPT system or combined with other anti-inflammatory/antitumor therapeutics, may facilitate translation of this promising strategy into clinical application.

AUTHOR CONTRIBUTIONS

WG and QL conceived and designed the scope of the review. MW, KW, XL, and HH collected the literature and wrote the manuscript. WG, LC, and LM critically revised this review. All of the authors read and approved the final manuscript, and they agreed to be responsible for the integrity and accuracy of all parts of the manuscript.

FUNDING

This work was supported by the National Natural Science Foundation of China (grant number: 82000086), the Shanghai Sailing Program (grant number: 20YF1440300) for WG, the National Natural Science Foundation of China (grant number: 81870064, 82070086) for QL, and the Shanghai Jiao Tong University Medical & Engineering Cross Fund (grant number: YG2019QNA65) for HH.

ACKNOWLEDGMENTS

We thank Biorender for providing fundamental materials of our scheme figures. We thank LetPub (www.letpub.com) for its linguistic assistance during the preparation of this manuscript.

REFERENCES

Agarwal, A. R., Yin, F., and Cadenas, E. (2014). Short-Term Cigarette Smoke Exposure Leads to Metabolic Alterations in Lung Alveolar Cells. *Am. J. Respir. Cel Mol. Biol.* 51, 284–293. doi:10.1165/rcmb.2013-0523OC

Al-Khami, A. A., Ghonim, M. A., Del Valle, L., Ibba, S. V., Zheng, L., Pyakurel, K., et al. (2017). Fuelling the Mechanisms of Asthma: Increased Fatty Acid Oxidation in Inflammatory Immune Cells May Represent a Novel Therapeutic Target. *Clin. Exp. Allergy* 47, 1170–1184. doi:10.1111/cea.12947

Aloia, A., Müllhaupt, D., Chabbert, C. D., Eberhart, T., Flückiger-Mangual, S., Vukolic, A., et al. (2019). A Fatty Acid Oxidation-Dependent Metabolic Shift Regulates the Adaptation of BRAF-Mutated Melanoma to MAPK Inhibitors. *Clin. Cancer Res.* 25, 6852–6867. doi:10.1158/1078-0432.CCR-19-0253

Bonnefont, J. P., Djouadi, F., Prip-Buus, C., Gobin, S., Munnich, A., and Bastin, J. (2004). Carnitine Palmitoyltransferases 1 and 2: Biochemical, Molecular and Medical Aspects. *Mol. Aspects Med.* 25, 495–520. doi:10.1016/j.mam.2004.06.004

Borghi-Silva, A., Baldissera, V., Sampaio, L. M., Pires-DiLorenzo, V. A., Jamami, M., Demonte, A., et al. (2006). L-carnitine as an Ergogenic Aid for Patients with Chronic Obstructive Pulmonary Disease Submitted to Whole-Body and Respiratory Muscle Training Programs. *Braz. J. Med. Biol. Res.* 39, 465–474. doi:10.1590/s0100-879x2006000400006

Bremer, J. (1963). Carnitine in Intermediary Metabolism. The Biosynthesis of Palmitylcarnitine by Cell Subfractions. *J. Biol. Chem.* 238, 2774–2779. doi:10.1016/s0021-9258(18)67896-2

Britton, C. H., Schultz, R. A., Zhang, B., Esser, V., Foster, D. W., and McGarry, J. D. (1995). Human Liver Mitochondrial Carnitine Palmitoyltransferase I: Characterization of its cDNA and Chromosomal Localization and Partial Analysis of the Gene. *Proc. Natl. Acad. Sci. U S A.* 92, 1984–1988. doi:10.1073/pnas.92.6.1984

Brosnan, J. T., Kopec, B., and Fritz, I. B. (1973). The Localization of Carnitine Palmitoyltransferase on the Inner Membrane of Bovine Liver Mitochondria. *J. Biol. Chem.* 248, 4075–4082. doi:10.1016/s0021-9258(19)43841-6

Brown, N. F., Hill, J. K., Esser, V., Kirkland, J. L., Corkey, B. E., Foster, D. W., et al. (1997). Mouse white Adipocytes and 3T3-L1 Cells Display an Anomalous Pattern of Carnitine Palmitoyltransferase (CPT) I Isoform Expression during Differentiation. Inter-tissue and Inter-species Expression of CPT I and CPT II Enzymes. *Biochem. J.* 327 (Pt 1), 225–231. doi:10.1042/bj3270225

Brown, N. F., Weis, B. C., Husti, J. E., Foster, D. W., and McGarry, J. D. (1995). Mitochondrial Carnitine Palmitoyltransferase I Isoform Switching in the Developing Rat Heart. *J. Biol. Chem.* 270, 8952–8957. doi:10.1074/jbc.270.15.8952

Brown, Z. J., Fu, Q., Ma, C., Kruhlak, M., Zhang, H., Luo, J., et al. (2018). Carnitine Palmitoyltransferase Gene Upregulation by Linoleic Acid Induces CD4+ T Cell Apoptosis Promoting HCC Development. *Cell Death Dis* 9, 620. doi:10.1038/s41419-018-0687-6

Castaño, C., Kalko, S., Novials, A., and Párrizas, M. (2018). Obesity-associated Exosomal miRNAs Modulate Glucose and Lipid Metabolism in Mice. *Proc. Natl. Acad. Sci. U S A.* 115, 12158–12163. doi:10.1073/pnas.1808855115

Chen, H., Li, Z., Dong, L., Wu, Y., Shen, H., and Chen, Z. (2019). Lipid Metabolism in Chronic Obstructive Pulmonary Disease. *Int. J. Chron. Obstruct. Pulmon. Dis.* 14, 1009–1018. doi:10.2147/COPD.S196210

Chen, T., Wu, G., Hu, H., and Wu, C. (2020). Enhanced Fatty Acid Oxidation Mediated by CPT1C Promotes Gastric Cancer Progression. *J. Gastrointest. Oncol.* 11, 695–707. doi:10.21037/jgo-20-157

Chung, K. W., Dhillon, P., Huang, S., Sheng, X., Shrestha, R., Qiu, C., et al. (2019). Mitochondrial Damage and Activation of the STING Pathway Lead to Renal Inflammation and Fibrosis. *Cell Metab.* 30, 784–799.e5. doi:10.1016/j.cmet.2019.08.003

Conlon, T. M., Bartel, J., Ballweg, K., Günter, S., Prehn, C., Krumsiek, J., et al. (2016). Metabolomics Screening Identifies Reduced L-Carnitine to Be Associated with Progressive Emphysema. *Clin. Sci.* 130, 273–287. doi:10.1042/CS20150438

Console, L., Giangregorio, N., Indiveri, C., and Tonazzi, A. (2014). Carnitine/acylcarnitine Translocase and Carnitine Palmitoyltransferase 2 Form a Complex in the Inner Mitochondrial Membrane. *Mol. Cell Biochem.* 394, 307–314. doi:10.1007/s11010-014-2098-z

Cox, K. B., Johnson, K. R., and Wood, P. A. (1998). Chromosomal Locations of the Mouse Fatty Acid Oxidation Genes Cpt1a, Cpt1b, Cpt2, Acadvl, and Metabolically Related Crat Gene. *Mamm. Genome* 9, 608–610. doi:10.1007/s003359900830

Cui, H., Xie, N., Banerjee, S., Ge, J., Guo, S., Liu, G., et al. (2019). Impairment of Fatty Acid Oxidation in Alveolar Epithelial Cells Mediates Acute Lung Injury. *Am. J. Respir. Cel Mol. Biol.* 60, 167–178. doi:10.1165/rcmb.2018-0152OC

Dai, Y., Wolfgang, M. J., Cha, S. H., and Lane, M. D. (2007). Localization and Effect of Ectopic Expression of CPT1c in CNS Feeding Centers. *Biochem. Biophys. Res. Commun.* 359, 469–474. doi:10.1016/j.bbrc.2007.05.161

Demaugre, F., Bonnefont, J. P., Cepanec, C., Scholte, J., Saudubray, J. M., and Leroux, J. P. (1990). Immunoquantitative Analysis of Human Carnitine Palmitoyltransferase I and II Defects. *Pediatr. Res.* 27, 497–500. doi:10.1203/00006450-199005000-00016

Dludla, P. V., Nkambule, B. B., Mazibuko-Mbeje, S. E., Nyambuya, T. M., Marcheggiani, F., Cirilli, I., et al. (2020). N-acetyl Cysteine Targets Hepatic Lipid Accumulation to Curb Oxidative Stress and Inflammation in NAFLD: A Comprehensive Analysis of the Literature. *Antioxidants (Basel)* 9, 1283. doi:10.3390/antiox9121283

Draoui, N., de Zeeuw, P., and Carmeliet, P. (2017). Angiogenesis Revisited from a Metabolic Perspective: Role and Therapeutic Implications of Endothelial Cell Metabolism. *Open Biol.* 7, 170219. doi:10.1098/rsob.170219

Eaton, S., Bartlett, K., and Pourfarzam, M. (1996). Mammalian Mitochondrial Beta-Oxidation. *Biochem. J.* 320 (Pt 2), 345–357. doi:10.1042/bj3200345

Eaton, S., Fukumoto, K., Stefanutti, G., Spitz, L., Zammit, V. A., and Pierro, A. (2003). Myocardial Carnitine Palmitoyltransferase I as a Target for Oxidative Modification in Inflammation and Sepsis. *Biochem. Soc. Trans.* 31, 1133–1136. doi:10.1042/bst0311133

Eelen, G., de Zeeuw, P., Treps, L., Harjes, U., Wong, B. W., and Carmeliet, P. (2018). Endothelial Cell Metabolism. *Physiol. Rev.* 98, 3–58. doi:10.1152/physrev.00001.2017

Erpicum, P., Rowart, P., Defraigne, J. O., Krzesinski, J. M., and Jouret, F. (2018). What We Need to Know about Lipid-Associated Injury in Case of Renal Ischemia-Reperfusion. *Am. J. Physiol. Ren. Physiol.* 315, F1714–F1719. doi:10.1152/ajprenal.00322.2018

Esser, V., Britton, C. H., Weis, B. C., Foster, D. W., and McGarry, J. D. (1993). Cloning, Sequencing, and Expression of a cDNA Encoding Rat Liver Carnitine Palmitoyltransferase I. Direct Evidence that a Single Polypeptide Is Involved in Inhibitor Interaction and Catalytic Function. *J. Biol. Chem.* 268, 5817–5822. doi:10.1016/s0021-9258(18)53392-5

Esser, V., Brown, N. F., Cowan, A. T., Foster, D. W., and McGarry, J. D. (1996). Expression of a cDNA Isolated from Rat Brown Adipose Tissue and Heart Identifies the Product as the Muscle Isoform of Carnitine Palmitoyltransferase I (M-CPT I). M-CPT I Is the Predominant CPT I Isoform Expressed in Both white (Epididymal) and Brown Adipocytes. *J. Biol. Chem.* 271, 6972–6977. doi:10.1074/jbc.271.12.6972

Esteves, P., Blanc, L., Celle, A., Dupin, I., Maurat, E., Amoedo, N., et al. (2021). Crucial Role of Fatty Acid Oxidation in Asthmatic Bronchial Smooth Muscle Remodelling. *Eur. Respir. J.* 8, 2004252. doi:10.1183/13993003.04252-2020

Evans, C. R., Karnovsky, A., Puskarich, M. A., Michailidis, G., Jones, A. E., and Stringer, K. A. (2019). Untargeted Metabolomics Differentiates L-Carnitine Treated Septic Shock 1-Year Survivors and Nonsurvivors. *J. Proteome. Res.* 18, 2004–2011. doi:10.1021/acs.jproteome.8b00774

Franz, K. (1904). Der Abbau aromatischer Fettsäuren im Tierkörper. *Beitr. Chem. Physiol. Pathol.* 6, 150–162.

Fraser, F., Corstorphine, C. G., and Zammit, V. A. (1997). Topology of Carnitine Palmitoyltransferase I in the Mitochondrial Outer Membrane. *Biochem. J.* 323 (Pt 3), 711–718. doi:10.1042/bj3230711

Fritz, I. (1955). The Effect of Muscle Extracts on the Oxidation of Palmitic Acid by Liver Slices and Homogenates. *Acta Physiol. Scand.* 34, 367–385. doi:10.1111/j.1748-1716.1955.tb01256.x

Fritz, I. B., and Yue, K. T. (1963). Long-chain Carnitine Acyltransferase and the Role of Acylcarnitine Derivatives in the Catalytic Increase of Fatty Acid Oxidation Induced by Carnitine. *J. Lipid. Res.* 4, 279–288. doi:10.1016/s0022-2275(20)40302-5

Fruchart, J. C., Duriez, P., and Staels, B. (1999). Peroxisome Proliferator-Activated Receptor-Alpha Activators Regulate Genes Governing Lipoprotein Metabolism, Vascular Inflammation and Atherosclerosis. *Curr. Opin. Lipidol.* 10, 245–257. doi:10.1097/00041433-199906000-00007

Fukumoto, K., Pierro, A., Spitz, L., and Eaton, S. (2002). Differential Effects of Neonatal Endotoxemia on Heart and Kidney Carnitine Palmitoyl Transferase I. *J. Pediatr. Surg.* 37, 723–726. doi:10.1053/jpsu.2002.32263

García-Lucio, J., Peinado, V. I., de Jover, L., Del Pozo, R., Blanco, I., Bonjoch, C., et al. (2018). Imbalance between Endothelial Damage and Repair Capacity in Chronic Obstructive Pulmonary Disease. *PLoS One* 13, e0195724. doi:10.1371/journal.pone.0195724

Gibbs, K. W., Chuang Key, C. C., Belfield, L., Krall, J., Purcell, L., Liu, C., et al. (2021). Aging Influences the Metabolic and Inflammatory Phenotype in an Experimental Mouse Model of Acute Lung Injury. *J. Gerontol. A. Biol. Sci. Med. Sci.* 76, 770–777. doi:10.1093/gerona/glaa248

Gong, J., Zhao, H., Liu, T., Li, L., Cheng, E., Zhi, S., et al. (2019). Cigarette Smoke Reduces Fatty Acid Catabolism, Leading to Apoptosis in Lung Endothelial Cells: Implication for Pathogenesis of COPD. *Front. Pharmacol.* 10, 941. doi:10.3389/fphar.2019.00941

Guan, L., Chen, Y., Wang, Y., Zhang, H., Fan, S., Gao, Y., et al. (2019). Effects of Carnitine Palmitoyltransferases on Cancer Cellular Senescence. *J. Cel Physiol.* 234, 1707–1719. doi:10.1002/jcp.27042

Gugiatti, E., Tenca, C., Ravera, S., Fabbi, M., Ghiotto, F., Mazzarello, A. N., et al. (2018). A Reversible Carnitine Palmitoyltransferase (CPT1) Inhibitor Offsets the Proliferation of Chronic Lymphocytic Leukemia Cells. *Haematologica* 103, e531–e536. doi:10.3324/haematol.2017.175414

Hada, T., Yamamoto, T., Yamamoto, A., Ohkura, K., Yamazaki, N., Takiguchi, Y., et al. (2014). Comparison of the Catalytic Activities of Three Isozymes of Carnitine Palmitoyltransferase 1 Expressed in COS7 Cells. *Appl. Biochem. Biotechnol.* 172, 1486–1496. doi:10.1007/s12010-013-0619-y

Herlitz, J., Malmberg, K., Karlson, B. W., Rydén, L., and Hjalmarson, A. (1988). Mortality and Morbidity during a Five-Year Follow-Up of Diabetics with Myocardial Infarction. *Acta Med. Scand.* 224, 31–38. doi:10.1111/j.0954-6820.1988.tb16735.x

Huizar, I., Malur, A., Patel, J., McPeek, M., Dobbs, L., Wingard, C., et al. (2013). The Role of PPARγ in Carbon Nanotube-Elicited Granulomatous Lung Inflammation. *Respir. Res.* 14, 7. doi:10.1186/1465-9921-14-7

Hwangbo, H., Kim, M. Y., Ji, S. Y., Kim, S. Y., Lee, H., Kim, G. Y., et al. (2020). Auranofin Attenuates Non-alcoholic Fatty Liver Disease by Suppressing Lipid Accumulation and NLRP3 Inflammasome-Mediated Hepatic Inflammation *In Vivo* and *In Vitro*. *Antioxidants* 9, 1040. doi:10.3390/antiox9111040

Ibrahim, S. A., Abdel-Gaber, S. A., Ibrahim, M. A., Amin, E. F., Mohammed, R. K., and Abdelrahman, A. M. (2021). Nitric Oxide Modulation as a Potential Molecular Mechanism Underlying the Protective Role of NaHS in Liver Ischemia Reperfusion Injury. *Curr. Mol. Pharmacol.* [Epub ahead of print]. doi:10.2174/1874467214666210909154609

Idrovo, J. P., Yang, W. L., Nicastro, J., Coppa, G. F., and Wang, P. (2012). Stimulation of Carnitine Palmitoyltransferase 1 Improves Renal Function and Attenuates Tissue Damage after Ischemia/reperfusion. *J. Surg. Res.* 177, 157–164. doi:10.1016/j.jss.2012.05.053

Ji, S., You, Y., Kerner, J., Hoppel, C. L., Schoeb, T. R., Chick, W. S., et al. (2008). Homozygous Carnitine Palmitoyltransferase 1b (Muscle Isoform) Deficiency Is Lethal in the Mouse. *Mol. Genet. Metab.* 93, 314–322. doi:10.1016/j.ymgme.2007.10.006

Jiang, Z., Knudsen, N. H., Wang, G., Qiu, W., Naing, Z. Z. C., Bai, Y., et al. (2017). Genetic Control of Fatty Acid β-Oxidation in Chronic Obstructive Pulmonary Disease. *Am. J. Respir. Cel Mol. Biol.* 56, 738–748. doi:10.1165/rcmb.2016-0282OC

Joshi, P. R., and Zierz, S. (2020). Muscle Carnitine Palmitoyltransferase II (CPT II) Deficiency: A Conceptual Approach. *Molecules* 25, 1784. doi:10.3390/molecules25081784

Kajihara, N., Kukidome, D., Sada, K., Motoshima, H., Furukawa, N., Matsumura, T., et al. (2017). Low Glucose Induces Mitochondrial Reactive Oxygen Species via Fatty Acid Oxidation in Bovine Aortic Endothelial Cells. *J. Diabetes Investig.* 8, 750–761. doi:10.1111/jdi.12678

Kalucka, J., Bierhansl, L., Conchinha, N. V., Missiaen, R., Elia, I., Brüning, U., et al. (2018). Quiescent Endothelial Cells Upregulate Fatty Acid β-Oxidation for Vasculoprotection via Redox Homeostasis. *Cel Metab* 28, 881–e13. doi:10.1016/j.cmet.2018.07.016

Kang, H. M., Ahn, S. H., Choi, P., Ko, Y. A., Han, S. H., Chinga, F., et al. (2015). Defective Fatty Acid Oxidation in Renal Tubular Epithelial Cells Has a Key Role in Kidney Fibrosis Development. *Nat. Med.* 21, 37–46. doi:10.1038/nm.3762

Karlic, H., Lohninger, S., Koeck, T., and Lohninger, A. (2002). Dietary L-Carnitine Stimulates Carnitine Acyltransferases in the Liver of Aged Rats. *J. Histochem. Cytochem.* 50, 205–212. doi:10.1177/002215540205000208

Lee, B. J., Lin, J. S., Lin, Y. C., and Lin, P. T. (2015). Antiinflammatory Effects of L-Carnitine Supplementation (1000 Mg/d) in Coronary Artery Disease Patients. *Nutrition* 31, 475–479. doi:10.1016/j.nut.2014.10.001

Lee, J., and Wolfgang, M. J. (2012). Metabolomic Profiling Reveals a Role for CPT1c in Neuronal Oxidative Metabolism. *BMC Biochem.* 13, 23. doi:10.1186/1471-2091-13-23

Lee, T. I., Kao, Y. H., Baigalmaa, L., Lee, T. W., Lu, Y. Y., Chen, Y. C., et al. (2019). Sodium Hydrosulphide Restores Tumour Necrosis Factor-α-Induced Mitochondrial Dysfunction and Metabolic Dysregulation in HL-1 Cells. *J. Cell. Mol. Med.* 23, 7641–7650. doi:10.1111/jcmm.14637

Lee, T. I., Kao, Y. H., Chen, Y. C., Tsai, W. C., Chung, C. C., and Chen, Y. J. (2014). Cardiac Metabolism, Inflammation, and Peroxisome Proliferator-Activated Receptors Modulated by 1,25-dihydroxyvitamin D3 in Diabetic Rats. *Int. J. Cardiol.* 176, 151–157. doi:10.1016/j.ijcard.2014.07.021

Li, L., and Davie, J. R. (2010). The Role of Sp1 and Sp3 in normal and Cancer Cell Biology. *Ann. Anat.* 192, 275–283. doi:10.1016/j.aanat.2010.07.010

Lin, C. W., Peng, Y. J., Lin, Y. Y., Mersmann, H. J., and Ding, S. T. (2020). LRRK2 Regulates CPT1A to Promote β-Oxidation in HepG2 Cells. *Molecules* 25, 4122. doi:10.3390/molecules25184122

Liou, C. J., Wei, C. H., Chen, Y. L., Cheng, C. Y., Wang, C. L., and Huang, W. C. (2018). Fisetin Protects against Hepatic Steatosis through Regulation of the Sirt1/AMPK and Fatty Acid β-Oxidation Signaling Pathway in High-Fat Diet-Induced Obese Mice. *Cell Physiol. Biochem.* 49, 1870–1884. doi:10.1159/000493650

Liu, M., O'Connor, R. S., Trefely, S., Graham, K., Snyder, N. W., and Beatty, G. L. (2019). Metabolic Rewiring of Macrophages by CpG Potentiates Clearance of Cancer Cells and Overcomes Tumor-Expressed CD47-Mediated 'don't-Eat-Me' Signal. *Nat. Immunol.* 20, 265–275. doi:10.1038/s41590-018-0292-y

Liu, P. P., Liu, J., Jiang, W. Q., Carew, J. S., Ogasawara, M. A., Pelicano, H., et al. (2016). Elimination of Chronic Lymphocytic Leukemia Cells in Stromal Microenvironment by Targeting CPT with an Antiangina Drug Perhexiline. *Oncogene* 35, 5663–5673. doi:10.1038/onc.2016.103

Lundström, S. L., Balgoma, D., Wheelock, Å. M., Haeggström, J. Z., Dahlén, S. E., and Wheelock, C. E. (2011). Lipid Mediator Profiling in Pulmonary Disease. *Curr. Pharm. Biotechnol.* 12, 1026–1052. doi:10.2174/138920111795909087

Luo, X., Wang, Y., Zhang, F., Wang, Y., and Wang, Y. (2021). Cpt1a Promoted ROS-Induced Oxidative Stress and Inflammation in Liver Injury via the Nrf2/HO-1 and NLRP3 Inflammasome Signaling Pathway. *Can. J. Physiol. Pharmacol.* 99, 468–477. doi:10.1139/cjpp-2020-0165

Maitra, U., Chang, S., Singh, N., and Li, L. (2009). Molecular Mechanism Underlying the Suppression of Lipid Oxidation during Endotoxemia. *Mol. Immunol.* 47, 420–425. doi:10.1016/j.molimm.2009.08.023

Makrecka-Kuka, M., Korzh, S., Videja, M., Vilskersts, R., Sevostjanovs, E., Zharkova-Malkova, O., et al. (2020). Inhibition of CPT2 Exacerbates Cardiac Dysfunction and Inflammation in Experimental Endotoxaemia. *J. Cel Mol. Med.* 24, 11903–11911. doi:10.1111/jcmm.15809

Malek Mahdavi, A., Mahdavi, R., and Kolahi, S. (2016). Effects of L-Carnitine Supplementation on Serum Inflammatory Factors and Matrix Metalloproteinase Enzymes in Females with Knee Osteoarthritis: A Randomized, Double-Blind, Placebo-Controlled Pilot Study. *J. Am. Coll. Nutr.* 35, 597–603. doi:10.1080/07315724.2015.1068139

Mao, S., Ling, Q., Pan, J., Li, F., Huang, S., Ye, W., et al. (2021). Inhibition of CPT1a as a Prognostic Marker Can Synergistically Enhance the Antileukemic Activity of ABT199. *J. Transl. Med.* 19, 181. doi:10.1186/s12967-021-02848-9

McGarry, J. D., and Brown, N. F. (1997). The Mitochondrial Carnitine Palmitoyltransferase System. From Concept to Molecular Analysis. *Eur. J. Biochem.* 244, 1–14. doi:10.1111/j.1432-1033.1997.00001.x

Miguel, V., Tituaña, J., Herrero, J. I., Herrero, L., Serra, D., Cuevas, P., et al. (2021). Renal Tubule Cpt1a Overexpression Protects from Kidney Fibrosis by Restoring Mitochondrial Homeostasis. *J. Clin. Invest.* 131, e140695. doi:10.1172/JCI140695

Mizumura, K., Justice, M. J., Schweitzer, K. S., Krishnan, S., Bronova, I., Berdyshev, E. V., et al. (2018). Sphingolipid Regulation of Lung Epithelial Cell Mitophagy and Necroptosis during Cigarette Smoke Exposure. *FASEB. J.* 32, 1880–1890. doi:10.1096/fj.201700571R

Nemati, A., Moghadam, R. A., Mazani, M., and Darvishi, A. (2019). Effect of L-Carnitine and Conjugated Linoleic Acid Supplements on Haemoglobin Levels and Haptoglobin Genotype in Chronic Kidney Disease. *J. Pak. Med. Assoc.* 69, 343–348.

Ni, Y., Ni, L., Zhuge, F., and Fu, Z. (2020). The Gut Microbiota and its Metabolites, Novel Targets for Treating and Preventing Non-alcoholic Fatty Liver Disease. *Mol. Nutr. Food Res.* 64, e2000375. doi:10.1002/mnfr.202000375

Nieman, K. M., Kenny, H. A., Penicka, C. V., Ladanyi, A., Buell-Gutbrod, R., Zillhardt, M. R., et al. (2011). Adipocytes Promote Ovarian Cancer Metastasis and Provide Energy for Rapid Tumor Growth. *Nat. Med.* 17, 1498–1503. doi:10.1038/nm.2492

Peng, S., Chen, D., Cai, J., Yuan, Z., Huang, B., Li, Y., et al. (2021). Enhancing Cancer-Associated Fibroblast Fatty Acid Catabolism within a Metabolically Challenging Tumor Microenvironment Drives colon Cancer Peritoneal Metastasis. *Mol. Oncol.* 15, 1391–1411. doi:10.1002/1878-0261.12917

Petrache, I., Natarajan, V., Zhen, L., Medler, T. R., Richter, A. T., Cho, C., et al. (2005). Ceramide Upregulation Causes Pulmonary Cell Apoptosis and Emphysema-like Disease in Mice. *Nat. Med.* 11, 491–498. doi:10.1038/nm1238

Petővári, G., Dankó, T., Tőkés, A.-M., Vetlényi, E., Krencz, I., Raffay, R., et al. (2020). *In Situ* Metabolic Characterisation of Breast Cancer and its Potential Impact on Therapy. *Cancers* 12, 2492. doi:10.3390/cancers12092492

Price, N., van der Leij, F., Jackson, V., Corstorphine, C., Thomson, R., Sorensen, A., et al. (2002). A Novel Brain-Expressed Protein Related to Carnitine Palmitoyltransferase I. *Genomics* 80, 433–442. doi:10.1006/geno.2002.6845

Puskarich, M. A., Finkel, M. A., Karnovsky, A., Jones, A. E., Trexel, J., Harris, B. N., et al. (2015). Pharmacometabolomics of L-Carnitine Treatment Response Phenotypes in Patients with Septic Shock. *Ann. Am. Thorac. Soc.* 12, 46–56. doi:10.1513/AnnalsATS.201409-415OC

Qiao, S., Lv, C., Tao, Y., Miao, Y., Zhu, Y., Zhang, W., et al. (2020). Arctigenin Disrupts NLRP3 Inflammasome Assembly in Colonic Macrophages via Downregulating Fatty Acid Oxidation to Prevent Colitis-Associated Cancer. *Cancer Lett.* 491, 162–179. doi:10.1016/j.canlet.2020.08.033

Reilly, P. T., and Mak, T. W. (2012). Molecular Pathways: Tumor Cells Co-opt the Brain-specific Metabolism Gene CPT1C to Promote Survival. *Clin. Cancer Res.* 18, 5850–5855. doi:10.1158/1078-0432.CCR-11-3281

Rennard, S. I., and Drummond, M. B. (2015). Early Chronic Obstructive Pulmonary Disease: Definition, Assessment, and Prevention. *Lancet* 385, 1778–1788. doi:10.1016/S0140-6736(15)60647-X

Roe, C. R. (2002). Inherited Disorders of Mitochondrial Fatty Acid Oxidation: a New Responsibility for the Neonatologist. *Semin. Neonatol.* 7, 37–47. doi:10.1053/siny.2002.0097

Rosca, M. G., Vazquez, E. J., Chen, Q., Kerner, J., Kern, T. S., and Hoppel, C. L. (2012). Oxidation of Fatty Acids Is the Source of Increased Mitochondrial Reactive Oxygen Species Production in Kidney Cortical Tubules in Early Diabetes. *Diabetes* 61, 2074–2083. doi:10.2337/db11-1437

Savica, V., Santoro, D., Mazzaglia, G., Ciolino, F., Monardo, P., Calvani, M., et al. (2005). L-carnitine Infusions May Suppress Serum C-Reactive Protein and Improve Nutritional Status in Maintenance Hemodialysis Patients. *J. Ren. Nutr.* 15, 225–230. doi:10.1053/j.jrn.2004.10.002

Scantlebery, A. M., Tammaro, A., Mills, J. D., Rampanelli, E., Kors, L., Teske, G. J., et al. (2021). The Dysregulation of Metabolic Pathways and Induction of the Pentose Phosphate Pathway in Renal Ischaemia-Reperfusion Injury. *J. Pathol.* 253, 404–414. doi:10.1002/path.5605

Schafer, Z. T., Grassian, A. R., Song, L., Jiang, Z., Gerhart-Hines, Z., Irie, H. Y., et al. (2009). Antioxidant and Oncogene rescue of Metabolic Defects Caused by Loss of Matrix Attachment. *Nature* 461, 109–113. doi:10.1038/nature08268

Schlaepfer, I. R., and Joshi, M. (2020). CPT1A-Mediated Fat Oxidation, Mechanisms, and Therapeutic Potential. *Endocrinology* 161, bqz046. doi:10.1210/endocr/bqz046

Schröder, T., Kucharczyk, D., Bär, F., Pagel, R., Derer, S., Jendrek, S. T., et al. (2016). Mitochondrial Gene Polymorphisms Alter Hepatic Cellular Energy Metabolism and Aggravate Diet-Induced Non-alcoholic Steatohepatitis. *Mol. Metab.* 5, 283–295. doi:10.1016/j.molmet.2016.01.010

Shapiro, S. D., and Ingenito, E. P. (2005). The Pathogenesis of Chronic Obstructive Pulmonary Disease: Advances in the Past 100 Years. *Am. J. Respir. Cel Mol. Biol.* 32, 367–372. doi:10.1165/rcmb.F296

Shimizu, T., Maruyama, K., Kawamura, T., Urade, Y., and Wada, Y. (2020). PERK Participates in Cardiac Valve Development via Fatty Acid Oxidation and Endocardial-Mesenchymal Transformation. *Sci. Rep.* 10, 20094. doi:10.1038/s41598-020-77199-4

Sierra, A. Y., Gratacós, E., Carrasco, P., Clotet, J., Ureña, J., Serra, D., et al. (2008). CPT1c Is Localized in Endoplasmic Reticulum of Neurons and Has Carnitine Palmitoyltransferase Activity. *J. Biol. Chem.* 283, 6878–6885. doi:10.1074/jbc.M707965200

Singh, D. P., Bhargavan, B., Chhunchha, B., Kubo, E., Kumar, A., and Fatma, N. (2012). Transcriptional Protein Sp1 Regulates LEDGF Transcription by Directly Interacting with its Cis-Elements in GC-Rich Region of TATA-Less Gene Promoter. *PLoS One* 7, e37012. doi:10.1371/journal.pone.0037012

Soliman, E., Elhassanny, A. E. M., Malur, A., McPeek, M., Bell, A., Leffler, N., et al. (2020). Impaired Mitochondrial Function of Alveolar Macrophages in Carbon

Nanotube-Induced Chronic Pulmonary Granulomatous Disease. *Toxicology* 445, 152598. doi:10.1016/j.tox.2020.152598

Squire, J. D., Vazquez, S. N., Chan, A., Smith, M. E., Chellapandian, D., Vose, L., et al. (2020). Case Report: Secondary Hemophagocytic Lymphohistiocytosis with Disseminated Infection in Chronic Granulomatous Disease-A Serious Cause of Mortality. *Front. Immunol.* 11, 581475. doi:10.3389/fimmu.2020.581475

Stamler, J., Vaccaro, O., Neaton, J. D., and Wentworth, D. (1993). Diabetes, Other Risk Factors, and 12-yr Cardiovascular Mortality for Men Screened in the Multiple Risk Factor Intervention Trial. *Diabetes Care* 16, 434–444. doi:10.2337/diacare.16.2.434

Tan, Z., Zou, Y., Zhu, M., Luo, Z., Wu, T., Zheng, C., et al. (2021). Carnitine Palmitoyl Transferase 1A Is a Novel Diagnostic and Predictive Biomarker for Breast Cancer. *BMC Cancer* 21, 409. doi:10.1186/s12885-021-08134-7

van der Leij, F. R., Huijkman, N. C., Boomsma, C., Kuipers, J. R., and Bartelds, B. (2000). Genomics of the Human Carnitine Acyltransferase Genes. *Mol. Genet. Metab.* 71, 139–153. doi:10.1006/mgme.2000.3055

Wang, G., Yu, Y., Wang, Y. Z., Zhu, Z. M., Yin, P. H., and Xu, K. (2020). Effects and Mechanisms of Fatty Acid Metabolism-mediated G-lycolysis R-egulated by B-etulinic A-cid-loaded N-anoliposomes in C-olorectal C-ancer. *Oncol. Rep.* 44, 2595–2609. doi:10.3892/or.2020.7787

Wang, R., Lou, X., Feng, G., Chen, J., Zhu, L., Liu, X., et al. (2019). IL-17A-stimulated Endothelial Fatty Acid β-oxidation Promotes Tumor Angiogenesis. *Life Sci.* 229, 46–56. doi:10.1016/j.lfs.2019.05.030

Wang, W., Hu, X., Xia, Z., Liu, Z., Zhong, Z., Lu, Z., et al. (2020). Mild Hypothermia Attenuates Hepatic Ischemia-Reperfusion Injury through Regulating the JAK2/STAT3-CPT1a-dependent Fatty Acid β-Oxidation. *Oxid. Med. Cell Longev.* 2020, 5849794. doi:10.1155/2020/5849794

Wang, Y. N., Zeng, Z. L., Lu, J., Wang, Y., Liu, Z. X., He, M. M., et al. (2018). CPT1A-mediated Fatty Acid Oxidation Promotes Colorectal Cancer Cell Metastasis by Inhibiting Anoikis. *Oncogene* 37, 6025–6040. doi:10.1038/s41388-018-0384-z

Wei, T., Xiong, F. F., Wang, S. D., Wang, K., Zhang, Y. Y., and Zhang, Q. H. (2014). Flavonoid Ingredients of Ginkgo Biloba Leaf Extract Regulate Lipid Metabolism through Sp1-Mediated Carnitine Palmitoyltranferase 1A Up-Regulation. *J. Biomed. Sci.* 21, 87. doi:10.1186/s12929-014-0087-x

Wen, Y. A., Xing, X., Harris, J. W., Zaytseva, Y. Y., Mitov, M. I., Napier, D. L., et al. (2017). Adipocytes Activate Mitochondrial Fatty Acid Oxidation and Autophagy to Promote Tumor Growth in colon Cancer. *Cell Death Dis* 8, e2593. doi:10.1038/cddis.2017.21

Wirthensohn, G., and Guder, W. G. (1986). Renal Substrate Metabolism. *Physiol. Rev.* 66, 469–497. doi:10.1152/physrev.1986.66.2.469

Woeltje, K. F., Esser, V., Weis, B. C., Cox, W. F., Schroeder, J. G., Liao, S. T., et al. (1990b). Inter-tissue and Inter-species Characteristics of the Mitochondrial Carnitine Palmitoyltransferase Enzyme System. *J. Biol. Chem.* 265, 10714–10719. doi:10.1016/s0021-9258(18)87005-3

Woeltje, K. F., Esser, V., Weis, B. C., Sen, A., Cox, W. F., McPhaul, M. J., et al. (1990a). Cloning, Sequencing, and Expression of a cDNA Encoding Rat Liver Mitochondrial Carnitine Palmitoyltransferase II. *J. Biol. Chem.* 265, 10720–10725. doi:10.1016/s0021-9258(18)87006-5

Xi, L., Brown, K., Woodworth, J., Shim, K., Johnson, B., and Odle, J. (2008). Maternal Dietary L-Carnitine Supplementation Influences Fetal Carnitine Status and Stimulates Carnitine Palmitoyltransferase and Pyruvate Dehydrogenase Complex Activities in Swine. *J. Nutr.* 138, 2356–2362. doi:10.3945/jn.108.095638

Xie, Y. H., Xiao, Y., Huang, Q., Hu, X. F., Gong, Z. C., and Du, J. (2021). Role of the CTRP6/AMPK Pathway in Kidney Fibrosis through the Promotion of Fatty Acid Oxidation. *Eur. J. Pharmacol.* 892, 173755. doi:10.1016/j.ejphar.2020.173755

Xiong, J., Kawagishi, H., Yan, Y., Liu, J., Wells, Q. S., Edmunds, L. R., et al. (2018). A Metabolic Basis for Endothelial-To-Mesenchymal Transition. *Mol. Cell* 69, 689–698.e7. doi:10.1016/j.molcel.2018.01.010

Xiong, X., Wen, Y. A., Fairchild, R., Zaytseva, Y. Y., Weiss, H. L., Evers, B. M., et al. (2020). Upregulation of CPT1A Is Essential for the Tumor-Promoting Effect of Adipocytes in colon Cancer. *Cell Death Dis* 11, 736. doi:10.1038/s41419-020-02936-6

Xiong, Y., Liu, Z., Zhao, X., Ruan, S., Zhang, X., Wang, S., et al. (2018). CPT1A Regulates Breast Cancer-Associated Lymphangiogenesis via VEGF Signaling. *Biomed. Pharmacother.* 106, 1–7. doi:10.1016/j.biopha.2018.05.112

Xu, L., Xia, H., Ni, D., Hu, Y., Liu, J., Qin, Y., et al. (2020). High-Dose Dexamethasone Manipulates the Tumor Microenvironment and Internal Metabolic Pathways in Anti-tumor Progression. *Int. J. Mol. Sci.* 21, 1846. doi:10.3390/ijms21051846

Yamazaki, N., Shinohara, Y., Shima, A., Yamanaka, Y., and Terada, H. (1996). Isolation and Characterization of cDNA and Genomic Clones Encoding Human Muscle Type Carnitine Palmitoyltransferase I. *Biochim. Biophys. Acta* 1307, 157–161. doi:10.1016/0167-4781(96)00069-3

Yao, H., Gong, J., Peterson, A. L., Lu, X., Zhang, P., and Dennery, P. A. (2019). Fatty Acid Oxidation Protects against Hyperoxia-Induced Endothelial Cell Apoptosis and Lung Injury in Neonatal Mice. *Am. J. .Respir. Cell Mol. Biol.* 60, 667–677. doi:10.1165/rcmb.2018-0335OC

Ye, G., Gao, H., Wang, Z., Lin, Y., Liao, X., Zhang, H., et al. (2019). PPARα and PPARγ Activation Attenuates Total Free Fatty Acid and Triglyceride Accumulation in Macrophages via the Inhibition of Fatp1 Expression. *Cell Death Dis* 10, 39. doi:10.1038/s41419-018-1135-3

Zehethofer, N., Bermbach, S., Hagner, S., Garn, H., Müller, J., Goldmann, T., et al. (2015). Lipid Analysis of Airway Epithelial Cells for Studying Respiratory Diseases. *Chromatographia* 78, 403–413. doi:10.1007/s10337-014-2787-5

Zeisberg, M., and Neilson, E. G. (2010). Mechanisms of Tubulointerstitial Fibrosis. *J. Am. Soc. Nephrol.* 21, 1819–1834. doi:10.1681/ASN.2010080793

Zhai, Y., Petrowsky, H., Hong, J. C., Busuttil, R. W., and Kupiec-Weglinski, J. W. (2013). Ischaemia-reperfusion Injury in Liver Transplantation-Ffrom Bench to Bedside. *Nat. Rev. Gastroenterol. Hepatol.* 10, 79–89. doi:10.1038/nrgastro.2012.225

Zhang, X. J., Cheng, X., Yan, Z. Z., Fang, J., Wang, X., Wang, W., et al. (2018). An ALOX12-12-HETE-GPR31 Signaling axis Is a Key Mediator of Hepatic Ischemia-Reperfusion Injury. *Nat. Med.* 24, 73–83. doi:10.1038/nm.4451

Zhao, F., Xiao, C., Evans, K. S., Theivanthiran, T., DeVito, N., Holtzhausen, A., et al. (2018). Paracrine Wnt5a-β-Catenin Signaling Triggers a Metabolic Program that Drives Dendritic Cell Tolerization. *Immunity* 48, 147–160.e7. doi:10.1016/j.immuni.2017.12.004

Zhao, Q., Yang, R., Wang, J., Hu, D. D., and Li, F. (2017). PPARα Activation Protects against Cholestatic Liver Injury. *Sci. Rep.* 7, 9967. doi:10.1038/s41598-017-10524-6

Conflict of Interest: The authors declare that the research was conducted in the absence of any commercial or financial relationships that could be construed as a potential conflict of interest.

Publisher's Note: All claims expressed in this article are solely those of the authors and do not necessarily represent those of their affiliated organizations, or those of the publisher, the editors, and the reviewers. Any product that may be evaluated in this article, or claim that may be made by its manufacturer, is not guaranteed or endorsed by the publisher.

frontiers in Pharmacology

ORIGINAL RESEARCH
published: 27 October 2021
doi: 10.3389/fphar.2021.727876

lncRNA OR3A4 Promotes the Proliferation and Metastasis of Ovarian Cancer Through KLF6 Pathway

Fangfang Guo[1,2], *Jianan Du*[3,4], *Lingling Liu*[3,4], *Yawei Gou*[3,4], *Mingming Zhang*[3,4], *Wei Sun*[3,4], *Hongmei Yu*[5]* and *Xueqi Fu*[1]*

[1]Edmond H. Fischer Signal Transduction Laboratory, College of Life Sciences, Jilin University, Changchun, China, [2]Department of Gynecology, Xinhua Hospital Affiliated to Dalian University, Dalian, China, [3]Department of Molecular Biology, College of Basic Medical Sciences Jilin University, Changchun, China, [4]Jilin Province Zebrafish Genetic Engineering Laboratory, Jilin Provincial Development and Reform Commission, Changchun, China, [5]Department of Blood Transfusion, China-Japan Union Hospital of Jilin University, Changchun, China

Aim: Ovarian cancer is a collaborative malignant tumor of the female reproductive system in clinical research. Some clinical studies have shown that OR3A4, which is a cancer-causing lncRNA, plays a major role in promoting the occurrence and development of a variety of tumors. And we also expressed the view that it expressed in ovarian tissue. However, the function of OR3A4 in ovarian cancer remains unclear.

Methods and Results: To further verify the function of lncRNA OR3A4 in ovarian cancer, we established the xenograft model in the zebra fish. In this study, cells transformed with OR3A4 shRNA plasmids were transplanted into the zebra fish, and the cell proliferation and migration ability were significantly reduced compared to the empty vector. While knocking out OR3A4, we further downregulated its expression by siRNA of KLF6. Our study found that the knocked out OR3A4 resulted in a decrease in cell proliferation and migration level, which can be found in the downregulated expression of KLF6. We also verify the relationship between OR3A4 and circulating tumor cells in the zebra fish xenograft model, the results indicate that lncRNA OR3A4 may be involved in the resistance of ovarian cancer to complain.

Conclusion: lncRNA OR3A4 promotes the proliferation and metastasis of ovarian cancer through the KLF6 pathway.

Keywords: ovarian cancer, lncRNA OR3A4, KLF6, inflammation, zebra fish

OPEN ACCESS

Edited by:
Zhaogang Yang,
University of Texas MD Anderson Cancer Center, United States

Reviewed by:
Tongzheng Liu,
Jinan University, China
Xiao Gong,
Wuhan University of Technology, China

***Correspondence:**
Xueqi Fu
fxq@jlu.edu.cn
Hongmei Yu
yuhongm@jlu.edu.cn

Specialty section:
This article was submitted to Inflammation Pharmacology, a section of the journal Frontiers in Pharmacology

Received: *20 June 2021*
Accepted: *26 August 2021*
Published: *27 October 2021*

Citation:
Guo F, Du J, Liu L, Gou Y, Zhang M, Sun W, Yu H and Fu X (2021) lncRNA OR3A4 Promotes the Proliferation and Metastasis of Ovarian Cancer Through KLF6 Pathway. Front. Pharmacol. 12:727876. doi: 10.3389/fphar.2021.727876

INTRODUCTION

Ovarian cancer is a joint malignant tumor of the female reproductive system in clinical research (Jemal et al., 2007; Bowtell et al., 2015). In China, its incidence rate ranks the third after cervical cancer and endometrial cancer, which seriously threaten women's health (Shi et al., 2017). At present, it has been observed that long non-coding RNA refers to RNA molecules with nucleotide length between 200 and 200,000 without translation function (Mercer et al., 2009; Zhang et al., 2013; Lorenzen and Thum, 2016). Its mechanism of action is mainly to interfere with the physiological activities of cells and play a role in the occurrence, progression, and metastasis of tumors by affecting the expression of downstream genes

and interfering with the normal shearing of mRNA (Maass et al., 2014; Schmitt and Chang, 2016; Luo et al., 2018; Chen et al., 2019).

Long non-coding RNA OR3A4 is the member of the olfactory receptor family 3 and subfamily A (Shang et al., 2019). Studies have reported that the expression of OR3A4 can be detected in the peripheral blood of primary gastric cancer tissues and gastric cancer patients, and it has also been found that OR3A4 can promote the growth, invasion, metastasis, and tumorigenesis of gastric cancer cells *in vitro* and *in vivo* (Guo et al., 2016). This indicates that OR3A4 is a cancer-causing lncRNA that promotes tumor progression. Clinical studies have confirmed that it plays an important role in promoting the occurrence and development of a variety of tumors , such as gastric cancer, breast cancer, liver cancer, and lung cancer (Gutschner and Diederichs, 2012; Guo et al., 2016; Liu et al., 2017; Li et al., 2019a; Zhong et al., 2019). However, the expression and function of long non-coding RNA OR3A4 in ovarian cancer remains unclear.

Kruppel-like factor 6 (KLF6) is a member of the Kruppel-like factor family and is considered a tumor suppressor (Zhang et al., 2018). Research proves that KLF6 in human cancer mainly by p53 independence means an increased expression of p21 (Lang et al., 2013; D'Astolfo et al., 2008), makes the cell cycle of tumor cells stranded in the G_1/S transition, and thus plays a role of inhibition of the proliferation of cancer cells, transfer, etc. In a variety of cancers, such as rectal cancer and liver cancer (Reeves et al., 2004; Watanabe et al., 2008), KLF6 can lead to a decreased protein expression level due to gene deletion or mutation, resulting in the occurrence and development of tumors. At present, studies have shown that KLF6 silencing in ovarian cancer can promote cell and tumor growth and blood vessel production, but whether it can promote apoptosis of ovarian cancer has yet to be further studied (DiFeo et al., 2006; Han and Gong, 2021; Zhang et al., 2021). Therefore, the role of long non-coding RNA OR3A4 and KLF6 in ovarian cancer, and whether they are related became the purpose of this study. By detecting the overexpression of long non-coding RNA OR3A4 in ovarian cancer tissues and ovarian cancer cells, this study found that the increased expression of OR3A4 could inhibit the expression of KLF6, and the knockdown of OR3A4 could inhibit the migration and invasion of ovarian cancer cells. In order to further prove the role of KLF6 in ovarian cancer, this study used siRNA technology to study the role of KLF6 in isolation-induced apoptosis of ovarian cancer cells, providing a theoretical basis for further revealing the role of KLF6 in the pathogenesis of ovarian cancer.

The results show that in ovarian cancer, lncRNA OR3A4 can inhibit the expression of KLF6 expression and, at the same time, promote the cell migration and invasion ability, and the declined KLF6 expression can also block the apoptosis induced by cisplatin. lncRNA OR3A4 promotes cell migration and invasion ability of important roles and molecular mechanism, provides a theoretical basis for the future of clinical trials and drug development, and provides a new potential therapeutic target and idea. In addition, studies have shown that inflammation and tumor progression are closely linked. It was reported that chronic inflammation was related to 15–20% of tumor occurrence, such as lung cancer, gastrointestinal tumors, and breast cancer are related to systemic inflammation (Tomita et al., 2011; Xu et al., 2017). Inflammation can upregulate tumor-causing cytokines and inflammatory mediators, inhibit tumor cell apoptosis, induce tumor angiogenesis, stimulate DNA damage, induce immunosuppressive microenvironment, and remodel the extracellular matrix (Coussens and Werb, 2002; Hanahan and Weinberg, 2011). Besides, studies have likewise reported the impact of antitumor drugs on the immune response, such as methotrexate (MTX) blocking the acute inflammatory immune response after wasp infection (Yadav et al., 2021). It suggests that the effects of inflammation and tumors are mutual. In this study, we have also observed that the administration of the antitumor drug cisplatin increases the migration and aggregation of neutrophils, which are among the most quickly responsive innate immune cells in inflammation. This model could be invoked as a basis for studying the correlation between immune cells and tumors in the further study.

MATERIALS AND METHODS

Cells and Drugs

SKOV3 cell lines were obtained from the Boster Biological Technology Co., Ltd. (Wuhan, Hubei, China). SKOV3 cell lines were cultured in an RPMI-1640 medium supplemented with 10% fetal bovine serum (FBS) in a 37°C incubator containing 5% CO2. Cisplatin was purchased from Sigma (St. Louis, MO, United States).

Cell Proliferation

For the CCK8 assay, a cell counting kit 8 (CCK8, Dojindo, Japan) was used according to the manufacturer's instructions. SKOV3+EV, SKOV3+OR3A4 shRNA, and SKOV3+OR3A4 shRNA + KLF6siRNA cells were respectively placed in a 1640 medium for 24 h, followed by incubation in 96-well plates at a density of 5 × 103 cells/well, and cultured for 24, 48, and 72 h, respectively. At the appropriate time points, 10 μL of CCK8 reagent was added to each well and mixed uniformly. Then all cells were incubated for another 3 h, and the optical absorbance at 450 nm was measured with an ELISA plate reader (Thermo Fisher, United States).

Cell Migration

SKOV3 cell migration was analyzed using a wound healing assay. A culture insert was set into a 12-well plate, following which SKOV3+EV, SKOV3+OR3A4 shRNA, and SKOV3+OR3A4 shRNA + KLF6siRNA cells were counted and seeded (8 × 105) into each well containing the culture insert with 70 μL of medium and incubated for 24 h. Suction was utilized to draw out the medium from the insert, and the insert was gently removed using sterile tweezers, followed by the addition of 2 ml of medium to each well of the plate. Finally, cell migration was observed for 0–8 h.

Western Blotting

Western blotting was done using the standard protocol. In brief, the samples were lysed and denatured in 5× sample buffer. The same amount of proteins was separated on a 10% SDS–polyacrylamide gel and transferred onto a nitrocellulose membrane. The nitrocellulose membrane was incubated with 5% non-fat milk in Tris-buffered saline (150 mM NaCl, 20 mM Tris–HCl, pH7.4) with a primary antibody overnight at 4°C. After washing, the membrane

was further incubated with a secondary antibody for 45 min, and proteins were detected with an ECL detection system. ImageJ software was used to measure the band intensity.

Zebra Fish Xenograft Model Experiment

Cells of shRNA were transfected for 24 h, and empty vectors were collected and washed three times with HBSS. The labeled cells were stained with the lipophilic fluorescent tracking dye CM-DiI. The cells were seen at 37°C for 5 min and then at 4°C for 15 min. Finally, the cells were washed three times with HBSS. The labeled cells were used only for injection. The zebra fish embryos at 48 hpf (hours post fertilization) were fixed using a low–melting point agarose gel; the tumor cell suspension is loaded into a capillary needle and injected into the protriptyline space with the amount of 300–400 cells in one strip. The zebra fish injected with the tumor cells is cultured in a 34°C incubator. The cells were transplanted for observation under a microscope on the second day (1 day post-injection, dpi). Zebra fish larvae with similar tumor cell sizes were selected and cultured in an incubator at 34°C for 96 h (4 dpi). Then they were fixed with the low–melting point gel and imaged using a fluorescence stereomicroscope (Olympus MVX10, Japan), with the magnifying power of ×3.2. The images were created with ImageJ software, and the statistical analysis was performed by GraphPad Prism 8 software.

Drug Screening in Zebra Fish

After the zebra fish xenograft model was established, the zebra fish larvae with similar tumor cell mass sizes were selected for drug screening for 1 day. The drug concentration of 0.6 mg/ml was added to the zebra fish culture solution and administered by immersion. Fresh culture solution containing the drug was replaced every 24 h and cultured in an incubator at 34°C. The drug was administered continuously for 3 days (4 dpi), respectively. The methods of microimaging, picture processing, and statistical analysis were the same as before.

Data Analysis

Group data were presented as mean ± SE. The unpaired *t*-test was used to compare between groups. Multiple group means were compared by ANOVA, followed by the least significant difference (LSD) post hoc *t*-test.

RESULTS

Correlation Between KLF6 and Ovarian Cancer and Pathway Enrichment Analysis

Based on the TCGA PanCancer Atlas database of the cBioPortal website, we obtained the relationship between KLF6 and the incidence of various cancers. The alteration frequency of KLF6 in bladder cancer was the highest, which had a total of 8.76% alteration in 411 cases. Followed by ovarian cancer, there was 5.14% alteration of KLF6 in 584 cases. Among them, 0.17% were mutations, 0.17% were fusions, and 4.29% were amplification. Then we evaluated the effect of the KLF6 expression level on the survival of ovarian cancer patients through the TCGA OV database of the UALCAN Website. We found that when the KLF6 gene is highly expressed, the probability of patients surviving more than 2,000 days is significantly lower than that of the KLF6 medium- to low-expression group, which indicates that the expression level of KLF6 may be negatively correlated with the survival rate of ovarian cancer ($p < 0.05$).

After evaluating the correlation between KLF6 and ovarian cancer, we obtained 20 genes co-expressed with KLF6 in ovarian cancer samples based on the TCGA mRNA expression profiles on the cBioPortal Website. Subsequently, enrichment of co-related genes was analyzed by R language. The GO analysis results showed that these genes were predominantly enriched in response to hormones such as steroid hormones, glucocorticoid, and corticosteroid; muscular organ development; skeletal muscle cell differentiation; p38MAPK signal cascade; and other biological process (BP). Molecular function (MF) is mainly enriched in the activity of RNA polymerase II–specific DNA-binding transcription activator, histone acetyltransferase binding, and protein tyrosine/serine/threonine phosphatase activity. The KEGG pathway of these 20 genes is significantly enriched in the MAPK signaling pathway, parathyroid hormone synthesis, secretion and action, osteoclast differentiation, and apoptosis (**Figure 1**).

Knocked Out of lncRNA OR3A4 Resulted in Decreased Proliferation and Migration Levels of SKOV3 in Zebra Fish Xenograft Model

To further verify the function of lncRNA OR3A4 on SKOV3 *in vivo*, we established the xenograft model in the zebra fish. The zebra fish xenograft model has been used in tumor-related research in recent years mainly because of its high efficient transplantation and intuitive and rapid observation. In this study, the cells transformed with OR3A4 shRNA plasmids were transplanted into the protriptyline space around the yolk sac of zebra fish embryos at 3 days post-fertilization (3 dpf). Then we imaged and analyzed the SKOV3 proliferation and migration at 4 days after transplantation. It was noted that after the knockdown of OR3A4 in SKOV3 cells, the cell proliferation and migration ability were significantly reduced compared with the empty vector (**Figure 2**).

KLF6 Mediated the Proliferation and Migration of lncRNA OR3A4 in SKOV3

To study the regulation of proliferation and migration of SKOV3 by lncRNA OR3A4 through the KLF6 pathway, we verified by cell rescue experiments. While knocking out OR3A4, we further downregulated its expression by siRNA of KLF6. Our study found that knocked out OR3A4 resulted in a decrease in cell proliferation and migration levels, which can be found by downregulating the expression of KLF6 (**Figure 3**). The result stated that OR3A4 could regulate the proliferation and migration of SKOV3 cells by downregulating the expression of KLF6.

Knocked Out OR3A4 in SKOV3 Cells Enhanced the Antitumor Effect of Cisplatin

To study the effect of lncRNA OR3A4 on cisplatin resistance of SKOV3 cells, we treated with cisplatin, and on this basis,

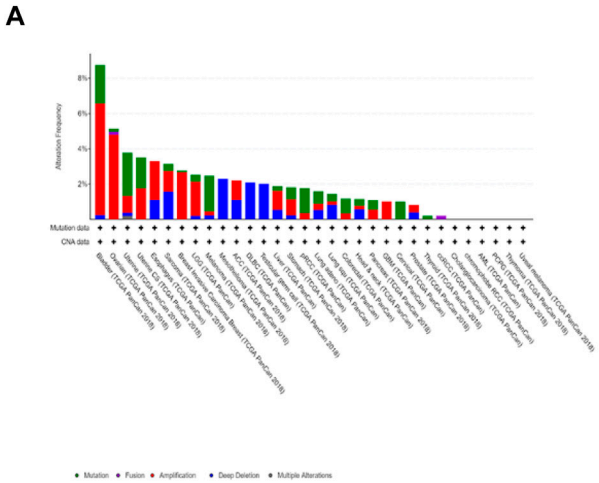

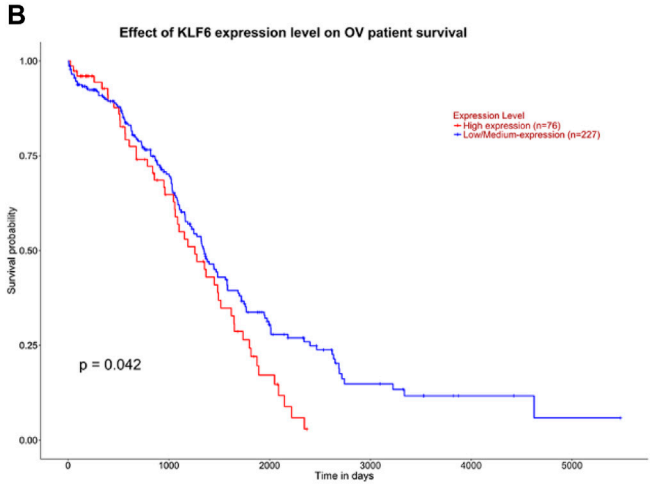

C

Correlated gene with KLF6 in ovarian cancer

Correlated Gene	*Cyto band*	*Spearman's Correlation*	*p-Value*	*q-Value*
ZFP36	19q13.2	0.673454	6.43E-28	1.22E-23
GADD45B	19p13.3	0.642627	8.37E-25	7.95E-21
DUSP1	5q35.1	0.624104	4.25E-23	2.69E-19
CCN1	1p22.3	0.59172	2.25E-20	1.07E-16
FOSB	19q13.32	0.577243	2.97E-19	1.13E-15
SOCS3	17q25.3	0.5748	4.54E-19	1.37E-15
RGS1	1q31.2	0.574195	5.04E-19	1.37E-15
CCN2	6q23.2	0.566681	1.81E-18	4.29E-15
MAFF	22q13.1	0.563884	2.88E-18	6.09E-15
EGR1	5q31.2	0.5627	3.51E-18	6.67E-15
SERPINE1	7q22.1	0.557683	8.00E-18	1.38E-14
DUSP5	10q25.2	0.555137	1.21E-17	1.91E-14
FOS	14q24.3	0.554256	1.39E-17	2.04E-14
GPR183	13q32.3	0.540311	1.25E-16	1.70E-13
ATF3	1q32.3	0.536666	2.18E-16	2.76E-13
MCL1	1q21.2	0.532424	4.13E-16	4.91E-13
SGK1	6q23.2	0.529879	6.03E-16	6.75E-13
HBEGF	5q31.3	0.527507	8.57E-16	9.05E-13
KLF9	9q21.12	0.515326	4.97E-15	4.98E-12
NR4A3	9q31.1	0.514417	5.66E-15	5.37E-12

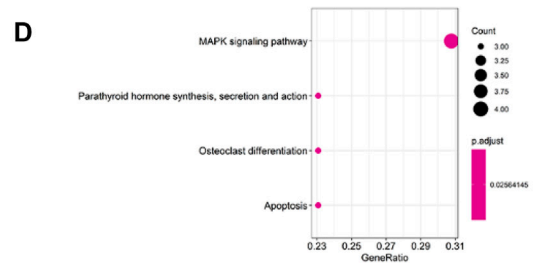

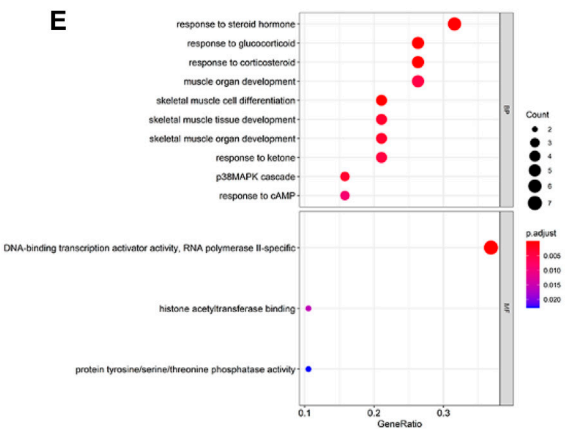

FIGURE 1 | Correlation between KLF6 and ovarian cancer and pathway enrichment analysis. **(A)** Using the TCGA PanCancer Atlas database of cBioPortal, the alteration frequency of KFL6 in various cancer was obtained. **(B)** Effect of the KLF6 expression level of ovarian cancer patient survival based on the TCGA OV database of UALCAN. **(C)** Co-expressed genes with KLF6 in ovarian cancer samples according to the mRNA expression profiles of the TCGA database. **(D, E)** KEGG and GO analysis of modular genes by the R package of clusterProfiler. The enrichment file is in KEEG. and GO. txt.

downregulated the expression of OR3A4, and then detected the cell proliferation and migration level. Studies have shown the same.

Proliferation and migration were significantly reduced after the concurrent use of circulating tumor cells, and the expression of OR3A4 was downregulated compared with that after a single treatment (**Figure 4**). The results indicate that lncRNA OR3A4 may be involved in the resistance of SKOV3 to cisplatin.

The Zebra Fish Xenograft Model Verified that the Knockdown of lncRNA OR3A4 Enhanced the Tumor Inhibition Effect of Cisplatin

To further verify the relationship between lncRNA OR3A4 and cisplatin in the zebra fish xenograft model, we first tested the treated concentration of cisplatin in zebra fish. Because there may be differences between the soaking concentration and the

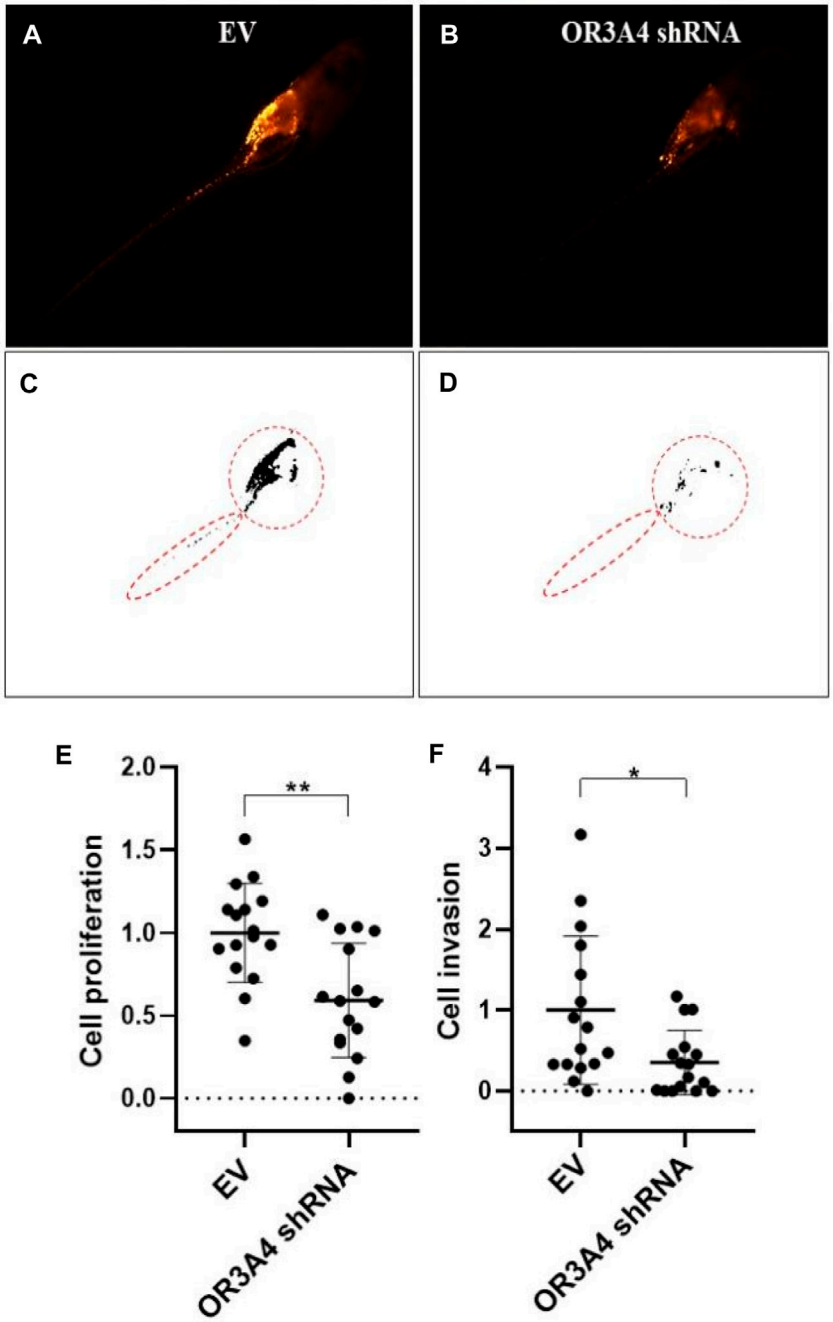

FIGURE 2 | Knocked out of lncRNA OR3A4 in the zebra fish xenograft model resulted in decreased proliferation and migration of SKOV3 **(A, B)** Representative fluoroscopy image at 4 days after transplantation of the empty vector (EV) transfected with shRNA and the SKOV3 cells transfected with the lncRNA OR3A4 shRNA plasmid into the protriptyline space of zebra fish larvae at 3d after fertilization**(C, D)** Fluorescent segment images corresponding to those pictures. The signals in the circles (transplant sites) are employed to the statistical analysis of cell proliferation, and the signals in the oval circles (migrated trunk sites) are used for the statistical analysis of cell migration **(E, F)** Statistical analysis of the effects of transfection of OR3A4 shRNA plasmid on the proliferation and migration of SKOV3 in the zebra fish xenograft model. $^{*}p < 0.05$, $^{**}p < 0.01$, n = 16.

concentration in zebra fish larvae, we started the experiment according to the general concentration of the cells of the experiment. We determined the appropriate concentration of cisplatin treatment according to the development of zebra fish larvae. We found that the concentration of cisplatin equal to or higher than 0.8 mg/ml had a significant effect on the development and survival of zebra fish, whereas when the concentration of cisplatin was equal to or lower than 0.6 mg/ml, the development of zebra fish larvae was unaffected.

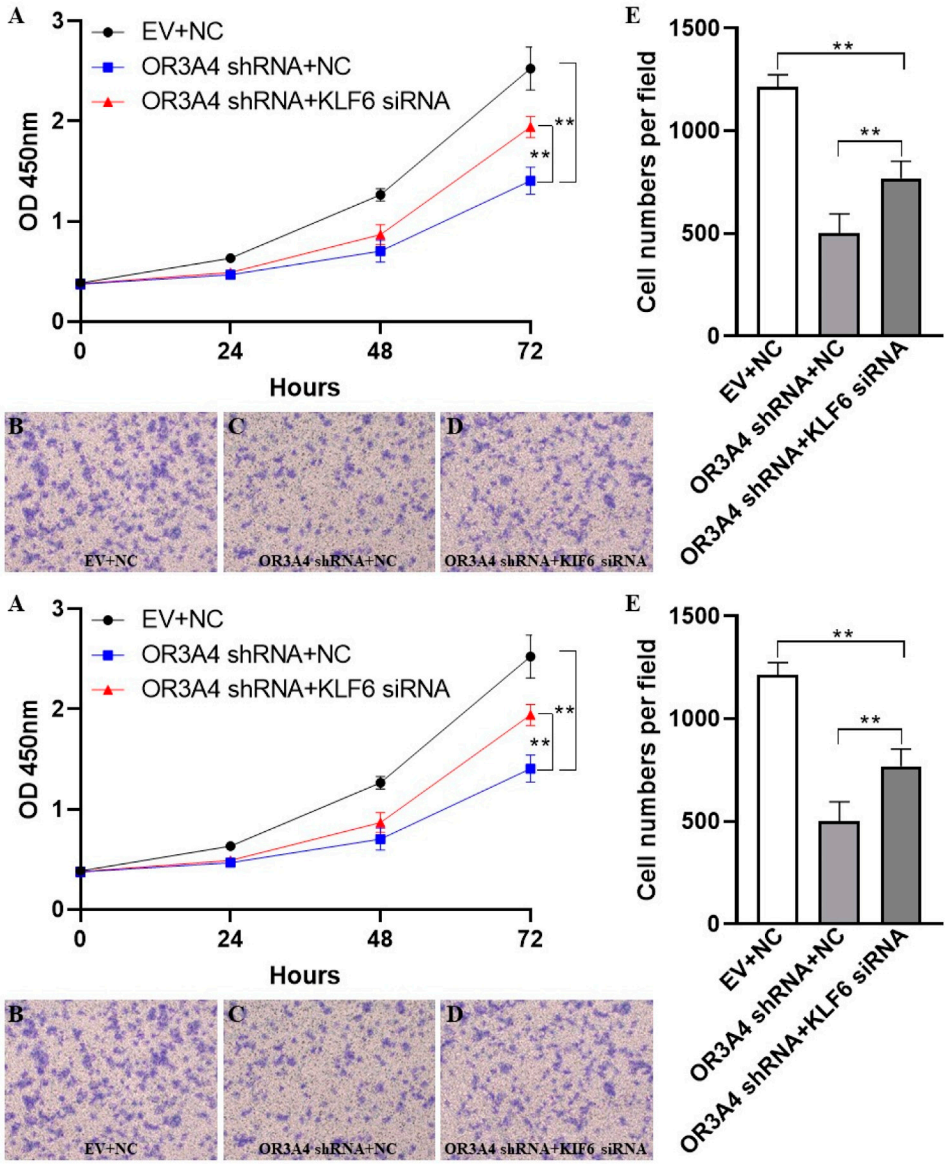

FIGURE 3 | KLF6 mediated the proliferation and migration of lncRNA OR3A4 in SKOV3 **(A)** Knocking out of OR3A4 and the downregulation of KLF6 expression can rescue the proliferation of SKOV3 cells **(B, E)** Knocked out OR3A4 while downregulated KLF6 saved the migration level of SKOV3 cells **(B–D)** Typical pictures of transwell experiments.

After determining the cisplatin treatment concentration in zebra fish larvae, we further performed the study based on the zebra fish xenograft model. Similar to the results from the cell experiment, we found that the proliferation and migration of tumor cells after simultaneous treatment with cisplatin and OR3A4 knockdown were significantly lower than those of a single treatment (**Figure 5**).

In addition, we used neutrophil EGFP-labeled juvenile zebra fish at 3 dpf to detect the effect of cisplatin treatment and OR3A4 knockdown on the immune cells. The results showed that compared with the DDP treatment alone, the migration and aggregation of neutrophils in zebra fish larvae after cisplatin combined with OR3A4 knockdown were significantly enhanced (**Figure 6**).

DISCUSSION

lncRNA is an important regulatory factor in the occurrence and development of ovarian cancer (Gutschner and Diederichs, 2012; Zhan et al., 2018; Long et al., 2019), which can be invoked as a potential biomarker and therapeutic target for ovarian cancer. For instance, the silencing of lncRNA MNX1-AS1 can inhibit the proliferation and migration of ovarian cancer cells (Gao et al., 2019), and lncRNA MNX1-AS1 may become a potential target of ovarian cancer. lncRNA BACE1-AS can inhibit the proliferation and invasion of ovarian cancer stem cells and can be utilized as a new target for ovarian cancer

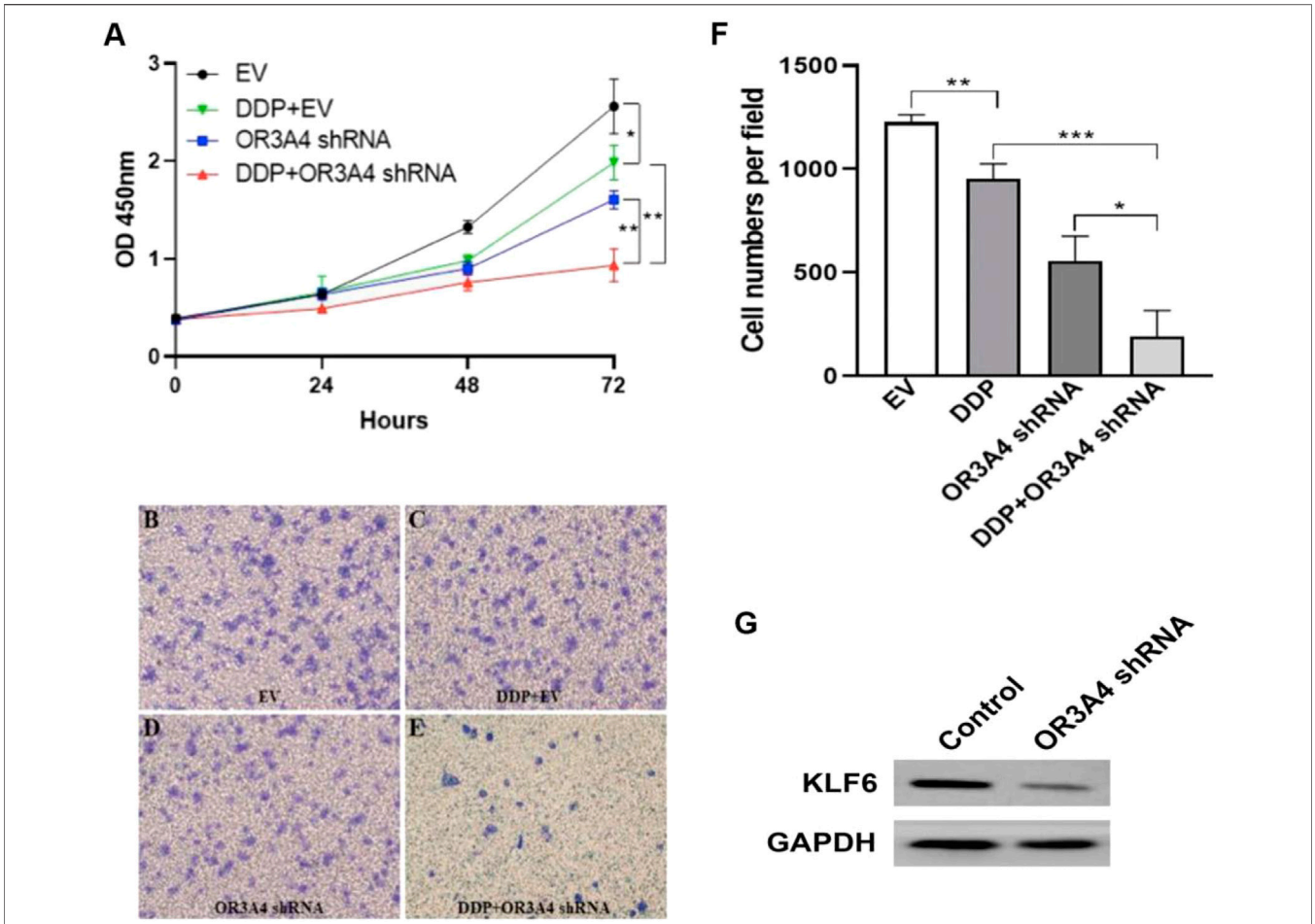

FIGURE 4 | Knockdown of OR3A4 in SKOV3 cells enhanced the antitumor effect of cisplatin **(A)** The proliferation level of cells processed by DDP and simultaneously knocked down OR3A4 was significantly lower than those treated individually **(B–F)** The migration level of cells treated with DDP while knocking down OR3A4 was considerably lower than those treated individually **(B–E)** The representative images of transwell experiments **(F)** The statistical analysis of cell migration **(G)** KLF6 expression in SKOV3 cells while knocking down OR3A4. *$p < 0.05$, **$p < 0.01$, ***$p < 0.001$.

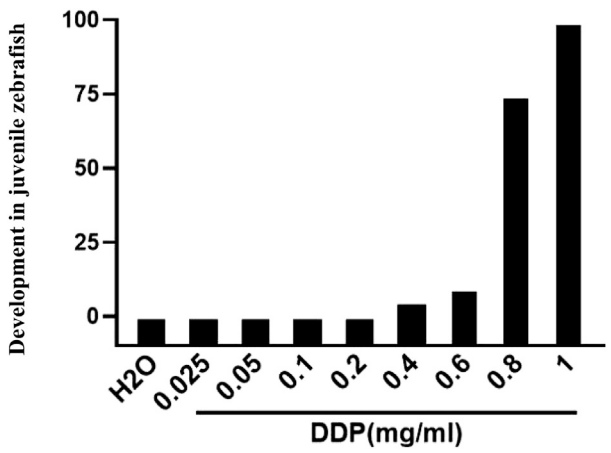

FIGURE 5 | Impacts of different cisplatin concentrations on the overall development in juvenile zebra fish (3–6 dpf).

treatment (Chen et al., 2016). lncRNA HOXA1 can promote the proliferation and migration of ovarian cancer cells, which is closely linked to the prognosis of the ovary (Li et al., 2019b). Downregulation of lncRNA SPRY4-IT1 can promote the metastasis of ovarian cancer cells by regulating epithelial–mesenchymal transition (Li et al., 2017; Yu et al., 2017). lncRNA ElncRNA1, an oncogene in the proliferation of epithelial ovarian cancer cells, was substantially upregulated by estrogen (Qiu et al., 2017).

Krüppel-like factor 6(KLF6) is a member of the Krüppel-like factor family. It has been proved that KLF6 plays the role of tumor suppressor in various tumors by regulating diverse biological processes (Narla et al., 2001; Reeves et al., 2004). Studies have shown that the mechanism of KLF6 inhibiting tumor is to increase the expression of p21 through the p53-independent pathway, thus inhibiting the occurrence and proliferation of cancer cells. At present, lncRNA OR3A4 in the occurrence and development of ovarian cancer is difficult to identify and the role of KLF6 as a tumor suppressor in

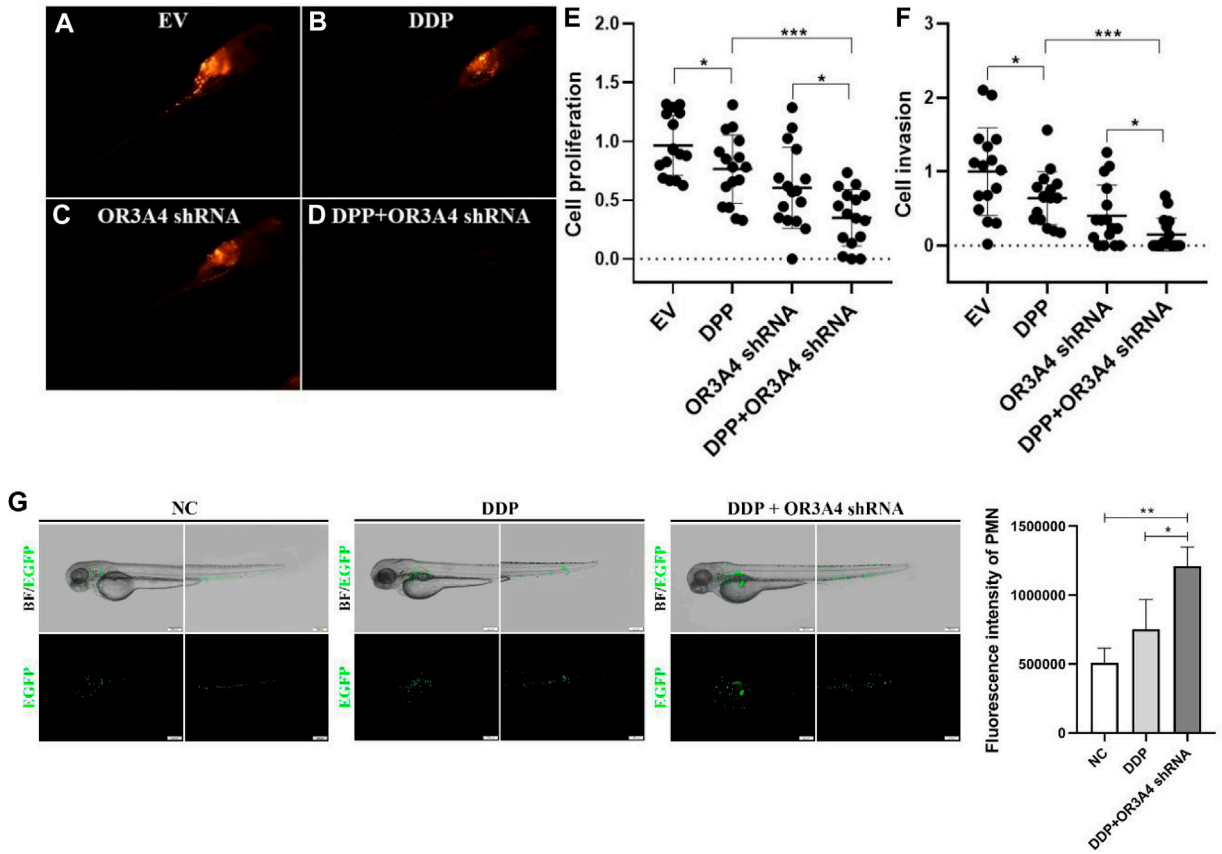

FIGURE 6 | Concurrent treatment with DDP and knockdown of OR3A4 enhanced the tumor inhibition of cisplatin in the zebra fish xenografts model **(A–D)** The representative imaging of zebra fish larvae treated with DDP, knockout OR3A4, and concurrent treatment **(E–F)** Statistical effects of DPP, knockdown of OR3A4, and concurrent treatment on the proliferation and migration of SKOV3 cells in a zebra fish xenograft model **(G)** The representative images of the effects on the migration and aggregation of neutrophils in zebra fish larvae treated with DDP and knocked out OR3A4. *$p < 0.05$, ***$p < 0.001$, $n = 16$.

ovarian cancer is also unknown. Therefore, this study aims to take lncRNA OR3A4 and KLF6 as research objects and try to explore their roles in ovarian cancer cells.

To study that lncRNA OR3A4 regulates the proliferation and migration of SKOV3 through the KLF6 pathway, we verified it by saving experiments in cells. The results showed that the knockdown of OR3A4 resulted in a decrease in cell proliferation and migration levels, which could be found by downregulating KLF6 expression. To further verify the relationship between lncRNA OR3A4 and cisplatin in the zebra fish xenograft model, we first tested the treated concentration of cisplatin in zebra fish. Because there may be differences between the soaking concentration and the concentration in zebra fish larvae, we started the experiment according to the general concentration of cells in experiment. We determined the appropriate concentration of cisplatin treatment according to the development of zebra fish larvae.

We found that the concentration of cisplatin equal to or higher than 0.8 mg/ml had a significant effect on the development and survival of zebra fish, whereas when the concentration of cisplatin was equal to or lower than 0.6 mg/ml, the development of zebra fish larvae was unaffected. Therefore, we used 0.6 mg/ml *in vivo* cisplatin treatment in zebra fish. Further studies have the responsibility for determining whether resistance to lncRNA OR3A4 is mediated by KLF6.

Moreover, cisplatin treatment combined with the knockdown of lncRNA OR3A4 enhanced tumor suppression, which may be related to the activation of innate immune cells, especially neutrophils. In this study, we first detected the role of neutrophils after tumor drug administration, which is a rapidly responsive cell in immunity. In further research, we will also study the role of macrophages, NK cells, T cells, B cells, and other immune cells in tumor killing.

DATA AVAILABILITY STATEMENT

The original contributions presented in the study are included in the article/supplementary material; further inquiries can be directed to the corresponding authors.

ETHICS STATEMENT

The animal study was reviewed and approved by Jilin University. Written informed consent was obtained from the owners for the participation of their animals in this study.

AUTHOR CONTRIBUTIONS

FG and JD conceived the project. HY and WS designed the experiments, and MZ and HY wrote the article. LL performed most of the experiments with help from YG and XF.

REFERENCES

Bowtell, D. D., Böhm, S., Ahmed, A. A., Aspuria, P. J., Bast, R. C., Beral, V., et al. (2015). Rethinking Ovarian Cancer II: Reducing Mortality from High-Grade Serous Ovarian Cancer. *Nat. Rev. Cancer* 15 (11), 668–679. doi:10.1038/nrc4019

Chen, J., Yu, Y., Li, H., Hu, Q., Chen, X., He, Y., et al. (2019). Long Noncoding RNA PVT1 Promotes Tumor Progression by Regulating the miR-143/HK2 axis in Gallbladder Cancer. *Mol. Cancer* 18 (1), 33. doi:10.1186/s12943-019-0947-9

Chen, Q., Liu, X., Xu, L., Wang, Y., Wang, S., Li, Q., et al. (2016). Long Noncoding RNA BACE1-AS Is a Novel Target for Anisomycin-Mediated Suppression of Ovarian Cancer Stem Cell Proliferation and Invasion. *Oncol. Rep.* 35 (4), 1916–1924. doi:10.3892/or.2016.4571

Coussens, L. M., and Werb, Z. (2002). Inflammation and Cancer. *Nature* 420 (6917), 860–867. doi:10.1038/nature01322

D'Astolfo, D. S., Gehrau, R. C., Bocco, J. L., and Koritschoner, N. P. (2008). Silencing of the Transcription Factor KLF6 by siRNA Leads to Cell Cycle Arrest and Sensitizes Cells to Apoptosis Induced by DNA Damage. *Cell Death Differ* 15 (3), 613–616. doi:10.1038/sj.cdd.4402299

DiFeo, A., Narla, G., Hirshfeld, J., Camacho-Vanegas, O., Narla, J., Rose, S. L., et al. (2006). Roles of KLF6 and KLF6-SV1 in Ovarian Cancer Progression and Intraperitoneal Dissemination. *Clin. Cancer Res.* 12 (12), 3730–3739. doi:10.1158/1078-0432.CCR-06-0054

Gao, Y., Xu, Y., Wang, J., Yang, X., Wen, L., and Feng, J. (2019). lncRNA MNX1-AS1 Promotes Glioblastoma Progression through Inhibition of miR-4443. *Oncol. Res.* 27 (3), 341–347. doi:10.3727/096504018X15228909735079

Guo, X., Yang, Z., Zhi, Q., Wang, D., Guo, L., Li, G., et al. (2016). Long Noncoding RNA OR3A4 Promotes Metastasis and Tumorigenicity in Gastric Cancer. *Oncotarget* 7 (21), 30276–30294. doi:10.18632/oncotarget.7217

Gutschner, T., and Diederichs, S. (2012). The Hallmarks of Cancer: a Long Noncoding RNA point of View. *RNA Biol.* 9 (6), 703–719. doi:10.4161/rna.20481

Han, X., and Gong, X. (2021). *In Situ*, One-Pot Method to Prepare Robust Superamphiphobic Cotton Fabrics for High Buoyancy and Good Antifouling. *ACS Appl. Mater. Inter.* 13 (26), 31298–31309. doi:10.1021/acsami.1c08844

Hanahan, D., and Weinberg, R. A. (2011). Hallmarks of Cancer: the Next Generation. *Cell* 144 (5), 646–674. doi:10.1016/j.cell.2011.02.013

Jemal, A., Siegel, R., Ward, E., Murray, T., Xu, J., and Thun, M. J. (2007). Cancer Statistics, 2007. *CA Cancer J. Clin.* 57 (1), 43–66. doi:10.3322/canjclin.57.1.43

Lang, U. E., Kocabayoglu, P., Cheng, G. Z., Ghiassi-Nejad, Z., Muñoz, U., Vetter, D., et al. (2013). GSK3β Phosphorylation of the KLF6 Tumor Suppressor Promotes its Transactivation of P21. *Oncogene* 32 (38), 4557–4564. doi:10.1038/onc.2012.457

Li, H., Liu, C., Lu, Z., Chen, L., Wang, J., Li, Y., et al. (2017). Upregulation of the Long Noncoding RNA SPRY4-IT1 Indicates a Poor Prognosis and Promotes Tumorigenesis in Ovarian Cancer. *Biomed. Pharmacother.* 88, 529–534. doi:10.1016/j.biopha.2017.01.037

Li, W., Fu, Q., Man, W., Guo, H., and Yang, P. (2019). LncRNA OR3A4 Participates in the Angiogenesis of Hepatocellular Carcinoma through Modulating AGGF1/akt/mTOR Pathway. *Eur. J. Pharmacol.* 849, 106–114. doi:10.1016/j.ejphar.2019.01.049

Li, X., Pang, L., Yang, Z., Liu, J., Li, W., and Wang, D. (2019). LncRNA HOTAIRM1/HOXA1 Axis Promotes Cell Proliferation, Migration and Invasion in Endometrial Cancer. *Onco Targets Ther.* 12, 10997–11015. doi:10.2147/OTT.S222334

Liu, G., Hu, X., and Zhou, G. (2017). Long Noncoding RNA OR3A4 Promotes Proliferation and Migration in Breast Cancer. *Biomed. Pharmacother.* 96, 426–433. doi:10.1016/j.biopha.2017.10.011

Long, X., Song, K., Hu, H., Tian, Q., Wang, W., Dong, Q., et al. (2019). Long Noncoding RNA GAS5 Inhibits DDP-Resistance and Tumor Progression of Epithelial Ovarian Cancer via GAS5-E2f4-PARP1-MAPK axis. *J. Exp. Clin. Cancer Res.* 38 (1), 345. doi:10.1186/s13046-019-1329-2

Lorenzen, J. M., and Thum, T. (2016). Long Noncoding RNAs in Kidney and Cardiovascular Diseases. *Nat. Rev. Nephrol.* 12 (6), 360–373. doi:10.1038/nrneph.2016.51

Luo, X., Qiu, Y., Jiang, Y., Chen, F., Jiang, L., Zhou, Y., et al. (2018). Long Noncoding RNA Implicated in the Invasion and Metastasis of Head and Neck Cancer: Possible Function and Mechanisms. *Mol. Cancer* 17 (1), 14. doi:10.1186/s12943-018-0763-7

Maass, P. G., Luft, F. C., and Bähring, S. (2014). Long Noncoding RNA in Health and Disease. *J. Mol. Med. (Berl)* 92 (4), 337–346. doi:10.1007/s00109-014-1131-8

Mercer, T. R., Dinger, M. E., and Mattick, J. S. (2009). Long Noncoding RNAs: Insights into Functions. *Nat. Rev. Genet.* 10 (3), 155–159. doi:10.1038/nrg2521

Narla, G., Heath, K. E., Reeves, H. L., Li, D., Giono, L. E., Kimmelman, A. C., et al. (2001). KLF6, a Candidate Tumor Suppressor Gene Mutated in Prostate Cancer. *Science* 294 (5551), 2563–2566. doi:10.1126/science.1066326

Qiu, J. J., Zhang, X. D., Tang, X. Y., Zheng, T. T., Zhang, Y., and Hua, K. Q. (2017). ElncRNA1, a Long Noncoding RNA that Is Transcriptionally Induced by Oestrogen, Promotes Epithelial Ovarian Cancer Cell Proliferation. *Int. J. Oncol.* 51 (2), 507–514. doi:10.3892/ijo.2017.4030

Reeves, H. L., Narla, G., Ogunbiyi, O., Haq, A. I., Katz, A., Benzeno, S., et al. (2004). Kruppel-like Factor 6 (KLF6) Is a Tumor-Suppressor Gene Frequently Inactivated in Colorectal Cancer. *Gastroenterology* 126 (4), 1090–1103. doi:10.1053/j.gastro.2004.01.005

Schmitt, A. M., and Chang, H. Y. (2016). Long Noncoding RNAs in Cancer Pathways. *Cancer Cell* 29 (4), 452–463. doi:10.1016/j.ccell.2016.03.010

Shang, J., Xu, Y. D., Zhang, Y. Y., and Li, M. (2019). Long Noncoding RNA OR3A4 Promotes Cisplatin Resistance of Non-small Cell Lung Cancer by Upregulating CDK1. *Eur. Rev. Med. Pharmacol. Sci.* 23 (10), 4220–4225. doi:10.26355/eurrev_201905_17926

Shi, T., Wang, P., Xie, C., Yin, S., Shi, D., Wei, C., et al. (2017). BRCA1 and BRCA2 Mutations in Ovarian Cancer Patients from China: Ethnic-Related Mutations in BRCA1 Associated with an Increased Risk of Ovarian Cancer. *Int. J. Cancer* 140 (9), 2051–2059. doi:10.1002/ijc.30633

Tomita, M., Shimizu, T., Ayabe, T., Yonei, A., and Onitsuka, T. (2011). Preoperative Neutrophil to Lymphocyte Ratio as a Prognostic Predictor after Curative Resection for Non-small Cell Lung Cancer. *Anticancer Res.* 31 (9), 2995–2998.

Watanabe, K., Ohnishi, S., Manabe, I., Nagai, R., and Kadowaki, T. (2008). KLF6 in Nonalcoholic Fatty Liver Disease: Role of Fibrogenesis and Carcinogenesis. *Gastroenterology* 135 (1), 309–312. doi:10.1053/j.gastro.2008.06.014

Xu, J., Ni, C., Ma, C., Zhang, L., Jing, X., Li, C., et al. (2017). Association of Neutrophil/lymphocyte Ratio and Platelet/lymphocyte Ratio with ER and PR in Breast Cancer Patients and Their Changes after Neoadjuvant Chemotherapy. *Clin. Transl Oncol.* 19 (8), 989–996. doi:10.1007/s12094-017-1630-5

Yadav, R. K., Gautam, D. K., Muj, C., Gajula Balija, M. B., and Paddibhatla, I. (2021). Methotrexate Negatively Acts on Inflammatory Responses Triggered in Drosophila Larva with Hyperactive JAK/STAT Pathway. *Dev. Comp. Immunol.* 123, 104161. doi:10.1016/j.dci.2021.104161

Yu, J., Han, Q., and Cui, Y. (2017). Decreased Long Noncoding RNA SPRY4-IT1 Contributes to Ovarian Cancer Cell Metastasis Partly via Affecting Epithelial-Mesenchymal Transition. *Tumour Biol.* 39 (7), 1010428317709129. doi:10.1177/1010428317709129

Zhan, L., Li, J., and Wei, B. (2018). Long Noncoding RNAs in Ovarian Cancer. *J. Exp. Clin. Cancer Res.* 37 (1), 120. doi:10.1186/s13046-018-0793-4

Zhang, B., Guo, D. D., Zheng, J. Y., and Wu, Y. A. (2018). Expression of KLF6-SV2 in Colorectal Cancer and its Impact on Proliferation and Apoptosis. *Eur. J. Cancer Prev.* 27 (1), 20–26. doi:10.1097/CEJ.0000000000000410

Zhang, H., Chen, Z., Wang, X., Huang, Z., He, Z., and Chen, Y. (2013). Long Noncoding RNA: a New Player in Cancer. *J. Hematol. Oncol.* 6, 37. doi:10.1186/1756-8722-6-37

Zhang, J., Zhang, L., and Gong, X. (2021). Large-Scale Spraying Fabrication of Robust Fluorine-free Superhydrophobic Coatings Based on Dual-Sized Silica Particles for Effective Antipollution and Strong Buoyancy. *Langmuir* 37 (19), 6042–6051. doi:10.1021/acs.langmuir.1c00706

Zhong, M., Wang, W. L., and Yu, D. J. (2019). Long Noncoding RNA OR3A4 Is Associated with Poor Prognosis of Human Non-small Cell Lung Cancer and Regulates Cell Proliferation via Up-Regulating SOX4. *Eur. Rev. Med. Pharmacol. Sci.* 23 (15), 6524–6530. doi:10.26355/eurrev_201908_18537

Conflict of Interest: The authors declare that the research was conducted in the absence of any commercial or financial relationships that could be construed as a potential conflict of interest.

Publisher's Note: All claims expressed in this article are solely those of the authors and do not necessarily represent those of their affiliated organizations, or those of the publisher, the editors, and the reviewers. Any product that may be evaluated in this article, or claim that may be made by its manufacturer, is not guaranteed or endorsed by the publisher.

frontiers in Pharmacology

REVIEW
published: 15 November 2021
doi: 10.3389/fphar.2021.779425

Therapeutic Development by Targeting the cGAS-STING Pathway in Autoimmune Disease and Cancer

Qiumei Li[1], *Shuoran Tian*[1], *Jiadi Liang*[1], *Jiqiang Fan*[1], *Junzhong Lai*[2]* *and Qi Chen*[1]*

[1]*Fujian Key Laboratory of Innate Immune Biology, Biomedical Research Center of South China, Fujian Normal University, Fuzhou, China,* [2]*The Cancer Center, Union Hospital, Fujian Medical University, Fuzhou, China*

DNA immune recognition regulation mediated by the cGAS-STING pathway plays an important role in immune functions. Under normal physiological conditions, cGAS can recognize and bind to invading pathogen DNA and activate the innate immune response. On the other hand, abnormal activation of cGAS or STING is closely related to autoimmune diseases. In addition, activation of STING proteins as a bridge connecting innate immunity and adaptive immunity can effectively restrain tumor growth. Therefore, targeting the cGAS-STING pathway can alleviate autoimmune symptoms and be a potential drug target for treating cancer. This article summarizes the current progress on cGAS-STING pathway modulators and lays the foundation for further investigating therapeutic development in autoimmune diseases and tumors.

Keywords: innate immunity, cGAS-STING pathway, autoimmune disease, cancer, therapeutic development

OPEN ACCESS

Edited by:
Gerard Bannenberg,
Global Organization for EPA and DHA Omega-3s (GOED), United States

Reviewed by:
Sam Campos,
The University of Arizona, United States
Chunfu Zheng,
University of Calgary, Canada

***Correspondence:**
Junzhong Lai
850408633@qq.com
Qi Chen
chenqi@fjnu.edu.cn

Specialty section:
This article was submitted to Inflammation Pharmacology, a section of the journal Frontiers in Pharmacology

Received: *20 September 2021*
Accepted: *18 October 2021*
Published: *15 November 2021*

Citation:
Li Q, Tian S, Liang J, Fan J, Lai J and Chen Q (2021) Therapeutic Development by Targeting the cGAS-STING Pathway in Autoimmune Disease and Cancer. Front. Pharmacol. 12:779425. doi: 10.3389/fphar.2021.779425

INTRODUCTION

Innate Immunity and Immune Diseases

Innate Immunity and cGAS-STING Signaling Pathway

The human immune system uses pattern recognition to sense infection and trigger an immune response against pathogen invasion. At the beginning of the 21st century, TLR9 was the only known foreign DNA pattern recognition receptor (PRR). In 2006, Medzhitov and Stetson reported a novel DNA-sensing immune response independent of TLR9 which can lead to interferon regulatory factor 3 (IRF3) mediated type I interferon production (Stetson and Medzhitov, 2006). They further found that the abnormal accumulation of cytoplasmic DNA caused by the abnormality of 3′ repair exonuclease 1 (Trex1) could be sensed by unknown DNA receptors leading to fatal autoimmune symptoms (Stetson et al., 2008). By the end of 2012, Chen's team discovered a novel second messenger molecule, guanine cyclic dinucleotide (cGAMP), and its synthase cGAMP synthase (cGAS), and demonstrated that cGAS could recognize abnormal DNA in the cytoplasm and induce an innate immune response named "the cGAS-STING signaling pathway" (Ablasser et al., 2013). In the absence of double-stranded DNA (dsDNA), cGAS is in a dormant state. When a virus invades the body or when cell damage causes abnormal dsDNA accumulation in the cytoplasm, cGAS can recognize and bind to dsDNA, actively form a dimer, and catalyze the synthesis of ATP and GTP into cGAMP with phosphodiester bonds (2′3′-cGAMP). cGAMP is an endogenous ligand of STING protein located on the endoplasmic reticulum membrane. After STING is activated, the conformation of STING changes and STING moves from the endoplasmic reticulum to the Golgi apparatus, and then recruits TANK-binding kinase 1 (TBK1) and phosphorylates IRF3. Phosphorylated IRF3 forms a dimer and enters the nucleus. At the same time, STING can also activate IKK kinase

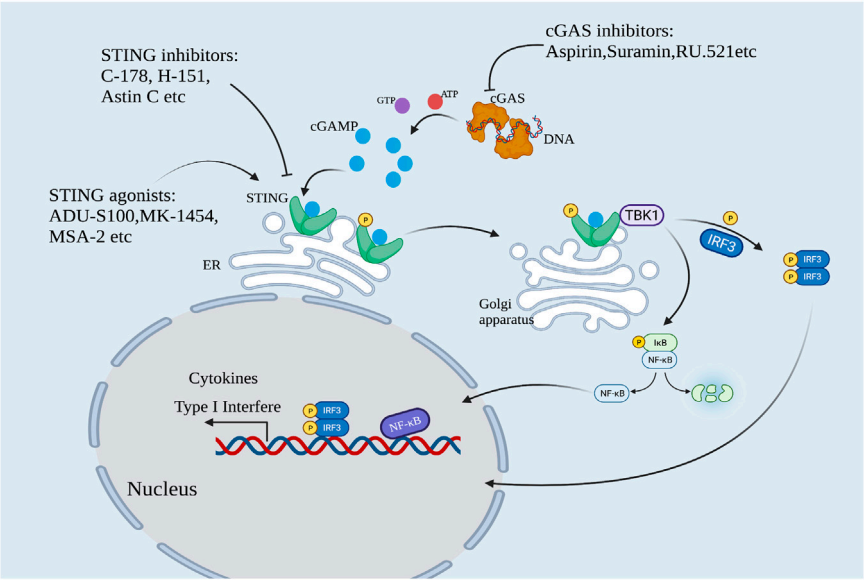

FIGURE 1 | The cGAS-STING pathway. cGAS is activated by sensing cytoplasmic DNA. Activated cGAS catalyzes the formation of cGAMP. cGAMP activates STING protein, and activated STING recruits TBK1 and phosphorylates IRF3. Meanwhile, STING activated IKK kinase and phosphorylated IκB, leading to the release of NF-κB. Phosphorylated IRF3 formed dimer and translocated with NF-κB into the nucleus to synergistically induce the expression of IFN-I and various inflammatory factors. This pathway can be regulated by cGAS and STING modulators.

(inhibitor of nuclear factor kappa-B kinase) and phosphorylate IκB, causing its degradation and the release of NF-κB. IRF3, NF-κB, and other regulatory factors in the nucleus work together to induce the expression of type I interferon (IFN-I) and various inflammatory factors (e.g., TNF, IL-6, and IL-1β), and initiate the innate immune response (**Figure 1**).

Autoimmune Diseases and the cGAS-STING Signaling Pathway

The cGAS-STING pathway plays an important role in innate immunity, but cGAS can also be activated by the body's abnormal DNA to cause tissue damage or autoimmune diseases, such as Aicardi-Goutières syndrome (AGS), systemic lupus erythematosus (SLE), primary biliary liver disease. Genetic studies have shown that mutations in the genes prevent abnormal accumulation of cytoplasmic DNA, such as DNA exonuclease Trex1 (Crow et al., 2006), deoxyribonuclease-II (DNAse-II) (Kawane et al., 2001), and adenosine deaminase ADAR1 (Hartner et al., 2009), can lead to these diseases. Our group constructed a Trex1-D18N point mutation model in mice by using the CRISPR/Cas9 technology. The mice exhibit a systemic inflammatory phenotype, similar to familial chilblain lupus (FCL) and SLE. In this model, the inactivation of TREX1 leads to abnormal accumulation of dsDNA in the cytoplasm, which leads to the overexpression of IFN-I. However, after the cGAS gene is knocked out, abnormal IFN-I levels return to normal, and systemic inflammatory response and abnormal activation of T cells are effectively alleviated (Xiao et al., 2019), underscoring the role of the cGAS-STING pathway in such diseases and making it an important target for the development of drugs to treat these diseases (Abe et al., 2013).

On the other hand, the cGAS-STING pathway is also an important monitoring mechanism in the body's antitumor immunity. In the process of immune surveillance, cGAS can detect the DNA leaked into the cytoplasm during abnormal mitosis that often occurs in malignant cells, induce the secretion of IFN-I, which stimulates the presentation of tumor antigens, and activates tumor-specific $CD8^+$ effector T cells to exert the antitumor effect (Duewell et al., 2014). In addition, dendritic cells (DCs) can recognize tumor-derived DNA to express IFN-I and initiate antitumor immunity (Deng et al., 2014). It is worth noting that the cGAS-STING pathway is defective in many cancer types, including melanoma and colorectal cancer (Ridker et al., 2017). Increasing evidence indicates that the specific activation of STING can stimulate innate immunity and promotes T cell infiltration into the tumor microenvironment (TME), thereby suppress tumor progression (Düwell et al., 2019).

Modulating the cGAS-STING pathway and expression of IFN-I and related inflammatory factors are important in alleviating autoimmune diseases caused by immune abnormalities. In addition, cGAS and STING can serve as a bridge connecting innate immunity and adaptive immunity and regulate the occurrence and development of malignant tumors (Parlato and Yeretssian, 2014). Therefore, targeting the cGAS-STING pathway has great therapeutic potential and is receiving much attention in the pharmaceutical field. In the following, we summarized the current progress in developing molecular agents targeting the cGAS-STING pathway, and their therapeutic potential is also discussed.

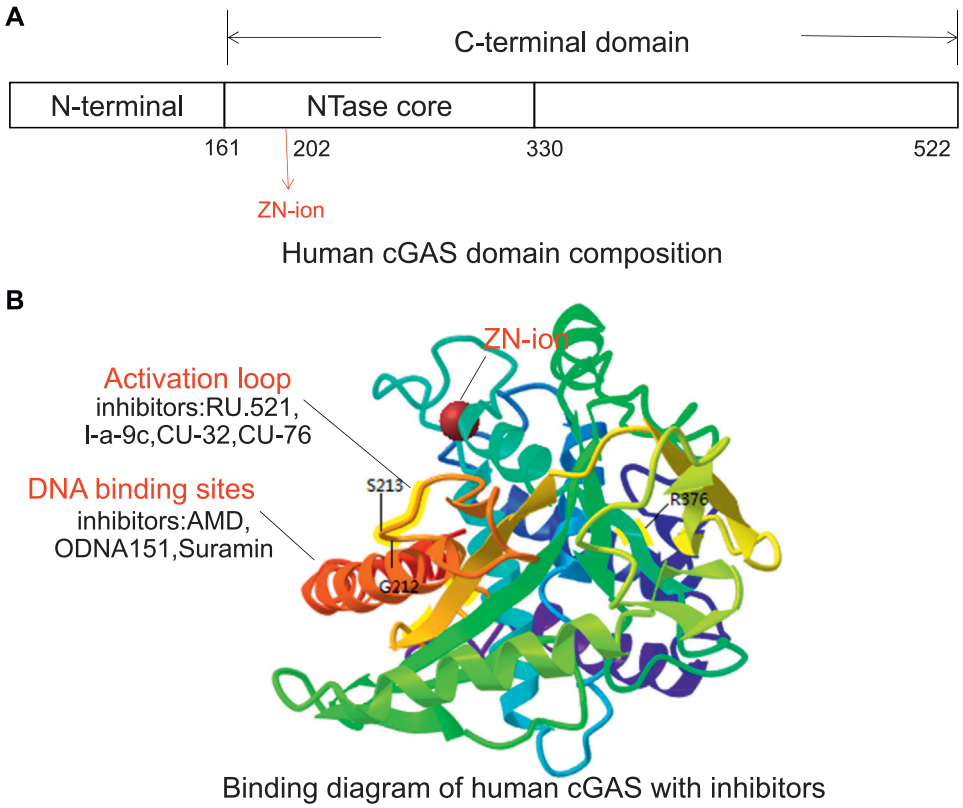

FIGURE 2 | The potential targeting sites of cGAS modulators, as shown on the X-ray crystal structure of human cGAS (Adopted from PDB ID: 4KM5). **(A)** Human cGAS domain composition. The human cGAS structure contains N-terminal helical extensions (amino acid residues 1–160) and C-terminal domains (amino acid residues 161–522). A unique zinc ion is located at position 202. **(B)** Binding diagram of human cGAS with inhibitors. The G212, S213, and R376 sites in the activation loop are the key sites of cGAS binging substrate (ATP + GTP). The inhibitors that target DNA binding sites include AMD, ODNA151, and suramin, and the inhibitors targeting ATP and GTP binding sites include RU.521, CU-32, CU-76, and I-a-9c.

cGAS INHIBITORS

Structural Features of cGAS

The cGAS protein is a member of the nucleotide transferase family. It contains an N-terminal domain and a C-terminal domain with a specific zinc-ion-binding module (**Figure 2**). The zinc-band structure mediates the binding of cGAS to the phosphate ribose backbone of dsDNA and the dimerization of cGAS and participates in the synthesis of 2′3′-cGAMP. The catalytic domain of cGAS is the NTase family, whose N-terminus contains all catalytic residues (Zhang et al., 2020). In 2013, Kranzusch et al. (2013), Kato et al. (2013), and Li et al. (2013a) reported the crystal structure of cGAS protein without binding dsDNA or ligand. Point mutation studies have shown that certain amino acid residues such as Lys335 (m-cGAS)/ Lys347 (h-cGAS) are important for forming cGAS dimers and cGAS functions. cGAS activity is eliminated by Lys335 and Lys382 (m-cGAS)/Lys394 (h-cGAS) point mutations (Zhang et al., 2014). In addition, Tyr436 and Arg376 can form π-π stacking and π-cation with the aromatic center of the ligand, respectively. The amino group of Lys362 can form a salt bridge with the phosphate group of cGAMP, and the amino hydrogen on Asp227 adenine can interact with Asp319. The carboxyl oxygen forms a hydrogen bond. These amino acids exert a synergistic effect in cGAS functions (Chen, 2019). The crystal structure analysis provides a foundation for structure-based drug design and development (Hall et al., 2017a).

Current cGAS Inhibitors

The development of cGAS inhibitors is at its initial stage. The currently known cGAS inhibitors can be divided into non-substrate competitive inhibitors and substrate competitive inhibitors according to whether they act on the active site of cGAS substrates. Non-substrate competitive inhibitors usually inhibit the activity of cGAS by binding to the necessary groups other than the active center, such as aspirin. Substrate competitive inhibitors usually share structural similarities with the substrate for binding, thereby reversibly inhibiting enzyme activity, such as RU.521. The following is a detailed description of the currently known cGAS inhibitors (**Table 1**).

Aspirin

The classic drug aspirin is a non-steroidal anti-inflammatory drug (NSAID), which is known to acetylate proteins such as

TABLE 1 | cGAS inhibitors.

cGAS inhibitors	Inhibition mechanism	Biological effect	Refs
Aspirin	Acetylated Lys amino group of cGAS protein	Improved DNA-mediated autoimmune responses in mouse and AGS patient cells	Shakespear et al. (2011); Dai et al. (2019)
AMDs	It binds to dsDNA and occupies the binding site of cGAS	In THP-1 cells, the IC_{50} dose range of AMDS was 3–25 μM	An et al. (2015); Bose et al. (2016)
ODN A151	Telomere sequences and thiophosphate mainchains compete with DNA for cGAS	Inhibit the expression of type I interferon in THP-1 cells and the activation of cGAS in its Trex1$^{-/-}$ cells	Steinhagen et al. (2018)
RU.521	Occupy the catalytic sites of cGAS and competes with ATP	The IC_{50} in macrophages is 700 nM	Vincent et al. (2017); Lama et al. (2019)
PF-06928215	Binding to cGAS active site	It was verified in THP-1 cells	Hall et al. (2017b); Zhao et al. (2020)
Suramin	As a nucleic acid analog, it prevents cGAS from binding to dsDNA	Regulates the production of IFN-I in THP-1 cells	Wang et al. (2018); Padilla-Salinas et al. (2020)
I-a-9c	At the DNA binding site of cGAS, Tyr436, Arg376, and Asp227 form forces	The inhibition rate of cGAS was 83.9% at the 10 μM level	Chen (2019)
CU-32 CU-76	The zinc capsule structure inserted into cGAS inhibits the formation of dimer	The cGAS-STING pathway was specifically inhibited	Hall et al. (2017b); Padilla-Salinas et al. (2020)

cyclooxygenase (COX) (Shakespear et al., 2011). Studies have shown that aspirin can inhibit the activity of human cGAS by regulating its post-translational modification in patient cells by acetylating Lys384, Lys394, or Lys494 (Dai et al., 2019). Aspirin improves DNA-mediated autoimmune responses in mice and patients with AGS by inhibiting the function of cGAS (Dai et al., 2019). At present, aspirin is widely used in clinical practice, with 2,269 items registered clinical trials on the NIH list. Its pharmacological action and pharmacological metabolism have been well defined. These findings suggest that aspirin can act as a human cGAS inhibitor for the treatment of immune diseases.

Antimalarial Drugs

Antimalarial drugs (AMDs), a family of widely used drugs for the treatment of malaria, have proved a safety profile. In 2015, An et al. reported a series of AMDs that can interfere with the binding of cGAS and dsDNA, including hydroxychloroquine sulfate (HCQ), chloroquine (CQ), and quinine (QN) (An et al., 2015). The results show that HCQ can inhibit cGAS activity by non-specific binding of aminoquinoline and aminoacridine, taking up the DNA binding sites R342 and K372. In addition, their inhibition of cGAS activity and IFN-β production is dose-dependent. For example, the half-maximal inhibitory concentration (IC_{50}) of AMDs in THP-1 cells is in the dose range of 3–25 μM, while the IC_{50} of QN is 13 μM (Bose et al., 2016). Because of the good safety profile of AMDs and its inhibitory capability on cGAS, the interaction between AMD and cGAS provides a new therapeutic strategy for the treatment of innate immune diseases.

An Oligodeoxynucleotide Containing a TTAGGG Modified Fragment (ODNs)

In 2018, Steinhagen et al. reported that ODNs containing the TTAGGG modified fragment could inhibit cGAS activity (Steinhagen et al., 2018). It inhibited the expression of type I interferon in THP-1 cells and the activation of cGAS in *Trex1*$^{-/-}$ cells. Among them, the inhibitory activity of ODN A151 depends on the telomere sequence and phosphorothioate backbone to prevent cGAS activation by competing with DNA (Steinhagen et al., 2018), laying the foundation for developing new immunosuppressive agents to treat autoimmune diseases caused by cGAS abnormal activation.

The RU Series of Compounds

Some drugs bind to cGAS, thereby affecting the affinity of ATP or GTP to cGAS, which is the key to inhibition. In 2017, Vincent et al. reported that the RU series of compounds could occupy the catalytic sites Arg364 and Tyr421 of cGAS in mice, reduce the binding affinity of cGAS to ATP and GTP suppress the expression of interferon in primary macrophages (Vincent et al., 2017). RU.521 showed good activity in the macrophages derived from the AGS mouse model (IC_{50} = 700 nM). Due to the low signal of human cGAS (h-cGAS) in RF mass spectrometry, accurate kinetic characterization cannot be carried out (Lama et al., 2019). Based on the significant inhibition of the RU series of compounds on murine cGAS, the RU series of compounds are expected to be used as human cGAS inhibitors but need further investigation.

The PF Series of Compounds

In 2017, Hall et al. reported the PF series of compounds with a high affinity for binding human cGAS by a novel fluorescence polarization method (Hall et al., 2017b). The study found that PF-06928215 bound to cGAS efficiently and showed high inhibitory activity *in vitro*. Later, Zhao's research group reported the discovery of a novel human cGAS catalytic domain ($H\text{-}cGAS^{CD}$) and screened out the PF compounds S2 (IC_{50} = 13.1 ± 0.09 μM) and S3 (IC_{50} = 4.9 ± 0.26 μM) as h-cGAS inhibitors (Zhao et al., 2020). These studies lay a foundation for the further application of PF compounds.

Suramin

Suramin has a variety of functions and many clinical applications. So far, there are 21 suramin-related clinical trials on the NIH list. Its toxicological characteristics and target structure are clear. In 2018, Wang et al. reported that

suramin could inhibit cGAS and regulate the production of type I interferon (Wang et al., 2018). It is showed that suramin, as a nucleic acid analog, blocks the binding of cGAS to dsDNA. However, suramin may interact with the Toll-like receptor 3 (TLR 3) pathway to produce off-target effects as well (Padilla-Salinas et al., 2020). Therefore, structure optimization of suramin needs to be further conducted.

Substituted Acetamides

At present, few skeleton structures of cGAS nucleoside site inhibitors have been reported. In 2019, Chen reported the synthesis of cGAS inhibitor pharmacophore based on the cGAS receptor-ligand complex structure (Chen, 2019). Conformational analysis shows that the original receptor-ligand binding effect between the compound I-a-9-c and cGAS. Tyr436 and Arg376 can form π-π stacking and π-cation with the aromatic center of the I-a-9c, respectively. In addition, the hydroxyl group on its propanol group can also form a hydrogen bond with the carboxyl group of Asp 227 in cGAS, and the hydrogen bond improves the inhibition of cGAS activity. The inhibitory rate of I-a-9c on the cGAS activity at 10 μM is 83.9% in THP-1 cells (Chen, 2019). These compounds have low toxicity and high efficiency, so it has potential for further development.

The CU Series of Compounds

Crystal structure studies have shown that the two DNA-binding surfaces and the protein-protein interface (PPI) of cGAS play an important role in IRF3 activation and IFN-β induction (Hall et al., 2017b). In 2019, Padilla-Salinas et al. reported a novel drug binding site of cGAS at Z9189 by targeting the PPI of human cGAS (Padilla-Salinas et al., 2020). Structural docking indicated that the inhibitor CU series of compounds targeting Z9189 might be inserted into the zinc capsule structure of cGAS, thus inhibiting dimer formation through the allosteric effect. It is worth noting that CU-32 and CU-76 specifically inhibit the cGAS-STING pathway but have no significant effect on the RIG-I-MAVs pathway or the TLR pathway. Further studies showed that the IC_{50} values of CU-32 and CU-76 in THP-1 cells were 0.66 and 0.27 μM, respectively, and the inhibitory effect was dose-dependent (Padilla-Salinas et al., 2020), which provides a new chemical scaffold for developing cGAS inhibitors.

RESEARCH STATUS OF STING MODULATORS

Increasing evidence indicates that persistent activation of STING is associated with the pathogenesis of autoimmune diseases induced by its gene mutations, such as AGS (Barber, 2015), autoimmune myocarditis (Kwon and Bakhoum, 2020), multiple arthritis, and other related vascular diseases (Feng et al., 2020). These diseases occur in infants with family history and pose a serious threat to human life and health. Therefore, STING is an attractive target for therapeutic intervention.

Structural Characteristics of STING

The human STING (h-STING) protein, as a homodimer, consists of a luminal N-terminal domain (four transmembranes helically anchored ER: TM1-4) and a cytoplasmic C-terminal domain (CTD) containing ligand binding pockets (Wang et al., 2014) (**Figure 3**). The crystal structure of CTD dimer shows that without cGAMP, the ligand-binding domain (LBD) is in an inactive open conformation. cGAMP binding induces the CTD of the STING dimer to turn clockwise relative to the transmembrane domain (TMD) (Wang et al., 2014). Rotating 180° causes the formation of β-sheets, covering the ligand-binding pocket, causing STING to become an active closed state. Point mutation studies have shown that the residues in the N-terminal helical loop, V147 L, N154 S, and V155 M, may contribute to the conformational change of STING. After the ligand binds to STING, the STING TMD is modified post-translationally, and STING was translocated from the endoplasmic reticulum to the Golgi apparatus, in which palmitoylation of Cys88/91 is crucial to the activation of STING. STING binds to the TBK1 dimer through the C-terminal, activates TBK1, and phosphorylates IRF3, and the main phosphorylation site is Ser366 at the C-terminal (Weerapana et al., 2010). The phosphorylation at Ser172 of TBK1 is required for its activation (Mukai et al., 2016). Although the specific mechanism of STING activation needs further investigation, these analyses lay the foundation for structure-based drug design to facilitate the research and development of novel immune regulatory agents with high efficiency and low toxicity. The currently known STING inhibitors are listed on **Table 2**.

STING Inhibitors

Nitrofuran Derivatives

Palmitoylation of STING is a post-translational modification critical for the assembly of STING into polymer complexes in the Golgi apparatus and recruitment of downstream signal factors (Zhang et al., 2013). In 2018, Haag et al. reported that nitrofuran derivative C-178 and indoles derivative H-151-Al (H-151) were irreversible inhibitors of mouse STING (m-STING) and human STING (h-STING), respectively (Haag et al., 2018). The main inhibitory mechanism was that C-178 forms covalent bonds with Cys91 and Cys88 of STING TMD, which affects the palmitoylation of STING. Unlike C-178 and H-151, Hansen et al. reported that nitro-fatty acids (NO_2-FAs/CXA-10) had an inhibitory effect on either mouse or human STING (Hansen et al., 2018). NO_2-FAs forms a covalent bond with Cys88/91 and N-terminal His16, which affects the palmitoylation of STING and inhibits TBK1 phosphorylation in the fibroblasts derived from patients of STING-associated vascular disease (SAVI). Additionally, CXA-10, a STING inhibitor, has also entered clinical trials as an oral peroxisome proliferator-activated receptor agonist (PPAR) for the treatment of primary focal segmental glomerulosclerosis (FSGS) (Hansen et al., 2018).

Astin C

STING can be directly associated with cyclic dinucleotides (CDNs) to activate the downstream immune response

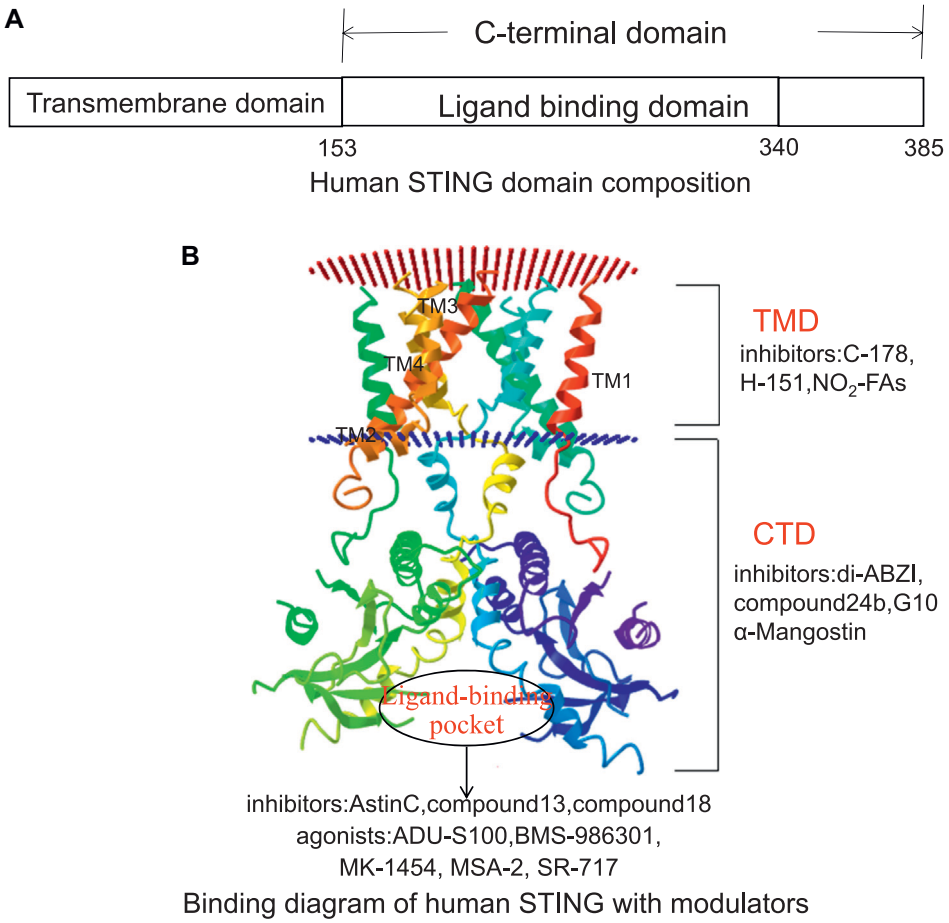

FIGURE 3 | The potential targeting sites of STING modulators, as shown on the Cryo-EM structure of human STING (Adopted from PDB ID: 6NT5). **(A)** Human STING domain composition. Human STING protein, as a homologous dimer, is composed of a luminal N-terminal domain (TMD, amino acid residues 1–152) and a cytoplasmic C-terminal domain (CTD, amino acid residues 153–385) containing ligand-binding domain (amino acid residues 153–340). **(B)** Binding diagram of human STING with modulators. The inhibitors targeting the TMD domain include C-178, H-151, and NO_2-FAs. The inhibitors targeting the CTD domain include di-ABZI, Compound 24b, G10, and α-Mangostin. The inhibitors targeting the ligand-binding sites include astin C, Compound13, and Compound18. Its agonists include ADU-S100, BMS-986301, MK-1454, MSA-2, and SR-717.

TABLE 2 | STING inhibitors.

STING inhibitors	Inhibition mechanism	Biological effect	Refs
C-178, H-151	It forms a covalent bond with TMD Cys91 and Cys88	The therapeutic effect was shown in the Trex1$^{-/-}$ mouse tumor model	Haag et al. (2018)
NO_2-FAs	It forms covalent bonds with Cys88/91 and N-terminal His16	It was demonstrated in fibroblasts from SAVI patients	Hansen et al. (2018)
Astin C	Binding to Ser162, Tyr163, and Arg238 occupy site pockets	The IC_{50} values in mouse and human fibroblasts were 3.4 and 10.8 μM, respectively	Burdette et al. (2011); Li et al. (2018)
Compound 18	Hydrogen bonding is formed with Thr263 by carboxyl group	EC_{50} = 30 μM, IC_{50} = 11 μM	Siu et al. (2019)

(Burdette et al., 2011). In 2018, Li et al. reported that astin C, a natural cyclic peptide from Aster, inhibited the innate immune CDN sensor STING (Li et al., 2018). Astin C specifically binds to the CTD region of STING and occupies the cGAMP binding pocket by interacting with Ser162, Tyr163, and Arg238 to inhibit h-STING functions. In isothermal titration calorimetry, astin C binding to STING can be abolished by high concentrations of cGAMP. In addition, astin C inhibited

TABLE 3 | STING agonists.

STING agonists	Activation mechanism	Biological effect	Refs
ADU-S100, BMS-986301, MK-1454	Binding with LBD in STING	They are indicated for the treatment of advanced solid tumors with monotherapy and combined ICIs	Dubensky et al. (2013); Corrales et al. (2015); Meric-Bernstam et al. (2019) Ding et al. (2020) Harrington et al. (2018)
Di-ABZI, Compound 24b	Binding with Ser241 and Ser162	EC_{50} of di-ABZI was 130 nM; Compound 24b EC_{50} = 0.287 μM	Ramanjulu et al. (2018) Xi et al. (2020)
C11, BNBC	Binding with h-STING	Specifically activate STING mediated immune responses and effectively block replication of multiple alphavirus types	Gall et al. (2018) Zhang et al. (2019)
Kitacinnamycins 8	Binding with STING	Increased poly (dA:dT) and cGAMP-induced IFN-β expression	Shi et al. (2019)
DMXAA	Binding with m-STING	Activates the TBK1-IRF3 pathway and shows good activity in mouse solid tumors	Kim et al. (2013a)
α-Mangostin, G10	Binding with the CTD region of h-STING	Activated the STING-TBK1-IRF3 pathway. The EC_{50} of G10 ranged from 2.5–4.3 μM. α -Mangosteen can repolarize M2 macrophages into M1 phenotype	Zhang et al. (2018) Banerjee et al. (2020)
DSDP	Binding with h-STING	Induces STING-dependent cytokine responses in HFF and PBMCs cells and effectively inhibits the replication of a variety of viruses	Liu et al. (2017)
MSA-2	Binding with STING	Persistent antitumor immunity and synergistic anti-PD-1 therapy	Pan et al. (2020)
SR-717	Binding with STING	Antitumor activity	Chin et al. (2020)

IFN-β mRNA expression in mouse and human fibroblasts with the IC_{50} values of 3.42 and 10.83 μM, respectively (Li et al., 2018). Based on the high efficiency and low toxicity. Astin C may be used to treat STING dysfunction-mediated diseases.

Derivatives Containing Carboxylic Acids

Targeting the large protein pocket in STING is a challenge since the molecular weight of its endogenous ligand cGAMP is relatively high (Burdette and Vance, 2013). In 2019, Siu et al. reported that by using the symmetry of STING protein, small molecules (derivatives containing carboxylic acids) were screened to bind to the open conformation of STING in the ratio of 2:1 (Siu et al., 2019). Such binding stoichiometry can fully occupy the large binding site while maintaining oral drugs' good physical and chemical properties. As the antagonists of h-STING, the selected carboxylic acid derivatives of Compound 13 (Siu et al., 2019) (EC_{50} = 30 μM, IC_{50} = 11.5 μM) and 18 (EC_{50} = 30 μM, IC_{50} = 11 μM) formed hydrogen bonds with Thr263 through carboxyl groups and stabilized the open conformation of STING. With a binding ratio of 2:1, there is a risk of instability in the drug potency. Therefore, two-dimensional optimization of protein-ligand and ligand-ligand interactions is needed to improve valence efficiency (Siu et al., 2019).

STING Agonists

Activating the cGAS-STING pathway can enhance the immune response and restrain tumor growth. In addition, STING agonists can be used as adjuvants to develop vaccines against certain infectious diseases, such as HIV and malaria. Currently, most STING activators are synthetic CDNs. The entry of cGAMP into cells can overcome the escape of cGAS recognition by pathogens (Li et al., 2013b), and activate the interferon response driven by STING in DCs, thereby promoting the formation of major histocompatibility complex presenting tumor-associated antigens to activate $CD8^+$ T cells for antitumor killing (Li et al., 2016). Several known STING agonists are described below (**Table 3**).

Cyclic Dinucleotides

In recent years, CDNs have become a class of STING agonists with anticancer effects (Dubensky et al., 2013). In 2015, Corrales et al. reported that CDNs can bind to the ligand-binding domain of STING and activate it, thereby affecting the vascular system and tumor microenvironment and initiating the activities of APC (antigen-presenting cells) and $CD8^+$ T cells (Corrales et al., 2015). Intratumoral injection of CDNs produces a significant antitumor T cell immune response, prevents distal metastasis of lung cancer, generates immune memory, and causes complete tumor regression (Corrales et al., 2015). One of their CDNs was named ADU-S100. In 2019, Meric-Bernstam et al. reported that in comparison to cGAMP, ADU-S100 shows better metabolic stability and higher effectivity in activating STING (Meric-Bernstam et al., 2019). Currently, ADU-S100 is undergoing clinical trials as a STING agonist.

BMS-986301, a cyclodinucleotide derivative originally developed by IFM Therapeutics, was presented by Bristol Myers Squibb (BMS) at the Cancer ImmunoTherapy Society (SITC) in 2018. In May of 2019, BMS-986301 entered a phase 1 trial (Clinical Trials.gov ID: NCT03956680) to treat advanced solid tumors with monotherapy combined with immune checkpoint inhibitors (ICIs). However, the structure of BMS-986301 has not been fully determined (Ding et al., 2020).

In 2018, Harrington et al. reported that cyclic dinucleotide MK-1454 induced complete tumor regression through intratumoral administration and enhanced the efficacy of anti-PD-1 therapy in a homologous mouse tumor model (Harrington

et al., 2018). MK-1454 has entered a clinical trial (NCT03010176) to treat advanced solid tumors (Harrington et al., 2018). These drugs have a high safety profile, and their maximum tolerated dose (MTD) has not been determined and should be further studied.

Nonnucleotide Agonists

Amide Compounds

Cyclic dinucleotide agonists are limited in their clinical application due to their high polarity and proteolytic tendency. In recent years, non-nucleotide derivatives have gained prominence due to their high specificity and effectiveness. In 2018, Ramanjulu et al. reported the synthesis of symmetrically related amide benzimidazole (ABZI) compound, which enhanced the binding and cellular function of STING (Ramanjulu et al., 2018). This formamide compound is anchored to Ser241 in the STING CTD region by hydrogen bonds. The pyrazole ring is located at the bottom of the binding pocket and connected to Ser162 by hydrogen bonds. In addition, two ABZI subunits on N1 benzimidazole bind to the pocket. These effects significantly enhance the binding affinity between STING and di-ABZI. In human peripheral blood mononuclear cells (h-PBMCs), di-ABZIs can induce IFN-β with EC_{50} of 130 nM, 400 times higher than cGAMP, without apparent toxicity. Furthermore, di-ABZI caused significant tumor volume regression by intravenous administration in a mouse model of colon tumors (Ramanjulu et al., 2018). In 2020, Xi et al. reported that amino benzimidazole derivatives - Compound 16g, 24b, and 24e, all STING agonists significantly increase the expression of IFN-β, CXCL10, and IL-6 and promote the phosphorylation of STING, TBK1, and IRF3 in h-PBMC and THP-1 cells (Xi et al., 2020). They also have significant antitumor effects when given intravenously in mice with colorectal tumors. Compounds 16g, 24b, and 24e in THP-1 cells showed high safety with the EC_{50} values of 1.24, 0.287, and 1.14 μM (Xi et al., 2020). Since then, N-(methylcarbamoyl)-2-{[5-(4-methylphenyl)-1,3,4-oxadiazol-2-yl]sulfanyl}-2-phenylacetamide (C11) (Gall et al., 2018) and 6-bromo-n -(naphthalen-1-yl)-benzo (d) (Stetson and Medzhitov, 2006; Ablasser et al., 2013) dioxole-5-carboxamide (BNBC) (Zhang et al., 2019) have been identified as h-STING agonists. In human fibroblasts (THF) and myeloid cell lines (MM6), C11 and BNBC can specifically activate STING-mediated transcription and translation of interferon and other antiviral genes, effectively blocking replication of multiple alphavirus types, including chikungunya fever, venezuelan equine encephalitis, mayaro virus. Moreover, the immune response is independent of MAVS and TRIF. However, C11 does not activate innate immune responses in mouse and THP-1 cells, and the specific mechanism is unclear.

Kitacinnamycins 8

The natural products of medicinal plants have been important resources for discovering novel drugs in recent decades (Newman and Cragg, 2016). In 2019, Shi et al. identified a new class of cinnamoyl-containing nonribosomal peptides (CCNPs) through the genomic collection and biosynthetic methods, named kitacinnamycins (Shi et al., 2019). Kitacinnamycins 8 increased poly (dA:dT) and cGAMP-induced IFN-β expression in a dose-dependent manner (Shi et al., 2019). However, the pharmacokinetics of kitacinnamycins 8 remain uncovered.

Flavonoids Compounds

In 2013, Kim et al. reported that 5,6-dimethylxanthenone-4-acetic acid (DMXAA) is a mouse STING agonist. In the mouse macrophage cell line Raw264.7 and L929 cells, DMXAA, similar to cyclic dinucleotide PAMPs and cyclic GMP-AMP, binds with m-STING to activate the TBK1-IRF3 pathway. In addition, DMXAA showed good activity in mouse solid tumors, causing tumor-specific vascular injury and other antitumor effects. However, its clinical trials failed, possibly because DMXAA does not bind to h-STING and lacks efficacy or mechanism-related toxicity in humans (Kim et al., 2013a). Unlike DMXAA, flavonoids α-Mangostin (Zhang et al., 2018) and G10 (Banerjee et al., 2020) were agonists of human STING. α-Mangostin and G10 bind to and stabilize the CTD region of STING in THP-1 cells and HEK293T (the human embryonic kidney cell line), respectively, and activate the STING-TBK1-IRF3 pathway. The EC_{50} values of G10 in STING R232 and H232 variants were 2.5 and 4.3 μM, respectively. In addition, α-Mangostin can repolarize human monocyte-derived M2 macrophages into the M1 phenotype, which has an antitumor function. However, α-Mangostin lacks *in vivo* biological activity and pharmacological properties, and G10 cannot activate all human STING, such as THP-1. In 2017, Liu identified a dispiro diketopiperzine (DSDP) compound as a h-STING agonist using a high-throughput cell-based screening method (Liu et al., 2017). DSDP induced STING-dependent cytokine responses in human foreskin fibroblasts (HFF) and h-PBMCs and effectively inhibited the replication of yellow fever virus, dengue virus, and Zika virus (Liu et al., 2017).

Other Compounds

In 2020, Pan et al. reported a non-nucleotide agonist, MSA-2, acting on STING (Pan et al., 2020). MSA-2 exists as an interconverting monomer or dimer, but only can it bind and activate STING in the dimer form. In mouse tumor models, MSA-2 was well tolerated by subcutaneous injection and oral administration. It can stimulate the secretion of IFN-β in tumors, induce tumor regression, have long-lasting antitumor immunity, and synergize with anti-PD-1 therapy. Moreover, in the acidic tumor microenvironment, the cellular efficacy of MSA-2 was enhanced with extracellular acidification (Pan et al., 2020). In 2020, Chin et al. reported another non-nucleotide STING agonist, SR-717 (Chin et al., 2020). SR-717 activates STING and induces "closure" of STING in a binding manner similar to that of cGAMP-STING. Through protein thermal transfer analysis, SR-717 can directly bind to recombinant STING and promote the cross-initiation of antigen and the activation of $CD8^+$ T cells, natural killer cells, and dendritic cells. In addition, SR-717 can induce the expression of relevant immune genes, including programmed cell death ligand 1 (PD-L1), and show antitumor activity (Chin et al., 2020). MSA-2 and SR-717 are STING

TABLE 4 | Indirect regulators targeting the cGAS-STING pathway.

Agents	Inhibition mechanism	Biological effect	Refs
Obtusilactone B, Brazilin	It inhibits dsDNA by inhibiting BAF	Indirect regulation of cGAS	Kim et al. (2013b); Kim et al. (2015)
Tucatinib	Inhibition of HER2 kinase activity	Indirect regulation of STING	Kulukian et al. (2020)
EGCG	Inhibits the enzyme activity of G3BP1	Indirect regulation of cGAS	Liu et al. (2019)
Compound C	Inhibit the accumulation of cGAMP	Indirect regulation of the cGAS-STING pathway	Lai et al. (2020)
Celastrol	Inhibit the activation of IRF3	Indirect regulation of the cGAS-STING pathway	Liu et al. (2020)
α,β–metADP/ATP,bzATP, ARL 67156	Inhibit the activation of ENPP1	Indirect regulation of the cGAMP	Lévesque et al. (2007); Lee et al. (2017)
$(TiW11CoO40)8^{-}$, SR-8314, MV-626	Inhibit the activation of ENPP1	Indirect regulation of the cGAMP	Lee and Müller, (2017); Weston et al. (2019)

agonists suitable for clinical application because of their oral characteristics and simplified administration mode, and their pharmacological metabolism should be further studied.

INDIRECT MODULATION OF THE cGAS-STING PATHWAY

Indirect Inhibition of cGAS by Targeting BAF

BAF is a self-integration disorder factor encoded by BANF1 and belongs to chromatin-binding protein, essential for nuclear membrane recombination in mitosis (Wang et al., 1996). BAF can dynamically bind to dsDNA, inhibit cGAS activity and suppress abnormal immune responses (Wang et al., 1998). Therefore, activating the cGAS-STING signaling pathway by inhibiting BAF may be an effective antitumor strategy (Zhao et al., 1998). Kim et al. found that a butanol lactone derivative, obtusilactone B, purified from spirea pernifolia, can inhibit BAF activity (Kim et al., 2013b). The specific binding of obtusilactone B to BAF inhibits vaccinia-associated kinase 1 (VRK1)-mediated BAF phosphorylation, leading to DNA nuclear membrane disintegration, thus inactivating BAF. In addition, Kim et al. isolated brazilin from legumes, which can inhibit BAF phosphorylation *in vitro* and *in vivo* by inhibiting VRK1, and disrupt BAF banding to DNA (Kim et al., 2015). Therefore, obtusilone B and brazilin can be candidates for the indirect regulation of cGAS-STING signaling. The above modulators are shown in **Table 4**.

Indirect Inhibition of STING by Targeting HER2

Studies have shown that tyrosine kinase receptor HER2 can effectively inhibit cGAS-STING signaling (Kroemer et al., 2015). Activated HER2 recruits the downstream protein kinase AKT1 and phosphorylates TBK1, thus blocking the formation of STING and TBK1 complex, and causing ubiquitination of TBK1 and ultimately weakening the STING signal (Wu et al., 2019). Therefore, inhibiting HER2 may effectively activate cGAS-STING-mediated signaling. Kulukian et al. reported a small molecule, tucatinib which could inhibit HER2 activity and blocks downstream signal transduction through MAPK and PI3K/AKT pathways (Kulukian et al., 2020). In addition, tucatinib was selectively cytotoxic to HER2-amplified breast cancer cells. Tucatinib has shown enhanced antitumor activity in combination with trastuzumab (therapeutic agents that target HER2 positive advanced metastatic tumors) or docetaxel (a newly developed taxoid anticancer agent), resulting in improved rates of partial and complete tumor regression (Kulukian et al., 2020).

Indirect Inhibition of cGAS by Targeting G3BP1

In 2019, Liu et al. reported a novel cGAS-regulatory factor G3BP1 (GTPase activating protein SH3 domain-binding protein 1) (Liu et al., 2019). G3BP1 promotes the binding and activation of cGAS with DNA by changing the structure or oligomerization state of cGAS. Epigallocatechin gallate (EGCG), a polyphenol isolated from tea, is a known inhibitor of G3BP1 and specifically inhibits the binding of G3BP1 to cGAS and prevents the activation of cGAS, thereby blocking IFN-I production *in vivo* and *in vitro*. EGCG administration attenuated autologous DNA-induced autoinflammation in AGS mouse models and reduced interferon gene expression (Liu et al., 2019). Currently, EGCG is undergoing clinical trials with the potential to treat cGAS-dependent immune disorders.

Modulation of the cGAS-STING Pathway by Compound C

Compound C is known to be a reversible inhibitor of AMPK and ALKs protein kinases. However, our group found that Compound C could inhibit the expression of IFN-β and related interferon stimulating factors (ISGs) by inhibiting the accumulation of cGAMP in the cytoplasm (Lai et al., 2020). Liquid chromatography-mass spectrometry (LC-MS) data showed that Compound C could inhibit the expression of type I interferon by decreasing the accumulation of cGAMP. It plays a modulator role in cGAS-STING-mediated DNA sensing pathway, but this effect is independent of AMPK protein activity. The IC_{50} of Compound C in L929 cells is 40 μM. In addition, Compound C can rescue the autoimmune phenotype of Trex1 gene deletion in mice (Lai et al., 2020), indicating that Compound C can inhibit the cGAS-STING pathway by acting on cGAMP, which will lay a foundation for further structural optimization of Compound C, and revealing the structure-

activity relationship between small molecule compounds and cGAS or STING proteins, and for the design, synthesis and bioactivity studies of related new compounds.

Indirect Inhibition of cGAS-STING Pathway by Targeting IRF3

Celastrol is a bioactive substance isolated from *Tripterygium wilfordii*. In 2020, our group found that celastrol could inhibit IRF3 activation *in vitro* and *in vivo*, thus effectively inhibits exogenous DNA-induced IFN-I response, with an IC_{50} value of 145.7 ± 23.6 nM (Liu et al., 2020). In addition, celastrol significantly rescued autoimmune phenotypes in *Trex1*$^{-/-}$ mice, including myocarditis and abnormal interferon response (Liu et al., 2020). Therefore, celastrol may be used to treat autoimmune and interferon-related diseases, but its specific targets need further clarification.

Indirect Inhibition of cGAMP by Targeting ENPP1

Exonucleotide pyrophosphatase/phosphodiesterase I (ENPP1), as a key phosphodiesterase, catalyzes the hydrolysis of ATP or GTP to AMP or GMP, which affect the activity of STING by degrading cGAMP (Onyedibe et al., 2019). ENPP1-targeting inhibitors are expected to treat diseases associated with the cGAS-STING pathway. ENPP1 inhibitors can be divided into two classes. The first group are nucleotide inhibitors. They are structurally similar to natural ENPP1 substrates and competitively bind ENPP1 with ATP or GTP, such as α,β-metADP/ATP, 2-mesADP/ATP and bzATP, with IC_{50} values ranging from 13 to 32 μM (Lee et al., 2017). In addition, γ-S-α,β-metATP derivative, ARL 67156 and Diadenosine boranophosphate derivative are also nucleotide inhibitors of ENPP1, but their pharmacological activities need to be further determined (Lévesque et al., 2007). The second class of non-nucleotide inhibitors include polyoxometalates (TiW11CoO40)8−, suramin, heparin, etc. (TiW11CoO40)8− is the most effective ENPP1 inhibitor at present, and its K_i is 1.46 nM (Lee and Müller, 2017). In addition, SR-8314 and MV-626 could increase tumor infiltration of $CD3^+$, $CD4^+$, and CD8+T cells and showed significant antitumor activity (Weston et al., 2019).

CLINICAL STUDIES OF REGULATORY AGENTS TARGETING THE cGAS-STING PATHWAY

Various modulators that target the cGAS-STING pathway have moved towards clinical trials (**Table 5**, data from https://www.clinicaltrials.gov/ October 13, 2021). Currently, two cGAS inhibitors are in clinical trials. In 2015, suramin combined with paclitaxel in treating stage IIIB-IV breast cancer (NCT00054028) proved effective. In 2019, aspirin was used in the clinical trial (NCT04132791) to prevent and treat cardiovascular diseases due to its ability to reduce the morning activity of platelets. A low-dose aspirin study is currently underway to prevent heart and vascular disease, colon and rectal cancer (NCT03603366). These clinical trials need to be followed up. It is believed that suramin and aspirin may be used as cGAS inhibitors to treat DNA-mediated immune diseases based on these pharmacological findings.

On the other hand, there are currently five STING modulators under clinical studies. From 2016 to 2019, ADU-S100 (NCT03937141, NCT02675439, NCT03172936), MK-1454 (NCT04220866, NCT03010176), and BMS-986301 (NCT03956680) were enrolled in clinical trials for the treatment of advanced/metastatic solid tumors or lymphomas. Compared with single-drug treatment, ADU-S100, MK-1454, or BMS-986301 combined with the ICIs therapy (Pembrolizumab/Ipilimumab/Nivolumab) to treat solid tumors and had shown good drug tolerance, has yet to reach maximum tolerated dose. Currently, CXA-10 has been used in 11 clinical trials. Among them, the clinical trial of oral CXA-10 in the treatment of primary focal segmental glomerulosclerosis has entered phase 2, but no clinical trial of CXA-10 as a STING inhibitor in the treatment of related immune diseases has been reported. In 2008, DMXAA was used as a STING agonist in clinical trial treating refractory tumors (DART). However, as it was an m-STING specific agonist, it did not react with h-STING, resulting in an unsatisfactory effect, and the experiment failed. Therefore, the structure of DMXAA needs to be further optimized. In addition, two indirect regulators targeting the cGAS-STING pathway have been tested clinically for pharmacologic metabolic research and cancer treatment.

In 2019, EGCG was studied in pharmacokinetics and liver safety pharmacology (NCT04177693). So far, 117 clinical trials related to EGCG have been enrolled.

By October 2021, tucatinib has been used in more than 30 clinical trials, particularly used for treating $HER2^+$ breast cancer. For example, tucatinib (NCT03054363) is combined with palbociclib (a drug used to treat advanced breast cancer) and letrozole (aromatase inhibitor) used for treating hormone-receptor-positive and HER2-positive metastatic breast cancer patients. Treatment protocol of tucatinib with capecitabine and trastuzumab has been approved for treating patients with unresectable previously treated $HER2^+$ breast cancer by US Food and Drug Administration on April 17, 2020.

SUMMARY AND PROSPECT

In recent years, rapid progress has been made in clarifying the structure and mechanism of key proteins in the cGAS-STING pathway and in revealing the important role of this pathway in human autoimmune disease and cancer. Therefore, targeting the cGAS-STING signaling pathway to activate innate immunity and enhance the immune function provides great potential for cancer treatments. On the other hand, abnormal activation of the cGAS-STING pathway is the main cause of inflammation and autoimmune diseases. Therefore, the research and development of appropriate compounds, delivery pathways, and treatment regimens to suppress the

TABLE 5 | Clinical trials of regulatory agents targeting cGAS-STING pathways.

Control agents	Control targets	Clinical trials	Disease
Aspirin	h-cGAS	Not applicable (NCT04132791) (NCT03603366) a total of 2,269 studies	Cardiovascular disease, cancer of the colon and rectum
Suramin	h-cGAS	Phase 1/2 (NCT00054028) a total of 21 studies	Stage IIIB-IV breast cancer
CXA-10	h-STING	Phase 2 (NCT03422510) a total of 11 studies	FSGS
ADU-S100	h-STING	Phase 2 (NCT03937141) phase 1 (NCT02675439) phase 1 (NCT03172936)	Head and neck cancer, advanced/metastatic solid tumors or lymphomas
MK-1454	h-STING	Phase 2 (NCT04220866) phase 1 (NCT03010176)	Neck squamous cell carcinoma, advanced/metastatic solid tumor, or lymphoma
BMS-986301	h-STING	Phase 1 (NCT03956680)	Advanced solid tumor
DMXAA (ASA404)	m-STING	Phase 1 (NCT00863733) phase 1 (NCT00856336) phase 1/2 (NCT00832494) a total of 18 studies	Solid tumors, DART, advanced non-small cell lung cancer
Tucatinib	HER2	Phase 1/2 (NCT03054363) phase 2 (NCT04579380) phase 2 (NCT03043313) phase 1/2 (NCT04430738) a total of 34 studies	Breast cancer, solid tumors, HER2+ colorectal cancer, HER2+ gastrointestinal cancers
EGCG	G3BP1	Phase 2 (NCT04553666) phase 0 (NCT02891538) phase 1 (NCT04177693) a total of 117 studies	Older cancer, colorectal cancer, pharmacokinetics, and hepatic safety

cGAS-STING pathway will benefit patients with autoimmune and infectious diseases.

The crystal structures of several cGAS-STING pathway-related proteins have been analyzed, laying a foundation for the design of structure-based drugs. We now understand more clearly that binding or catalytic sites targeting cGAS and STING proteins and post-translational modifications can influence the enzyme activity and thus regulate immune responses. However, the high-resolution structures of some key protein complexes in the cGAS-STING pathway have not been resolved, such as the STING oligomer -TBK1 oligomer. It was found that the function of STING was strictly regulated by membrane transport, and retrograde membrane transport was crucial for silencing signaling pathways. This transportation defect is the basis of the pathogenesis of COPA syndrome, a single-gene autoinflammatory disease. The membrane transport of STING is co-mediated by COP-II and COP-I. Thus, using the regulatory agents to target membrane transport is likely to be a novel strategy for treating autoimmune diseases (Taguchi et al., 2021). However, the regulatory factors of STING transfer from the Golgi apparatus to the lysosome and the mechanisms of STING, NF-κB, and autophagy remain to be further studied. In addition, how post-translational modifications regulate the STING and other related enzyme activities, such as the relationship between palmitoylation of STING and oligomerization and activity, also remains unknown (Zhang et al., 2020). In recent years, cGAS has been closely related to the functions of histone and chromatin in the nucleus, and its interaction can affect the activity, but its structural basis and mechanism remain unclear (Kim et al., 2015).

On the other hand, agonists of the cGAS-STING pathway have potential value in the treatment of cancer. Some modified CDN analogs have entered clinical trials, but their clinical application may be hindered by their drug similarity, which needs to be treated in combination with ICIs, with collaborative administration. Small molecule non-CDN agonists provide a new strategy for systemic delivery, but clinical data have not been reported and need to be further verified. A potentially serious problem with agonist immunotherapy is the occurrence of "cytokine storms" (Ng et al., 2018). Continuous activation of immune signals can lead to excessive production of cytokines, causing severe toxicity or even death (Fu et al., 2020). Therefore, how much patients with autoimmune disease or cancer will benefit from cGAS-STING immunotherapy requires further investigation.

The pharmacodynamics optimization of cGAS-STING regulators and the rediscovery of natural drugs are important strategies for its immunopharmacology research. In addition, the compounds that indirectly regulate this pathway will also be a good focus for the study. Recently, inhibition of the cGAS-STING signaling pathway by nucleosomes (Boyer et al., 2020) and circRNAs (Xia et al., 2018) has been reported. Targeting the cGAS-STING pathway has promoted the vigorous development of immunotherapy. The combination of immunoregulatory agents and ICI_S therapy has become a hot spot in recent years. We anticipate that there will be more efficient and less toxic immune regulatory agents targeting cGAS-STING available in the future and applied for clinical practice to provide safer and more effective treatments for autoimmune disease and cancer.

AUTHOR CONTRIBUTIONS

QC and JuL proposed the review idea, while QL, JiL, and JF collected literature and QL wrote the first draft. QC and ST revised the manuscript.

FUNDING

The present study was supported by the National Natural Science Foundation of China (Grant No. 81770222). Project Title: Targeted optimization and signaling molecular modification of CAR-T cells in the treatment of multiple myeloma and its mechanism.

REFERENCES

Abe, J., Izawa, K., Nishikomori, R., Awaya, T., Kawai, T., Yasumi, T., et al. (2013). Heterozygous TREX1 p.Asp18Asn Mutation Can Cause Variable Neurological Symptoms in a Family With Aicardi-Goutieres Syndrome/Familial Chilblain Lupus. *Rheumatology (Oxford)*. 52, 406–408. doi:10.1093/rheumatology/kes181

Ablasser, A., Goldeck, M., Cavlar, T., Deimling, T., Witte, G., Röhl, I., et al. (2013). cGAS Produces a 2'-5'-linked Cyclic Dinucleotide Second Messenger That Activates STING. *Nature*. 498, 380–384. doi:10.1038/nature12306

An, J., Woodward, J. J., Sasaki, T., Minie, M., and Elkon, K. B. (2015). Cutting Edge: Antimalarial Drugs Inhibit IFN-β Production Through Blockade of Cyclic GMP-AMP Synthase-DNA Interaction. *J. Immunol.* 194, 4089–4093. doi:10.4049/jimmunol.1402793

Banerjee, M., Middya, S., Shrivastava, R., Basu, S., Ghosh, R., Pryde, D. C., et al. (2020). G10 Is a Direct Activator of Human STING. *PLoS One*. 15, e0237743. doi:10.1371/journal.pone.0237743

Barber, G. N. (2015). STING: Infection, Inflammation and Cancer. *Nat. Rev. Immunol.* 15, 760–770. doi:10.1038/nri3921

Bose, D., Su, Y., Marcus, A., Raulet, D. H., and Hammond, M. C. (2016). An RNA-Based Fluorescent Biosensor for High-Throughput Analysis of the cGAS-cGAMP-STING Pathway. *Cell Chem. Biol.* 23, 1539–1549. doi:10.1016/j.chembiol.2016.10.014

Boyer, J. A., Spangler, C. J., Strauss, J. D., Cesmat, A. P., Liu, P., McGinty, R. K., et al. (2020). Structural Basis of Nucleosome-Dependent cGAS Inhibition. *Science*. 370, 450–454. doi:10.1126/science.abd0609

Burdette, D. L., Monroe, K. M., Sotelo-Troha, K., Iwig, J. S., Eckert, B., Hyodo, M., et al. (2011). STING Is a Direct Innate Immune Sensor of Cyclic Di-GMP. *Nature* 478, 515–518. doi:10.1038/nature10429

Burdette, D. L., and Vance, R. E. (2013). STING and the Innate Immune Response to Nucleic Acids in the Cytosol. *Nat. Immunol.* 14, 19–26. doi:10.1038/ni.2491

Chen, Y. (2019), Rational Design, Synthesis and Biological Evaluation of cGAS in Inhibitors Based on the Virtual Screening & the Study of the Computational Approach for the Bindig Mode of S1P1R Agonists Base on the Active-Like Receptor Model. doi:10.27648/d.cnki.gzxhu.2019.000372

Chin, E. N., Yu, C., Vartabedian, V. F., Jia, Y., Kumar, M., Gamo, A. M., et al. (2020). Antitumor Activity of a Systemic STING-Activating Non-Nucleotide cGAMP Mimetic. *Science* 369, 993–999. doi:10.1126/science.abb4255

Corrales, L., Glickman, L. H., McWhirter, S. M., Kanne, D. B., Sivick, K. E., Katibah, G. E., et al. (2015). Direct Activation of STING in the Tumor Microenvironment Leads to Potent and Systemic Tumor Regression and Immunity. *Cell Rep.* 11, 1018–1030. doi:10.1016/j.celrep.2015.04.031

Crow, Y. J., Hayward, B. E., Parmar, R., Robins, P., Leitch, A., Ali, M., et al. (2006). Mutations in the Gene Encoding the 3'-5' DNA Exonuclease TREX1 Cause Aicardi-Goutières Syndrome at the AGS1 Locus. *Nat. Genet.* 38, 917–920. doi:10.1038/ng1845

Dai, J., Huang, Y. J., He, X., Zhao, M., Wang, X., Liu, Z. S., et al. (2019). Acetylation Blocks cGAS Activity and Inhibits Self-DNA-Induced Autoimmunity. *Cell*. 176, 1447–e14. e14. doi:10.1016/j.cell.2019.01.016

Deng, L., Liang, H., Xu, M., Yang, X., Burnette, B., Arina, A., et al. (2014). STING-Dependent Cytosolic DNA Sensing Promotes Radiation-Induced Type I Interferon-Dependent Antitumor Immunity in Immunogenic Tumors. *Immunity* 41, 843–852. doi:10.1016/j.immuni.2014.10.019

Ding, C., Song, Z., Shen, A., Chen, T., and Zhang, A. (2020). Small Molecules Targeting the Innate Immune cGAS–STING–TBK1 Signaling Pathway. *Acta Pharm. Sin B.* 10 (12), 2272–2298. doi:10.1016/j.apsb.2020.03.001

Dubensky, T. W., Jr., Kanne, D. B., and Leong, M. L. (2013). Rationale, Progress and Development of Vaccines Utilizing STING-Activating Cyclic Dinucleotide Adjuvants. *Ther. Adv. Vaccin.* 1, 131–143. doi:10.1177/2051013613501988

Duewell, P., Steger, A., Lohr, H., Bourhis, H., Hoelz, H., Kirchleitner, S. V., et al. (2014). RIG-I-Like Helicases Induce Immunogenic Cell Death of Pancreatic Cancer Cells and Sensitize Tumors Toward Killing by CD8(+) T Cells. *Cell Death Differ.* 21, 1825–1837. doi:10.1038/cdd.2014.96

Düwell, P., Heidegger, S., and Kobold, S. (2019). Innate Immune Stimulation in Cancer Therapy. *Hematol. Oncol. Clin. North. Am.* 33, 215–231. doi:10.1016/j.hoc.2018.12.002

Feng, X., Liu, D., Li, Z., and Bian, J. (2020). Bioactive Modulators Targeting STING Adaptor in cGAS-STING Pathway. *Drug Discov. Today.* 25, 230–237. doi:10.1016/j.drudis.2019.11.007

Fu, Y., Lin, Q., Zhang, Z., and Zhang, L. (2020). Therapeutic Strategies for the Costimulatory Molecule OX40 in T-Cell-Mediated Immunity. *Acta Pharm. Sin B.* 10, 414–433. doi:10.1016/j.apsb.2019.08.010

Gall, B., Pryke, K., Abraham, J., Mizuno, N., Botto, S., Sali, T. M., et al. (2018). Emerging Alphaviruses Are Sensitive to Cellular States Induced by a Novel Small-Molecule Agonist of the STING Pathway. *J. Virol.* 92, e01913. doi:10.1128/JVI.01913-17

Haag, S. M., Gulen, M. F., Reymond, L., Gibelin, A., Abrami, L., Decout, A., et al. (2018). Targeting STING With Covalent Small-Molecule Inhibitors. *Nature* 559, 269–273. doi:10.1038/s41586-018-0287-8

Hall, J., Brault, A., Vincent, F., Weng, S., Wang, H., Dumlao, D., et al. (2017a). Discovery of PF-06928215 as a High Affinity Inhibitor of cGAS Enabled by a Novel Fluorescence Polarization Assay. *PLoS One* 12, e0184843. doi:10.1371/journal.pone.0184843

Hall, J., Ralph, E. C., Shanker, S., Wang, H., Byrnes, L. J., Horst, R., et al. (2017b). The Catalytic Mechanism of Cyclic GMP-AMP Synthase (cGAS) and Implications for Innate Immunity and Inhibition. *Protein Sci.* 26, 2367–2380. doi:10.1002/pro.3304

Hansen, A. L., Buchan, G. J., Rühl, M., Mukai, K., Salvatore, S. R., Ogawa, E., et al. (2018). Nitro-Fatty Acids Are Formed in Response to Virus Infection and Are Potent Inhibitors of STING Palmitoylation and Signaling. *Proc. Natl. Acad. Sci. U S A.* 115, E7768–e7775. doi:10.1073/pnas.1806239115

Harrington, K. J., Brody, J., Ingham, M., Strauss, J., Cemerski, S., Wang, M., et al. (2018). Preliminary Results of the First-In-Human (FIH) Study of MK-1454, an Agonist of Stimulator of Interferon Genes (STING), as Monotherapy or in Combination with Pembrolizumab (Pembro) in Patients With Advanced Solid Tumors or Lymphomas. *Ann. Oncol.* 29, viii712. doi:10.1093/annonc/mdy424.015

Hartner, J. C., Walkley, C. R., Lu, J., and Orkin, S. H. (2009). ADAR1 Is Essential for the Maintenance of Hematopoiesis and Suppression of Interferon Signaling. *Nat. Immunol.* 10, 109–115. doi:10.1038/ni.1680

Kato, K., Ishii, R., Goto, E., Ishitani, R., Tokunaga, F., and Nureki, O. (2013). Structural and Functional Analyses of DNA-Sensing and Immune Activation by Human cGAS. *PLoS One* 8, e76983. doi:10.1371/journal.pone.0076983

Kawane, K., Fukuyama, H., Kondoh, G., Takeda, J., Ohsawa, Y., Uchiyama, Y., et al. (2001). Requirement of DNase II for Definitive Erythropoiesis in the Mouse Fetal Liver. *Science* 292, 1546–1549. doi:10.1126/science.292.5521.1546

Kim, S., Li, L., Maliga, Z., Yin, Q., Wu, H., and Mitchison, T. J. (2013a). Anticancer Flavonoids Are Mouse-Selective STING Agonists. *ACS Chem. Biol.* 8, 1396–1401. doi:10.1021/cb400264n

Kim, W., Lyu, H. N., Kwon, H. S., Kim, Y. S., Lee, K. H., Kim, D. Y., et al. (2013b). Obtusilactone B From Machilus Thunbergii Targets Barrier-To-Autointegration Factor to Treat Cancer. *Mol. Pharmacol.* 83, 367–376. doi:10.1124/mol.112.082578

Kim, S. H., Lyu, H. N., Kim, Y. S., Jeon, Y. H., Kim, W., Kim, S., et al. (2015). Brazilin Isolated from Caesalpinia Sappan Suppresses Nuclear Envelope Reassembly by Inhibiting Barrier-To-Autointegration Factor Phosphorylation. *J. Pharmacol. Exp. Ther.* 352, 175–184. doi:10.1124/jpet.114.218792

Kranzusch, P. J., Lee, A. S., Berger, J. M., and Doudna, J. A. (2013). Structure of Human cGAS Reveals a Conserved Family of Second-Messenger Enzymes in Innate Immunity. *Cell Rep.* 3, 1362–1368. doi:10.1016/j.celrep.2013.05.008

Kroemer, G., Senovilla, L., Galluzzi, L., André, F., and Zitvogel, L. (2015). Natural and Therapy-Induced Immunosurveillance in Breast Cancer. *Nat. Med.* 21, 1128–1138. doi:10.1038/nm.3944

Kulukian, A., Lee, P., Taylor, J., Rosler, R., de Vries, P., Watson, D., et al. (2020). Preclinical Activity of HER2-Selective Tyrosine Kinase Inhibitor Tucatinib as a Single Agent or in Combination with Trastuzumab or Docetaxel in Solid Tumor Models. *Mol. Cancer Ther.* 19, 976–987. doi:10.1158/1535-7163.MCT-19-0873

Kwon, J., and Bakhoum, S. F. (2020). The Cytosolic DNA-Sensing cGAS-STING Pathway in Cancer. *Cancer Discov.* 10, 26–39. doi:10.1158/2159-8290.CD-19-0761

Lai, J., Luo, X., Tian, S., Zhang, X., Huang, S., Wang, H., et al. (2020). Compound C Reducing Interferon Expression by Inhibiting cGAMP Accumulation. *Front. Pharmacol.* 11, 88. doi:10.3389/fphar.2020.00088

Lama, L., Adura, C., Xie, W., Tomita, D., Kamei, T., Kuryavyi, V., et al. (2019). Development of Human cGAS-Specific Small-Molecule Inhibitors for Repression of dsDNA-Triggered Interferon Expression. *Nat. Commun.* 10, 2261. doi:10.1038/s41467-019-08620-4

Lee, S. Y., and Müller, C. E. (2017). Nucleotide Pyrophosphatase/Phosphodiesterase 1 (NPP1) and its Inhibitors. *Medchemcomm.* 8, 823–840. doi:10.1039/c7md00015d

Lee, S. Y., Sarkar, S., Bhattarai, S., Namasivayam, V., De Jonghe, S., Stephan, H., et al. (2017). Substrate-Dependence of Competitive Nucleotide Pyrophosphatase/Phosphodiesterase1 (NPP1) Inhibitors. *Front. Pharmacol.* 8, 54. doi:10.3389/fphar.2017.00054

Lévesque, S. A., Lavoie, E. G., Lecka, J., Bigonnesse, F., and Sévigny, J. (2007). Specificity of the Ecto-ATPase Inhibitor ARL 67156 on Human and Mouse Ectonucleotidases. *Br. J. Pharmacol.* 152, 141–150. doi:10.1038/sj.bjp.0707361

Li, S., Hong, Z., Wang, Z., Li, F., Mei, J., Huang, L., et al. (2018). The Cyclopeptide Astin C Specifically Inhibits the Innate Immune CDN Sensor STING. *Cell Rep.* 25, 3405–e7. e7. doi:10.1016/j.celrep.2018.11.097

Li, T., Cheng, H., Yuan, H., Xu, Q., Shu, C., Zhang, Y., et al. (2016). Antitumor Activity of cGAMP via Stimulation of cGAS-cGAMP-STING-IRF3 Mediated Innate Immune Response. *Sci. Rep.* 6, 19049. doi:10.1038/srep19049

Li, X., Shu, C., Yi, G., Chaton, C. T., Shelton, C. L., Diao, J., et al. (2013a). Cyclic GMP-AMP Synthase Is Activated by Double-Stranded DNA-Induced Oligomerization. *Immunity* 39, 1019–1031. doi:10.1016/j.immuni.2013.10.019

Li, X. D., Wu, J., Gao, D., Wang, H., Sun, L., and Chen, Z. J. (2013b). Pivotal Roles of cGAS-cGAMP Signaling in Antiviral Defense and Immune Adjuvant Effects. *Science* 341, 1390–1394. doi:10.1126/science.1244040

Liu, B., Tang, L., Zhang, X., Ma, J., Sehgal, M., Cheng, J., et al. (2017). A Cell-Based High Throughput Screening Assay for the Discovery of cGAS-STING Pathway Agonists. *Antivir. Res.* 147, 37–46. doi:10.1016/j.antiviral.2017.10.001

Liu, Y., Xiao, N., Du, H., Kou, M., Lin, L., Huang, M., et al. (2020). Celastrol Ameliorates Autoimmune Disorders in Trex1-Deficient Mice. *Biochem. Pharmacol.* 178, 114090. doi:10.1016/j.bcp.2020.114090

Liu, Z. S., Cai, H., Xue, W., Wang, M., Xia, T., Li, W. J., et al. (2019). G3BP1 Promotes DNA Binding and Activation of cGAS. *Nat. Immunol.* 20, 18–28. doi:10.1038/s41590-018-0262-4

Meric-Bernstam, F., Kaur Sandhu, S., Hamid, O., Spreafico, A., and Kasper, S. (2019). Phase Ib Study of MIW815 (ADU-S100) in Combination With Spartalizumab (PDR001) in Patients (Pts) With Advanced/Metastatic Solid Tumors or Lymphomas. *J. Clin. Oncol.* 37, 2507. doi:10.1200/JCO.2019.37.15_suppl.2507

Mukai, K., Konno, H., Akiba, T., Uemura, T., Waguri, S., Kobayashi, T., et al. (2016). Activation of STING Requires Palmitoylation at the Golgi. *Nat. Commun.* 7, 11932. doi:10.1038/ncomms11932

Newman, D. J., and Cragg, G. M. (2016). Natural Products as Sources of New Drugs From 1981 to 2014. *J. Nat. Prod.* 79, 629–661. doi:10.1021/acs.jnatprod.5b01055

Ng, K. W., Marshall, E. A., Bell, J. C., and Lam, W. L. (2018). cGAS-STING and Cancer: Dichotomous Roles in Tumor Immunity and Development. *Trends Immunol.* 39, 44–54. doi:10.1016/j.it.2017.07.013

Onyedibe, K. I., Wang, M., and Sintim, H. O. (2019). ENPP1, an Old Enzyme With New Functions, and Small Molecule Inhibitors-A STING in the Tale of ENPP1. *Molecules* 24, 4192. doi:10.3390/molecules24224192

Padilla-Salinas, R., Sun, L., Anderson, R., Yang, X., Zhang, S., Chen, Z. J., et al. (2020). Discovery of Small-Molecule Cyclic GMP-AMP Synthase Inhibitors. *J. Org. Chem.* 85, 1579–1600. doi:10.1021/acs.joc.9b02666

Pan, B. S., Perera, S. A., Piesvaux, J. A., Presland, J. P., Schroeder, G. K., Cumming, J. N., et al. (2020). An Orally Available Non-nucleotide STING Agonist With Antitumor Activity. *Science* 369, eaba6098. doi:10.1126/science.aba6098

Parlato, M., and Yeretssian, G. (2014). NOD-Like Receptors in Intestinal Homeostasis and Epithelial Tissue Repair. *Int. J. Mol. Sci.* 15, 9594–9627. doi:10.3390/ijms15069594

Ramanjulu, J. M., Pesiridis, G. S., Yang, J., Concha, N., Singhaus, R., Zhang, S. Y., et al. (2018). Design of Amidobenzimidazole STING Receptor Agonists With Systemic Activity. *Nature* 564, 439–443. doi:10.1038/s41586-018-0705-y

Ridker, P. M., MacFadyen, J. G., Thuren, T., Everett, B. M., Libby, P., and Glynn, R. J. (2017). Effect of Interleukin-1β Inhibition With Canakinumab on Incident Lung Cancer in Patients With Atherosclerosis: Exploratory Results From a Randomised, Double-Blind, Placebo-Controlled Trial. *Lancet* 390, 1833–1842. doi:10.1016/S0140-6736(17)32247-X

Shakespear, M. R., Halili, M. A., Irvine, K. M., Fairlie, D. P., and Sweet, M. J. (2011). Histone Deacetylases as Regulators of Inflammation and Immunity. *Trends Immunol.* 32, 335–343. doi:10.1016/j.it.2011.04.001

Shi, J., Liu, C. L., Zhang, B., Guo, W. J., Zhu, J., Chang, C.-Y., et al. (2019). Genome Mining and Biosynthesis of Kitacinnamycins as a STING Activator. *Chem. Sci.* 10, 4839–4846. doi:10.1039/c9sc00815b

Siu, T., Altman, M. D., Baltus, G. A., Childers, M., Ellis, J. M., Gunaydin, H., et al. (2019). Discovery of a Novel cGAMP Competitive Ligand of the Inactive Form of STING. *ACS Med. Chem. Lett.* 10, 92–97. doi:10.1021/acsmedchemlett.8b00466

Steinhagen, F., Zillinger, T., Peukert, K., Fox, M., Thudium, M., Barchet, W., et al. (2018). Suppressive Oligodeoxynucleotides Containing TTAGGG Motifs Inhibit cGAS Activation in Human Monocytes. *Eur. J. Immunol.* 48, 605–611. doi:10.1002/eji.201747338

Stetson, D. B., Ko, J. S., Heidmann, T., and Medzhitov, R. (2008). Trex1 Prevents Cell-Intrinsic Initiation of Autoimmunity. *Cell.* 134, 587–598. doi:10.1016/j.cell.2008.06.032

Stetson, D. B., and Medzhitov, R. (2006). Recognition of Cytosolic DNA Activates an IRF3-Dependent Innate Immune Response. *Immunity* 24, 93–103. doi:10.1016/j.immuni.2005.12.003

Taguchi, T., Mukai, K., Takaya, E., and Shindo, R. (2021). STING Operation at the ER/Golgi Interface. *Front. Immunol.* 12, 646304. doi:10.3389/fimmu.2021.646304

Vincent, J., Adura, C., Gao, P., Luz, A., Lama, L., Asano, Y., et al. (2017). Small Molecule Inhibition of cGAS Reduces Interferon Expression in Primary Macrophages From Autoimmune Mice. *Nat. Commun.* 8, 750. doi:10.1038/s41467-017-00833-9

Wang, M., Sooreshjani, M. A., Mikek, C., Opoku-Temeng, C., and Sintim, H. O. (2018). Suramin Potently Inhibits cGAMP Synthase, cGAS, in THP1 Cells to Modulate IFN-β Levels. *Future Med. Chem.* 10, 1301–1317. doi:10.4155/fmc-2017-0322

Wang, Q., Liu, X., Cui, Y., Tang, Y., Chen, W., Li, S., et al. (2014). The E3 Ubiquitin Ligase AMFR and INSIG1 Bridge the Activation of TBK1 Kinase by Modifying the Adaptor STING. *Immunity* 41, 919–933. doi:10.1016/j.immuni.2014.11.011

Wang, W., Chi, T., Xue, Y., Zhou, S., Kuo, A., and Crabtree, G. R. (1998). Architectural DNA Binding by a High-Mobility-Group/Kinesin-Like Subunit in Mammalian SWI/SNF-related Complexes. *Proc. Natl. Acad. Sci. U S A.* 95, 492–498. doi:10.1073/pnas.95.2.492

Wang, W., Côté, J., Xue, Y., Zhou, S., Khavari, P. A., Biggar, S. R., et al. (1996). Purification and Biochemical Heterogeneity of the Mammalian SWI-SNF Complex. *Embo J.* 15, 5370–5382. doi:10.1002/j.1460-2075.1996.tb00921.x

Weerapana, E., Wang, C., Simon, G. M., Richter, F., Khare, S., Dillon, M. B., et al. (2010). Quantitative Reactivity Profiling Predicts Functional Cysteines in Proteomes. *Nature* 468, 790–795. doi:10.1038/nature09472

Weston, A., Thode, T., Munoz, R., Daniel, S., Soldi, R., Kaadige, M., et al. (2019). Abstract 3077: Preclinical Studies of SR-8314, a Highly Selective ENPP1 Inhibitor and an Activator of STING Pathway. *Cancer Res.* 79, 3077. doi:10.1158/1538-7445.AM2019-3077

Wu, S., Zhang, Q., Zhang, F., Meng, F., Liu, S., Zhou, R., et al. (2019). HER2 Recruits AKT1 to Disrupt STING Signalling and Suppress Antiviral Defence and Antitumour Immunity. *Nat. Cell Biol.* 21, 1027–1040. doi:10.1038/s41556-019-0352-z

Xi, Q., Wang, M., Jia, W., Yang, M., Hu, J., Jin, J., et al. (2020). Design, Synthesis, and Biological Evaluation of Amidobenzimidazole Derivatives as Stimulator of Interferon Genes (STING) Receptor Agonists. *J. Med. Chem.* 63, 260–282. doi:10.1021/acs.jmedchem.9b01567

Xia, P., Wang, S., Ye, B., Du, Y., Li, C., Xiong, Z., et al. (2018). A Circular RNA Protects Dormant Hematopoietic Stem Cells from DNA Sensor cGAS-Mediated Exhaustion. *Immunity* 48, 688–e7. e7. doi:10.1016/j.immuni.2018.03.016

Xiao, N., Wei, J., Xu, S., Du, H., Huang, M., Zhang, S., et al. (2019). cGAS Activation Causes Lupus-like Autoimmune Disorders in a TREX1 Mutant Mouse Model. *J. Autoimmun.* 100, 84–94. doi:10.1016/j.jaut.2019.03.001

Zhang, X., Bai, X. C., and Chen, Z. J. (2020). Structures and Mechanisms in the cGAS-STING Innate Immunity Pathway. *Immunity* 53, 43–53. doi:10.1016/j.immuni.2020.05.013

Zhang, X., Liu, B., Tang, L., Su, Q., Hwang, N., Sehgal, M., et al. (2019). Discovery and Mechanistic Study of a Novel Human-Stimulator-Of-Interferon-Genes Agonist. *ACS Infect. Dis.* 5, 1139–1149. doi:10.1021/acsinfecdis.9b00010

Zhang, X., Shi, H., Wu, J., Zhang, X., Sun, L., Chen, C., et al. (2013). Cyclic GMP-AMP Containing Mixed Phosphodiester Linkages Is an Endogenous High-Affinity Ligand for STING. *Mol. Cell.* 51, 226–235. doi:10.1016/j.molcel.2013.05.022

Zhang, X., Wu, J., Du, F., Xu, H., Sun, L., Chen, Z., et al. (2014). The Cytosolic DNA Sensor cGAS Forms an Oligomeric Complex With DNA and Undergoes Switch-Like Conformational Changes in the Activation Loop. *Cell Rep.* 6, 421–430. doi:10.1016/j.celrep.2014.01.003

Zhang, Y., Sun, Z., Pei, J., Luo, Q., Zeng, X., Li, Q., et al. (2018). Identification of α-Mangostin as an Agonist of Human STING. *ChemMedChem.* 13, 2057–2064. doi:10.1002/cmdc.201800481

Zhao, K., Wang, W., Rando, O. J., Xue, Y., Swiderek, K., Kuo, A., et al. (1998). Rapid and Phosphoinositol-Dependent Binding of the SWI/SNF-Like BAF Complex to Chromatin After T Lymphocyte Receptor Signaling. *Cell.* 95, 625–636. doi:10.1016/s0092-8674(00)81633-5

Zhao, W., Xiong, M., Yuan, X., Li, M., Sun, H., and Xu, Y. (2020). In Silico Screening-Based Discovery of Novel Inhibitors of Human Cyclic GMP-AMP Synthase: A Cross-Validation Study of Molecular Docking and Experimental Testing. *J. Chem. Inf. Model.* 60, 3265–3276. doi:10.1021/acs.jcim.0c00171

Conflict of Interest: The authors declare that the research was conducted in the absence of any commercial or financial relationships that could be construed as a potential conflict of interest.

Publisher's Note: All claims expressed in this article are solely those of the authors and do not necessarily represent those of their affiliated organizations, or those of the publisher, the editors and the reviewers. Any product that may be evaluated in this article, or claim that may be made by its manufacturer, is not guaranteed or endorsed by the publisher.

frontiers in Pharmacology

ORIGINAL RESEARCH
published: 05 January 2022
doi: 10.3389/fphar.2021.801493

Targeting TIGIT Inhibits Bladder Cancer Metastasis Through Suppressing IL-32

Kang Wu[1,2,3†], *Jun Zeng*[4†], *Xulian Shi*[1,3†], *Jiajia Xie*[1,3†], *Yuqing Li*[1,2,3], *Haoxiang Zheng*[1,3], *Guoyu Peng*[1,3], *Guanghui Zhu*[1,3], *Dongdong Tang*[1,3] *and Song Wu*[1,5,6,7*]

[1]*Department of Urology, The Third Affiliated Hospital of Shenzhen University (Luohu Hospital Group), Shenzhen, China,* [2]*Key Laboratory of Regenerative Biology, Guangdong Provincial Key Laboratory of Stem Cell and Regenerative Medicine, South China Institute for Stem Cell Biology and Regenerative Medicine, Guangzhou Institutes of Biomedicine and Health, Chinese Academy of Sciences, Guangzhou, China,* [3]*Shenzhen Following Precision Medicine Research Institute, Shenzhen, China,* [4]*Department of Genetics and Cell Biology, College of Life Sciences, Chongqing Normal University, Chongqing, China,* [5]*Medical Laboratory of Shenzhen Luohu People's Hospital, Shenzhen, China,* [6]*Teaching Center of Shenzhen Luohu Hospital, Shantou University Medical College, Shantou, China,* [7]*Department of Urology and Guangdong Key Laboratory of Urology, The First Affiliated Hospital of Guangzhou Medical University, Guangzhou, China*

Bladder cancer is a highly metastatic tumor and one of the most common malignancies originating in the urinary tract. Despite the efficacy of immune checkpoints, including programmed cell death-1 (PD-1) and cytotoxic T-lymphocyte-associated protein 4 (CTLA-4), the effect of immunotherapy for bladder cancer remains unsatisfactory. Therefore, it is urgent to develop new targets to expand immunotherapeutic options. In this study, we utilized single-cell sequencing to explore the cell composition of tumors and detected a subset of Treg cells with high expression of T-cell immunoreceptor with immunoglobulin and immunoreceptor tyrosine-based inhibitory motif domain (TIGIT) and interleukin (IL)-32. The antitumor immune response was suppressed by this subset of Treg cells, while IL-32 promoted bladder cancer metastasis. Nevertheless, targeting TIGIT not only reversed immunosuppression by restoring the antitumor immune response mediated by T cells but also suppressed the secretion of IL-32 and inhibited the metastasis of bladder cancer cells. Thus, our study provided novel insights into immunosuppression in bladder cancer and highlighted TIGIT as a novel target for immunotherapy of bladder cancer. We also illustrated the mechanism of the dual effect of targeting TIGIT and revealed the metastasis-promoting effect of IL-32 in bladder cancer. Collectively, these findings raise the possibility of utilizing TIGIT as a target against bladder cancer from the bench to the bedside.

Keywords: bladder cancer, TIGIT, IL-32, metastasis, immunotherapy

OPEN ACCESS

Edited by:
Xuefeng Li,
Guangzhou Medical University, China

Reviewed by:
Yubin Li,
University of Pennsylvania, United States
Lei Guo,
University of Texas Southwestern Medical Center, United States

***Correspondence:**
Song Wu
wusong@szu.edu.cn

†These authors have contributed equally to this work

Specialty section:
This article was submitted to Inflammation Pharmacology, a section of the journal Frontiers in Pharmacology

Received: *25 October 2021*
Accepted: *24 November 2021*
Published: *05 January 2022*

Citation:
Wu K, Zeng J, Shi X, Xie J, Li Y, Zheng H, Peng G, Zhu G, Tang D and Wu S (2022) Targeting TIGIT Inhibits Bladder Cancer Metastasis Through Suppressing IL-32. Front. Pharmacol. 12:801493. doi: 10.3389/fphar.2021.801493

INTRODUCTION

Treatment strategies for patients with solid tumors have traditionally been based on three different options: surgery, targeted therapies, and cytotoxic therapy (chemotherapy or radiation therapy) (Chauvin and Zarour, 2020). Immunotherapy has only recently emerged as a novel therapeutic paradigm in our armamentarium (Solomon and Garrido-Laguna, 2018). Unfortunately, the vast majority of patients cannot benefit from immunotherapy (Ma et al., 2021). Thus, it is necessary to explore new targets for immunotherapy to facilitate the improved treatment of solid tumors.

T-cell immunoreceptor with immunoglobulin and ITIM domain (TIGIT, also called WUCAM, Vstm3, or VSIG9) is a receptor of the Ig superfamily, which plays a critical role in the regulation of immunoresponses (Chauvin and Zarour, 2020). In particular, TIGIT is an immunoreceptor inhibitor checkpoint that has been implicated in tumor immunosurveillance (Manieri et al., 2017; Harjunpaa and Guillerey, 2020). Preclinical models, such as colorectal cancer and melanoma models, have suggested the synergy of anti-TIGIT antibodies with anti-PD-1/PD-L1 antibodies (Curran, 2018). Interestingly, TIGIT molecules have been identified on the surface of $CD8^+$ T cells in bladder cancer, but their function has not been well characterized (Han et al., 2021).

Interleukin-32 (IL-32) is a novel cytokine regulating cancer development and inflammation (Kwon et al., 2018). IL-32 is initially expressed selectively in mitogen-activated T cells and NK cells, and its expression is strongly augmented by microbes, mitogens, and other cytokines (Kim, 2014; Lee et al., 2019). Despite IL-32 being induced mainly by pathogens and proinflammatory cytokines, its expression is more prominent in immune cells than in nonimmune tissues (Khawar et al., 2016). Moreover, IL-32 is expressed in various human tissues and organs such as the spleen, thymus, leukocytes, lung, small intestine, colon, prostate, heart, placenta, liver, muscle, kidney, pancreas, and brain (Oh et al., 2011; Yun et al., 2018; Baselli et al., 2020). Previous studies have demonstrated that IL-32 regulates cell proliferation, metabolism, and immune response and is also involved in the pathological regulation or protection against inflammatory diseases (Netea et al., 2008; Kwon et al., 2018; Palstra et al., 2018). IL-32 has also been involved in various cancers, including renal cancer, esophageal cancer, lung cancer, gastric cancer, breast cancer, pancreatic cancer, lymphoma, osteosarcoma, breast cancer, colon cancer, and thyroid carcinoma (Tsai et al., 2014; Hong et al., 2017; Wen et al., 2019). However, other studies have suggested that IL-32 decreases tumor development, including cervical cancer, colon cancer, prostate cancer, melanoma, pancreatic cancer, liver cancer, and chronic myeloid leukemia (Nishida et al., 2009; Lee et al., 2011; Park et al., 2012; Sloot et al., 2018). Notably, the expression of IL-32 receptor (IL-32R) on the surface of epithelial cells is mediated by the stimulation of interferon gamma (IFN-γ), as previously reported (Aass et al., 2021). Although a higher expression of IL-32 has been demonstrated in bladder cancer, its function has not been well characterized (Yang et al., 2020).

Taken together, our study demonstrated the enrichment of $TIGIT^+$ Treg cells in bladder cancer tissues. Furthermore, Treg cells expressed IL-32 to promote the migration and invasion of bladder cancer cells. In addition, targeting TIGIT with anti-TIGIT monoclonal antibodies suppressed the metastasis of bladder cancer and reversed its antitumor activities. Thus, we have provided novel insights into the function of IL-32 in bladder cancer and the effect of anti-TIGIT monoclonal antibodies against bladder cancer.

MATERIALS AND METHODS

Single-Cell RNA Sequencing

The BD Rhapsody system was used to capture the transcriptomic information of bladder-derived single cells with BD Rhapsody WTA Amplification Kit (Becton, Dickinson and Company, BD Biosciences). Single-cell capture was achieved by random distribution of a single-cell suspension across >200,000 microwells using a limited dilution approach. Beads with oligonucleotide barcodes were added to saturation, so that a single bead was paired with a single cell in a microwell. Cell lysis buffer was added so that the polyadenylated RNA molecules hybridized to beads. Beads were collected in a single tube for reverse transcription. Upon complementary DNA (cDNA) synthesis, each cDNA molecule was tagged on the 5 end, that is, the 3 end of the messenger RNA (mRNA) transcript, with a unique molecular identifier (UMI) and cell label indicating its cell of origin. Whole transcriptome libraries were prepared using the BD Rhapsody single-cell whole-transcriptome amplification workflow. In brief, second-strand cDNA was synthesized, followed by ligation of the WTA adaptor for universal amplification. Eighteen PCR cycles were used to amplify adaptor-ligated cDNA products. Sequencing libraries were prepared using random priming PCR of whole-transcriptome amplification products to enrich the 3 end of transcripts linked with the cell label and UMI. Sequencing libraries were quantified using a High-Sensitivity DNA chip (Agilent) on a Bioanalyzer 2200 and the Qubit High-Sensitivity DNA assay (Thermo Fisher Scientific). The library for each sample was sequenced using an Illumina sequencer (Illumina) on a 150-bp paired-end run.

Single-Cell RNA Statistical Analysis

scRNA-seq data analysis was performed by NovelBio Co., Ltd. using the NovelBrain cloud analysis platform. We applied fast p using default parameter settings that filtered the adaptor sequence and removed low-quality reads to achieve clean data (Chen et al., 2018). UMI tools were applied for single-cell transcriptome analysis to identify the cell barcode whitelist (Smith et al., 2017). UMI-based clean data were mapped to the human genome (Ensemble version 91) utilizing STAR mapping with customized parameters from the UMI tools standard pipeline to obtain the UMI counts of each sample (Dobin et al., 2013). Cells containing over 200 expressed genes and mitochondrial UMI rates below 20% passed the cell quality filtering, and mitochondrial genes were removed from the expression table. The Seurat package (version: 2.3.4, https://satijalab.org/seurat/) was used for cell normalization and regression based on the expression table according to the UMI counts of each sample and percentage of mitochondrial rate to obtain scaled data. Principal component analysis (PCA) was constructed based on the scaled data with the top 2,000 highly variable genes, whereas the top 10 principals were used for the construction of t-SNE and UMAP.

Utilizing the graph-based cluster method (resolution = 0.8), we acquired the results of unsupervised cell clusters based on the PCA top 10 principals and calculated the marker genes using the FindAllMarkers function with the Wilcoxon rank-sum test

algorithm under the following criteria: (1) lnFC >0.25; 2. p value < 0.05; 3. min. pct >0.1. To identify the cell type in detail, clusters of the same cell type were selected for re-tSNE analysis, graph-based clustering, and marker analysis.

Estimation of Copy Number Variations

Cells were defined as endothelial cells, fibroblast cells, macrophages, epithelial cells, T cells, and B cells and were used as a reference to identify somatic copy number variations (CNVs) with the R package infercnv (v0.8.2). We scored each cell according to the extent of the CNV signal, defined as the mean of squares of CNV values across the genome. Putative malignant cells were then defined as those with a CNV signal above 0.05 and CNV correlation above 0.5.

Patient Specimens

Specimens were collected from 24 patients with bladder cancer at the Luohu Hospital. The protocol adopted in this study conformed to the ethical guidelines of the 1975 Helsinki Declaration and was approved by the Ethics Review Committee of Luohu Hospital. Clinical data, pathological features, AJCC staging, and other data were collected for follow-up visits and subsequent analyses. Tumor staging was estimated according to the histological classification criteria proposed by the International Union for Cancer. A total of 24 tumor and adjacent normal tissue pairs were collected from patients who underwent bladder cancer resection between 2018 and 2019. Clinical samples are listed in **Supplementary Table I**.

Cell Culture

T24 and EJ human bladder cancer cell lines, and the MBT2 mouse bladder cancer cell line, were purchased from the American Type Culture Collection (ATCC). All cell lines were identified by short-tandem repeat analysis and were guaranteed to be used within 6 months. The most recent test was performed 3 months ago. All cell lines were maintained in Roswell Park Memorial Institute (RPMI) 1640 (Invitrogen) supplemented with 1×10^7 U/L penicillin (Invitrogen), 10 mg/L streptomycin (Sigma-Aldrich), and 10% fetal bovine serum (FBS) (Gibco) in a humidified incubator at 37°C and 5% CO_2 atmosphere, following cell culture guidelines.

In Vivo Tumor Model

MBT2-luciferase cells were established as previously described. Briefly, the full-length cDNA sequence of the luciferase gene was synthesized (Shanghai Generay Biotech Co., Ltd.) and cloned into the pMSCV-puro retroviral vector plasmid (Clontech Laboratories Inc.) to generate the pMSCV-luciferase plasmid. pMSCV-luciferase was cotransfected with the pIK packaging plasmid into 293T cells using the calcium phosphate transfection method. Then, 48 h after transfection, the supernatants were collected and incubated with MBT2 cells. The infectious mixture was incubated for 24 h in the presence of polybrene (2.5 μg/ml). Puromycin (4 μg/ml) was then used to select stably transfected cells over a 12-day period. Female C57B6/J mice (6–8 weeks of age) were housed under specific pathogen-free (SPF) conditions. All animal care and experiments were conducted in accordance with the guidelines provided by the Animal Center of Luohu Hospital and were approved by the Experimental Animal Ethics Committee of Luohu Hospital. In the mouse lung metastasis model, 1×10^6 MBT2-luciferase cells were intravenously injected into two groups of mice. Mice were euthanized at 4 and 6 weeks after injection to observe tumor cell metastasis in the lungs. Metastases were confirmed by hematoxylin and eosin (H&E) staining. The bladder cancer orthotropic mouse model was established by injecting 1×10^6 MBT2-luciferase cells into the bladder wall of mice after anesthesia. After 18 days, each mouse was intravenously injected with 100 μg of neutralizing antibodies every 3 days. Mice were examined daily, and the date of death was recorded for each mouse. To establish the subcutaneous model, MBT2 cells (1×10^6 in 50 μl FBS-free medium containing 20% Matrigel) were injected into the left flank of recipient mice. After 18 days, each mouse was intravenously injected with 100 μg of neutralizing antibodies every 3 days. Mice were examined daily, and the date of death was recorded for each mouse.

In Vivo Bioluminescence

C57B6/J mice inoculated with MBT2-luciferase cells were anesthetized by intraperitoneal injection of sodium pentobarbital (50 mg/kg) and then injected with D-luciferin potassium salt (150 mg/kg). After 15 min, the bioluminescence of mice was tracked and imaged (AniView100, Biolight Biotechnology Co., Ltd.).

Flow Cytometry

Cells were analyzed by flow cytometry, as previously described (Wu et al., 2019a). Single-cell suspensions were prepared from the bladder, spleen, blood, or tumors of individual mice. For cell staining, cells were preincubated in 0.1% bovine serum albumin (BSA)/phosphate-buffered saline (PBS) solution containing 10 μg/ml anti-FcgRII/III (2.4 G2) (BD Pharmingen) for 10 min at 4°C. Cells were then stained for 20 min at 4°C with primary antibodies. For intracellular cytokine staining, cells were stimulated with 100 ng/ml phorbol 12-myristate 13-acetate (PMA) (Sigma-Aldrich) and 1 μg/ml ionomycin (Sigma-Aldrich) in the presence of 5 μg/ml brefeldin A (Sigma-Aldrich) for 4 h. Cells were washed twice in PBS, fixed, and permeabilized using the BD Cytofix/Cytoperm™ fixation/permeabilization kit. Stained samples were analyzed using the BD FACSAria II system (BD Biosciences). Flow cytometric data were analyzed using the FlowJo software (Tree Star).

The primary antibodies used in the study included anti-FOXP3 (MF-14), anti-CD25 (3C7), anti-CD3 (145-2C11), anti-TIGIT (1G9), anti-CD8 (53-6.7), anti-IFN-γ (XMG1.2), and anti-CD4 (RM4-5).

Mice

C57BL/6J mice were purchased from Vital River Laboratories (Beijing, China) and bred under specific pathogen-free (SPF) conditions at Luohu Hospital. All mouse experiments were approved by the Institutional Animal Care and Use Committee of Luohu Hospital.

Scratch Wound Healing Assay

To evaluate their migration ability after treatment, T24 cells and EJ cells were seeded into six-well cell culture plates and grown in RPMI 1640 medium containing 10% FBS for 24 h to form an adherent monolayer with a degree of fusion approaching 70%–80%. A cross was scratched in the culture plate using a 200-μl sterile pipette tip, and detached cells were removed by gently washing the well twice with PBS. Fresh medium was added to the culture wells, and cells were cultured with IFN-γ (10 ng/ml) or IL-32 (10 ng/ml) for an additional 24 h. Transplanted cells were photographed (40×) using an inverted optical microscope (Zeiss) at 0 and 24 h to monitor the migration of cells to the wound area and calculate wound closure.

Invasion Assays

To assess the invasion ability of T24 and EJ cells, matrix gel (Corning) was thawed overnight at 4°C and diluted in serum-free medium RPMI 1640 at a scale of 1:7. Next, a Transwell was coated in a 24-well plate with 50 μl diluted matrix gel and incubated at 37°C for 30 min. Then, 1×10^5 cells in serum-free medium were seeded into the Transwell upper chamber. Concomitantly, 500 μl RPMI 1640 medium supplemented with 10% FBS was added to the lower Transwell chamber and incubated with IFN-γ (10 ng/ml) or IL-32 (10 ng/ml) at 37°C and 5% CO_2 for 24 h. The Transwell chamber was removed, washed thrice with PBS, and dried using a cotton swab. Cells were fixed with 4% paraformaldehyde (Sigma-Aldrich) and stained with crystal violet for 5 min. The Transwell chamber was photographed, and cells were counted under an optical microscope (40×) (Zeiss).

Immunohistochemistry

Tumor and animal tissues were fixed with paraformaldehyde, dehydrated, and cleared using a gradient of alcohol solutions and xylene, respectively. Subsequently, tissues were embedded in paraffin. Paraffin-embedded tissues were sliced continuously (3.5°C) using a HistoCore AUTOCUT system (Leica), mounted, dewaxed, and rehydrated. For antigen retrieval, sections (3–4 μm) were pretreated in a microwave oven with citric acid buffer (pH 6.0) for 12 min and then cooled to 25°C in deionized water. Sections were then incubated in methanol containing 3% hydrogen peroxide to inhibit endogenous peroxidase activity. After washing with PBS for 5 min, sections were incubated with normal goat serum at 37°C for 1 h, and incubated overnight with anti-IL-32 and anti-TIGIT (Proteintech) at 4°C. Sections were then washed again with PBS containing 0.1% BSA and incubated with rabbit anti-goat IgG and horseradish peroxidase (HRP)-linked antibodies (Proteintech). Specific binding was assessed using diaminobenzidine; hematoxylin and eosin staining (Solarbio) was performed as counterstaining. Paraffin sections were photographed using the imaging system of an ortho DM6 B microscope (Leica).

Real-Time Quantitative PCR

Total RNA was extracted and purified using a standard procedure. Total purified RNA was reverse-transcribed into cDNA using a reverse transcription kit (k1622, Thermo Scientific, United States). Primers were designed using the Primer-BLAST tool (https://www.ncbi.nlm.nih.gov/tools/primer-blast/): forward primer, 5′-CGGAATTCATGTGCT TCCCGAAGGTCC-3′; reverse primer, 5′-CCGCTCGAGTCA TTTTGAGGATTGGGGTTC-3′. Quantitative real-time PCR (qRT-PCR) was performed on an ABI 7500 real-time fluorescent quantitative PCR instrument using SYBR Green (420A, Takara). Cycle threshold values of genes of interest were normalized to that of GAPDH: forward primer, 5′-CCC AGCTTAGGTTCATCAGGT-3′; reverse primer, 5′-TACGGC CAAATCCGTTCACA-3′.

Immunofluorescence Staining

Immunofluorescence staining was performed as previously described (Wu et al., 2019b). Briefly, tumor and animal tissues were fixed with paraformaldehyde, dehydrated, and cleared with a gradient of alcohol solutions and xylene, respectively. Consecutively, tissues were embedded in paraffin. Paraffin-embedded tissues were sliced continuously (3.5°C) using a HistoCore AUTOCUT system (Leica), mounted, dewaxed, and rehydrated. For antigen retrieval, sections (3–4 μm) were pretreated in a microwave oven with citric acid buffer (pH 6.0) for 12 min and then cooled to 25°C in deionized water. After washing with PBS for 5 min, sections were incubated with 5% normal goat and donkey serum at 37°C for 1 h at 25°C and then incubated with the primary antibody (1:800, ab37647, Abcam) at 4°C overnight. After washing at least thrice with PBS, sections were incubated with the following secondary antibodies: Alexa 633-conjugated donkey anti-rat antibody (1:500, Invitrogen), Alexa 596-conjugated goat anti-rabbit (1:500, Invitrogen), and Alexa 488-conjugated goat anti-mouse antibody (1:250, Invitrogen) for 1 h at 25°C. Afterward, cells were extensively washed with PBS, and their nuclei were labeled using 4′,6-diamidino-2-phenylindole (DAPI). Free-floating sections with positive immunofluorescence staining were captured and analyzed using a laser scanning confocal microscope (Zeiss).

Cell Counting Kit-8 Assay

Cell proliferation was measured using the Cell Counting Kit-8 (CCK-8) reagent (Solarbio), as previously described (Wang et al., 2021). Briefly, cells were cultured in 96-well plates with corresponding treatments. At 0, 24, 48, and 72 h, 10 μl CCK-8 reagent was added to each well. After 2 h of incubation at 37°C, the optical density at 450 nm was measured using a microplate reader.

Statistical Analysis

Data were analyzed using the GraphPad Prism 8.0.2 software, SPM 12, and REST software. All quantitative data are shown as the mean ± SD of at least three independent experiments. Two-group comparisons were assessed using the Student's *t*-test. Multigroup comparisons were analyzed using one-way ANOVA, followed by the Bonferroni *post-hoc* test on dependent experimental designs. Statistical significance was set at $p < 0.05$.

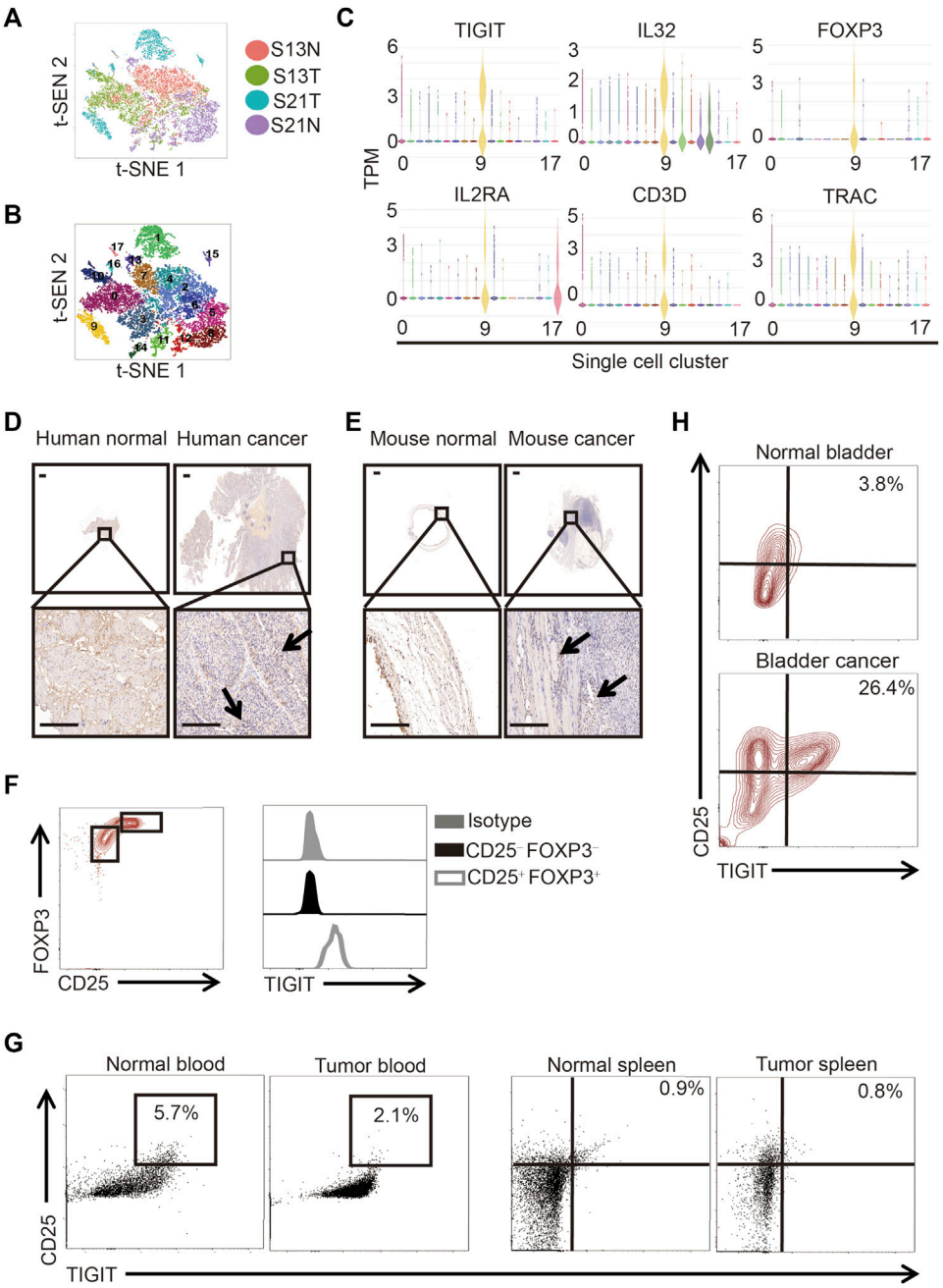

FIGURE 1 | TIGIT$^+$ Treg cells in bladder cancer tissues. **(A)** Schematic showing the single-nucleus RNA sequencing process. Samples of bladder tissues were surgically removed. Single cells were obtained from cancerous (n = 2) or paracancerous (n = 2) bladder tissues of patients and processed by plate-based scRNA-seq.**(B)** Two-dimensional t-distributed stochastic neighbor embedding (t-SNE) visualization from single-nucleus RNA sequencing showing the distribution of all nuclei. Eighteen major nuclear classes were identified. Each dot represents a single nucleus colored according to cluster assignment. Background is colored by major cell types (epithelial cells, T cells, B cells, endothelial cells, fibroblasts, stromal cells, umbrella cells, and smooth muscle cells). **(C)** Gene expression for each TIGIT + IL-32 + IL2RA + FOXP3+ CD3$^+$ TRAC + single cell plotted as log2 counts per million. **(D,E)** Higher expressions of TIGIT in human **(D)** and murine **(E)** bladder cancer tissues. Immunohistochemistry images showing the expression of TIGIT in bladder tissues collected from different anatomical sites and groups of animals. Representative data from four independent experiments (n = 5). Scale bar = 1 mm. **(F)** Higher level of expression of TIGIT on the surface of Treg cells. Overlaid histogram plots showing the levels of expression of TIGIT in different CD4$^+$ T-cell subsets. Data are representative of three independent experiments (n = 6). **(G)** TIGIT + Treg cells in the blood and spleen of mice with bladder cancer. The numbers in the dot plots represent the frequencies of TIGIT + Treg cells. Data are representative of three independent experiments (n = 8). **(H)** Higher frequencies of TIGIT + Treg cells in murine bladder cancer tissues. The numbers in the dot plots represent the frequencies of TIGIT + Treg cells. Data are representative of four independent experiments (n = 8).

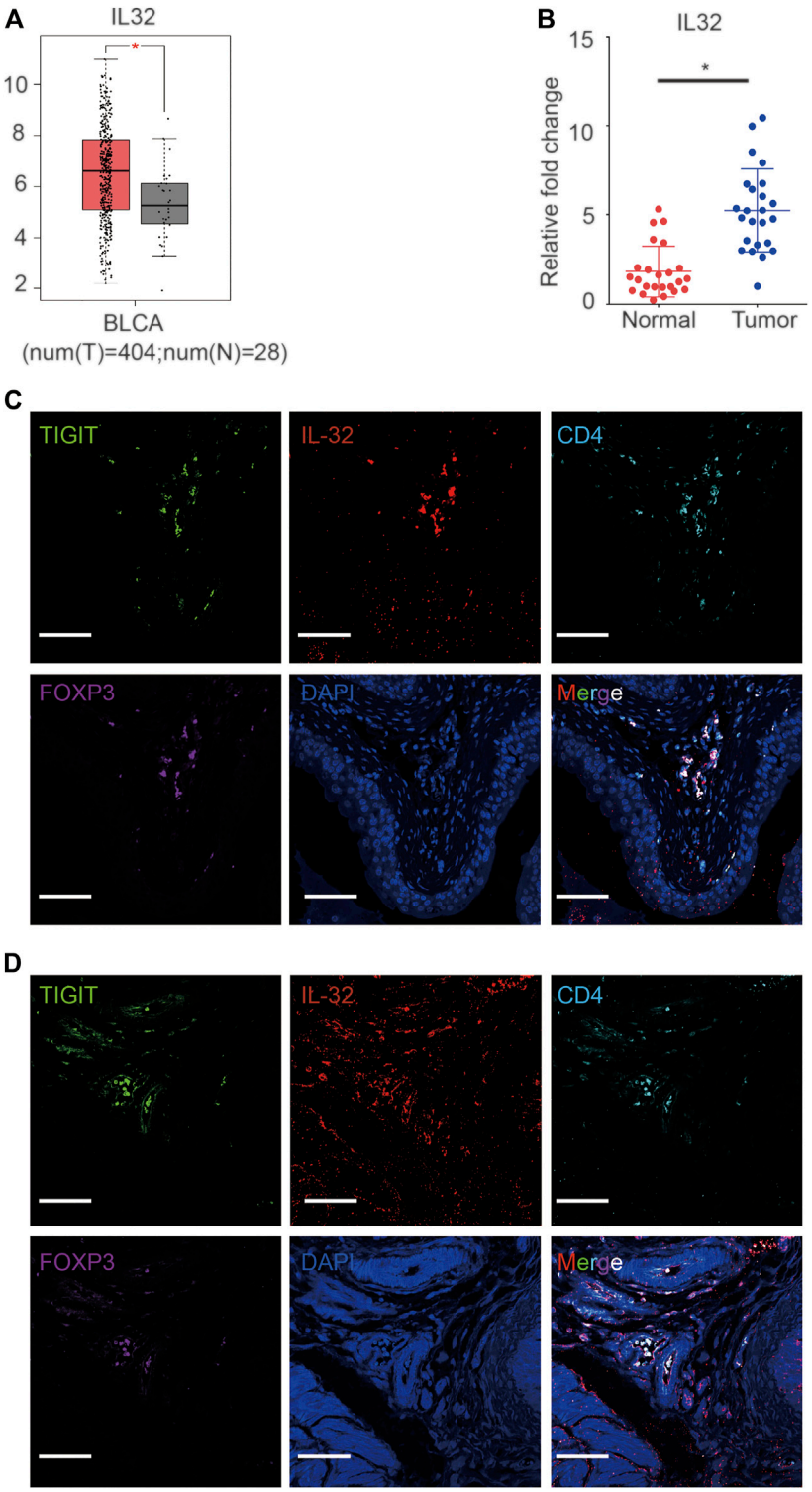

FIGURE 2 | Expression of IL-32 in Treg cells in bladder cancer tissues. **(A)** Higher expression of IL-32 in the bladder cancer cohort in the TCGA and GTEx databases. Data are shown as the mean ± standard deviation (SD). *$p < 0.05$; *t*-test. **(B)** Higher relative expression of IL-32 in bladder cancer tissues. qRT-PCR analysis showing the relative expression of IL-32 in healthy and cancerous bladder tissues. Data are shown as the mean ± SD. *$p < 0.05$; *t*-test. **(C)** IL-32 colocalizes with Treg cells in human bladder cancer tissues. Representative immunofluorescence images showing cells stained with anti-FOXP3 (violet), IL-32 (red), CD4 (light blue), TIGIT (green), and DAPI (blue). Scale bar = 100 μm.**(D)** IL-32 colocalizes with Treg cells in murine bladder cancer tissues. Representative immunofluorescence images showing cells stained with anti-FOXP3 (violet), IL-32 (red), CD4 (light blue), TIGIT (green), and DAPI (blue). Scale bar = 100 μm.

RESULTS

Existence of TIGIT$^+$ Treg Cells in Bladder Cancer Tissues

To determine the cell composition of bladder cancer tissues, we compared the cells in clinical samples of bladder cancer tissues to those of paracancerous tissues using single-cell sequencing. Following the employment of PCA for the reduction of the dimensionality of single-cell gene expression profiles, in both bladder cancer and paracancerous tissues, we identified 18 clusters based on principal components. We used t-distributed stochastic neighbor embedding (t-SNE) to visualize the gene expression profiles (**Figures 1A, B**). In particular, we detected the presence of a subset of regulatory T (Treg) cells in bladder cancer tissues but not in paracancerous tissues (**Figure 1B**). Interestingly, we found that this subset of Treg cells not only highly expressed IL-2Rα (also called CD25) and forkhead box protein 3 (FOXP3) but also TIGIT and IL-32 (**Figure 1C**). To verify the protein expression of TIGIT in bladder cancer tissues, we performed immunohistochemistry (IHC) analysis of TIGIT in both bladder cancer and paracancerous tissues in patients and mice. We observed that in both human and mice, the expression of IL-32 was much higher in bladder cancer than in paracancerous tissues (**Figures 1D, E**). Furthermore, we examined the expression of TIGIT in Treg cells from murine bladder cancer tissues. As expected, TIGIT was highly expressed on the surface of Treg cells from bladder cancer tissues (**Figure 1F**). In addition, we detected higher frequencies of TIGIT$^+$ Treg cells only in bladder cancer tissues but not in spleen tissues or peripheral blood cells (**Figures 1G,H**). Thus, TIGIT$^+$ Treg cells were unambiguously enriched in bladder cancer tissues.

Expression of IL-32 in Treg Cells in Bladder Cancer Tissues

Based on single-cell sequencing results, Tregs infiltrating bladder cancer tissues also expressed IL-32. To confirm the high expression of IL-32 in bladder cancer, we analyzed data from The Cancer Genome Atlas Program (TCGA) and The Genotype-Tissue Expression Project (GTEx) as previously reported (Tang et al., 2017). As expected, we noticed that the expression of IL-32 in the bladder cancer cohort was higher than that in the healthy cohort (**Figure 2A**). To validate the upregulation of IL-32 in bladder cancer tissues, we measured the expression of IL-32 using quantitative real-time PCR (qRT-PCR). We found that the expression of IL-32 was indeed upregulated in bladder cancer tissues to a certain extent (**Figure 2B**). However, whether IL-32 was expressed in Treg cells from bladder cancer tissues remains unknown. To verify the expression of IL-32 in Treg cells in bladder cancer tissues, we analyzed the abundances of IL-32, TIGIT, FOXP3, and CD25 in the TCGA and GTEx as previously reported (Tang et al., 2017). We accordingly detected that the expression of IL-32 was correlated with the abundance of TIGIT, FOXP3, and CD25 (**Supplementary Figure S1**). To validate the expression of IL-32 in Treg cells, we analyzed the colocalization of IL-32 and Treg cells using immunofluorescence. We found that IL-32 was colocalized with FOXP3 and TIGIT in clinical bladder cancer samples (**Figure 2C**). To establish an animal model to test the function of targeting TIGIT or IL-32 against bladder cancer, we inoculated C57B6/J mice with MBT-2 cells and analyzed the colocalization of IL-32 and Treg cells. As expected, we noticed that IL-32 was also colocalized with FOXP3 and TIGIT in murine bladder cancer tissues (**Figure 2D**). Collectively, our data suggested that IL-32 is highly expressed in Treg cells in bladder cancer tissues.

IL-32 Promoted the Metastasis of Bladder Cancer

As previously reported, IL-32 has multiple potential functions (Hong et al., 2017). To explore the specific function of IL-32 in bladder cancer, we incubated bladder cancer cells with a minimal concentration of IL-32 to mimic the effect of the secretion of IL-32 from Treg cells on bladder cancer cells. Similar to the effect of IL-32 on colorectal cancer, we found that IL-32 enhanced the migration of T24 and EJ cells (**Figure 3A**) (Yang et al., 2015). Moreover, IL-32 increased the invasion of bladder cancer cells (**Figure 3B**). However, we observed that IL-32 did not mediate the proliferation of bladder cancer cells (**Figure 3C**). To explore the mechanism of the IL-32-mediated invasion and migration of bladder cancer cells, we analyzed the relationship between the abundance of IL-32 and the expression of molecules that mediate the invasion and migration of bladder cancer cells in the TCGA and GTEx databases (Tang et al., 2017). We found that the expression of IL-32 was associated with the abundance of the C–C motif chemokine ligand 4 (CCL4) (**Figure 3D**). Hence, IL-32 promoted the metastasis of bladder cancer.

Targeting TIGIT Suppressed Bladder Cancer

Given the good performance of the monoclonal antibody of TIGIT (α-TIGIT) against some carcinomas, we explored the antitumor capacity of TIGIT antibodies against bladder cancer. To ensure the specificity of α-TIGIT and minimize any side effects, we analyzed the distribution of TIGIT in the whole body of patients. Using the Protein Atlas database, we detected that the expression of TIGIT was higher in the urinary tract than in other tissues, except for lymphatic tissues (**Supplementary Figure S2**). Thus, we aimed to establish a bladder cancer orthotropic model and then compare the antitumor capacity of α-PD-1 and α-TIGIT. To visually compare the long-term efficacy of these antibodies, we established a murine model transfected with luciferase-expressing MBT-2 cells. Then, 18 days after inoculation, we intravenously administered mice with α-PD-1 or α-TIGIT (**Figure 4A**). We found that the tumor size in mice administered α-TIGIT was suppressed to a greater extent compared with that in mice administered α-PD-1 (**Figure 4A**). In addition, we observed that compared with mice injected with α-PD-1, the weights of bladders in mice administered α-TIGIT were greatly reduced (**Figure 4B**). Moreover, the survival rates of mice administered α-TIGIT

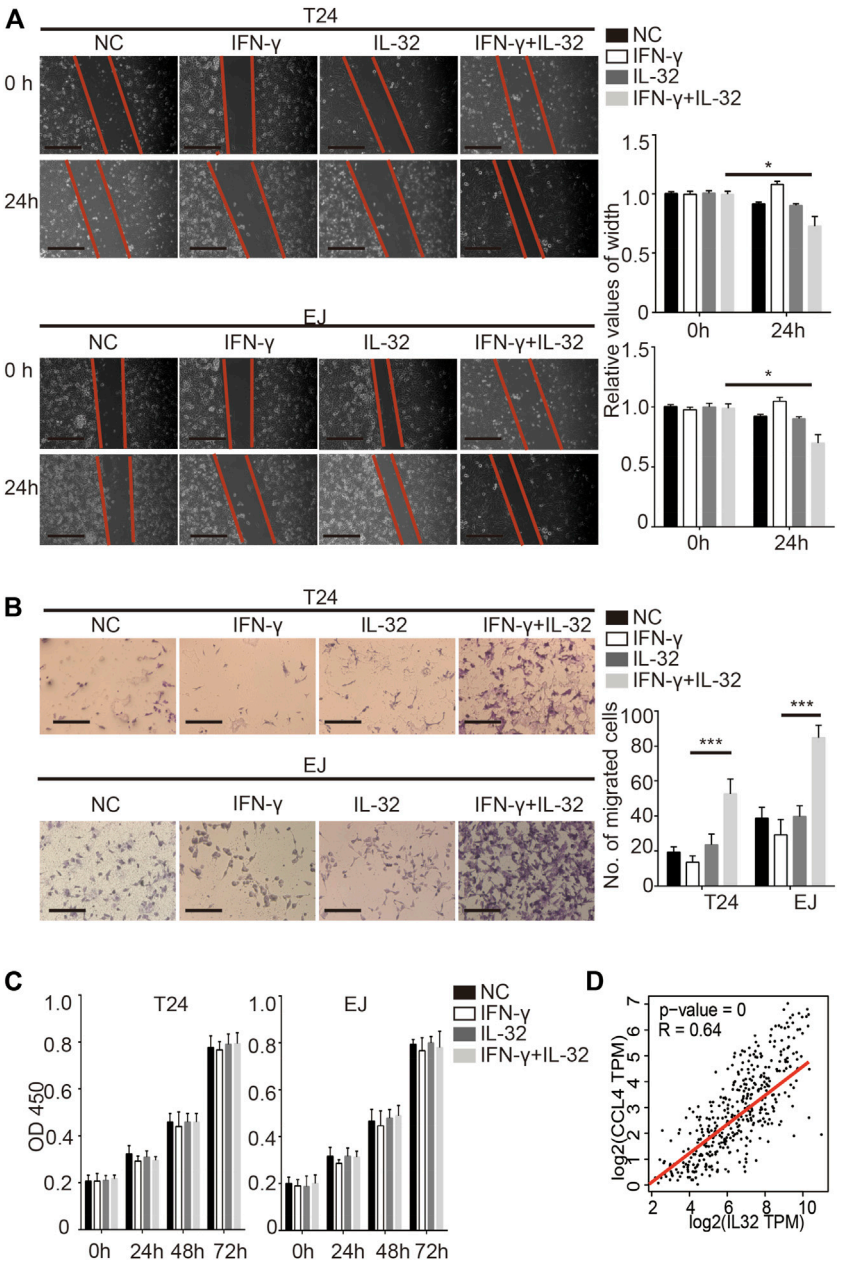

FIGURE 3 | IL-32 promotes the metastasis of bladder cancer. **(A)** IL-32 enhances the migration ability of bladder cancer cells. Representative data of 3 independent experiments from wound healing migration assays performed with the indicated bladder cancer cells. Scale bar = 100 μm **(left panel)**. The relative values of width are shown as the mean ± SD. *$p < 0.05$; one-way ANOVA **(right panel)**. **(B)** IL-32 increases the invasion ability of bladder cancer cells. Representative data of three independent experiments from crystal violet staining showing the invasive capacities of bladder cancer cells. Scale bar = 100 μm **(left panel)**. The number of migrated cells is shown as the mean ± SD. ***$p < 0.001$; one-way ANOVA **(right panel)**. **(C)** IL-32 does not disrupt the proliferation of bladder cancer cells. Cell viability was measured using the CCK8 assay. Data are shown as the mean ± SD. **(D)** The association between IL-32 and CCL4. The relationship between IL-32 and CCL4 in the TCGA and GTEx databases is shown. Spearman's rank correlation coefficient is shown.

were also higher than those of mice administered α-PD-1 (**Figure 4C**). Surprisingly, we did not observe any significant difference between mice administered a-TIGIT or a-PD-1 in the subcutaneous tumor model (**Figure 4D**). Our results clearly demonstrated that targeting TIGIT suppressed bladder cancer.

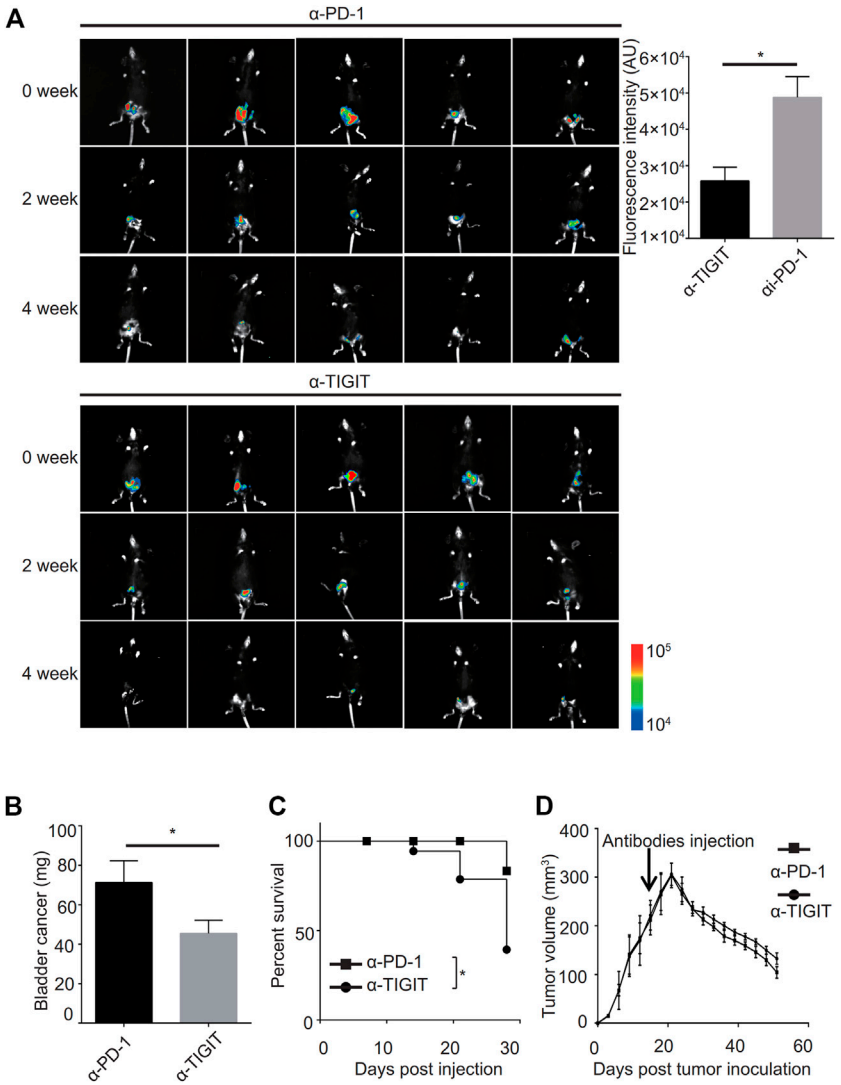

FIGURE 4 | Targeting TIGIT suppressed bladder cancer. **(A, B)** α-TIGIT suppresses bladder cancer. *In vivo* bioluminescent imaging of C57B6/J mice transplanted with MBT2-luciferase cells **(left panel)**. Bioluminescence intensities are shown as the mean ± SD. *$p < 0.05$; *t*-test. Data are representative of three independent experiments (n = 8) **(right panel)**. **(C)** α-TIGIT suppresses the growth of bladder tissues. Bladder weight of mice are shown as the mean ± SD. *$p < 0.05$; *t*-test. Data are representative of three independent experiments (n = 8). **(D)** Tumor-bearing mice administered α-TIGIT show a better prognosis. The relative survival rates of mice in different groups were recorded. Data are representative of four independent experiments (n = 6). *$p < 0.05$; log-rank (Mantel-Cox) test.

Targeting TIGIT Promoted the Capability of Antitumor of T Cells

Given the efficiency of α-TIGIT against bladder cancer, we investigated the mechanisms underlying the antitumor effects of α-TIGIT. As TIGIT is known to be functionally related to the immune system, we compared the immune activities of mice administered with α-PD-1 or α-TIGIT. We noticed that the ratios of $CD4^+$ and $CD8^+$ T cells were not disrupted by the administration of α-PD-1 or α-TIGIT (**Figure 5A**). However, we found that IFN-γ was upregulated in $CD4^+$ and $CD8^+$ T cells of mice administered α-TIGIT compared with that in mice administered α-PD-1 (**Figure 5B**). As with the enhancement of the tumor-killing capacities of immune cells, the changes in immunosuppressive cells caused by the tumor microenvironment, especially the changes in Treg cells, remain unknown. To explore the regulation of α-TIGIT in Treg cells, we analyzed the expression of CD25, TIGIT, and FOXP3 in murine bladder cancer tissues. Flow cytometric analysis showed that the ratio of $TIGIT^+$ $CD25^+$ $CD4^+$ T cells was downregulated in those tissues following the administration of α-TIGIT (**Figure 5C**). Similarly, we noticed that the ratio of Treg cells ($CD25^+$ $FOXP3^+$) in bladder cancer tissues was also downregulated after the administration of α-TIGIT (**Figure 5D**). Collectively, these data indicated that targeting TIGIT with α-TIGIT upregulated

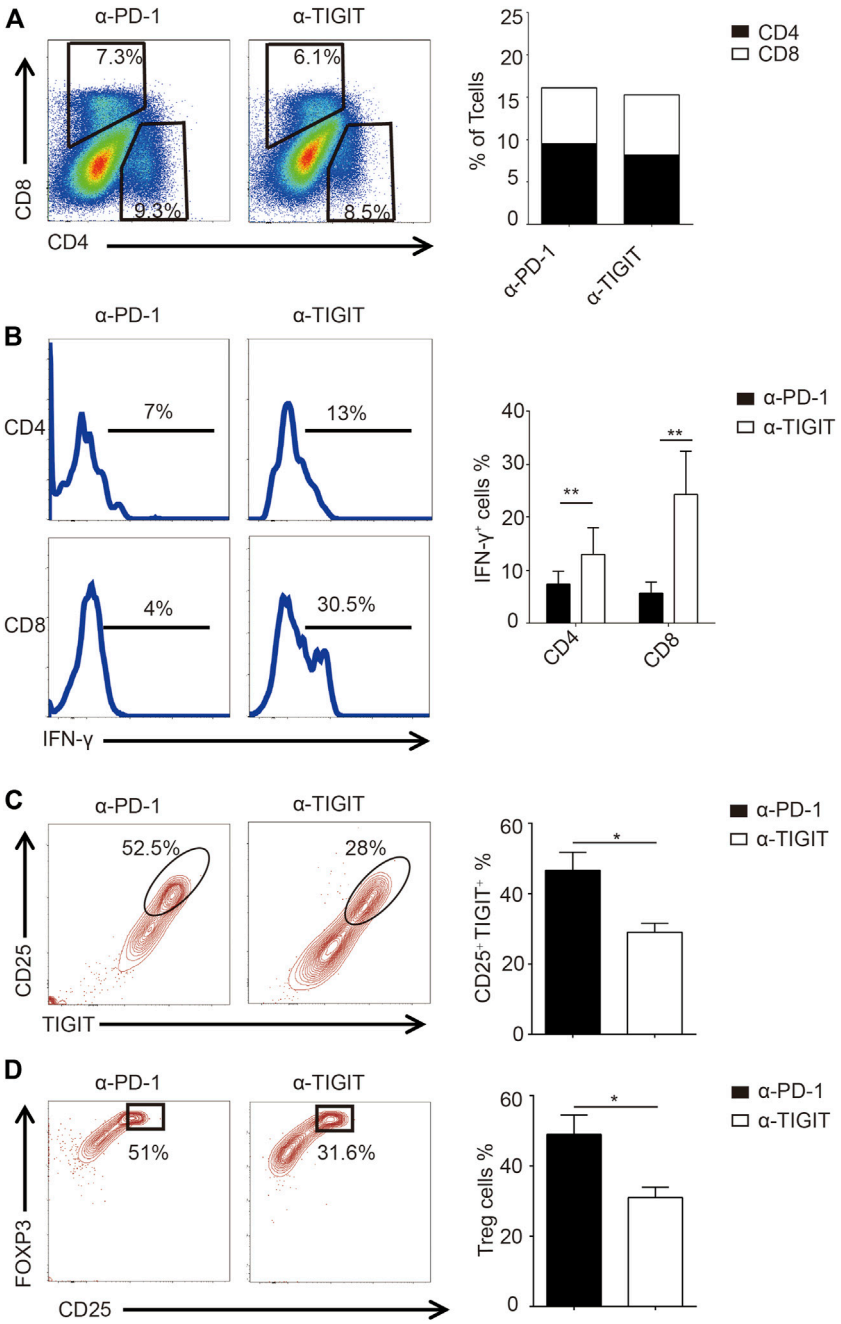

FIGURE 5 | Targeting TIGIT promoted the antitumor capability of T cells. **(A)** Administration of α-TIGIT does not affect the ratios of $CD4^+$ and $CD8^+$ T-cells in bladder cancer tissues. Dot plots represent the frequencies of $CD4^+$ and $CD8^+$ T cells in murine bladder cancer tissues from three independent experiments (n = 6) **(left panel)**. The ratios of $CD4^+$ and $CD8^+$ T cells are shown as the mean **(right panel)**. **(B)** Administration of α-TIGIT upregulates the secretion of IFN-γ in T cells. Numbers in histograms show the representative ratios of IFN-γ+ T cells from three independent experiments (n = 6) **(left panel)**. The ratios of IFN-γ+ cells are shown as the mean ± SD. $^{**}p < 0.01$; one-way ANOVA **(right panel)**. **(C)** Administration of α-TIGIT suppresses the expression of TIGIT in Treg cells. Dot plots represent the ratios of TIGIT + $CD25^+$ subsets in $CD4^+$ T cells from three independent experiments (n = 6) **(left panel)**. The ratios of TIGIT + $CD25^+$ cells are shown as the mean ± SD. $^*p < 0.05$; *t*-test **(right panel)**. **(D)** Administration of α-TIGIT suppresses the generation of Treg cells in mice with bladder cancer. Dot plots represent the ratios of $CD25^+$ FOXP3+ subsets in $CD4^+$ T cells from three independent experiments (n = 6) **(left panel)**. The ratios of $CD25^+$ FOXP3+ cells are shown as the mean ± SD. $^*p < 0.05$; *t*-test **(right panel)**.

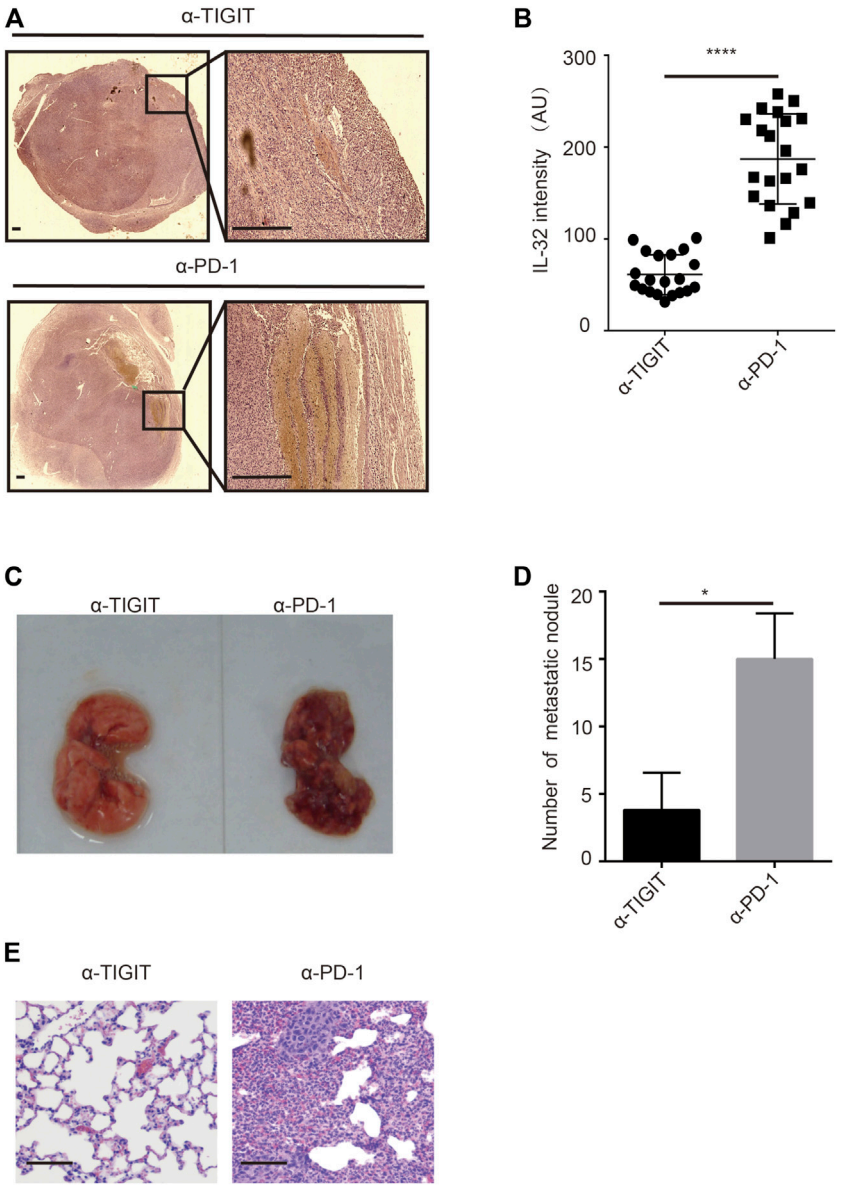

FIGURE 6 | Targeting TIGIT inhibits the metastasis of bladder cancer through suppressing IL-32. **(A,B)** Targeting TIGIT suppresses the expression of IL-32. Immunohistochemistry images showing the expression of IL-32 in bladder tissues collected from different groups of animals. Scale bar = 1 mm **(A)**. The levels of expression of IL-32 are shown as the mean ± SD. ****$p < 0.0001$; *t*-test **(B)**. Data are representative of four independent experiments (n = 7). **(C–E)** Targeting TIGIT inhibits the metastasis of bladder cancer. Metastatic nodules in lungs of mice inoculated with bladder cancer cell lines **(C)**. The number of metastatic nodules is shown as the mean ± SD. *$p < 0.05$; *t*-test **(D)**. Images showing HE-stained bladder tissues collected from different groups of animals. Scale bar = 100 μm **(E)**. Data are representative of four independent experiments (n = 7).

the antitumor capability of T cells, whereas it downregulated the induction of immunosuppression.

Targeting TIGIT Inhibited the Metastasis of Bladder Cancer Through Suppressing IL-32

Given the high abundance of IL-32 in Treg cells in bladder cancer tissues, we investigated whether targeting TIGIT with α-TIGIT suppresses the secretion of IL-32. As expected, we found that administration of α-TIGIT antibody suppressed the expression of IL-32 in bladder cancer tissues 3 days post-injection (**Figures 6A,B**). Because IL-32 mediates the metastasis and invasion of bladder cancer cells, targeting TIGIT might inhibit the metastasis of bladder cancer by suppressing the expression of IL-32. To verify this hypothesis, we intravenously injected MBT-2 cells into mice to establish a bladder cancer metastasis mouse model. After 3 days, mice were intravenously injected with α-TIGIT or α-PD-1. We accordingly detected that administration of α-TIGIT significantly reduced the number of metastatic nodules (**Figures 6C–E**). Thus, our data indicated that targeting TIGIT

inhibited the metastasis of bladder cancer cells by suppressing the expression of IL-32.

DISCUSSION

In this study, we identified a specific subset of Treg cells in human bladder cancer tissues that highly expressed TIGIT and IL-32. Furthermore, IL-32 from Treg cells promoted the metastasis of bladder cancer cells, while Treg cells mediated immunosuppression. Conversely, targeting TIGIT with anti-TIGIT antibodies enhanced the antitumor immune capacity of the host against bladder cancer. Importantly, targeting TIGIT with anti-TIGIT antibodies not only enhanced the antitumor activities of T cells but also suppressed the abundance of IL-32, in turn inhibiting the metastasis of bladder cancer cells. Thus, we have demonstrated a novel function of Treg cells in bladder cancer tissues. Hence, as an immune checkpoint, TIGIT not only enhances the antitumor immune response but also inhibits the metastasis of bladder cancer cells by suppressing the expression of IL-32.

The main function of regulatory T cells (Tregs) is to regulate immune responses, especially immunosuppression; however, functions other than immunological functions have rarely been reported (Togashi et al., 2019). In our study, we identified the accessory nonimmune function of Treg cells, that is, secreting IL-32 to promote the metastasis of bladder cancer cells. Our study showed that as immunosuppressive cells, Treg cells mediate tumor metastasis in a different way from tumor-related macrophages (Lin et al., 2019). Instead of carrying tumor cell metastasis, they secrete cytokines that mediate tumor metastasis. Meanwhile, their immunosuppressive function, that is, their canonical function, was preserved in bladder cancer tissues.

Antitumor immunotherapy is one of the most effective tumor treatments after chemotherapy and radiotherapy, but its effective rate is almost impossible to exceed 50% (Kruger et al., 2019). This is because current therapeutic targets are not suitable for all patients. In the era of precision medicine, new immunotherapy targets can be identified through sequencing technology (Zhang et al., 2021). In this study, using single-cell sequencing technology, we found that Treg cells in bladder cancer tissues highly expressed TIGIT, demonstrating it as a more suitable therapeutic target. Fortunately, targeting TIGIT had a dual effect, not only upregulating the immune response against bladder cancer but also inhibiting its metastasis. Thus, our study confirmed that this is a new way to develop and verify new immunotherapeutic targets. In particular, the CTLA-4 antibody is usually adapted to depleted Treg cells. However, administration of CTLA-4 antibodies did not downregulate the ratio of Treg cells in bladder cancer (Rouanne et al., 2018). Therefore, application of TIGIT antibodies might provide an effective option for the depletion of Treg cells in bladder cancer tissues to enhance antitumor activities. Surprisingly, in the subcutaneous tumor model, administration of a-TIGIT did not achieve better effects than injection of a-PD-1; we speculated that this was because only the bladder tumor microenvironment exhibited a higher expression of TIGIT. More importantly, we used TIGIT monoclonal antibodies as a single agent against bladder cancer and did not explore whether their combination with other drugs could achieve a better curative effect. As such, the efficacy of TIGIT in clinical practice remains inconclusive, and further research is needed.

The origin of IL-32 has been reported in different cells from distinct tumors. In contrast to breast cancer and small cell lung cancer, we have identified that IL-32 is derived from Treg cells in bladder cancer tissues (Sorrentino and Di Carlo, 2009). However, although the expression of IL-32 was positively correlated with Treg cell markers, the relationship between the expression of IL-32 and the prognosis of patients with bladder cancer in clinical practice remains unknown. Furthermore, the function of IL-32 in tumors is complex and controversial. In this study, we verified the positive effect of IL-32 for the invasion and migration of bladder cancer cells *in vitro* and identified the correlation between IL-32 and CCL4 (as a chemoattractant induced by inflammation, also known as macrophage inflammatory protein-1β) according to the TCGA and GTEx databases, but its function *in vivo* remains unknown. IL-32 is known to be an inflammation factor (Hong et al., 2017). However, the specific pathway by which IL-32 mediates the migration and invasion of tumor cells remains unknown. Meanwhile, it also remains unknown whether IL-32 first induces inflammation and then causes tumor metastasis in bladder cancer, especially by inducing the generation of cancer-associated fibroblasts through inflammation. In addition, although the TIGIT antibodies used in this study achieved a good effect of inhibiting the abundance of IL-32, the direct development of IL-32 monoclonal antibodies for the inhibition of IL-32 is a very attractive therapeutic option. Of note, regardless of breast cancer, colorectal cancer, and bladder cancer, the expression of IL-32 has been identified in several tumor tissues (Diakowska and Krzystek-Korpacka, 2020). However, IL-32 exhibits flowing characteristics and remains unclear whether it can be detected in blood or urine to be used as a diagnostic marker.

Overall, our study revealed the existence of $TIGIT^+$ $IL\text{-}32^+$ Treg cells in bladder cancer tissues. These cells not only suppressed antitumor immunoresponses but also promoted tumor metastasis. Surprisingly, targeting TIGIT not only relieved immunosuppression and enhanced immunity but also inhibited tumor metastasis, providing a double therapeutic benefit. Thus, our study provided an alternative option for bladder cancer therapy.

DATA AVAILABILITY STATEMENT

The datasets presented in this study can be found in online repositories. The names of the repository/repositories and accession number(s) can be found below: https://www.ncbi.nlm.nih.gov/geo, GSE186520.

ETHICS STATEMENT

All mice experiments were approved by the Institutional Animal Care and Use Committee of Luohu Hospital. Written informed

consent was obtained from the individual(s), and minor(s)' legal guardian/next of kin, for the publication of any potentially identifiable images or data included in this article.

AUTHOR CONTRIBUTIONS

Conceptualization: KW and XS. Methodology: YL, DT, HZ, GP, and GZ. Writing—original draft preparation: KW. Writing—review and editing: JZ, YL. Supervision: SW. Funding acquisition: JX, JZ, and SW.

FUNDING

This work was supported by the National Key Research and Development Program of China (No. 2017YFA0105900), National Natural Science Foundation of China (Nos. 81922046 and 61931024), Shenzhen Science and Technology Innovation Commission (No. RCJC20200714114557005), the Shenzhen Basic Research Project (No. JCYJ20170818110900404), the Natural Science Foundation of Chongqing (No. cstc2018jcyjAX0573), Shenzhen Key Laboratory Program (No. ZDSYS20190902092857146), and the Special Funds for Strategic Emerging Industries Development in Shenzhen (No. 20180309163446298).

SUPPLEMENTARY MATERIAL

The Supplementary Material for this article can be found online at: https://www.frontiersin.org/articles/10.3389/fphar.2021.801493/full#supplementary-material

REFERENCES

Aass, K. R., Kastnes, M. H., and Standal, T. (2021). Molecular Interactions and Functions of IL-32. *J. Leukoc. Biol.* 109, 143–159. doi:10.1002/JLB.3MR0620-550R

Baselli, G. A., Dongiovanni, P., Rametta, R., Meroni, M., Pelusi, S., Maggioni, M., et al. (2020). Liver Transcriptomics Highlights Interleukin-32 as Novel NAFLD-Related Cytokine and Candidate Biomarker. *Gut* 69, 1855–1866. doi:10.1136/gutjnl-2019-319226

Chauvin, J. M., and Zarour, H. M. (2020). TIGIT in Cancer Immunotherapy. *J. Immunother. Cancer* 8, e000957. doi:10.1136/jitc-2020-000957

Chen, S., Zhou, Y., Chen, Y., and Gu, J. (2018). Fastp: an Ultra-fast All-In-One FASTQ Preprocessor. *Bioinformatics* 34, i884–i890. doi:10.1093/bioinformatics/bty560

Curran, M. A. (2018). Preclinical Data Supporting Antitumor Activity of PD-1 Blockade. *Cancer J.* 24, 2–6. doi:10.1097/PPO.0000000000000298

Diakowska, D., and Krzystek-Korpacka, M. (2020). Local and Systemic Interleukin-32 in Esophageal, Gastric, and Colorectal Cancers: Clinical and Diagnostic Significance. *Diagn. Basel* 10, 785. doi:10.3390/diagnostics10100785

Dobin, A., Davis, C. A., Schlesinger, F., Drenkow, J., Zaleski, C., Jha, S., et al. (2013). STAR: Ultrafast Universal RNA-Seq Aligner. *Bioinformatics* 29, 15–21. doi:10.1093/bioinformatics/bts635

Han, H. S., Jeong, S., Kim, H., Kim, H. D., Kim, A. R., Kwon, M., et al. (2021). TOX-expressing Terminally Exhausted Tumor-Infiltrating CD8+ T Cells Are Reinvigorated by Co-blockade of PD-1 and TIGIT in Bladder Cancer. *Cancer Lett.* 499, 137–147. doi:10.1016/j.canlet.2020.11.035

Harjunpää, H., and Guillerey, C. (2020). TIGIT as an Emerging Immune Checkpoint. *Clin. Exp. Immunol.* 200, 108–119. doi:10.1111/cei.13407

Hong, J. T., Son, D. J., Lee, C. K., Yoon, D. Y., Lee, D. H., and Park, M. H. (2017). Interleukin 32, Inflammation and Cancer. *Pharmacol. Ther.* 174, 127–137. doi:10.1016/j.pharmthera.2017.02.025

Khawar, M. B., Abbasi, M. H., and Sheikh, N. (2016). IL-32: A Novel Pluripotent Inflammatory Interleukin, towards Gastric Inflammation, Gastric Cancer, and Chronic Rhino Sinusitis. *Mediators Inflamm.* 2016, 8413768. doi:10.1155/2016/8413768

Kim, S. (2014). Interleukin-32 in Inflammatory Autoimmune Diseases. *Immune Netw.* 14, 123–127. doi:10.4110/in.2014.14.3.123

Kruger, S., Ilmer, M., Kobold, S., Cadilha, B. L., Endres, S., Ormanns, S., et al. (2019). Advances in Cancer Immunotherapy 2019 - Latest Trends. *J. Exp. Clin. Cancer Res.* 38, 268. doi:10.1186/s13046-019-1266-0

Kwon, O. C., Kim, S., Hong, S., Lee, C. K., Yoo, B., Chang, E. J., et al. (2018). Role of IL-32 Gamma on Bone Metabolism in Autoimmune Arthritis. *Immune Netw.* 18, e20. doi:10.4110/in.2018.18.e20

Lee, S., Kim, J. H., Kim, H., Kang, J. W., Kim, S. H., Yang, Y., et al. (2011). Activation of the Interleukin-32 Pro-inflammatory Pathway in Response to Human Papillomavirus Infection and Over-expression of Interleukin-32 Controls the Expression of the Human Papillomavirus Oncogene. *Immunology* 132, 410–420. doi:10.1111/j.1365-2567.2010.03377.x

Lee, Y. S., Kim, K. C., Mongre, R. K., Kim, J. Y., Kim, Y. R., Choi, D. Y., et al. (2019). IL-32γ Suppresses Lung Cancer Stem Cell Growth via Inhibition of ITGAV-Mediated STAT5 Pathway. *Cell Death Dis* 10, 506. doi:10.1038/s41419-019-1737-4

Lin, Y., Xu, J., and Lan, H. (2019). Tumor-associated Macrophages in Tumor Metastasis: Biological Roles and Clinical Therapeutic Applications. *J. Hematol. Oncol.* 12, 76. doi:10.1186/s13045-019-0760-3

Ma, G., Li, C., Zhang, Z., Liang, Y., Liang, Z., Chen, Y., et al. (2021). Targeted Glucose or Glutamine Metabolic Therapy Combined with PD-1/pd-L1 Checkpoint Blockade Immunotherapy for the Treatment of Tumors - Mechanisms and Strategies. *Front. Oncol.* 11, 697894. doi:10.3389/fonc.2021.697894

Manieri, N. A., Chiang, E. Y., and Grogan, J. L. (2017). TIGIT: A Key Inhibitor of the Cancer Immunity Cycle. *Trends Immunol.* 38, 20–28. doi:10.1016/j.it.2016.10.002

Netea, M. G., Lewis, E. C., Azam, T., Joosten, L. A., Jaekal, J., Bae, S. Y., et al. (2008). Interleukin-32 Induces the Differentiation of Monocytes into Macrophage-like Cells. *Proc. Natl. Acad. Sci. U S A.* 105, 3515–3520. doi:10.1073/pnas.0712381105

Nishida, A., Andoh, A., Inatomi, O., and Fujiyama, Y. (2009). Interleukin-32 Expression in the Pancreas. *J. Biol. Chem.* 284, 17868–17876. doi:10.1074/jbc.M900368200

Oh, J. H., Cho, M. C., Kim, J. H., Lee, S. Y., Kim, H. J., Park, E. S., et al. (2011). IL-32γ Inhibits Cancer Cell Growth through Inactivation of NF-Kb and STAT3 Signals. *Oncogene* 30, 3345–3359. doi:10.1038/onc.2011.52

Palstra, R. J., De Crignis, E., Röling, M. D., Van Staveren, T., Kan, T. W., Van Ijcken, W., et al. (2018). Allele-specific Long-Distance Regulation Dictates IL-32 Isoform Switching and Mediates Susceptibility to HIV-1. *Sci. Adv.* 4, e1701729. doi:10.1126/sciadv.1701729

Park, M. H., Song, M. J., Cho, M. C., Moon, D. C., Yoon, D. Y., Han, S. B., et al. (2012). Interleukin-32 Enhances Cytotoxic Effect of Natural Killer Cells to Cancer Cells via Activation of Death Receptor 3. *Immunology* 135, 63–72. doi:10.1111/j.1365-2567.2011.03513.x

Rouanne, M., Roumiguié, M., Houédé, N., Masson-Lecomte, A., Colin, P., Pignot, G., et al. (2018). Development of Immunotherapy in Bladder Cancer: Present and Future on Targeting PD(L)1 and CTLA-4 Pathways. *World J. Urol.* 36, 1727–1740. doi:10.1007/s00345-018-2332-5

Sloot, Y. J. E., Smit, J. W., Joosten, L. A. B., and Netea-Maier, R. T. (2018). Insights into the Role of IL-32 in Cancer. *Semin. Immunol.* 38, 24–32. doi:10.1016/j.smim.2018.03.004

Smith, T., Heger, A., and Sudbery, I. (2017). UMI-tools: Modeling Sequencing Errors in Unique Molecular Identifiers to Improve Quantification Accuracy. *Genome Res.* 27, 491–499. doi:10.1101/gr.209601.116

Solomon, B. L., and Garrido-Laguna, I. (2018). TIGIT: a Novel Immunotherapy Target Moving from Bench to Bedside. *Cancer Immunol. Immunother.* 67, 1659–1667. doi:10.1007/s00262-018-2246-5

Sorrentino, C., and Di Carlo, E. (2009). Expression of IL-32 in Human Lung Cancer Is Related to the Histotype and Metastatic Phenotype. *Am. J. Respir. Crit. Care Med.* 180, 769–779. doi:10.1164/rccm.200903-0400OC

Tang, Z., Li, C., Kang, B., Gao, G., Li, C., and Zhang, Z. (2017). GEPIA: a Web Server for Cancer and normal Gene Expression Profiling and Interactive Analyses. *Nucleic Acids Res.* 45, W98–W102. doi:10.1093/nar/gkx247

Togashi, Y., Shitara, K., and Nishikawa, H. (2019). Regulatory T Cells in Cancer Immunosuppression - Implications for Anticancer Therapy. *Nat. Rev. Clin. Oncol.* 16, 356–371. doi:10.1038/s41571-019-0175-7

Tsai, C. Y., Wang, C. S., Tsai, M. M., Chi, H. C., Cheng, W. L., Tseng, Y. H., et al. (2014). Interleukin-32 Increases Human Gastric Cancer Cell Invasion Associated with Tumor Progression and Metastasis. *Clin. Cancer Res.* 20, 2276–2288. doi:10.1158/1078-0432.CCR-13-1221

Wang, J., Zhang, Y., Song, H., Yin, H., Jiang, T., Xu, Y., et al. (2021). The Circular RNA circSPARC Enhances the Migration and Proliferation of Colorectal Cancer by Regulating the JAK/STAT Pathway. *Mol. Cancer* 20, 81. doi:10.1186/s12943-021-01375-x

Wen, S., Hou, Y., Fu, L., Xi, L., Yang, D., Zhao, M., et al. (2019). Cancer-associated Fibroblast (CAF)-derived IL32 Promotes Breast Cancer Cell Invasion and Metastasis via Integrin β3-p38 MAPK Signalling. *Cancer Lett.* 442, 320–332. doi:10.1016/j.canlet.2018.10.015

Wu, K., Li, Y., Zhang, S., Zhou, N., Liu, B., Pan, T., et al. (2019a). Preferential Homing of Tumor-specific and Functional CD8+ Stem Cell-like Memory T Cells to the Bone Marrow. *J. Immunother.* 42, 197–207. doi:10.1097/CJI.0000000000000273

Wu, K., Wang, F., Guo, G., Li, Y., Qiu, L. J., and Li, X. (2019b). CD4+ TSCMs in the Bone Marrow Assist in Maturation of Antibodies against Influenza in Mice. *Mediators Inflamm.* 2019, 3231696. doi:10.1155/2019/3231696

Yang, J., Jian, Z., Shen, P., Bai, Y., Tang, Y., and Wang, J. (2020). Associations between Interleukin-32 Gene Polymorphisms Rs12934561 and Rs28372698 and Susceptibilities to Bladder Cancer and the Prognosis in Chinese Han Population. *Dis. Markers* 2020, 8860445. doi:10.1155/2020/8860445

Yang, Y., Wang, Z., Zhou, Y., Wang, X., Xiang, J., and Chen, Z. (2015). Dysregulation of Over-expressed IL-32 in Colorectal Cancer Induces Metastasis. *World J. Surg. Oncol.* 13, 146. doi:10.1186/s12957-015-0552-3

Yun, J., Park, M. H., Son, D. J., Nam, K. T., Moon, D. B., Ju, J. H., et al. (2018). IL-32 Gamma Reduces Lung Tumor Development through Upregulation of TIMP-3 Overexpression and Hypomethylation. *Cel Death Dis* 9, 306. doi:10.1038/s41419-018-0375-6

Zhang, Z., Lu, M., Qin, Y., Gao, W., Tao, L., Su, W., et al. (2021). Neoantigen: A New Breakthrough in Tumor Immunotherapy. *Front. Immunol.* 12, 672356. doi:10.3389/fimmu.2021.672356

Conflict of Interest: The authors declare that the research was conducted in the absence of any commercial or financial relationships that could be construed as a potential conflict of interest.

The handling editor declared a past co-authorship with several of the authors KW, JZ, and SW.

Publisher's Note: All claims expressed in this article are solely those of the authors and do not necessarily represent those of their affiliated organizations, or those of the publisher, the editors, and the reviewers. Any product that may be evaluated in this article, or claim that may be made by its manufacturer, is not guaranteed or endorsed by the publisher.

Advantages of publishing in Frontiers

OPEN ACCESS
Articles are free to read for greatest visibility and readership

FAST PUBLICATION
Around 90 days from submission to decision

HIGH QUALITY PEER-REVIEW
Rigorous, collaborative, and constructive peer-review

TRANSPARENT PEER-REVIEW
Editors and reviewers acknowledged by name on published articles

Frontiers
Avenue du Tribunal-Fédéral 34
1005 Lausanne | Switzerland

Visit us: www.frontiersin.org
Contact us: frontiersin.org/about/contact

REPRODUCIBILITY OF RESEARCH
Support open data and methods to enhance research reproducibility

DIGITAL PUBLISHING
Articles designed for optimal readership across devices

FOLLOW US
@frontiersin

IMPACT METRICS
Advanced article metrics track visibility across digital media

EXTENSIVE PROMOTION
Marketing and promotion of impactful research

LOOP RESEARCH NETWORK
Our network increases your article's readership